

Alkaloid-Like Molecules as AChE Inhibitors and Anticancer Agents for Therapeutic Relief of Alzheimer's Disease and Cancer

A thesis submitted in fulfilment of the requirements

for the award of the degree of

Doctor of Philosophy

From

University of Technology Sydney



Steven Gareth Williams

B. Sci Applied Chemistry (Hons)

Supervisor: Associate Professor Alison T. Ung

Co-supervisors: Dr Jason Ashmore and Dr Ronald Shimmon

School of Mathematical and Physical Sciences

January 2017

Declaration / Certificate of authorship and originality

I certify that the work in this thesis has not previously been submitted for a degree nor has it been submitted as part of the requirements for a degree except as fully acknowledged within the text.

I also certify that the thesis has been written by me. Any help that I have received in my research work and the preparation of the thesis itself has been acknowledged. In addition, I certify that all the information sources and literature used are indicated in the thesis.

Steven Williams

January 2017

This research is supported by an Australian Government Research Training Program Scholarship.

Acknowledgments

First and foremost I would like to thank my supervisors, Associate Professor Alison Ung, Dr Jason Ashmore and Dr Ronald Shimmon for helping me through this project from start to finish. In particular to Alison for the endless hours of work, support and guidance she has provided me with to bring this thesis to fruition. Your significant contribution of personal time has not gone unnoticed. I would also like to take this chance to thank the University of Technology Sydney for the opportunity to carry out this research that has helped me to learn and grow as a scientist and for the funding provided to make it possible.

I would like to thank my friends and family for their support over the last three years, in particular my Dad for always trying to relieve the stresses of time by taking care of household tasks and cooking for me without ever asking for help for all the time I lived with him over the period of this project as well as trying to help by reading over my work to find grammatical errors, despite how tedious it must be to read pages and pages of work not in your field. To the research group and organic lab group, Xixi Xu (partner in crime), Curtis Pazderka, Matt Payne, Matt Phillips, Callum Clarke, Alex Angeloski, Ariane Roseblade, Dan Pasin (and the rest of the 'o-o' forensic family) and all the honours people who passed through over the years, for the hours of garbage we would talk about during lunch but also all the adventures we had outside of uni, without you guys I don't think I would have made it through the last three years. To Sarah Fox, for the tedious proof reads that have kept me up to the highest quality work. To all the guys at St. Ives Rugby for the hours of stress relief provided by you and the club. There are many more that could be mentioned but will not be forgotten.

I am in great debt to Dr Mohan Bhadbhade for his tireless efforts in not only running the X-ray crystallography for me but also helping me understand how to analyse the data on my visits to UNSW, use the crystallography software and preparing the cif files required for publication of crystals grown during this project. The same extends to Emeritus Professor Roger Bishop from UNSW for his generous contribution of nitriles used in this project, for passing on his wisdom and insight into the Ritter chemistry and for reviewing the work published from this project.

The following people also require a special mention; Dr Tristan Rawling for teaching me how to perform all the cell work and his constant support and advice in regards to the many things I would ask him, especially when they were often not related to this project, Associate Professor Andrew McDonagh for his support, advice and for assessing and reviewing

my internal assessments, Dr David Bishop, Alexander Angeloski and Dr Regina Verena Taudte for their technical support for the GC-MS and QTF instruments, Dr Blair Nield for helping me understand the enzyme kinetics, Tanya Badal for teaching me the experimental procedure and data analysis for STD NMR even though this work did not make the cut for this thesis, Ariane Roseblade for helping me with cell work and showing me flow cytometry but also for always being up for a chat and relieving the stresses of research by always helping me see we are in the same boat and the boat ride will end soon enough, Joyce To for induction on the plate readers, Mercedes Ballesteros and Sarah Osvath for PC2 lab inductions and technical support in those labs, Dr Tapan Rai for help with understanding the statistical analysis of biological data collected, Anthea Harris for her endless alternative ideas and approaches when I was stuck for ideas and for letting me use her instruments, Dr Thanapat Sastraruji for helping me understand the data analysis process for the Ellman assay and the UTS Science IT department, in particular Keith Fung and Dobby (Thomas Dobson) for always making time to help me, chat about the rugby and giving me ice cream from your fridge.

Table of Contents

Declaration / Certificate of authorship and originality	i
Acknowledgments	ii
Table of Contents	iv
List of Figures	x
List of Schemes	xiv
List of Tables	xviii
List of Abbreviations	xx
Publications from this Thesis	xxiii
Abstract	xxiv
CHAPTER 1: Introduction	1
1.1 A Brief Overview of Medicinal Chemistry	1
1.1.1 Drug Development	1
1.1.2 Structure-based Design	1
1.1.3 Molecular Modelling	2
1.1.4 Discovering a Hit	2
1.2 Natural Products in Drug Discovery	3
1.2.1 Alkaloids	4
1.2.2 Pharmacology of Alkaloids and Drug Development	4
1.2.3 Challenges in Using Natural Products for Drug Discovery	5
1.3 Alkaloid-like Molecules	5
1.3.1 Alkaloid and Alkaloid-like Drug Development	5
1.3.2 Introduction to Alkaloids as Anticancer Drugs	7
1.4 Cancer	9
1.4.1 A Brief History of the Developments in Chemotherapy	10
1.4.2 Mechanisms of Chemotherapy	11
1.4.3 Issues with Current Chemotherapies	14
1.4.4 Breast Cancer	15
1.5 Alzheimer's Disease	16
1.5.1 AChE and Alzheimer's Disease	18
1.5.2 AChE Structure and Functionality	19
1.5.3 Treatment of Alzheimer's Disease	22
1.5.4 AChE Inhibitors	22

1.5.5 SAR of AChE Inhibitors	24
1.5.6 Other Applications of AChE Inhibitors	25
1.5.7 Other Treatments for Alzheimer's Disease	26
1.5.8 AChE Inhibitor Design by Molecular Modelling	27
CHAPTER 2: An Alkaloid-like 3-Azabicyclo[3.3.1]non-3-ene Library Obtained from the Bridged Ritter Reaction	31
2.1 General Introduction.....	31
2.2 Introduction to Ritter Reactions	31
2.2.1 Background	31
2.2.2 Ritter Reaction Conditions and Mechanism	31
2.2.3 Bridged Ritter Reactions	33
2.3 Synthesis of Alkaloid-like Molecules with the 3-azabicyclo[3.3.1]non-3-ene Core Structure	35
2.3.1 Preparation of 6- <i>N</i> -amides, 6-alkene and 6-alcohols with 3-azabicyclo[3.3.1]non-3-ene Core Structure	36
2.3.2 Outcomes of the Bridged Ritter Reactions with (-)- β -pinene	38
2.3.3 Preparation of 3-Azabicyclo[3.3.1]non-3-en-6-yl) acetate Products	50
2.3.4 Investigation of Reaction Time	54
2.3.5 Influence of the Nitriles	54
2.3.6 Proposed Mechanism for the Bridged Ritter Reaction with (-)- β -pinene.....	55
2.3.7 Attempted Bridged Ritter Reactions.....	56
2.3.8 Alternative Bridged Ritter Reaction Catalysis	62
2.4 Mixed Bridged Ritter Reactions	64
2.4.1 Outcomes of the Controlled Mixed Ritter Reaction	66
2.4.2 Outcomes of the One-Pot Mixed Ritter Reaction	66
2.5 Conclusions and Future Directions	72
CHAPTER 3: Synthesis of Alkaloid-like Molecules <i>via</i> Derivatisation of 3-azabicyclo[3.3.1]non-3-enes.....	74
3.1 General Introduction.....	74
3.2 Reduction of Cyclic Imines	75
3.2.1 Crystal Packing of (+)-101l and (+)-101b	78
3.3 Amide Deprotection of (+)-102m	81
3.4 Reductive <i>N</i> -Alkylation of <i>N</i> -3 Amines.....	81
3.5 Attempted Derivatisation Reactions.....	82

3.5.1 Amide Hydrolysis	82
3.5.2 N-6 Amine Derivatisation and Rational Drug Design	84
3.5.2.1 Petasis-Borono Mannich Multicomponent Reaction of (+)-103m	85
3.5.2.3 Reductive <i>N</i> -alkylation of (+)-105I with Benzaldehyde.....	88
3.5.3 Alkene Reactions.....	90
3.5.4 Reaction of (+)-101I with Benzenesulfonyl Chloride	91
3.5.5 Imine Reactions with (+)-60a	92
3.6 Reaction of (+)-59I with DMAD	94
3.7 Conversion of Imine to Nitron and Subsequent 1,3-Dipolar Cycloaddition of Maleic Anhydride.....	95
3.8 1,3-Dipolar Cycloaddition of Cyclic Nitrones with Maleic Anhydride.....	97
3.9 Conclusions and Future Directions	97
CHAPTER 4: Anticancer Biological Results	99
4.1 General Introduction to Assessment of Cytotoxicity.....	99
4.1.1 MTS Assay	99
4.1.2 Screening for Cytotoxicity	100
4.1.3 Dose-response analysis of cytotoxicity	102
4.1.4 SAR of Cytotoxic Activity Against MDA-MB-231.....	105
4.2 External Screening of Cytotoxicity	106
4.3 Conclusions and Future Directions	107
CHAPTER 5: AChE inhibition biological results.....	108
5.1 Introduction to Alzheimer's Disease and AChE inhibition	108
5.1.1 Ellman Assays.....	108
5.1.2 TLC Bioautographic Method	109
5.1.3 Other AChE Inhibition Methods.....	110
5.2 Review and Validation of Ellman Methods.....	110
5.3 AChE Inhibition Results	114
5.3.1 Ellman Assay Results	116
5.4 Assessment of Rationally Designed AChE Inhibitors.....	118
5.5 Conclusions and Future Directions	120
CHAPTER 6: External Broad Screening.....	122
6.1 General Introduction.....	122
6.2 The <i>In Vitro</i> Screening Process.....	122

6.2.1 <i>In Silico</i> Screening Results	122
6.2.2 Therapeutic Screening Targets and Results	125
6.3 Summary and Conclusion of Broad Screening Results	130
CHAPTER 7: Computer-Aided Molecular Modeling	132
7.1 General Introduction.....	132
7.2 Evaluation of Drug-Like Properties	132
7.2.1 Evaluation of ADMET Descriptors	134
7.3 Ligand Docking and Interactions.....	139
7.3.1 Preparing for Docking	139
7.3.2 Docking and Scoring Method Validation.....	141
7.3.3 Alkaloid-like Library AChE Docking Results.....	144
7.4 Docking Result Directed Rational Drug Design of a Better AChE Inhibitor	148
7.5 Conclusion.....	155
CHAPTER 8: Conclusion and Future Directions.....	156
8.1 Chemical Synthesis Conclusions	156
8.2 Biological Assays Conclusions	157
8.3 Future Directions	158
CHAPTER 9: Experimental.....	160
9.1 General Experimental	160
9.1.1 Nuclear Magnetic Resonance (NMR) Spectroscopy	160
9.1.2 Mass Spectrometry (MS).....	160
9.1.3 Chromatography	161
9.1.4 Infrared Spectroscopy.....	161
9.1.5 Melting Points	161
9.1.6 Optical Rotation	161
9.1.7 Plate Readers for Bio-Assays.....	161
9.1.8 Reagents and Solvents	162
9.1.9 Partial Characterisation.....	162
9.2 General Chemical Reaction Methods	162
9.2.1 Standard Bridged Ritter Reaction Conditions	162
9.2.2 Alternative Condition Bridged Ritter Reactions.....	169
9.2.3 Polar Bridged Ritter Reaction Conditions	169
9.2.4 Mixed Ritter Reactions.....	171

9.2.5 Hydride Reduction Reactions.....	173
9.3 Miscellaneous Chemical Reaction Methods	177
9.3.1 Mild Amide De-protection of (+)-101m	177
9.3.2 C-6 Amide Hydrolysis with HCl.....	178
9.3.3 S _N 2 reaction of C-6 Amines with Benzyl Bromide	179
9.3.4 Reductive Alkylation of (+)-101I	179
9.3.5 Reductive <i>N</i> -alkylation of N-6 Amine (+)-105I with Anisaldehyde	180
9.3.6 Conversion of (+)-59I Imine to Nitrone.....	181
9.3.7 DMAD addition of (+)-59I	182
9.4 Attempted Reactions	183
9.4.1 Bridged Ritter Reaction with Forced Oxidation	183
9.4.2 Bridged Ritter Reaction with Alternative Catalysts.....	183
9.4.3 Controlled Mixed Ritter Reactions.....	184
9.4.4 Reaction of (+)-101I with Benzenesulfonyl Chloride	185
9.4.5 Petasis-Borono Mannich Multicomponent Reaction.....	185
9.4.6 C-6 Amide Hydrolysis with NaOH.....	186
9.4.7 C-6 Alkene Reactions with (+)-60I	186
9.4.8 Reactions with (+)-60a Imine	186
9.4.9 1,3-Dipolar Cycloaddition of (+)-128 with Maleic Anhydride	187
9.4.10 Hinsberg Reaction of (+)-101I with Benzenesulfonyl Chloride	188
9.4.11 Methylchlorine Elimination of IBA with Base	188
9.5 X-ray Structure Analysis	188
9.5.1 Diffraction Data Collection.....	188
9.5.2 Solution and Refinement	189
9.5.3 Crystal Structure Data	195
9.6 Biological Assays	195
9.6.4 MTS Assay	195
9.6.5 External Cancer Cell Growth Inhibition Assay.....	195
9.6.6 AChE TLC Bioautographic Method	196
9.6.7 Ellman Assay Procedure	197
9.7 Molecular Modeling	197
CHAPTER 10: Appendices.....	198
10.1 Docking Parameters	198
10.1.1 Protein Preparation.....	198

10.1.2 Ligand Minimisation.....	198
10.1.3 Ligand Preparation.....	198
10.1.4 Docking with CDOCKER.....	199
10.1.5 In Situ Ligand Minimization.....	199
10.1.6 Ligand Scoring.....	200
10.2 Common Feature Pharmacophore Generation.....	202
CHAPTER 11: References.....	204

List of Figures

Figure 1.1 Common alkaloids.....	4
Figure 1.2 <i>Erythroxylon coca</i> . ^[16]	5
Figure 1.3 The 3-aza-bicyclo[3.3.1]nonane core structure found in alkaloids.	6
Figure 1.4 Structural comparisons of cyclic imines 10 and 11 with known <i>Aristotelia</i> alkaloids. 6	
Figure 1.5 <i>Picea abies</i> . ^[31]	7
Figure 1.6 The <i>Catharanthus roseus</i> flower and the structure of vincristine 14 , vinblastine 15 and vinorelbine 16	8
Figure 1.7 The structure of the hexacyclic pyrrole alkaloid lamellarin D 17	9
Figure 1.8 The formation and spread of cancer. ^[40]	10
Figure 1.9 The structure of sulfur and nitrogen mustards.....	10
Figure 1.10 Structures of folic acid 22 and methotrexate 23	11
Figure 1.11 Structures of uracil 24 and 5-fluorouracil 25	11
Figure 1.12 Stages of the cell cycle.	12
Figure 1.13 The structures of different alkaloid chemotherapy agents.	13
Figure 1.14 The structure of the variolin A 32 and B 33 alkaloids and first kinase inhibitor, imatinib 34	14
Figure 1.15 Simplified structure of the monoclonal antibody Trastuzumab.....	16
Figure 1.16 Pathology of Alzheimer’s disease. ^[64]	18
Figure 1.17 ACh and AChE in the synaptic cleft. ^[69]	19
Figure 1.18 1EVE: TcAChE with Donepezil in the binding site (sphere highlighted in red), generated using Discovery Studio 4.5.....	20
Figure 1.19 AChE active site interactions responsible for the hydrolysis of acetylcholine. ^[71] ...	20
Figure 1.20 The PAS site of TcAChE, generated using Discovery Studio 4.5.....	21
Figure 1.21 AChE active site residues coloured according to site type. ^[75]	22
Figure 1.22 Alkaloid AChE inhibitors.....	23
Figure 1.23 Structures of significant activity relationships.....	25
Figure 1.24 Stemofoline 44 and didehydrostemofoline 45 alkaloids.	25
Figure 1.25 Memantine 48 and structurally similar alkaloid-like molecules.	26
Figure 2.1 Transition state: hydrogen sulfate counter ion pairing with the carbenium ion.....	32
Figure 2.2 Product core numbering and nitrile letter assignment.	38
Figure 2.3 ORTEP diagram for compound (+)-59b	40
Figure 2.4 Colours obtained from the purification of the crude product of the bridged Ritter reaction with succinonitrile.	43

Figure 2.5 ORTEP diagram of (-)-66h molecule in the crystal structure of racemic, showing the intramolecular H-bonding between NH---O=C.	49
Figure 2.6 Enantiomers of (-)-66h (grey) and (+)-66h (magenta, glide plane related) in the unit cell looking down the <i>a</i> axis.	50
Figure 2.7 ORTEP diagram for the compound (+)-67	53
Figure 2.8 AChE protein file 1DX6 containing 2-[2-[2-(2-hydroxyethoxy)ethoxy]ethoxy]ethanol (pink) in the gorge leading down to the active site where Galantamine (red) interacts.	58
Figure 2.9 ORTEP diagram of the crystal structure of compound (+)-80	67
Figure 2.10 Mass spectrum for the mixed product (+)-80 , showing the identifying fragment. .	69
Figure 2.11 Mass spectrum for the mixed product (+)-79 , showing the identifying fragment. .	70
Figure 2.12 TIC chromatogram for the mixed bridged Ritter products of acetonitrile and benzonitrile.	70
Figure 3.1 NOESY correlations for compound (-)-102l generated by Spartan Pro 8. (AM1).	77
Figure 3.2 ORTEP diagram of (+)-101l (left) and (+)-101b (right), showing the configuration of stereocenter at C-4.	78
Figure 3.3 The NH---O=C and CH---O=C hydrogen bonding observed in the crystal structures of a, compound (+)-101l and b, compound (+)-101b	80
Figure 3.4 Space filling diagrams of (+)-101l (left) and (+)-101b (right), showing the crowding of the amine NH.	81
Figure 3.5 Imino-alkene (+)-60l with the alkene bond represented as a resonance stabilised structure.	90
Figure 3.6 Overlaid ¹ H NMR spectra of (+)-60m at 5 °C temperature intervals to observe a change in integral values of the C-7 CH and C-6α CH ₂ resonances.	91
Figure 4.1 All compounds % viability at 50 μM. Data represented is the mean of replicate ±SD.	101
Figure 4.6 The structures of compounds for visual comparison of SAR properties.	103
Figure 4.2 MDA-MB-231 cytotoxicity dose-response curve for (+)-59m	103
Figure 4.3 MDA-MB-231 cytotoxicity dose-response curve for (+)-60m	104
Figure 4.4 MDA-MB-231 cytotoxicity dose-response curve for (+)-101m	104
Figure 4.5 The effects of (+)-60m on MDA-MB-231 cells after 48 hours. Images were viewed at 10 x magnification using light microscopy. A) (+)-60m at 50 μM; B) (+)-60m at 10 μM; C) healthy untreated control cells.	105
Figure 5.1 Example of the TLC bioautographic with the Galantamine control.	110
Figure 5.2 Example Lineweaver-Burk Plot for competitive inhibitors.	111

Figure 5.3 Lineweaver-Burk plot of the Ellman assay kinetics experiment data.....	112
Figure 5.4 Michaelis-Menten plot of the Ellman assay kinetics experiment data.....	112
Figure 5.5 Dose-response curves for the % inhibition of active compounds.	117
Figure 5.6 Structures of compounds that showed AChE inhibition with the Ellman assay.	117
Figure 5.7 Molecular modeling guided rational drug designed compounds (+)-112 and (+)-114 and Ellman assay AChE inhibition IC ₅₀ values.....	119
Figure 5.8 Dose-response curve for the IC ₅₀ value calculated for (+)-112	120
Figure 5.9 Dose-response curve for the IC ₅₀ value calculated for (+)-114	120
Figure 6.1 Compounds submitted to OIDD program that are undergoing <i>in vitro</i> screening. .	124
Figure 6.2 Compounds submitted to OIDD program that failed <i>in silico</i> screening.	125
Figure 6.3 3D representation of OIDD primary screening results for each compound and corresponding assay.	131
Figure 7.1 Summary of a standard drug discovery pipeline.	132
Figure 7.2 ADMET plot of alkaloid-like molecules synthesised.	139
Figure 7.3 Summarised outline of the protocols used for docking in Discovery Studio 4.5.....	141
Figure 7.4 Crystal structure binding interactions of Galantamine in the AChE active site for protein file PDB: 1DX6.	142
Figure 7.5 Binding interactions for docked of Galantamine in the AChE active site for protein file PDB: 1DX6.	143
Figure 7.6 Superimposed Galantamine from the x-ray structure (green) and docked (blue)..	143
Figure 7.7 2D representation of the binding pose for (-)-65j in the AChE active site.	145
Figure 7.8 2D representation of the binding pose for (+)-59n in the AChE active site.....	146
Figure 7.9 2D representation of the binding pose for (+)-60n in the AChE active site.....	146
Figure 7.10 3D surface representation of the protein and the docked pose of (-)-65j , looking down the gorge from the top of the entrance.	147
Figure 7.11 3D surface representation of the protein and the docked pose of (-)-65j , looking side-on at the gorge with N3 and C6 labelled.....	147
Figure 7.12 Best theoretical docking products of the Petasis reaction.	150
Figure 7.13 Best theoretical docking products from <i>N</i> -alkylation.....	151
Figure 7.14 2D docking pose of 2-naphthylboronic acid, glyoxylic acid and 111	152
Figure 7.15 2D docking pose of 2-naphthylboronic acid, formaldehyde and 110	152
Figure 7.16 2D docking pose of 2-naphthylboronic acid, formaldehyde and 105n Petasis Product.....	153

Figure 7.17 ADMET plot for the proposed docked compounds, with the best scoring compounds listed in Table 7.6 highlighted in yellow.....	155
Figure 9.1 Layout of TLC bioautograph showing the inhibition of acetylcholinesterase activity by an inhibitor (0.5-1000 ng) with Galantamine as a positive control.	197

List of Schemes

Scheme 1.1 Total synthesis of (+)-aristoline 8	7
Scheme 1.2 Hydrolysis of ACh by AChE.	19
Scheme 1.3 Total Synthesis of Galantamine.....	24
Scheme 1.4 Useful alkaloid-like molecules formed <i>via</i> the bridged Ritter reaction.	28
Scheme 1.5 The bridged Ritter reaction between (-)- β -pinene and nitrile with functionality –R.	29
Scheme 2.1 General Ritter reaction.....	31
Scheme 2.2 Example Ritter reaction between butanol and 2-hydroxypropanenitrile. ^[103]	32
Scheme 2.3 Ritter reaction mechanism.....	33
Scheme 2.4 An example intramolecular cyclisation Ritter reaction.....	34
Scheme 2.5 General scheme for the bridged Ritter reaction between (-)- β -pinene and various nitriles under the standard reaction conditions.	34
Scheme 2.6 General scheme for the bridged Ritter reaction between (-)- β -pinene and various nitriles under the mild reaction conditions.	36
Scheme 2.7 The bridged Ritter reaction between (-)- β -pinene and trimethylsilyl cyanide.	39
Scheme 2.8 The bridged Ritter reaction between (-)- β -pinene and propionitrile.	39
Scheme 2.9 The bridged Ritter reaction between (-)- β -pinene and butyronitrile.	41
Scheme 2.10 The bridged Ritter reaction between (-)- β -pinene and valeronitrile.	41
Scheme 2.11 The bridged Ritter reaction between (-)- β -pinene and succinonitrile.	42
Scheme 2.12 Hydrolysis of (-)- 60d nitrile to form the amide derivative.	42
Scheme 2.13 Proposed mechanism for the formation of tri-cyclic alkaloid-like products from the intramolecular cyclisation of nitrile and carbocation.....	43
Scheme 2.14 The bridged Ritter reaction between (-)- β -pinene and 3,4-dimethoxybenzonitrile.	44
Scheme 2.15 The bridged Ritter reaction between (-)- β -pinene and cinnamonitrile.	45
Scheme 2.16 The bridged Ritter reaction between (-)- β -pinene and benzyl cyanides 4-bromophenylacetonitrile and 4-nitrophenylacetonitrile.	45
Scheme 2.17 Autoxidation of benzylic products.	46
Scheme 2.18 The bridged Ritter reaction between (-)- β -pinene and methyl cyanoacetate and ethyl cyanoacetate.....	47
Scheme 2.19 Interconversion of the enol and keto forms of (-)- 60g and (-)- 60h	48
Scheme 2.20 A possible mechanism for the rearmament of cyanoacetate product (-)- 66h	48

Scheme 2.21 Expected outcome from the bridged Ritter reaction between (-)- β -pinene and potassium cyanide.	51
Scheme 2.22 Actual outcome from the bridged Ritter reaction between (-)- β -pinene and potassium cyanide.	52
Scheme 2.23 A proposed mechanism for the formation of compound (+)-67	54
Scheme 2.24 Proposed mechanism for the bridged Ritter reaction with (-)- β -pinene.	56
Scheme 2.25 Attempted bridged Ritter reaction between (-)- β -pinene and 3-methoxypropionitrile.	58
Scheme 2.26 Attempted bridged Ritter reaction between (-)- β -pinene and 4-aminobenzonitrile.	59
Scheme 2.27 Protection of 4-aminobenzonitrile with acetic anhydride.	59
Scheme 2.28 Attempted bridged Ritter reaction between (-)- β -pinene and <i>N</i> -(4-cyanophenyl)acetamide.	60
Scheme 2.29 Attempted bridged Ritter reaction between (-)- β -pinene and aminoacetonitrile hydrogen sulfate.	60
Scheme 2.30 Attempted bridged Ritter reaction between (-)- β -pinene and <i>N</i> -(cyanomethyl)acetamide.	60
Scheme 2.31 General scheme for attempted bridged Ritter reactions between (-)- β -pinene and terminal chloronitrile's where chain length = <i>n</i>	61
Scheme 2.32 Halide elimination of the bridged Ritter reaction product and <i>N</i> -isobornylamides.	62
Scheme 2.33 Attempted bridged Ritter reaction between (-)- β -pinene and bromoacetonitrile.	62
Scheme 2.34 Halide elimination of (+)-59m to give the alkene product.	62
Scheme 2.35 Attempted bridged Ritter reaction between (-)- β -pinene and acetonitrile with I ₂ catalyst.	63
Scheme 2.36 The bridged Ritter reaction between (-)- β -pinene and acetonitrile with copper triflate catalyst.	64
Scheme 2.37 The bridged Ritter reaction between (-)- β -pinene and acetonitrile with zinc triflate catalyst.	64
Scheme 2.38 General reaction scheme for a controlled mixed Ritter reaction.	65
Scheme 2.39 General reaction scheme for a one-pot mixed Ritter reaction.	65
Scheme 2.40 Attempted controlled mixed Ritter reactions.	66
Scheme 3.1 Scaffold derivatisation <i>via</i> the imine functionality.	74

Scheme 3.2 Scaffold derivatisation <i>via</i> the alkene functionality.....	75
Scheme 3.3 Scaffold derivatisation <i>via</i> the amine functionality.	75
Scheme 3.4 Reduction of imino-amide scaffolds to amino-amides.	76
Scheme 3.5 Reduction of imino-alkene scaffolds to amino-alkenes.....	76
Scheme 3.6 Amide deprotection of amino-amide (+)-101m to diamine (+)-103m	81
Scheme 3.7 Reductive <i>N</i> -methylation of amino-amide (+)-101l to (+)-104l	82
Scheme 3.8 Expected outcome of the amide hydrolysis of (+)-59l and (+)-101l by NaOH.	83
Scheme 3.9 Imine-Enamine tautomerisation that protects the imine from hydrolysis.	83
Scheme 3.10 Expected outcome of the amide hydrolysis of (+)-59l and (+)-101l by HCl.	84
Scheme 3.11 Actual outcome of the amide hydrolysis of (+)-101l by HCl.	84
Scheme 3.12 The hydride reduction of (+)-105l to give (+)-103l	84
Scheme 3.13 Attempted Petasis reaction of (+)-103m with glyoxylic acid and 2-naphthylboronic acid.....	86
Scheme 3.14 Petasis reaction of (+)-103m with formaldehyde and 2-naphthylboronic acid....	86
Scheme 3.15 Petasis reaction of (+)-105l with formaldehyde and 2-naphthylboronic acid.	87
Scheme 3.16 Reductive <i>N</i> -alkylation of 6-N amine (+)-105l with <i>p</i> -anisaldehyde.	88
Scheme 3.17 Reductive <i>N</i> -alkylation of 6-N amine (+)-105l with benzaldehyde.	89
Scheme 3.18 Reaction of (+)-103l with benzyl bromide.....	89
Scheme 3.19 Potential proposed reaction of (+)-105l with benzyl bromide.....	89
Scheme 3.20 Conversion of the internal alkene 116 into the internal alkene (+)-60m	91
Scheme 3.21 The attempted reaction of (+)-101l with benzenesulfonyl chloride.	92
Scheme 3.22 Reaction of (+)-60a with 3-mercaptopropionic acid.	93
Scheme 3.23 Attempted reaction of (+)-60a with ethyl acetoacetate.....	93
Scheme 3.24 Attempted reaction of (+)-60a with malonic acid.....	94
Scheme 3.25 The reaction of (+)-59l with DMAD to give (-)-121	94
Scheme 3.26 Imine to nitron conversion by methyltrioxorhenium catalysed urea hydrogen peroxide. ^[160]	95
Scheme 3.27 Tungstate catalysed oxidation of structurally similar amines with hydrogen peroxide. ^[161]	95
Scheme 3.28 Synthesis of nitron (+)-125 <i>via</i> oxaziridine 124 from reacting (+)-59l with <i>m</i> -CPBA.....	96
Scheme 3.29 Formation of 126 and 127 from <i>N</i> -oxide (+)-125	96
Scheme 3.30 Synthesis of nitron (+)-125 using the method by Soldaini <i>et al.</i> ^[160]	97
Scheme 3.31 Attempted 1,3-dipolar cycloaddition of maleic anhydride to (+)-125	97

Scheme 4.1 Mitochondrial cleavage of MTS 129 to formazan 130	100
Scheme 4.2 Reduction of resazurin 134 to resorufin 135 by NADH.	106
Scheme 5.1 Hydrolysis of ATCh by AChE and the subsequent formation of yellow TNB (133).108	
Scheme 5.2 Hydrolysis of naphthyl acetate by AChE and the subsequent formation of the purple dye in the TLC bioautographic assay.	109
Scheme 7.1 Reaction pathway to functionalise C-6 through amine 105	148
Scheme 7.2 The four different possible compounds that could be formed by derivatising the C-6 amine <i>via</i> either the Petasis reaction, shown in green, or reductive <i>N</i> -alkylation, shown in blue.	149

List of Tables

Table 2.1 List of products obtained from the bridged Ritter reaction between (-)- β -pinene and the various nitriles used.....	37
Table 2.2 List of nitriles unsuccessfully used for the bridged Ritter reaction and the hypothesised reasons.	57
Table 2.3 Nitrile combinations attempted with the one-pot mixed bridged Ritter reaction.....	72
Table 3.1 Yields of amine-scaffolds obtained from the reduction of corresponding imines.	77
Table 3.2 Hydrogen-bond geometry for (+)-101I	78
Table 3.3 Hydrogen-bond geometry for (+)-101b	79
Table 4.1 MDA-MB-231 MTS screening results as % viability normalised to control.....	102
Table 4.2 MTS assay IC ₅₀ results with the standard errors.	103
Table 4.3 Cytotoxicity results from external screening performed at BIOTEC.	106
Table 5.1 Ellman assay kinetics experiment data.	113
Table 5.2 Summary of differences in Ellman methods reported.....	113
Table 5.3 TLC bioautographic AChE inhibition assay results.	115
Table 5.4 Ellman assay AChE inhibition results.....	117
Table 5.5 Comparison of functionality on AChE inhibitors.	118
Table 5.6 AChE inhibition properties of (+)-112 and (+)-114 , from the TLC bioautographic and Ellman assays.	119
Table 6.1 List of compounds that did not pass <i>in silico</i> screening.....	123
Table 6.2 Summary of primary screening results for OIDD endocrine & cardiovascular targets.	127
Table 6.3 Summary of primary screening results for OIDD neuroscience targets.....	127
Table 6.4 Summary of primary screening results for OIDD autoimmune targets.	128
Table 6.5 Summary of primary screening results for OIDD oncology target.	129
Table 6.6 Summary of primary screening results for OIDD tuberculosis target.....	129
Table 6.7 Summary of primary screening results for OIDD malaria target.....	129
Table 7.1 List of physicochemical properties corresponding to each compound made.	133
Table 7.2 ADMET results of the alkaloid-like library.....	135
Table 7.3 Ludi_3 scores for the docked pose for each of the compounds synthesised.	144
Table 7.4 List of docking scores for hypothetical products of the Petasis reaction.	149
Table 7.5 List of docking scores for hypothetical products of reductive <i>N</i> -alkylation.....	150
Table 7.6 Evaluation of the best docking compounds ADMET descriptors.	154
Table 9.1 X-ray crystal data for (-)-66h	190

Table 9.2 X-ray crystal data for (+)-101l	191
Table 9.3 X-ray crystal data for (+)-101b	192
Table 9.4 X-ray crystal data for (+)-67	193
Table 9.5 X-ray crystal data for (+)-80	194

List of Abbreviations

Å	Angstrom
δ	Chemical Shift (NMR)
λ	Wavelength
ν_{\max}	Maximum absorbance
$[\alpha]_D^{25}$	Specific rotation for a Na lamp at 589 nm at 25°C
[L]	Ligand concentration
$[M]^{+}$	Molecular ion
$[M + H]^{+}$	Protonated molecular ion
ACh	Acetylcholine
AChE	Acetylcholinesterase
AChR	Acetylcholine receptor
AD	Alzheimer's disease
Ar	Aromatic
Asp	Aspartic acid
ATCh	Acetylthiocholine
BChE	Butyrylcholinesterase
br	Broad (NMR)
c	Concentration in g/100 mL
calc	Calculated
CAS	Catalytic Active Site
d	Doublet (NMR)
Da	Dalton
DCM	Dichloromethane
dd	Doublet of doublets (NMR)
ddd	Doublet of doublets of doublets (NMR)
DEPT	Distortionless enhancement by polarization transfer
DMAD	Dimethyl acetylenedicarboxylate
DMSO	Dimethyl sulfoxide
dq	Doublet of quartets (NMR)
dsep	Doublet of septets (NMR)
dsex	Doublet of sextets (NMR)
dt	Doublet of triplets (NMR)
DTNB	5,5'-Dithiobis(2-nitrobenzoic acid)

eeAChE	Electric eel acetylcholinesterase (EC 3.1.1.7)
EtOAc	Ethyl Acetate
Equiv.	Equivalents
F ₂₅₄	Fluorescent at 254nm
FDA	Food and Drug Authority
FTIR	Fourier transform infrared spectroscopy
g	Gram
GC-MS	Gas chromatography-mass spectroscopy
Glu	Glutamic acid
Gly	Glycine
COSY	Correlation spectroscopy
HSQC	Heteronuclear single quantum correlation
hAChE	Human acetylcholinesterase
His	Histidine
HRMS	High-resolution mass spectroscopy
HTS	High throughput screening
Hz	Hertz
IC ₅₀	The half maximal inhibitory concentration
IR	Infrared
<i>J</i>	Coupling constant (NMR)
K _D	Ligand dissociation constant
LRMS	Low-resolution mass spectroscopy
m	Multiplet (NMR)
<i>m/z</i>	Mass to charge ratio
mg	Milligrams
mL	Millilitre
mmol	Millimole
m.p.	Melting point
NCE	New Chemical Entity
ng	Nanogram
nmol	Nanomole
NMR	Nuclear Magnetic Resonance
NOE	Nuclear Overhauser Effect
non	nonet (NMR)

PAS	Peripheral Active Site
PDB	Protein database
Ph	Phenyl
Phe	Phenylalanine
ppm	Part per million
Pet. spir.	Petroleum spirits
PSA	Polar surface area
q	Quartet (NMR)
qin	Quintet (NMR)
Q-TOF	Quadrupole Time-of-Flight
R_f	Retention factor
R_t	Retention time
r.t.	Room temperature
s	Singlet (NMR)
SAR	Structure-activity relationship
s	Second
Ser	Serine
sp.	Species
STD	Saturation Transfer Difference
t	Triplet (NMR)
TcAChE	<i>Torpedo californica</i> acetylcholinesterase (EC 3.1.1.7)
td	Triplet of doublets (NMR)
TLC	Thin layer chromatography
TMS	Trimethylsilane
Try	Tryptophan
Tyr	Tyrosine
U	The enzyme unit

Publications from this Thesis

1. An alkaloid-like 3-azabicyclo[3.3.1]non-3-ene library obtained from the bridged Ritter reaction, Steven Gareth Williams, Mohan Bhadbhade, Roger Bishop and Alison Thavary Ung, *Tetrahedron* **2017**, *73*, 116-128.
2. Synthesis and Crystal Structure of Unexpected (1S,4R,5R,6S)-4-cyano-2,2,6-trimethyl-3-azabicyclo[3.3.1]nonan-6-yl acetate, Steven Gareth Williams, Mohan Bhadbhade, Roger Bishop and Alison Thavary Ung, *Aus J Chem*, **submitted**.

Presented Conference Posters with Accepted Abstracts from This Thesis

1. Alkaloid-like molecules as AChE inhibitors. Steven Gareth Williams, Alison Thavary Ung. Presented at 'RACI Medicinal Chemistry and Chemical Biology NSW Symposium', 28 September 2015, The University of Sydney, NSW, Australia.
2. Alkaloid-like Molecules for Drug Discovery. Steven Gareth Williams, Tristan Rawling and Alison Thavary Ung. Presented at 'RACI Medicinal Chemistry and Chemical Biology Meeting', 6-9 November 2016, Crowne Plaza Coogee Beach, Australia.

Abstract

Due to the prevalence of alkaloids in the chemical drug space and the broad range of biological properties held by the *Aristolelia* alkaloids, including anticancer properties, a library of structurally similar alkaloid-like compounds has been synthesised, containing the 3-aza-bicyclo[3.3.1]nonane architecture, in order to explore the cytotoxicity of it and its derivatives.

The 3-aza-bicyclo[3.3.1]nonane core was obtained *via* the bridged Ritter reaction with (-)- β -pinene and various nitriles to afford 18 compounds (Chapter 2). Several of the compounds obtained from the bridged Ritter reaction were derivatised to give an additional 17 compounds (Chapter 3). The information obtained from these reaction outcomes, were used to further understand the bridged Ritter reaction mechanism. X-ray crystallography was used for analysis of the projection of the scaffold and substituents within the 3D space of the crystal lattice to further understand the reactivity of the synthesised scaffolds.

The library of alkaloid-like compounds was tested for their biological properties. The breast cancer cell lines MDA-MB-231 and MCF-7 were investigated due to in-house data that showed activity for a related series of compounds (Chapter 4). The MDA-MB-231 cell line was tested in-house and 3 of 28 compounds showed significant activity in the reduction of cell viability, however, it is believed that they possess general toxicity, as opposed to having a cytotoxic nature. This library was deemed not viable for developing as cytotoxic agents within this project.

Acetylcholine esterase (AChE) was chosen as an alternative target to be screened against (Chapter 5). Two complementary assays were used to determine the activity were 9 of the 27 tested compounds showed weak activity. SAR data and molecular modeling was used to develop a rational drug design approach to synthesise an improved inhibitor. Two of the designed compounds were synthesised and evaluated for their AChE inhibition properties and both showed relative increase in activity compared to their precursors. In addition to the docking studies used to guide the design of improved AChE inhibitors, molecular modeling was utilised to assess the drug-like properties and ADMET descriptors for each of the synthesised compounds.

Lastly, broad screening of the biological properties of a selection of the synthesised compounds is currently being investigated by the services of the Lily OIDD program with 16 of the 31 submitted compounds are currently undergoing screening and results from five compounds have been returned so far.

CHAPTER 1: Introduction

1.1 A Brief Overview of Medicinal Chemistry

Drug development began over a century ago with the investigation of derivatives of aliphatic and aromatic hydrocarbons extracted from coal-tar. In the 1870's, Paul Ehrlich postulated that these compounds should be able to selectively target chemoreceptors of cancer cells, parasites or microorganisms. This was based on the observation of dyes he was working with, that showed selective affinities for specific biological tissues.^[1] Furthermore, the concept of enzymes and receptors being used as drug targets was developed in 1905 by John Newport Langley. He stated that receptors are essentially switches that receive and send specific signals, and that this mechanism could be either blocked by an antagonist or turned on by an agonist. Many drugs have since been developed on this basis.^[1]

Comprehending biological structure and biochemical mechanisms became essential in the creation of new bioactive chemical structures. By 1996, about 500 molecular targets were addressed by therapies used at the time. It is claimed that there are at least 5,000-10,000 unused possible drug targets in the body,^[1] highlighting the significant potential for designing new drugs for targets we have not yet discovered. Drug development is the central role of a modern medicinal chemist.

1.1.1 Drug Development

Drug development often proceeds *via* the generation of large libraries of compounds, either virtual or synthetic, that are screened for desirable properties such as toxicity, potency and efficacy.^[1] From the collection of this type of data, structural activity relationships (SARs) can be determined or hypothesised. Libraries are often designed based on descriptors of structural and biological features, regularly achieved by high-throughput screening (HTS) to determine a compound's binding affinity against functionally different proteins.^[1]

1.1.2 Structure-based Design

More recently, the 3D structures of drug target proteins are utilised in the development stages, to design compounds in a way that will optimise their selectivity and potency as drugs. There are already drugs on the market that have been designed in this manner^[2] and one important aspect involves the identification of areas within the protein where intermolecular interactions can occur, thus defining a potential binding site. Molecular modelling is becoming increasingly important for this.

1.1.3 Molecular Modelling

Many computer programs have been developed to calculate the physical properties of molecules and hypothesise the way they may behave in biological systems. The calculation of polar surface area (PSA), lipophilicity descriptors (such as logD and logP), solubility and pK_a, helps to predict behaviour such as the rate of drug transport into hydrophilic and hydrophobic media. This gives medicinal chemists an indication of whether the compound will be able to cross the blood-brain barrier or be absorbed efficiently by the intestine before it can reach its target.^[3] Several other techniques, such as docking studies, quantitative structure–activity relationship (QSAR) models and pharmacophore models are techniques that focus on the biological target.

Docking is a method for predicting the interactions between a ligand and a protein, or the interactions between two proteins. The target structure must be known and represented as a protein file based on X-ray crystallography or Nuclear Magnetic Resonance (NMR) data. Docking can provide a ‘score’ representing the interaction affinity and it is an effective way of prioritising chemical library’s synthesis and biological assay experiments.^[4] QSAR is used as a predictive model for important drug properties such as physicochemical properties, pharmacokinetics and toxicology. QSAR uses the relationship between the structural properties of a compound and measured biological activity, normally where the biological target is unknown, to calculate the activity of new compounds or an established compounds activity against other targets.^[5] This technique utilises large databases of known compounds and activities towards specific targets. Furthermore, pharmacophore modelling is a way of identifying descriptive features of a set of compounds (ligand-based) or the active site of a target (receptor-based), which are necessary for a pharmacological interaction. These include regions of hydrogen bond donors (HBD) or acceptors (HBA), cationic or anionic sites, hydrophobic and aromatic regions.^[6]

Each of these techniques are powerful computer-aided tools used by medicinal chemists for performing rational drug design and *in silico* compound screening. Although this can accelerate the discovery of drug-like compounds, it is still only a guide and results must be supported with follow-up bio-assays.

1.1.4 Discovering a Hit

Synthesis directed by the results of molecular modelling and bio-assays often aim to develop weak binding fragments (showing target affinity at concentrations between 100 µM and 10 mM) into ‘hit’ compounds. ‘Hits’ are typically compounds that have IC₅₀ values lower

than 10 μM or show initial biological activity that warrants further investigation into 'leads'.^[2] The pharmaceutical industry has experienced great success with innovative and rational approaches to drug discovery; from computer-aided drug design to looking to nature for new chemical spaces in drug design. Medicinal chemists often look for 'hit' compounds in nature and a recent review by Newman and Cragg^[7] stated natural products have a pivotal role in drug discovery.

1.2 Natural Products in Drug Discovery

Natural products have played an important role in the pharmaceutical industry, with about 49% of the new chemical entities (NCE's) introduced between 1981 and 2002 being either natural, semi-synthetic (analogues of natural products) or synthetic compounds, based on the pharmacophores of natural products.^[8] Natural products provide good lead structures for drug discovery, as they often have favourable properties such as high biochemical specificity and high chemical diversity.

Of the large number of natural products reported, many show 'drug-like' properties, that is, they share characteristics with other compounds that are drugs. These properties include shape, size and solubility. Libraries of natural products and synthetic compounds are often examined and screened for these properties. Other properties such as molecular mass, molecular/structural flexibility (the number of rotatable bonds and ring topology), the number of chiral centres (which is found to be higher in natural products) and distribution of heavy atoms, are also evaluated.

Lipinski introduced a simple method for assessing some of these factors in 1997,^[9] known as 'Lipinski's rule-of-five'. The rule states that for small molecules intended to be administered orally, the molecular mass should be less than 500 Da, there should be less than five hydrogen-bond donors and less than 10 hydrogen bond acceptors, and the logP (calculated octanol-water partition coefficient) should be less than five.

A study by Schneider and Lee^[10] found that only 10% of both natural products and commercial synthetic drugs analysed had two or more violations of the rule-of-five. The use of natural products has provided lead compounds as well as the discovery of "privileged structures," that is, compounds that show an inherent ability to bind to multiple protein targets and confer biological activities.

A high percentage of currently employed chemotherapeutic drugs, more than 60% for cancer and more than 75% for infectious disease, are of plant origin. Approximately 50% of

pharmaceuticals currently being used are derived from naturally occurring amines. For this reason, alkaloids have been and will continue to be an in-depth area of research for promising drug development.^[11]

1.2.1 Alkaloids

Alkaloids are a class of naturally occurring organic compounds derived from plants and another natural source.^[11] They contain an amino nitrogen, giving them a basic nature. This nitrogen is of great significance as it opens a window to biological interactions and therefore potential medicinal properties. Due to this, out of the thousands of biologically active alkaloids, many are commonly used for their effect as drugs. Typical examples include cocaine **1**, morphine **2**, galantamine **3** and quinine **4**^[12] as seen in Figure 1.1.

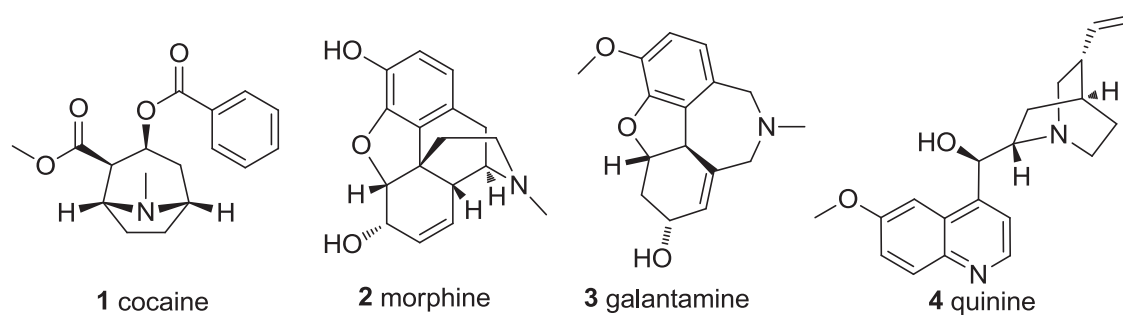


Figure 1.1 Common alkaloids.

Some of these alkaloids are well known for their analgesic and local anaesthetic properties.^[13] In many cases, their influence on biological function was discovered by accident, when people ingested plant or fungi material that contained significant levels of alkaloids. The use of plants containing alkaloids in ancient rituals has also been well documented.^{[14],[15]} It was on this basis that studies were performed to identify alkaloids in many plants and fungi with the aim of determining their typical molecular structures and properties.

1.2.2 Pharmacology of Alkaloids and Drug Development

As there is such a wide range of alkaloids with significant structural variation, they exhibit a variety of biological activities and pharmacological outcomes. For instance, ergot alkaloids (originating from the fungus *Claviceps purpurea*) are selectively active towards the endocrine system. Anaesthetic and analgesic alkaloids, such as morphine and cocaine (obtained from the coca bush *Erythroxylon coca* as seen in Figure 1.2), bind to the sodium channels within the nerve cell's membrane. This results in numbing pain by inhibiting sodium from crossing the cell membrane, thus stopping the formation of action potentials.^[11] Other well-documented pharmacological outcomes of alkaloids include AChE inhibitory and antineoplastic (anticancer) properties, as will be discussed in depth in the following sections.

Knowledge of all these properties and the corresponding molecular structures is crucial to alkaloid drug development.



Figure 1.2 *Erythroxylon coca*.^[16]

1.2.3 Challenges in Using Natural Products for Drug Discovery

Despite the advantages of natural products previously mentioned, there are limitations and challenges that beset the use of alkaloids in drug discovery. These include complexities of natural product chemistry, slowness in isolation and structural elucidation, concerns about IP rights and the costs and resource limitations of alkaloids required for further biological development and structure-activity relationship (SAR) investigations.^{[12],[17],[18]} This is why there is an imperative to develop synthetically accessible and biologically active compounds that mimic natural product chemical scaffolds. Thus, efficient synthetic methods that can provide rapid access to alkaloid-like chemical scaffolds would be a practical method of generating libraries of biologically active compounds used for drug discovery and development.

1.3 Alkaloid-like Molecules

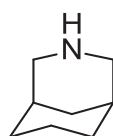
Alkaloid-like molecules are synthetic molecules that have close structural similarity to that of natural alkaloids.^[19] The properties of alkaloid-like molecules have a strong statistical correlation with the properties of established pharmaceutical drugs and thus alkaloid-like molecules often display biological and drug-like properties.^{[20],[21],[22]} Furthermore, synthetic molecules are designed to mimic the useful properties of their natural counterparts, including diverse structures and biological activities, good solubility, oral bioavailability and target selectivity.^[23]

1.3.1 Alkaloid and Alkaloid-like Drug Development

Analysing the literature has revealed that many natural alkaloids contain the 3-azabicyclo[3.3.1]nonane architecture **5**, seen in Figure 1.3. It is found in the core of known

bioactive alkaloids such as makomakine **6**, (+)-aristolone^[24] **7** and (-)-serratoline **9**. (+)-Aristolone is found in four of the five known *Aristolonia* species. Infusions of the leaves of *A. chilensis* were used in folk medicine in Central and South Chile and Western Argentina to treat sore throats, kidney pains, stomach ulcers, digestive conditions, fever, scarring injuries and as an anti-inflammatory agent.^{[25],[26]}

The leaf extracts which contain (+)-aristolone and its derivatives were shown to have anti-inflammatory, analgesic, antioxidant, anti-haemorrhagic, anticancer properties (against human epidermoid carcinoma)^{[26],[27]} and can alter human erythrocytes.^[24] This broad spectrum of biological activities exhibited amongst *Aristolonia* alkaloids would most likely be similar for alkaloid-like compounds that contain the same core structure.



5

Figure 1.3 The 3-aza-bicyclo[3.3.1]nonane core structure found in alkaloids.

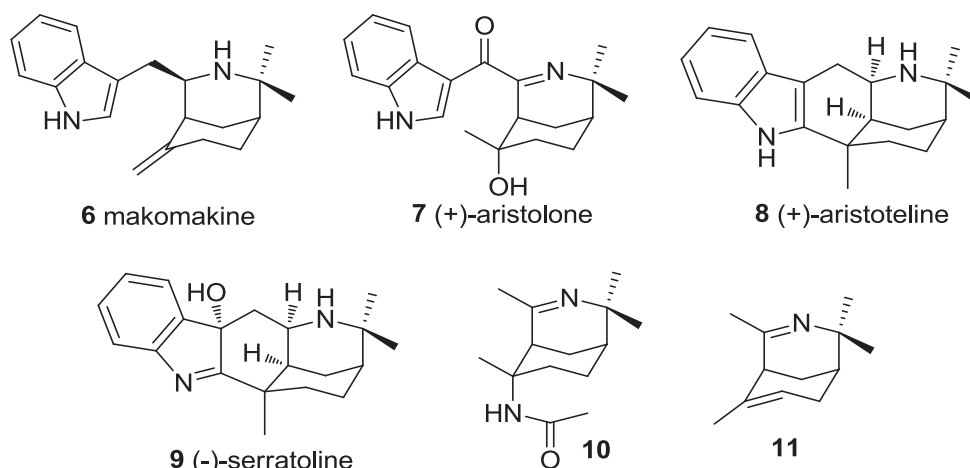
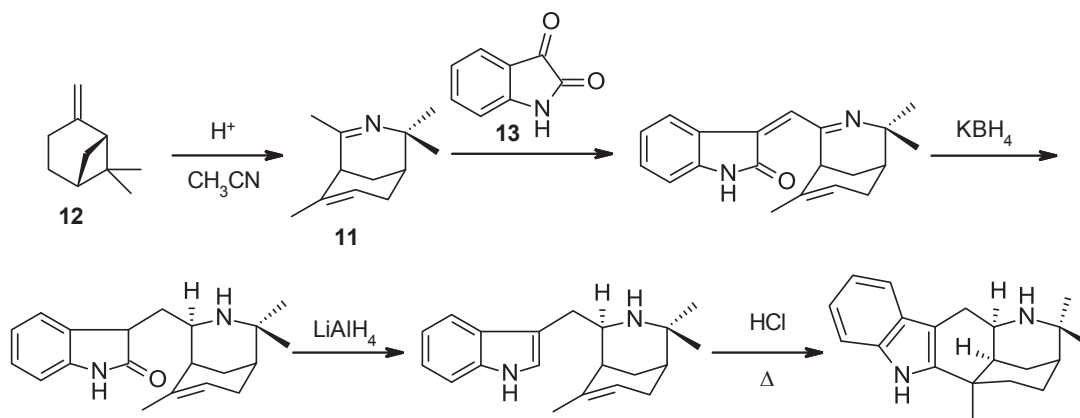


Figure 1.4 Structural comparisons of cyclic imines **10** and **11** with known *Aristolonia* alkaloids.

Compounds **10** and **11** (Figure 1.4) are alkaloid-like compounds that share the same core chemical scaffold as that found in the *Aristolonia* alkaloids. They are also capable of undergoing further reactions with various reagents to produce an extensive range of derivatives.^[28] For example, the total synthesis of (+)-aristolone **8** has been reported by Mirand *et al.*,^[29] in a five-step pathway from (-)- β -pinene **12** and subsequent reaction of alkaloid-like alkene **11** with isatin **13**, as shown in Scheme 1.1. This research has, therefore, focused on the development of many alkaloid-like molecules based on the core structure **5**.



Scheme 1.1 Total synthesis of (+)-aristoteline **8**.

1.3.1.1 Natural Product Starting Materials

Many terpenes exhibit biological properties,^[14] one such example is (-)- β -pinene, found in the species *Picea abies*^[30] shown in Figure 1.5. Terpenes also provide a pathway to produce an assortment of diverse alkaloid-like molecules. The type of chemistry capable of producing alkaloid-like molecules from these starting materials is also of great importance. One type of reaction known to be capable of this is the bridged Ritter reaction,^[19] which will be discussed in depth in Chapter 2.

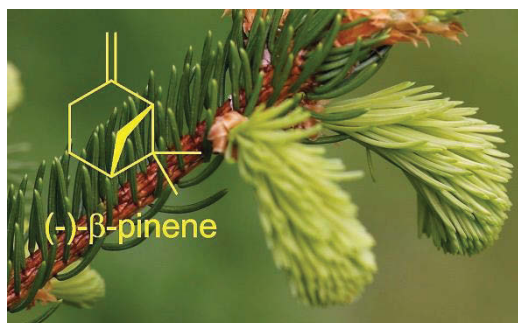


Figure 1.5 *Picea abies*.^[31]

The use of readily available and optically pure natural products as the starting materials in the bridged Ritter reaction constitutes an excellent approach for providing natural product derived and alkaloid-like scaffolds with rich structural diversity. One of the areas in which large amounts of research has been performed is on alkaloid-like molecules derived in such a way and their use as anticancer drugs.^[19]

1.3.2 Introduction to Alkaloids as Anticancer Drugs

Certain alkaloids are known to exhibit anticancer properties and there are many reports of alkaloids that display antineoplastic^[32] and immunomodulating^[33] properties. Particularly notable examples include the *Vinca* alkaloids vincristine **14**, vinblastine **15** and

vinorelbine **16** (Figure 1.6), which are mitotic inhibitors that work by inhibiting tubulin, tyrosine kinase and cyclin-dependent kinases (CDKs).^[34] The discovery of vincristine, found in the *Catharanthus roseus* plant, provided a breakthrough in the treatment of leukaemia and Hodgkin's disease. The semi-synthetic *Vinca* alkaloid, vinorelbine, is also used for treating breast and lung cancer. This highlights the usefulness of natural product derived compounds.^[35]

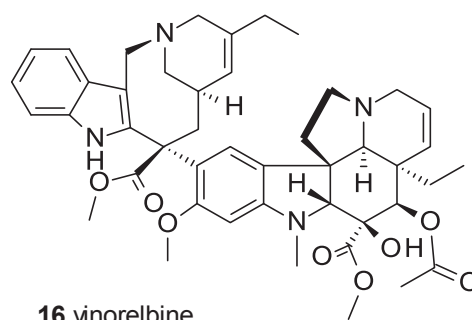
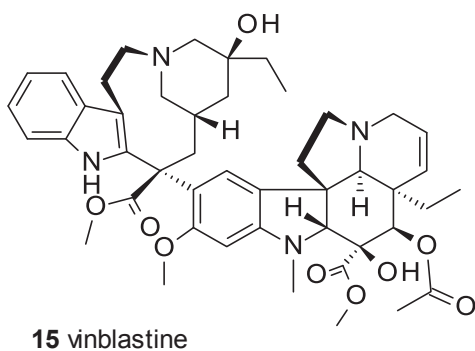
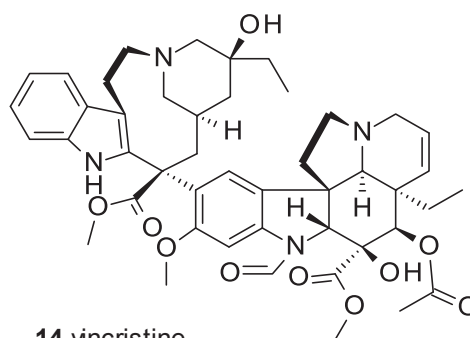
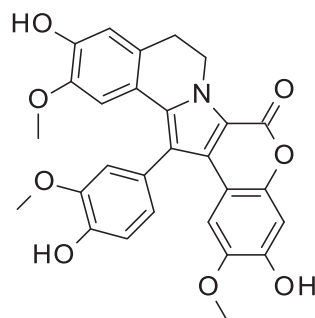


Figure 1.6 The *Catharanthus roseus* flower and the structure of vincristine **14**, vinblastine **15** and vinorelbine **16**.

Another example is the Lamellarins (hexacyclic pyrrole alkaloids), such as lamellarin D **17**, Figure 1.7. Hexacyclic pyrrole alkaloids are natural products of marine origin that have been extracted from species of ascidians and sponges and were first isolated from a prosobranch mollusc of the *Lamellaria* genus in 1985.^[36] Baunbæk *et al.*^[36] reported Lamellarins to demonstrate inhibition of several cancer protein kinases, as well as a number of other multi-target mechanisms that cause apoptotic cell death.



17 lamellarin D

Figure 1.7 The structure of the hexacyclic pyrrole alkaloid lamellarin D **17**.

Several other cytotoxic alkaloids and their mechanisms of action are listed in Section 1.4.2. If the properties of these alkaloids could be mimicked in novel alkaloid-like molecules, without the poor target selectivity which most current anticancer drugs have, they would make an ideal substitute.^[37] For any anticancer properties observed in the compounds synthesised from this research, it would be worthwhile investigating if they work *via* the same mechanisms as those of currently employed cytotoxic alkaloids.

1.4 Cancer

Cancer is one of the most common diseases in the world and is one of the leading causes of mortality and economic expenditure. The World Health Organisation (WHO) has predicted that the burden of cancer will increase by 70% over the next two decades.^[38] Advances in treatment and early diagnosis have increased life expectancies in developed countries, however, there were still over 44,000 cancer-related deaths in Australia in 2013, with one in two men and one in three women developing some form of the disease before the age of 85.^[39] This is why it is imperative that research continues to develop new methods for diagnosis and treatment.

Cancer is the result of mutations in the deoxyribonucleic acid (DNA) that cause cells to grow abnormally. Mutations can result from external environmental factors or by errors that naturally occur during DNA replication. Despite natural mechanisms existing to repair damaged DNA, or remove cells formed from mutated DNA, some are missed and replicate to form tumours. As a person ages, cancer becomes more prevalent because their bodies accumulate a higher number of these mutations and the immune system has weakened ability to eliminate abnormal cells. When a tumour begins to grow uncontrollably and spreads out of the primary growth site, it is called cancer (Figure 1.8). Cancers that have spread and are found in other parts of the body are known as metastases of the primary tumour.

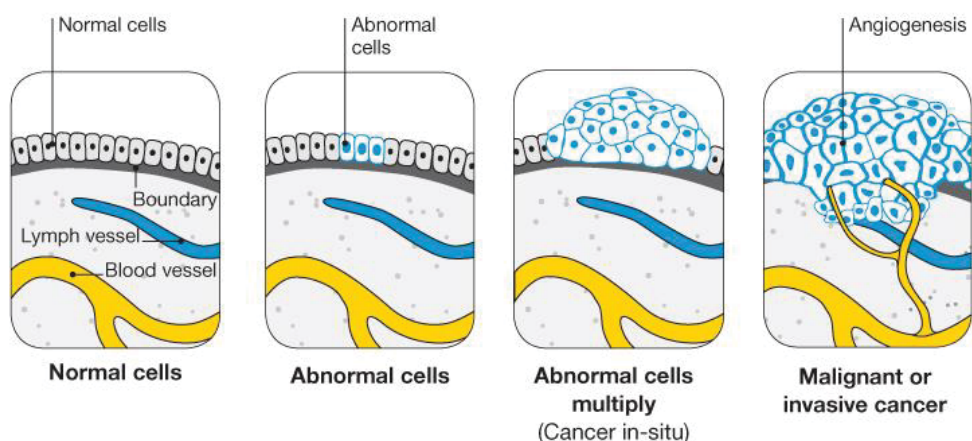


Figure 1.8 The formation and spread of cancer.^[40]

1.4.1 A Brief History of the Developments in Chemotherapy

The word ‘chemotherapy’ was termed by Paul Ehrlich in the early 1900s and was used to define the method of treating disease with chemicals. Although radiotherapy and surgery were the leading treatments for cancer until the 1960s, it was determined that the cure rates using these methods alone could not exceed 33% due to metastases that remained after treatment. Combining these established treatments with chemotherapy increased their effectiveness and patient outcomes were significantly improved.^[41]

Development of the first chemotherapeutic agents stemmed from research into vesicant war gases, in particular, an accident during the second world war where troops were exposed to sulphur mustards that leaked after their ship was bombed in Bari Harbor, Italy. Observations that the exposed troops had depleted lymph nodes and bone marrow concentration lead to research in 1943, where nitrogen mustards (Figure 1.9) were administered to patients to initiate the regression of cancer of the lymphatic system. Nitrogen mustards are alkylating agents and reacted with cellular nucleophiles. This initiated the synthesis of derivative alkylating agents and established the potential for using chemicals to treat cancer.

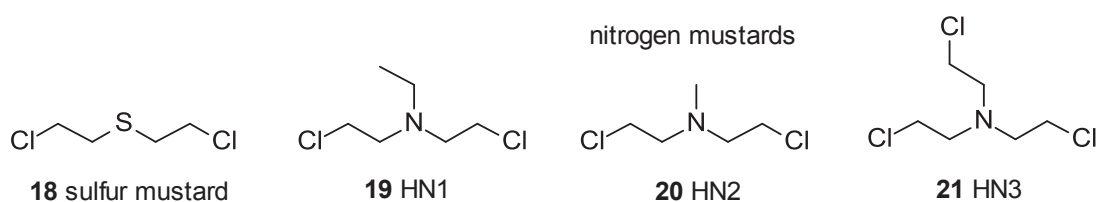


Figure 1.9 The structure of sulfur and nitrogen mustards.

Another important, yet initially incorrect observation, made in 1948 was that folic acid **22** sourced from green leafy vegetables accelerated leukaemia growth. This idea was based on

folate deficiency exhibiting similar effects to nitrogen mustard. After the development of a series of folic acid analogues, subsequent testing revealed that they result in the remission of leukaemia in children. Methotrexate, **23** (Figure 1.10), is a folic acid derivative that interferes with the synthesis of folate and either stops DNA replication or causes mistakes in the DNA. This leads to apoptosis and, therefore, methotrexate is classified as an anti-metabolite.

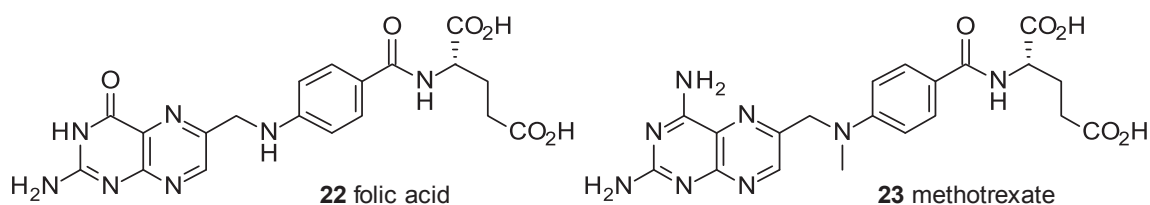


Figure 1.10 Structures of folic acid **22** and methotrexate **23**.

The next stage in the development of chemotherapy was the concept of targeted therapy, with the first example emerging in the mid-1950s with 5-fluorouracil **25**, as seen in Figure 1.11. Charles Heidelberger and his colleagues noticed that liver cancer metabolism in rats uniquely resulted in a greater uptake of uracil **24**, which is one of the nucleobases that makes up ribonucleic acid (RNA). The substitution of H-5 with fluorine led to the newly synthesised 5-fluorouracil which exhibited broad spectrum antitumor activity against many solid tumours.

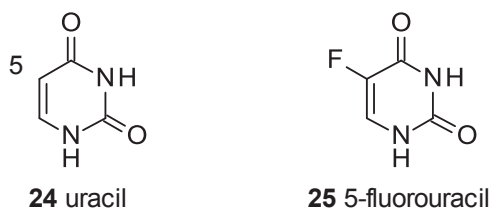


Figure 1.11 Structures of uracil **24** and 5-fluorouracil **25**.

Since the discovery of chemotherapy, extensive research has resulted in abundant information about the mechanisms by which different chemotherapies work becoming available. Understanding these mechanisms is important when considering the development of novel cytotoxic compounds.

1.4.2 Mechanisms of Chemotherapy

Chemotherapy works by targeting rapidly dividing cells such as cancer, hair follicle cells, gastrointestinal tract lining cells, skin cells and red and white blood cells. Although cancerous cells are most sensitive, the wide range of cell types that are affected is what accounts for the side effects and adverse effects of treatment, such as hair loss, diarrhoea, skin sensitivity and immunosuppression. These cells are targeted because they spend more time in

the S and M phase of the cell cycle, where the cell's DNA is replicated and the cell divides, respectively. By comparison, other healthy cells spend most of their time in the G₀ stage where the cells 'rest' and therefore do not proliferate as quickly. By introducing chemotherapies that damage DNA, the DNA is prevented from being replicated and hence the cells do not divide correctly, leading to apoptosis or mitotic catastrophe. Chemotherapies that target these stages of the cell cycle are known as 'phase-specific'. Finding new chemotherapeutic agents with potentially new mechanisms of action may lead to drugs that do not have the same side-effects.

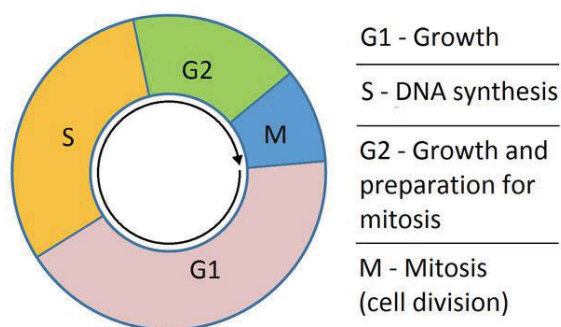


Figure 1.12 Stages of the cell cycle.

There are several types of commonly used chemotherapies, each with different biological targets. Many of these mechanisms can be targeted with alkaloids, as shown below, showing the significance of alkaloids and hence the potential of alkaloid-like compounds to be developed for chemotherapy. Alkylating agents prevent DNA replication by introducing alkyl groups that impede DNA function. Intercalating agents stop transcription by preventing DNA and RNA polymerases from binding to DNA by binding to the double helix grooves, for example acronycine **26**^[42] and berberine **27**.^[43] Antimetabolites are non-functioning analogues of DNA base pairs which substitute into the DNA, resulting in loss of function. Topoisomerase inhibitors, as the name suggests, inhibit the topoisomerase proteins which are responsible for unwinding the DNA when required for replication and transcription, for example the quinoline alkaloid camptothecin **28** is an example of a topoisomerase I inhibitor.^[44] Mitotic inhibitors either stop the synthesis of or destroy proteins such as tubulin, microtubules and mitotic spindles, which are required for moving chromosomes during mitosis. A few examples of alkaloids which target microtubule dynamics include cryptophycin B **29** and sarcodictyin A **30**,^[45] as well as the commonly used compound paclitaxel (or Taxol®) **31**.

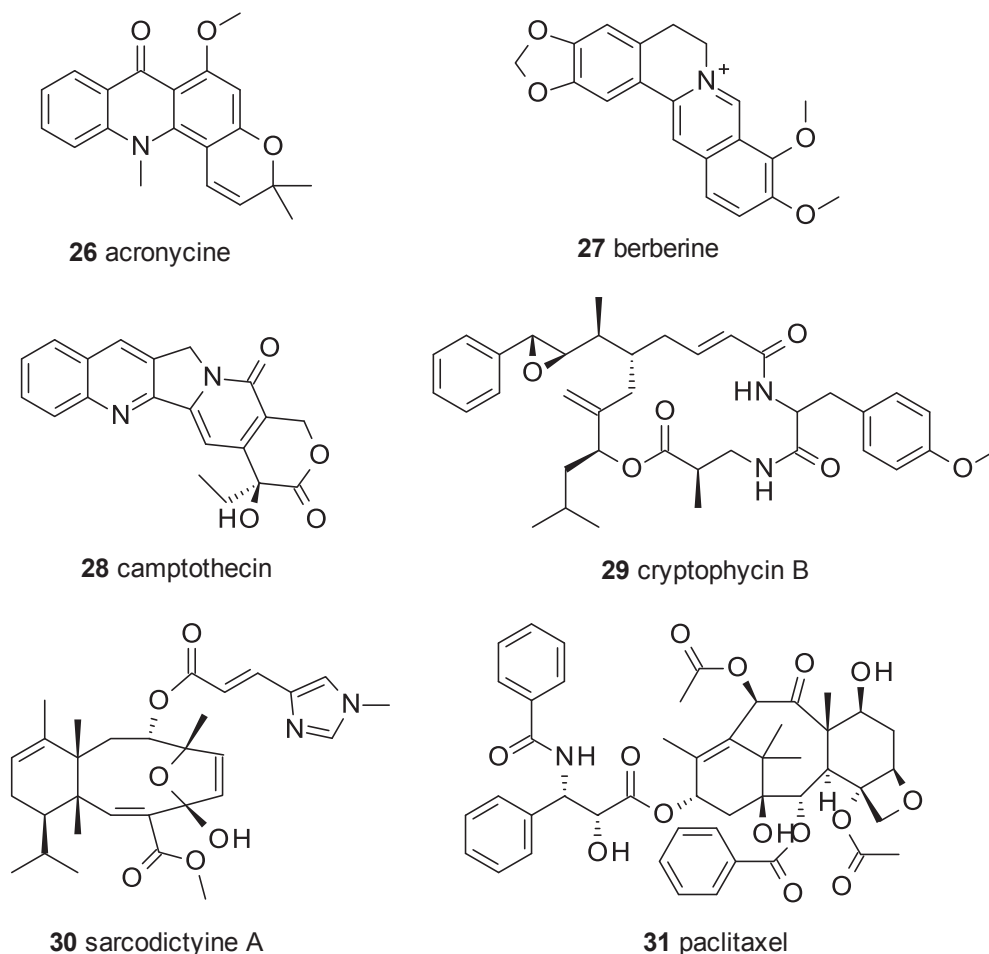


Figure 1.13 The structures of different alkaloid chemotherapy agents.

Another important group of targets are cyclin-dependent kinases, which are proteins responsible for cellular regulation such as apoptosis, transcription and cell cycle progression – making them good chemotherapeutic targets. In addition to the Lamellarins mentioned earlier, the Variolins are another group of alkaloids that have shown specific action towards inhibition of cyclin-dependent kinases.^[46] The structures of variolin A **32** and B **33** are seen in Figure 1.14. A structural investigation of inhibitors that bind to the ATP-site, indicated that slight changes in the chemical structure of kinase inhibitors result in variations in the binding mode and kinetics. The outcome of this investigation eventually led to the development of imatinib **34**, the first kinase inhibitor anticancer agent.^[2] It remains difficult, however, to synthesise highly selective kinase target molecules due to the large number of kinase enzymes and the similarity of their ATP-binding sites.

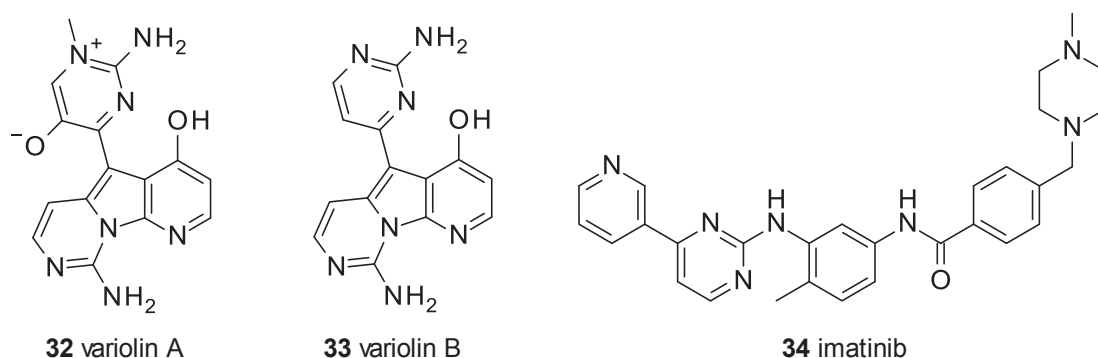


Figure 1.14 The structure of the variolin A **32** and B **33** alkaloids and first kinase inhibitor, imatinib **34**.

1.4.3 Issues with Current Chemotherapies

Despite the success of treatment methods using these mechanisms, both individually and as combinational therapies, cancers can still develop resistance to drugs. Cancers can become resistant to the mechanism of action of individual chemotherapies in as little as one mutation. For this reason, most chemo-regimens used today involve several different drugs, each with different modes of action. One of the primary causes for a tumour to develop resistance is the result of errors made by the enzymes that assemble the DNA. In addition, drugs that cause DNA damage can have their toxicity lowered by the cell cycle checkpoints that respond to damaged DNA. Although disruption of DNA is an effective way to prevent cancer cells from dividing, the same damage to healthy cell DNA can lead to the development of new secondary cancers, even though healthy cells have mechanisms and checkpoints for preventing the replication of damaged DNA. Normal healthy cells are often also affected by drugs that target cell division or DNA replication due to the normal cells and cancer cells sharing major metabolic pathways and DNA.

There are several other mechanisms for the development of resistance. These include the increase of cell membrane proteins that remove the drug from the cell or reduction in the expression of proteins that transport drugs across the cell membrane into the cell, increased metabolism of the drug, modification of proteins so that the drugs no longer interact or bind to them lose function and even the ability of the cells to repair the DNA damage the drugs cause or avoid cell death as a consequence of the DNA damage.

Once a tumour acquires the ability to remove drugs from the intracellular matrix by development and expression of transporters, the cell will be resistant to almost all drugs of the same class, despite differences in chemical structure and mechanisms of action.^[47] These are

all reasons why it is important to discover new mechanisms for cancer prevention and develop new chemotherapeutic agents.

1.4.4 Breast Cancer

Breast cancer is the most common cancer among women worldwide, with the World Health Organisation (WHO) reporting its incidence at 25.2% of the total occurrence of all cancer types. For this reason, breast cancer has been the primary focus of this research. There are several established subtypes of breast cancer, which offer oncologists a way of providing patients with targeted treatments by using chemotherapies that utilise a biological mechanism specific to certain subtypes.^[48] One way that the subtypes have been classified is based on their molecular features, such as the presence of receptors on the cell surface, nucleus or in the cytoplasm. The three most noteworthy receptors are the progesterone receptor (PR), the estrogen receptor (ER) and the tyrosine kinase receptor (ERBB2).^[49]

As well as the general mechanisms for cytotoxicity which can be applied to several cancer types, there are also mechanisms specific to the cell type. For this reason, breast cancer is a good example of targeted treatment. Breast cancer cells can be positive (+) or negative (-) for each of the previously mentioned receptors, hence providing specific chemotherapeutic targets. Estrogen receptors are responsible for regulating the activity of certain genes, which, once activated by the hormone estrogen, can be treated by administering hormone therapies that block the receptors of ER-positive cells. The story behind the discovery of the HER2 gene provides another example of developing targeted treatments.

Research led by Denis Salmon at the University of California, Los Angeles in 1987 found that some breast cancers showed amplification or overexpression of the human epidermal growth factor receptor 2 (or HER2) gene, which encodes the ERBB2 tyrosine kinases receptor responsible for the regulation of cellular processes such as stimulating cell proliferation.^[50] Consequently, this led to a lower survival rate in patients. For this reason, HER2 was identified as a potential therapeutic target for the treatment of ERBB2+ breast cancer. Following this discovery, it was the work of the biotechnology company Genentech in 1991 that led to the development of the monoclonal antibody trastuzumab (Herceptin®), which was approved by the FDA in 1998 for treating metastatic breast cancer. It is still used today for HER2 positive breast cancers. Trastuzumab binds to the HER2 receptors on the extracellular portion and prevents the binding of signalling mitogens that activate the receptor and prevents its role in pathways responsible for cell proliferation. Cell arrest then occurs and the rate of proliferation is reduced, preventing the cancer from growing.

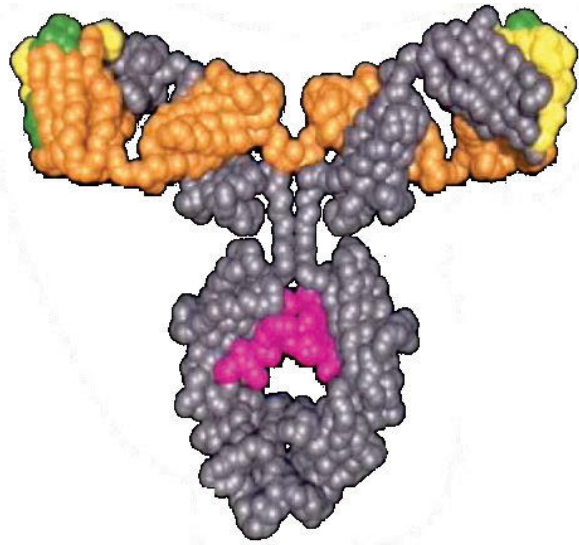


Figure 1.15 Simplified structure of the monoclonal antibody Trastuzumab.

Other established receptors that are important for the control of breast cancer growth include the progesterone receptor (PR)^[51] and p53.^[52] The presence of these receptors are referenced to classify breast cancers into their subtypes. Cell lines that are positive for both ER and PR but not HER2 are classified as luminal A. Those that are ER, PR and HER2 positive are classified as luminal B. Cell lines containing no ER, PR or HER2 are known as triple negative.^[53] Cancers with none of the known receptors are more challenging to treat.

As not all cancers are the same, the prevalence of different strains of cancer has attributed to extensive research into personalised medicine. Previously explained examples highlight the potential of the development of target specific treatments, however further research is required to effectively and cheaply individualise treatments. Discovering new biological pathways will assist this process.

1.5 Alzheimer's Disease

Alzheimer's Disease (AD) was first reported by Alois Alzheimer in 1907 and is defined as a neurodegenerative disease which accounts for an astonishing 60-80% of dementia cases,^[54] where dementia is an umbrella term used to describe any life effecting decline in mental ability. The symptoms of AD include an initial decrease in cognitive function and short-term memory, which eventually develops into difficulties with rationality, long-term memory, speaking and reading, then possible psychosis, depression and aggression.^[54]

AD is not only a significant problem now, with 1 in 3 people over the age of 85 and 1 in 9 over 65 having the disease,^[55] but the number of affected people is expected to greatly increase as the current Baby Boomer population enters this age bracket. Furthermore, this

figure is expected to increase, with the life expectancy of people in developed countries passing 80 due to medical advances available to the younger generations.^[54] AD is suffered by 35–40 million patients worldwide^[56] and there is currently no cure. As a result, it was the 2nd leading cause of death in Australia in 2013.

Many scientific papers^{[12],[14],[57]} have highlighted the use of natural products, in particular, alkaloids, as useful drugs targeting AD. In order to treat AD with drugs in a target based fashion, the disease must first be thoroughly understood. This is difficult because the initial cause of AD development is still unknown. Theories as to the development of the disease pathology include genetics, oxidative stress and biometal mediated aggregation. The pathological signs associated with AD in the literature are quite diverse and include ACh depletion, oxidative stress,^[58] τ -protein aggregation and β -amyloid deposits,^[59] with the two major biomarkers associated with AD being the development of plaques and tangles that damage the brain.

Brain damaging plaques are a result of the precipitation of high concentrations of β -amyloid, a peptide by-product of the amyloid precursor protein (APP) found in the synapse where it is required for synapse and neurone development.^[60] On the other hand, brain damaging tangles that form around dendrites, axons and microglia within the neurones are a result of the accumulation and clumping together of unbound hyperphosphorylated forms of the *tau* protein.^[61] *Tau* proteins are essential for healthy cognitive function^[62] as they are responsible for assembly and stabilisation of axonal microtubules, which provide neurones with structure and a means of intracellular vesicle transport.^[54] It has also been discovered that there may be a link between β -amyloid and increases in the phosphorylation of the *tau* protein.^[63]

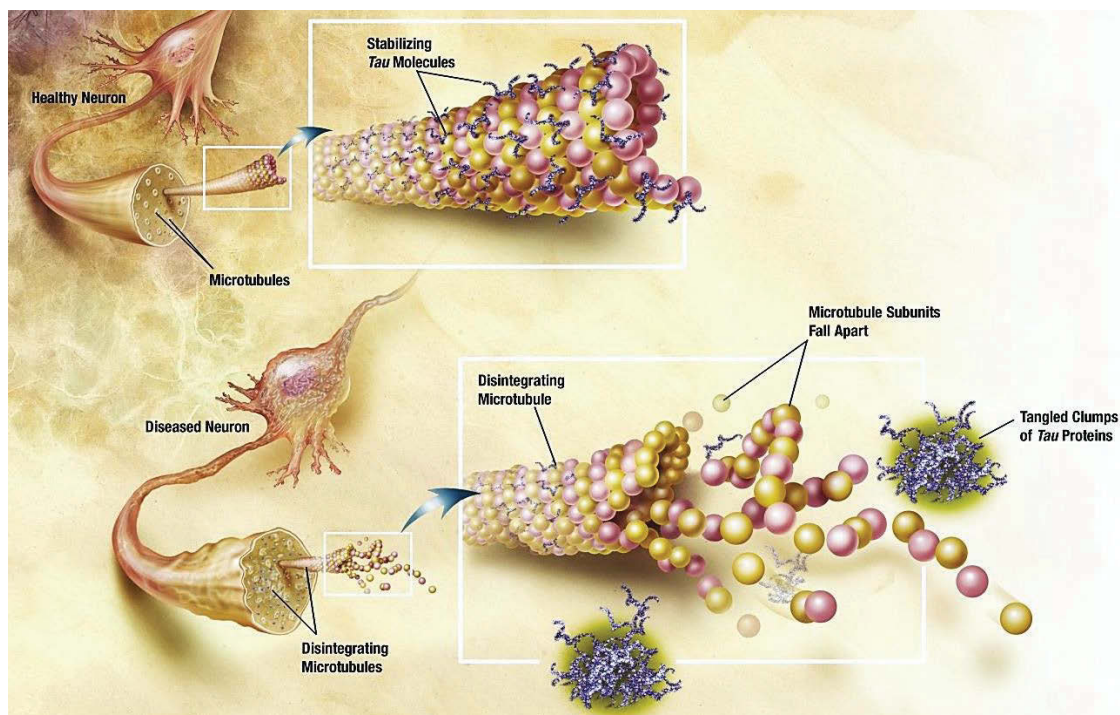


Figure 1.16 Pathology of Alzheimer's disease.^[64]

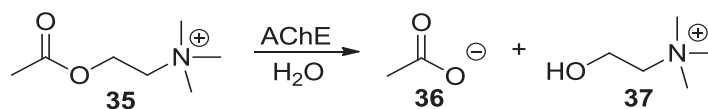
When brain cells are damaged from the build-up of plaques and tangles, neurones struggle to produce enough neurotransmitters required for normal cognitive function. For this reason, there is a correlation between the symptoms of the disease and the levels of neurotransmitter in the synapse. The regulation of this concentration is, therefore, a good target for AD drugs. One such mechanism for this regulation is the hydrolysis of the neurotransmitter acetylcholine.

1.5.1 AChE and Alzheimer's Disease

It is well established that symptoms of AD are related to low levels of the neurotransmitter acetylcholine (ACh) within the synaptic cleft^[65], mainly in the cerebral cortex and hippocampus, as determined by post-mortem analysis of the brains of AD sufferers.^[54] Within the brain, there are two main types of cholinergic or acetylcholine receptors (AChRs) on which ACh acts, both of which are affected by degeneration in AD. For both types of receptors, the nerve impulse is triggered by ACh binding to them after its release into the synaptic cleft. These impulses are terminated by the decomposition of ACh into the inactive components, choline and acetate, *via* rapid hydrolysis by the acetylcholinesterase (AChE) enzyme.^[66]

In the nervous system, AChE is a membrane-bound enzyme that is responsible for hydrolysis of ACh **35**,^[67] to give acetate **36** and choline **37** (Scheme 1.2). This natural process is summarised in Figure 1.17 and is required for the termination of transfer of signals between

neurons. Butyrylcholinesterase (BChE) is another enzyme that can hydrolyse ACh, however, BChE is a soluble protein found mainly in the liver and blood plasma.^[68] AChE is, therefore, the primary target for existing AD drugs. In people with AD and low levels of acetylcholine, it is possible to restore the levels of this neurotransmitter to a more natural level by inhibiting the AChE enzyme and hence relieving the symptoms of the disease.



Scheme 1.2 Hydrolysis of ACh by AChE.

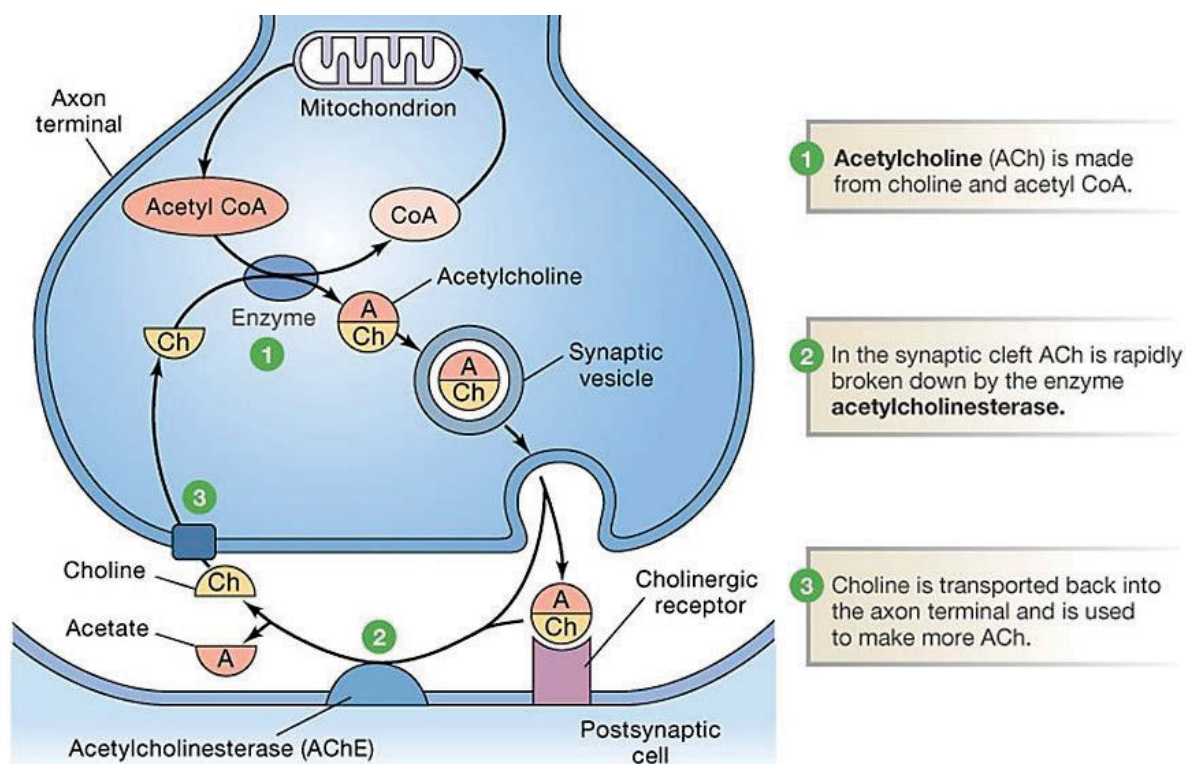


Figure 1.17 ACh and AChE in the synaptic cleft.^[69]

1.5.2 AChE Structure and Functionality

It is important to intimately understand the structure of a protein and its catalytic site when considering the design of inhibitors. There are many available X-ray structures of AChE, derived mainly from the following three organisms; native electric eel AChE (eeAChE), human AChE (hAChE) and *Torpedo California* (TcAChE). The amino acid sequence of each active site is well conserved across species. Two *Torpedo californica* AChE crystal structures that are commonly used in the literature are 1EVE (Donepezil complex, Figure 1.18) and 1DX6 (Galantamine complex). These X-ray structures are well-resolved and therefore will be discussed and used for molecular modelling.

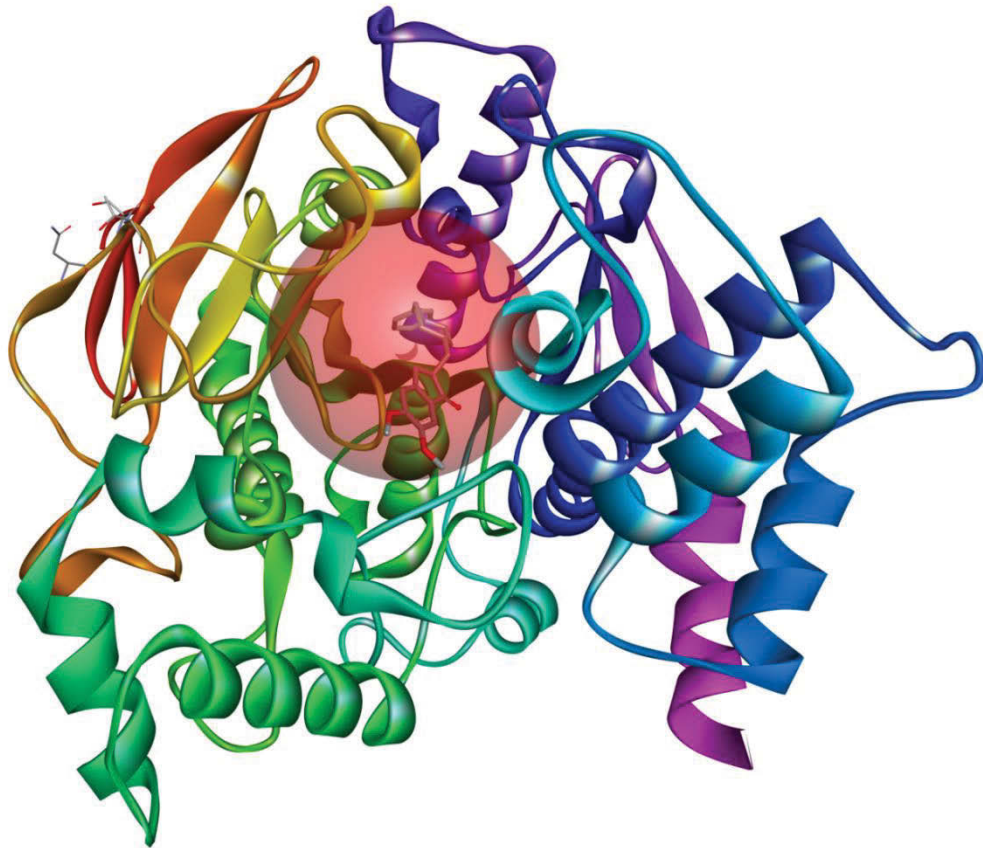


Figure 1.18 1EVE: TcAChE with Donepezil in the binding site (sphere highlighted in red), generated using Discovery Studio 4.5.

The dimensions of the AChE enzyme are approximately 45x60x65 Å. It contains an α/β protein monomer with 537 amino acids, which make up 12-stranded mixed β sheets surrounded by 14 α helices.^[70] The AChE active site is buried at the bottom of a 20 Å deep, narrow gorge, lined with conserved aromatic residues. The active site comprises four catalytic sub-sites: the esteric site (Ser200, His440 and Glu327), the oxyanion hole (Gly118, Gly119 and Ala201), the acyl pocket (Phe288 and Phe290) and the anionic sub-site (Trp84, Phe330 and Glu199). These sites are cooperatively responsible for the hydrolysis of acetylcholine (ACh) into acetate and choline (Figure 1.19).^[71]

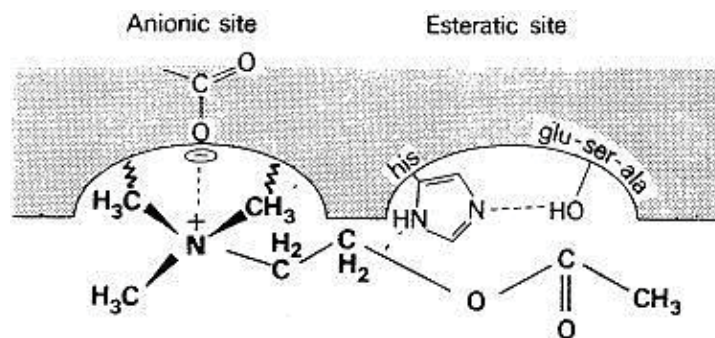


Figure 1.19 AChE active site interactions responsible for the hydrolysis of acetylcholine.^[71]

At the entrance of the active-site gorge is the peripheral active site (PAS). The PAS is made up of residues Tyr70, Asp72, Tyr121, Trp279 and Tyr334 (the yellow sphere in Figure 1.20), which are reported to attract the substrate to the gorge through cation- π and hydrophobic interactions. Non-catalytic functions of the PAS site include the mediation of heterologous protein association (during synaptogenesis it contributes to cell recognition, differentiation and adhesion)^[72] and nucleation of amyloid peptides.^[58] In addition to this, the PAS site is where amyloid- β fibrils that are associated with plaque deposition are formed. For this reason, the PAS site has become of high interest for developing dual action inhibitors that disrupt this interaction, with the aim of slowing the progression of the disease.

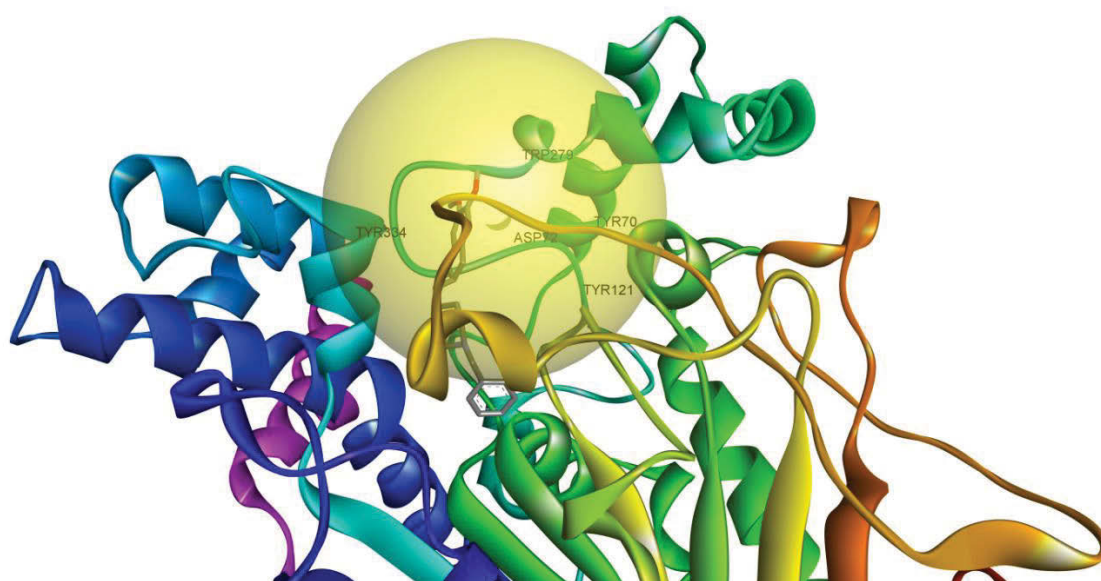


Figure 1.20 The PAS site of TcAChE, generated using Discovery Studio 4.5.

The PAS site opens up to a gorge that leads ACh down into the active site. The top of the gorge contains the residues Asp285 and Glu273. Around 12 Å away from the sub-site, the Asp72 residue is hydrogen-bonded to Tyr334 while Glu199 is found the bottom of the gorge.^[70] These residues guide ACh due to their interactions between the π electrons and ACh's quaternary ammonium.^[66] The gorge also has a sub-site that contains Trp84, to which ligands may also bind *via* the lipophilic and cation- π interactions.^[73] It has been proposed that the choline and acetate products do not leave the active site the same way that ACh enters but rather through an opening in the bottom of the cavity.^[74] Twenty water molecules occupy the gorge tunnel and it has been shown that they are required for hydrolysis of acetylcholine. Many of the amino acids that represent the active site components of protein file 1EVE are shown in Figure 1.21, as reported by Bajda *et al.*^[75]

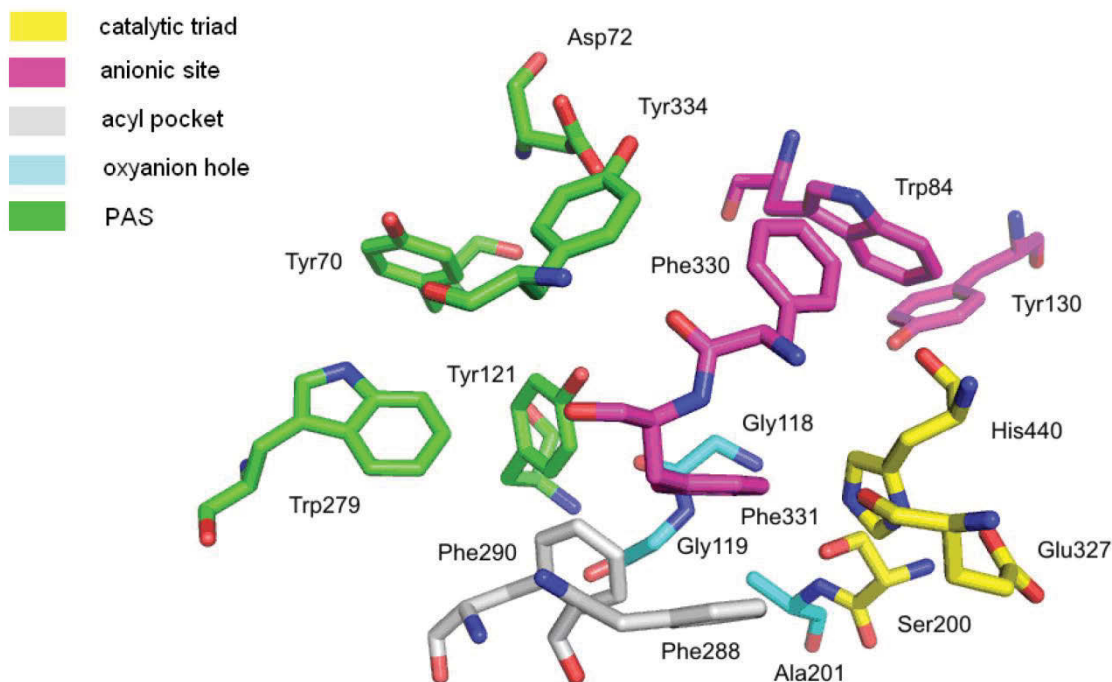


Figure 1.21 AChE active site residues coloured according to site type.^[75]

1.5.3 Treatment of Alzheimer's Disease

As previously stated, one method for relieving the symptoms of AD is the administration of AChE inhibitors. The inhibition of AChE in the synaptic cleft can reduce the amount of ACh being hydrolysed, allowing for the physiological concentration of ACh in the brain to be restored, hence, relieving the symptoms of AD.^[19] AChE inhibitors are molecules that often contain a positively charged nitrogen,^[14] capable of entering the active site of AChE and binding to the esteratic active site. This blocks ACh from entering and subsequently being broken down, prolonging its existence.^[76] The inhibitory process can be reversible or irreversible^[77] but, for the purpose of treating AD, reversible AChE inhibitors must be used because irreversible inhibitors result in the build-up of ACh and, as a result, neurone cell death.

The active site of AChE is a good target because of its high specific activity, although it will still hydrolyse many other esters. There are, however, several other modes of action that are possible for inhibitors, agonists and substrates, to bind to AChE. For instance, if ligands are too large to travel the complex gorge, they may still block the entrance by binding to the PAS. The binding of ligands to the PAS *via* hydrophobic interactions may block the passage of ACh or change the conformation of the active site allosterically and inhibit its function.^[78]

1.5.4 AChE Inhibitors

Many sources indicate that alkaloids are the strongest inhibitors of AChE.^{[14],[79]} Numerous natural products have been identified as having AChE inhibitory properties as listed

by Filho *et al.*^[80] For example, tacrine **38** was the first FDA-approved AChE inhibitor to be used for the treatment of AD in 1953.^[81] Since then many other compounds have also been used including donepezil **39**, rivastigmine **40**, huperzine A **41** and galantamine **3**.^[54] The last of these is the first Food and Drug Administration (FDA) approved natural product, extracted from *Galanthus caucasicus*.^[54]

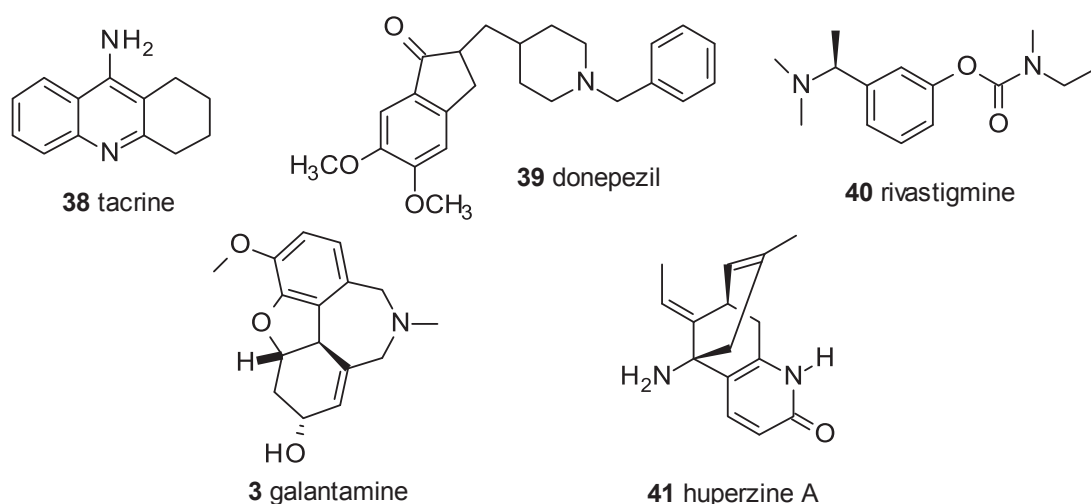
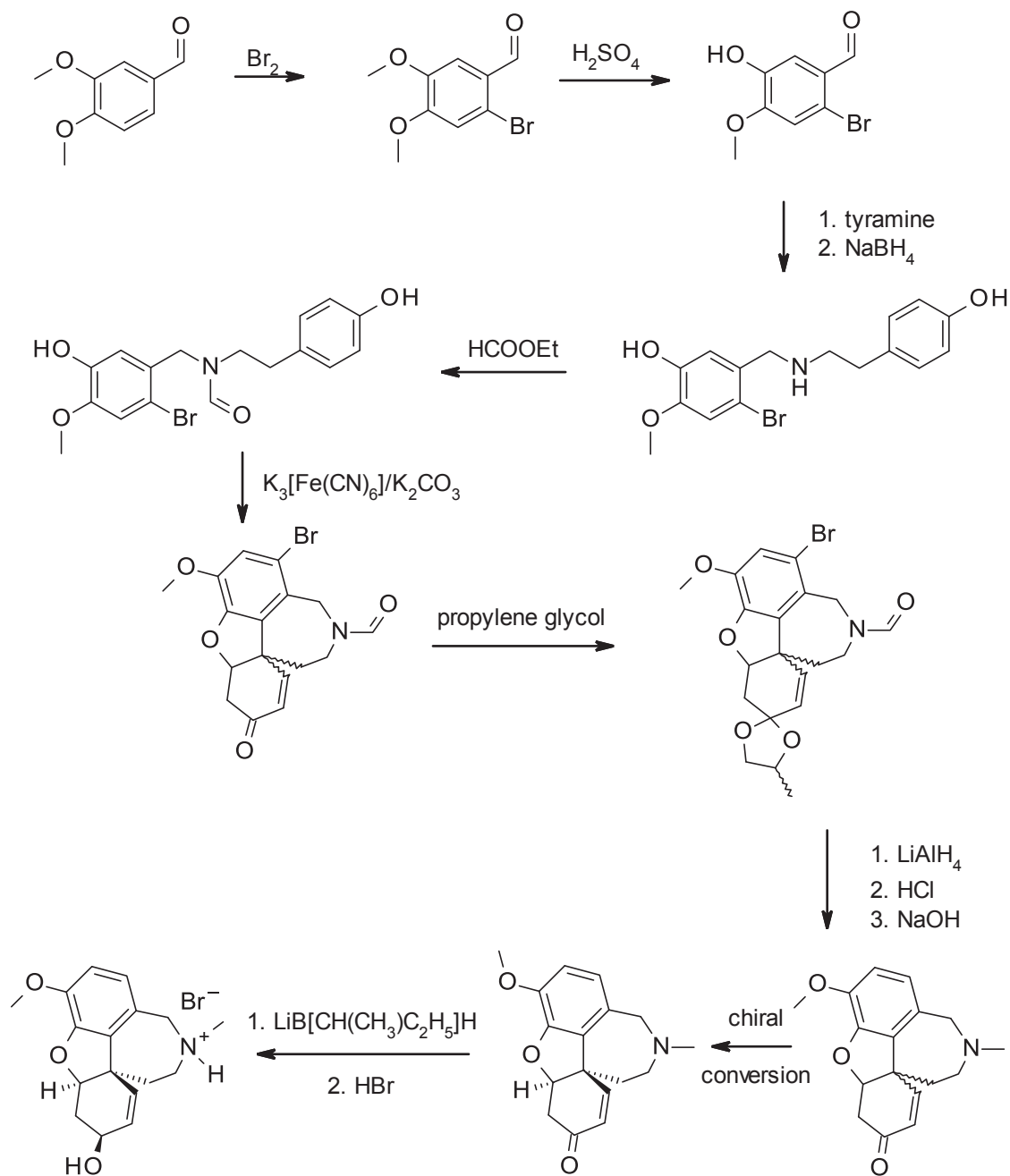


Figure 1.22 Alkaloid AChE inhibitors.

Galantamine and huperzine A are natural alkaloids and have emerged as potent AChE inhibitors. They are selective, long-lasting and show reversible receptor-binding, which produces beneficial cognitive effects in the patient.^{[82],[83]} All current inhibitors, however, exhibit undesirable side-effects, including headaches, dizziness, nausea, indigestion, vomiting, diarrhoea, weight loss and anorexia, muscle cramping, skin rashes and even insomnia.^[54] Some have also been shown to have poor bio-availability.^[84]

Galantamine and Huperzine A are approved as prescription drugs in the US and China, respectively, to treat the symptoms of mild-to-moderate AD. Despite the recent progress with Galantamine and Huperzine A, there is still an urgent need to discover AChE inhibitors that have effective and efficient brain penetration, extended action duration and reduced toxicity. Galantamine also remains a challenging and consequently expensive synthetic product, as outlined in Scheme 1.3, it can be seen that there are several complex steps involved which results in an overall final yield reported at 12.4%.^[85] Despite the increase in drug research for the treatment of AD, the number of therapeutic options on the market remains severely limited.



Scheme 1.3 Total Synthesis of Galantamine.

1.5.5 SAR of AChE Inhibitors

Numerous papers have listed the structural activity relationships (SARs) identified for alkaloids and other classes of existing AChE inhibitors. These should be considered in the design of new inhibitors and for developing a pharmacophore-like understanding of enzyme activity used to aid the development of alkaloid-like molecules used to target AChE.

Several structural features of alkaloids that are crucial for AChE inhibitory activities have been noted by Houghton *et al.*^[14] Apart from a positively charged nitrogen, other features

include the presence of carbamate **42** (interactions between the carbonyl group and the serine **43** –OH deactivates the enzyme) and the presence of an aromatic ring (to facilitate the molecules binding in the gorge).^[14] Structures containing tertiary amines, as opposed to a quaternary nitrogen, have difficulty crossing the blood-brain barrier due to their high degree of hydrophilicity.^[14] Steric hindrance can lower AChE inhibitory properties, whereas higher hydrophobicity increases it, as it allows further penetration into the active site.^[14]

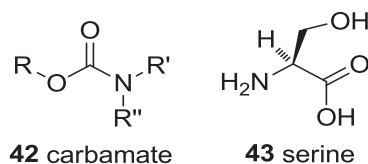


Figure 1.23 Structures of significant activity relationships.

Cationic ligands have been found to diffuse across the surface of the AChE enzyme towards the active site due to the interactions with the ring systems of aromatic amino acids in the enzyme's gorges.^[73] Rampa *et al.*^[86] found that for 11*H*-Indeno-[1,2-*b*]-quinolin-10-ylamine derivatives there is usually an increased inhibition activity with the introduction of substituents like fluorine or chlorine. They also proposed that atoms that are larger than hydrogen or fluorine impair inhibitor-enzyme interactions or the process of the inhibitor reaching the binding site. They also found strong electron-attracting groups such as NO₂ resulted in a drop in inhibition potency.

1.5.6 Other Applications of AChE Inhibitors

Work by Ung *et al.*^[87] on *Stemona* plants has shown that *Stemona* alkaloids (Figure 1.24) are strong inhibitors of AChE (at 1 ng/mL). The extracts of *Stemona* roots have been used in traditional medicine in South East Asia, China and Japan to treat the symptoms of bronchitis and tuberculosis due to their antitussive activities. They have also been identified as an effective internal antiparasitic in humans and animals. Similarly, Ung *et al.*^[87] successfully showed that stemofoline **44** and didehydrostemofoline **45** alkaloids are antifeedants on the larvae of *Plutella xylostella* (Diamondback moth).^{[88],[89]}

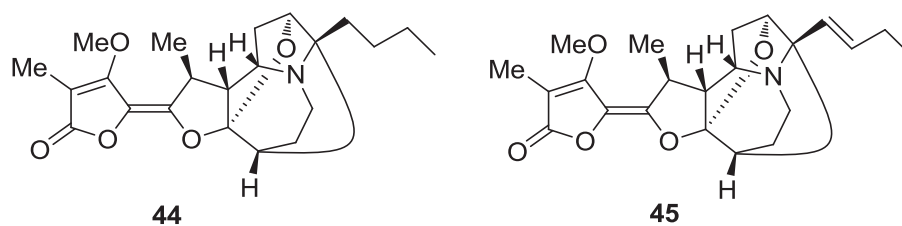


Figure 1.24 Stemofoline **44** and didehydrostemofoline **45** alkaloids.

AChE inhibitors can also be used as pharmaceutical drugs for the treatment of glaucoma and myasthenia gravis diseases.^{[70],[90]} Other uses for AChE inhibitors include

biological warfare agents^[14] via the use of irreversible AChE inhibitors and pesticides by overstimulating the cholinergic system in insects.^[91]

1.5.7 Other Treatments for Alzheimer's Disease

The synthesised alkaloid-like compounds **46** and **47** (Figure 1.25) are structurally similar to Memantine **48**, a compound already used as a drug for treating mild to severe AD. This highlights how these compounds have the potential for use in other mechanisms of treatment. Memantine works by binding to a type of ionotropic glutamate receptor, known as *N*-methyl-*D*-aspartate (NMDA) receptors.^[92] Glutamate is one of the most prominent neurotransmitters found in the brain and if the NMDA receptor is over-activated by excessive levels of glutamate, neurodegeneration can occur.^{[93],[94]} This results in diseases such as AD and hence deactivating NMDA with non-competitive binding of Memantine counteracts neurodegeneration.

Due to the similarity of the 3-azabicyclo[3.3.1]nonane core structure to that of Memantine, it is possible that alkaloid-like compounds with the core structure **5** could have dual modes of action and therefore be used to act as both an AChE inhibitor as well as a NMDA receptor antagonist.

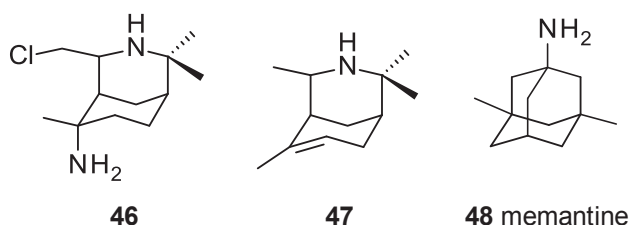


Figure 1.25 Memantine **48** and structurally similar alkaloid-like molecules.

Another mechanism is the use of histamine H₃ receptor antagonists because they cause the release of additional acetylcholine into the synapse. As previously stated, compounds could be designed to have a dual mode of action, whereby they interact with both receptors resulting in increased release of ACh (from H₃ receptor antagonistic effects) and prolonged biological half-life in the synapse (from AChE inhibition). This would result in strong cognition enhancement even when using an AChE inhibitor with reduced efficacy and, in turn, have fewer side effects. ACh concentration can also be increased by the use of cholinergic receptor ligands.^[86]

Despite these alternative methods showing potential for fewer side effects, there is still warrant in developing AChE inhibitors, in particular, those which bind to the peripheral active site. It was suggested in a recent study by Inestrova *et al.*^[95] that an inhibitor that binds to

the PAS site may, in fact, be able to slow the progression of AD. Although AChE inhibitors have been known to improve memory function and decrease cognitive decline with no change to the underlying pathology, PAS bound inhibitors show disruption in interactions between AChE and β -amyloid, believed to be the same site where AChE- β A interactions occur. This disruption may consequently decrease the aggregating effect of the enzyme on β -amyloid peptides and consequently slow the progression of the disease.^[96]

1.5.8 AChE Inhibitor Design by Molecular Modelling

Both the dual action scenarios mentioned above leave a great deal of possible exploration using molecular modelling. Pharmaceutical companies have already begun developing AChE inhibitors that also act as serotonin reuptake inhibitors to reduce the psychiatric symptoms often observed in patients with AD.^[97]

A recent study by Bembenek *et al.*^[98] used molecular modelling to design a dual action AChE and histamine H₃ inhibitor. The H₃ receptor antagonist, like AChE, is known to improve cholinergic neurotransmission in the cortex, whereas histamine H₃ inhibitors act primarily in the brain on the CNS, unlike AChE inhibitors. AChE inhibitors, especially non-selective inhibitors that act on butyrylcholinesterase as well, effect the whole body, resulting in mechanism-based side effects. It is believed that the combination of the AChE inhibition and histamine H₃ inhibition will lead to an increased potency of cholinergic neurotransmission and hence provide a safer more tolerable medication for patients.

1.6 Project Aims

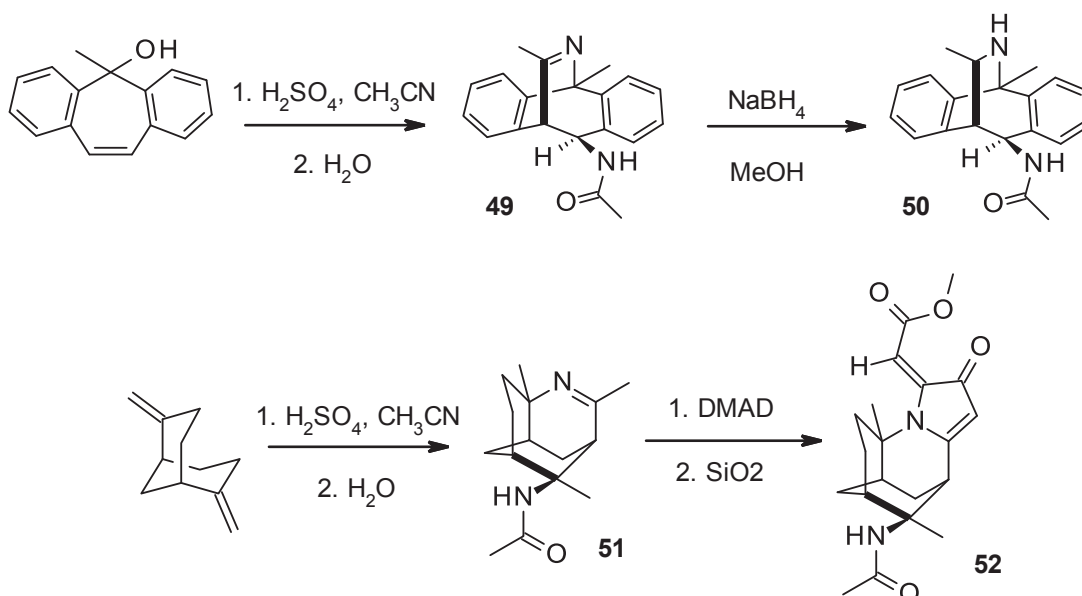
Over the past few decades the pharmaceutical industry has provided, on average, 15-25 New Chemical Entities (NCEs) per year (those are drugs not previously approved by the FDA). FDA approved drug are the NCEs that result from the development and selection from as many as 5000 compounds, each of which would cost the developing companies an average of \$359 million to develop over an average of 12 years.^[99]

Despite the significant investment in drug discovery, it is still difficult to produce quality 'hit' compounds. This study aims to accelerate this process by focussing on filling a gap in chemical and biological knowledge in this critical area and in doing so, contribute to the scientific community and provide justification for the continued investment aimed at improving the lives of thousands of people.

It aimed to achieve this by using the concept of 'target tractability' as an alternative to HTS. The probability of a new chemical entity to become a drug is rationally assessed based on

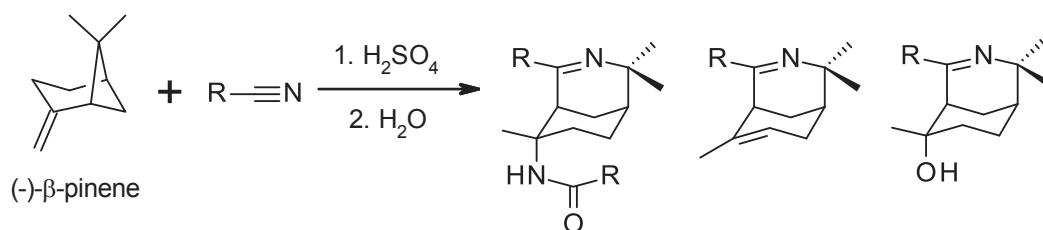
the knowledge of the previous success of the class of compounds regarding drug-likeness and knowledge of binding sites and protein structure. It has been stated that for tractable targets, focused screening is more appropriate than HTS for defining information about ligands and their target. This is, therefore, the approach of this project, specifically for AChE. An understanding of the structure of the biological targets and NMR structural screening of compounds has resulted in a significant acceleration of the early stages of drug discovery.^[2]

In Scheme 1.4, **50** is known to have AChE inhibitory properties and is a product of the imine **49**, formed by the bridged Ritter reaction.^[19] In-house data shows that **52** has anticancer properties (IC_{50} 7.1 μ M against MCF-7 and IC_{50} 38.9 μ M against MDA-MB-231) and is a compound derived from the imine **51**, which is a product of the Bridged Ritter reaction.^{[100],[101]}



Scheme 1.4 Useful alkaloid-like molecules formed *via* the bridged Ritter reaction.

Based on this knowledge, it was proposed that a library of alkaloid-like molecules containing the 3-aza-bicyclo[3.3.1]nonane architecture, synthesised *via* the bridged Ritter reaction and (-)- β -pinene (Scheme 1.5), would show biological activity. These scaffolds could then be derivatised to produce products that mimic their natural counterparts. New synthetic approaches for introducing structural variations and controlled derivatives of the core scaffold will be covered in Chapters 2 and 3.



Scheme 1.5 The bridged Ritter reaction between (-)-β-pinene and nitrile with functionality –R.

Once a library of alkaloid-like molecules is established they will be screened for their biological activities. The in-house anticancer screening will be performed *via* the MTS assay against the triple negative breast cancer cell line MDA-MD-231. In addition, external anticancer testing will provide information on target-selectivity through the screening of additional cancerous and healthy cell lines. The library's AChE inhibition properties will be screened using the TLC autobiographic method and Ellman method, to determine their potential as AChE inhibitors for treating AD. Also, broad-spectrum biological activities will be investigated through collaboration with Lilly's Open Innovation Drug Discovery program. This will be covered in Chapter 4.

Using the results obtained from the bio-assays, structure-activity relationship studies will evaluate the library's properties for any observed activity. This information, along with computer aided molecular modelling, will be used to assess the drug-like properties and the potential for further rational drug design and derivatisation to generate a second generation of compounds with improved potency towards the targets, as discussed in Chapters 5 and 6.

Broad screening can be used as the groundwork for investigating other uses reported for alkaloid-like molecules in the drug space. These include anti-bacterial properties, alimentary tract and metabolic control for gastrointestinal disorders, anti-malarial medication, pain control and anti-Parkinson's disease drugs.^{[20],[22]} The aims of the project can be summarised as follows:

1. To synthesise a library of alkaloid-like molecules from:
 - a. The bridged Ritter reaction (Chapter 2)
 - b. Derivatisation of bridged Ritter reaction products (Chapter 3)
2. To determine any cytotoxic properties of the synthesised library (Chapter 4)
3. To determine any AChE inhibition activity of the synthesised library (Chapter 5)
4. To identify any SAR for the synthesised library for:
 - a. MDA-MB-231 breast cancer cell line (Chapter 4)
 - b. AChE (Chapter 5)

5. To perform *in silico* evaluation of the synthesised library for drug-like properties and protein interactions (Chapter 7)
 - a. Calculation of molecular properties
 - b. Docking studies
6. To design and develop an improved library of compounds based on *in silico* and *in vitro* results (Chapter 3 and Chapter 7)
7. To evaluate the biological results from external broad screening by Lilly OIDD (Chapter 6)

CHAPTER 2: An Alkaloid-like 3-Azabicyclo[3.3.1]non-3-ene Library Obtained from the Bridged Ritter Reaction

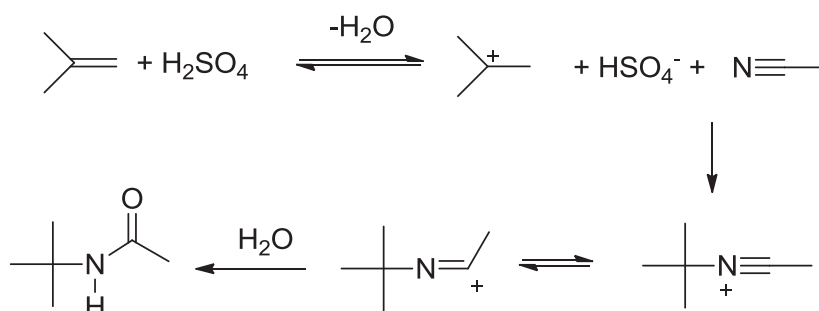
2.1 General Introduction

This chapter describes the synthesis of an alkaloid-like 3-azabicyclo[3.3.1]non-3-ene library using the bridged Ritter reaction of (-)- β -pinene with various nitriles. A discussion of the results follows an introduction to Ritter reactions.

2.2 Introduction to Ritter Reactions

2.2.1 Background

The Ritter reaction was first published by John Ritter and Paul Minieri in 1948.^[102] It is a nucleophilic addition reaction performed under strong acidic conditions that allows for a carbenium ion to be generated, which is then susceptible to nucleophilic attack by a nitrile. The nitrilium ion that forms then reacts with water to form an amide, typically as a 'one-pot' reaction, as shown in Scheme 2.1.^[103]



Scheme 2.1 General Ritter reaction.

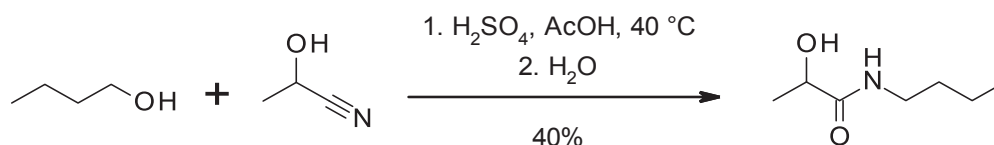
This reaction has been performed under various conditions and with numerous starting materials, affording a wide range of products. These reactions can be classified into two categories known as general Ritter reactions and intramolecular Ritter reactions. The latter is capable of cyclisation and so can yield a variety of heterocyclic compounds, such as alkaloid-like molecules or their precursors.

2.2.2 Ritter Reaction Conditions and Mechanism

2.2.2.1 Reaction Conditions

Ritter reactions involve the addition of nitriles to carbenium ions.^[102] The nitriles can contain many functional groups, provided that they are stable in acid,^[103] while the source of the carbenium ion can be any compound that will produce a carbenium ion in strong acidic conditions.^[104] The most commonly used sources for carbenium ions are alkenes and alcohols^[104] but saturated hydrocarbons may be used if a compatible hydride acceptor is

present.^[105] In general, the most common reaction temperature is between 20-50 °C, running for 1-24 hours.^[104] An example reaction can be seen in Scheme 2.2.



Scheme 2.2 Example Ritter reaction between butanol and 2-hydroxypropanenitrile.^[103]

The strong acidic conditions, such as those generated by concentrated H₂SO₄, are most favourable and often result in the best yields.^[106] This is due to the way the hydrogensulfate counter ion, pairing with the carbenium ion, can associate with the nitrile group during the reaction's transition state^[107] as seen in Figure 2.1. Any water supplied from H₂SO₄ (concentrations of 85-90%) can suppress side reactions by allowing rapid hydrolysis of the carbenium ion to form the amide. The best solvents to use are polar solvents because they increase the nucleophilicity of the nitrile, while non-polar solvents produce poor yields.^[108] It is important to note that Bishop^[103] claims that acetic acid is the best solvent despite resulting in the possibility of significant side reactions that form acetates.^[109] Benson *et al.*,^[110] however, reported some cases of the reaction not proceeding due to dilution with large quantities of solvent.

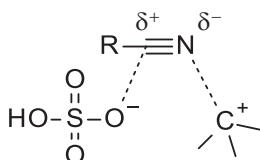


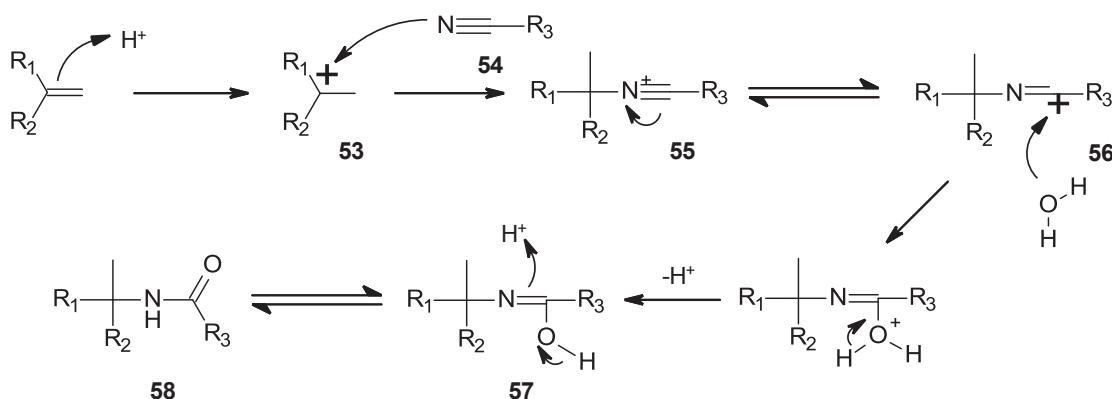
Figure 2.1 Transition state: hydrogen sulfate counter ion pairing with the carbenium ion.

The reaction's major product is that resulting from the most stable carbenium ion formed if rearrangements are possible.^[104] While lowering the strength of the acidic conditions and temperature may lead to greater regioselectivity, the disadvantage is the reduction of the yield.^[111] Different products can be generated depending on whether the reaction is controlled kinetically or thermodynamically,^[104] as well as by the order of addition of reagents.^[112] Sasaki *et al.*^[113] have also noted that the use of aluminium chloride as a catalyst increases the amount of the fastest forming kinetic product, as it has the smallest activation energy to the transition state.

2.2.2.2 Reaction Mechanisms

For alkenes, as seen in Scheme 2.3, the carbenium **53** ion is generated by the acid *via* protonation of the double bond, forming a carbocation centre that is susceptible to nucleophilic attack. The lone pair of electrons on the nitrile group **54** undergoes nucleophilic

addition with **53** to form a nitrilium ion **55** and the resonance stabilised structure derived from **56**. The lone pair of the nitrile is still available to take part, as it is only about 50% protonated in H_2SO_4 of 89-100% concentration.^[114] Water then attacks the positive charge on the nitrile carbon (in **56**) and after deprotonation forms **57**, which when basified condenses to form the carbonyl group of the amide **58**. The reaction between the carbenium and nitrile is first order with respect to both reagents.^[103] If water is not added to the reaction, the nitrilium ion can form an imidate with the HSO_4^- counter ion.^[103]



Scheme 2.3 Ritter reaction mechanism.

2.2.2.3 Unconventional Ritter Reaction Pathways

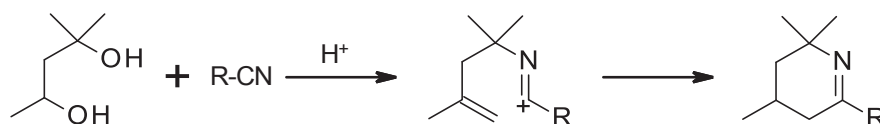
The reaction conditions for traditional Ritter reactions are relatively harsh due to the strong acid used. Many alternative conditions have been developed in an attempt to make the reaction more environmentally-friendly because this is important when considering performing the reaction on an industrial-size scale. The most common alteration is the way the carbenium ion is generated.^[103] Some alternative methods published include oxidation by free radicals,^[115] photochemical reactions,^[116] electrochemistry^[117] and metal-assisted catalysis.^{[118],[119]} Organometallic complexes have also been reported to be an effective way of stabilising the carbenium ion and hence controlling its reactivity.^[120]

These alternatives give a wide range of overall yields, from 90% to as low as 35%,^[103] however the acidic conditions remains the most effective procedure with respect to yield and reproducibility. The development of catalytic conditions using protic (Brønsted) acid or Lewis acid reagents, in quantities stoichiometrically to the nitrile used, is also an effective method.^[121]

2.2.3 Bridged Ritter Reactions

As previously mentioned, Ritter reactions are capable of producing heterocyclic systems^[102] through the intramolecular cyclisation of a nucleophilic group existing within a 6 or 7 membered acyclic nitrilium ion or *via* the addition of a nucleophile to a cyclic nitrilium ion

which will then cyclise.^[122] This allows two reactive groups to be within close enough proximity to undergo intramolecular addition.^[123] This type of transannular reaction is limited to forming a secondary ring comprising 5 or 6 members^[122] and contains a cyclic imine (C-N=C), as seen in Scheme 2.4.

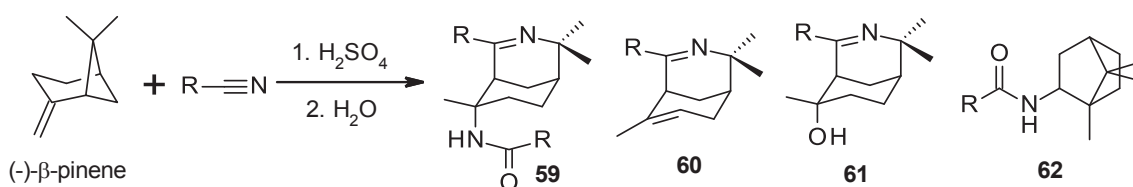


Scheme 2.4 An example intramolecular cyclisation Ritter reaction.

The imine nitrogen is of great biological significance as it is a functional group that can be derivatised into functional groups capable of biological interactions. It was determined in 1978 by Kaboré *et al.*^[124] that intramolecular cyclisation *via* the Ritter reaction could also result in bridged products on the least hindered face of the reactant ring system, to provide stereospecific compounds.

The imine containing scaffolds obtained from the bridged Ritter reaction are versatile in reactivity, allowing architecturally complex structures such as alkaloid-like molecules to be achieved. The similarity between synthesised alkaloid-like molecules and natural bioactive alkaloids deems them as good candidates for screening against properties such as AChE inhibitory activity^{[125],[14]} for the treatment of Alzheimer's disease as well as proteins associated with anticancer properties.

Our research group recently reported the synthesis of optically active **3-aza-bicyclic [3.3.1]non-2-ene** cyclic imines *via* the bridged-Ritter reaction.^[126] These cyclic imines can be easily obtained in one single step from (-)- β -pinene and various nitriles, as shown in Scheme 2.5. This synthetic pathway is of significant interest as it provides optically pure products with three stereocentres in a 'one-pot' reaction.



Scheme 2.5 General scheme for the bridged Ritter reaction between (-)- β -pinene and various nitriles under the standard reaction conditions.

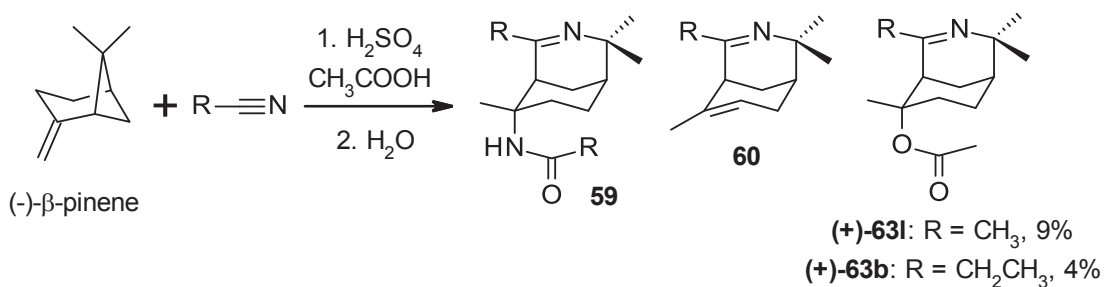
Herein, the detailed stereospecific synthesis of chiral 3-azabicyclo[3.3.1]non-3-enes *via* the bridged-Ritter reaction conditions, starting from (-)- β -pinene with various nitriles, is

described. The selectivity outcome of the products under different reaction conditions is also explored.

2.3 Synthesis of Alkaloid-like Molecules with the 3-azabicyclo[3.3.1]non-3-ene Core Structure

The following describes the two main sets of reaction conditions that were successfully employed for the preparation of optically active alkaloid-like molecules containing the 3-azabicyclo[3.3.1]non-3-ene core structure, from (-)- β -pinene with various nitriles, *via* a one-step bridged Ritter reaction. The first set of conditions is herein referred to as the 'standard' reaction conditions which used concentrated sulfuric acid to generate the carbocation and benzene as the reaction solvent. As shown in Scheme 2.5, these conditions form imino-amides **59**, imino-alkenes **60**, imino-alcohols **61** and *N*-isobornylamides **62**. The *N*-isobornylamide products form *via* the addition of the nitrile to the isobornyl carbocation generated by (-)- β -pinene rearrangement. These compounds were disregarded as 'of interest' to this project for several reasons, including that they are not novel, our previous work showed they had no AChE inhibition activity, and the core norbornane motif has been reported to show specific cardiac toxicity,^[127] deeming it to be unsuitable for pharmaceutical investigation within the scope of this project. The effect of reaction time was also investigated using the standard conditions with acetonitrile.

The second set of reaction conditions, herein referred to as the 'polar' reaction conditions, were developed in an attempt to optimise the reaction. Christol^[108] stated that the use of polar solvents increased yields by increasing the nucleophilicity of the nitrile. There are several alternative catalysts for the generation of carbocations reported,^[128] however this thesis focused only on the use of concentrated sulfuric acid and the use of acetic acid as a polar solvent in replacement of benzene used in the standard conditions, as listed in the experimental section. These polar conditions were used with acetonitrile and propionitrile and resulted in the formation of additional acetate products **(+)-63a** and **(+)-63b**, as seen in Scheme 2.6, with 9 and 4% yield respectively. They did not, however, result in an increased yield. Formation of the acetate products resulted from the nucleophilic addition of the acetate ion to the carbocation generated at C-6 as per suggested mechanism shown in Scheme 2.24.

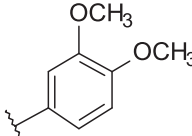
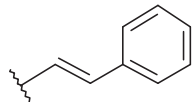
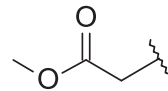
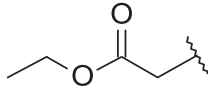
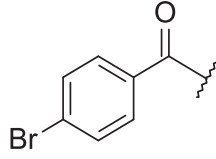
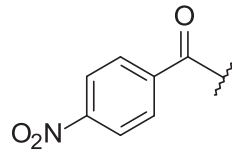


Scheme 2.6 General scheme for the bridged Ritter reaction between (-)- β -pinene and various nitriles under the mild reaction conditions.

2.3.1 Preparation of 6-*N*-amides, 6-alkene and 6-alcohols with 3-azabicyclo[3.3.1]non-3-ene Core Structure

The bridged Ritter reaction was successfully attempted with each of the nitriles listed in Table 2.1. This table also lists the yields of the obtained imino-alkene, -amide or -alcohol products. The assigned numbering corresponds to the type of product (either -amide, -alkene or -alcohol at the scaffolds C-6 location) and is associated with the letter corresponding to the nitrile entries from Table 2.1. These are represented again in Figure 2.2 for ease of interpretation. This table includes the products obtained previously from the reaction with acetonitrile, benzonitrile and chloroacetonitrile, as these products are screened for their biological properties which are reported for the first time in Chapters 4, 5 and 6. This summary highlights the significant difference in yields obtained due to the nitrile, as explained in the following sections.

Table 2.1 List of products obtained from the bridged Ritter reaction between (-)- β -pinene and the various nitriles used.

Entry	Nitrile	-R	Product/s (% Yield)
a	Trimethylsilyl cyanide	-H	(+)-60a (57)
b	Propionitrile	-CH ₂ CH ₃	(+)-59b (25), (-)-60b (14), (+)-63b (4)
c	Valeronitrile	-CH ₂ CH ₂ CH ₂ CH ₃	(+)-59c (12), (+)-60c (12)
d	Succinonitrile	-CH ₂ CH ₂ CN	(-)-60d (7)
e	3,4-Dimethoxybenzonitrile		(+)-60e (42)
f	Cinnamonitrile		(-)-60f (53)
g	Methyl cyanoacetate		(-)-60g (2)
h	Ethyl cyanoacetate		(-)-60h (7), (-)-66h (3)
i	4-Bromophenylacetonitrile		(-)-65i (14) ^b
j	4-Nitrophenylacetonitrile		(-)-65j (12) ^b
k	Butyronitrile	-CH ₂ CH ₂ CH ₃	(+)-59k (10), (-)-60k (6)
l	Acetonitrile	-CH ₃	(+)-59l (64)*, (+)-60l (23)*, (+)-63l (9)
m	Chloroacetonitrile	-CH ₂ Cl	(+)-59m (31)*, (+)-60m (23)*
n	Benzonitrile	-Ph	(+)-59n (42)*, (+)-60m (24)*

* Values from work published prior to PhD project.^[126]

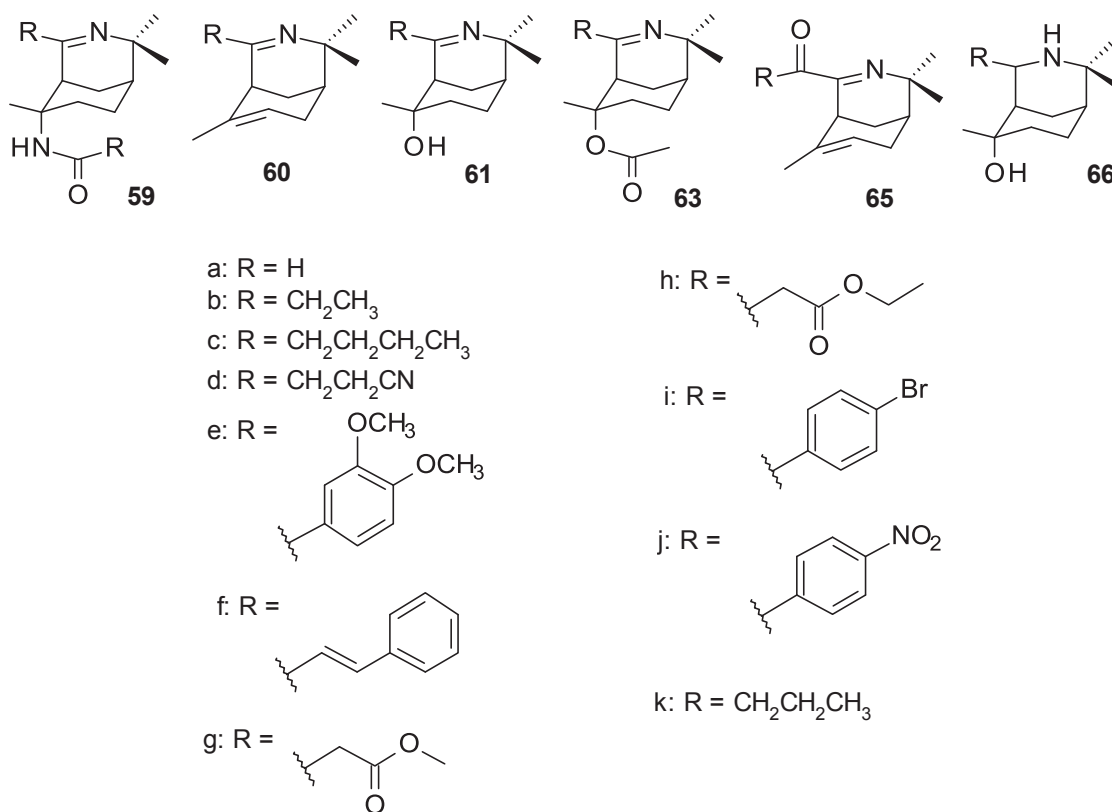


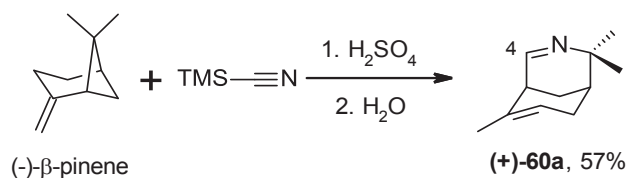
Figure 2.2 Product core numbering and nitrile letter assignment.

2.3.2 Outcomes of the Bridged Ritter Reactions with (-)- β -pinene

2.3.2.1 Trimethylsilyl Cyanide

Trimethylsilyl cyanide was used as a safer alternative to the highly toxic gas hydrogen cyanide, to achieve functionality where $-R = H$. Under the bridged Ritter reaction conditions employed, trimethylsilyl cyanide generates HCN *in situ*, contained within the reaction flask, sealed and set up with a gas trap containing NaOH solution (4 M) to neutralise any escaping HCN. The entire reaction was carried out within a sealed system and the same was done for the reaction work up. Interestingly, this reaction formed almost exclusively the alkene product **(+)-60a**, in a reasonable yield of 57% as a pale yellow liquid with a plant-like odour, as shown in Scheme 2.7. The C-4 hydrogen was assigned as a multiplet at δ 5.63 ppm in the ¹H NMR spectrum, while the ¹³C resonance for C-4 was assigned at δ 125.88 ppm, corresponding to the nature of the imine functionality. Other key characteristic peaks include the bridgehead hydrogen at C-5, assigned as a singlet at 2.28 ppm and the alkene CH proton singlet at 3.67 ppm, confirming the formation of the bridged product. The specific rotation was found to be $[\alpha]_D^{21} + 3.99$ (*c* 1.00, CHCl₃). The HRMS showed the $[M+H]^+$ exact mass to be 164.1436, corresponding to the molecular formula C₁₁H₁₇N.

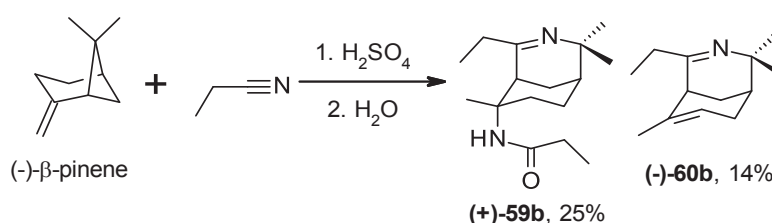
Although none of the amide product **59a** was isolated, it appears trace amounts may have formed, as the expected mass was detected in the GC-MS analysis of the crude product with m/z 208 at 17.606 minutes.



Scheme 2.7 The bridged Ritter reaction between (-)-β-pinene and trimethylsilyl cyanide.

2.3.2.2 Propionitrile

The bridged Ritter reaction with propionitrile provided a continuation to the alkyl series of -R substituents, as an extension to the previously reported reaction with acetonitrile. The yields of the bridged Ritter products were 25% for the imino-amide **(+)-59b** and 14% for the imino-alkene **(-)-60b** (Scheme 2.8). The imino-alkene was challenging to purify, because the imino-amide tended to co-elute on column chromatography, despite the difference in retention factor at R_f 0.8 for the alkene and 0.64 for the amide on alumina with EtOAc. The alkene was successfully isolated on preparative TLC.



Scheme 2.8 The bridged Ritter reaction between (-)-β-pinene and propionitrile.

For the imino-amide **(+)-59b** the ethyl CH_3 groups were both assigned as triplets with coupling constants of 7.5 Hz in the 1H NMR spectrum, with the C-6 propanamide CH_3 occurring at δ 1.16 ppm and the C-4 imino CH_3 occurring at 1.09 ppm. The corresponding CH_2 groups were seen at δ 2.21 ppm as a ddd ($J = 11.5, 7.5, 2.0$ Hz) for the propanamide and 2.31 and 2.27 ppm, both dt ($J = 7.5, 6.0$ Hz) for the two inequivalent CH_2 hydrogens adjacent to the imine. The specific rotation was found to be $[\alpha]_D^{18} + 125.95$ (c 0.95, $CHCl_3$) and the $[M+H]^+$ exact mass was found to be 265.2271, corresponding to the molecular formula $C_{16}H_{28}N_2O$. Single crystals of **(+)-59b** were also obtained from recrystallization in DCM/hexane, of which a suitable crystal was analysed by X-ray diffraction to give the unambiguous structure shown as an ORTEP diagram in Figure 2.3.

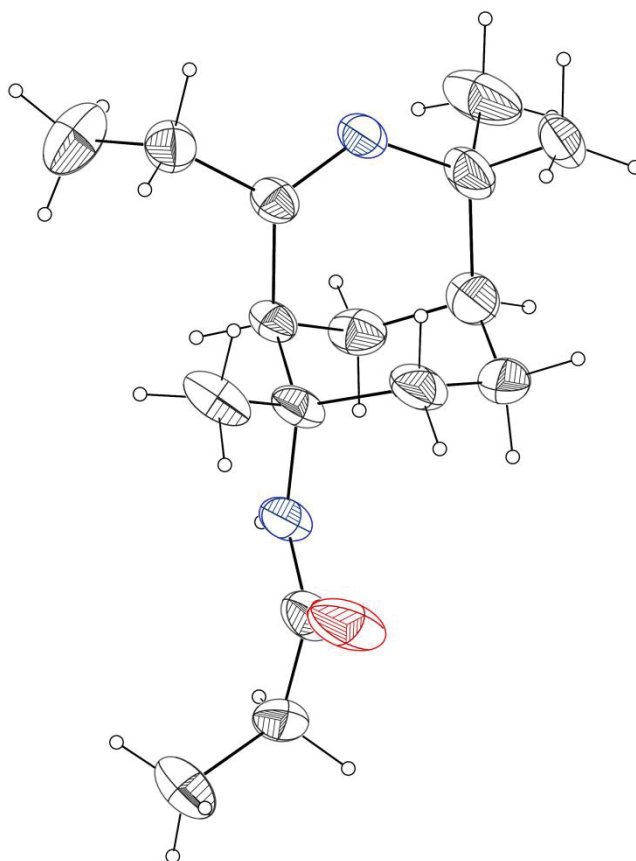
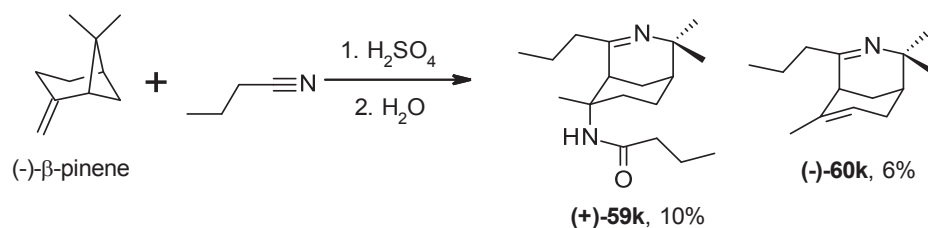


Figure 2.3 ORTEP diagram for compound **(+)-59b**.

For the imino-alkene **(-)-60b** the ^1H NMR spectrum showed the ethyl CH_3 group at C-4 as a triplet ($J = 7.5$ Hz) at δ 1.11 ppm, split by the adjacent CH_2 assigned as a quartet ($J = 7.5$ Hz) at 2.27 ppm. The bridgehead proton occurs as a broad singlet at 2.60 ppm and the C-7 CH as a singlet at 5.34 ppm. The specific rotation was found to be $[\alpha]_{\text{D}}^{23} - 22.56$ (c 1.00, CHCl_3) and the $[\text{M}+\text{H}]^+$ exact mass was 192.1751, corresponding to the molecular formula $\text{C}_{13}\text{H}_{21}\text{N}$.

2.3.2.3 Butyronitrile

The bridged Ritter reaction with butyronitrile successfully gave the imino-amide **(+)-59k** as a thick yellow oil and imino-alkene **(-)-60k** as a pale yellow liquid, in considerably lower yields than both the shorter alkyl chain nitriles and the longer valeritrile, with 10 and 6%, respectively (Scheme 2.9). The low yield may be attributed to the large amount of butanamide that was formed as a side product of the reaction. This was removed by recrystallization before the bridged Ritter products were isolated by column chromatography. Sufficient quantities of both products were isolated for characterisation and for submitting for broad screening. The method was not optimised to achieve a higher yield, although, in future work, attempting the reaction under dry conditions may reduce the formation of the butanamide.

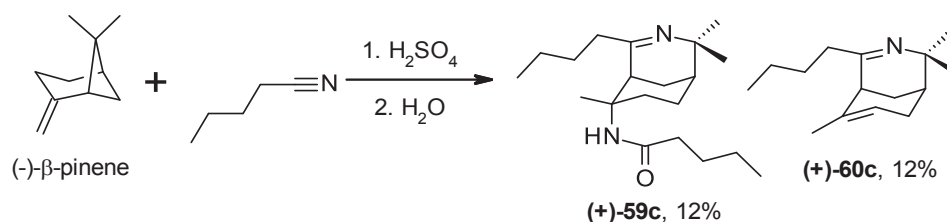


Scheme 2.9 The bridged Ritter reaction between (-)-β-pinene and butyronitrile.

For (+)-59k, the ^1H NMR NH resonance was assigned as a singlet at δ 5.44 ppm, with the C-5 bridge-head singlet at 3.42 ppm. The specific rotation was found to be $[\alpha]_{\text{D}}^{21} + 33.70$ (c 1.00, CHCl_3) and the $[\text{M}+\text{H}]^+$ exact mass was 293.2593, corresponding to the molecular formula $\text{C}_{18}\text{H}_{32}\text{N}_2\text{O}$. For (-)-60k, the ^1H NMR resonance for the C-7 alkene was assigned as a septet ($J = 1.5$ Hz) at δ 5.35 ppm, while the C-5 bridgehead proton is assigned as a singlet at 2.58 ppm. The specific rotation was found to be $[\alpha]_{\text{D}}^{21} - 2.38$ (c 1.00, CHCl_3) and the $[\text{M}+\text{H}]^+$ exact mass was 206.1908, corresponding to the molecular formula $\text{C}_{14}\text{H}_{23}\text{N}$.

2.3.2.4 Valeronitrile

The bridged Ritter reaction with valeronitrile successfully gave the imino-amide (+)-59c and imino-alkene (+)-60c, both with yields of 12% (Scheme 2.10). Both of the products were yellow oils and were relatively easy to purify by column chromatography. For the imino-amide (+)-59c, the usual ^1H resonances such as the C-5 bridgehead proton and the position 6 amide proton, were assigned as broad singlets at δ 3.27 and 5.31 ppm respectively, confirming the formation of the bridged structure and addition of the second nitrile to afford the amide. The large number of $-\text{CH}_2$ groups in the two alkyl chains resulted in a great deal of overlap on the ^1H spectrum due to the similarity of their chemical environments. ^{13}C DEPT and HSQC experiments were used to confirm that the correct number of $-\text{CH}_2$ groups were present and to identify the region they appear in the ^1H spectrum. The terminal $-\text{CH}_3$ groups at both C-4 and C-6 were seen as triplets ($J = 7.5$ Hz) at 0.94 and 0.90 ppm respectively. The specific rotation was found to be $[\alpha]_{\text{D}}^{22} + 81.82$ (c 1.35, CHCl_3) and the $[\text{M}+\text{H}]^+$ exact mass was 321.2884, corresponding to the molecular formula $\text{C}_{20}\text{H}_{36}\text{N}_2\text{O}$.

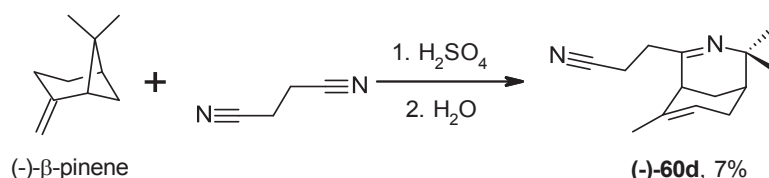


Scheme 2.10 The bridged Ritter reaction between (-)-β-pinene and valeronitrile.

The imino-alkene **(+)-60c** was characterised in the same way but was easier to interpret due to the relatively more simple structure involving one less alkyl chain. The bridgehead proton was identified in the ^1H spectrum as a broad singlet at δ 2.59 ppm and the alkene proton as a singlet at 5.34 ppm. The C-4 terminal $-\text{CH}_3$ was assigned as a triplet ($J = 7.0$ Hz) at 0.93 ppm. The specific rotation was found to be $[\alpha]_{\text{D}}^{21} + 9.22$ (c 1.00, CHCl_3) and the $[\text{M}+\text{H}]^+$ exact mass was 220.2048, corresponding to the molecular formula $\text{C}_{15}\text{H}_{25}\text{N}$.

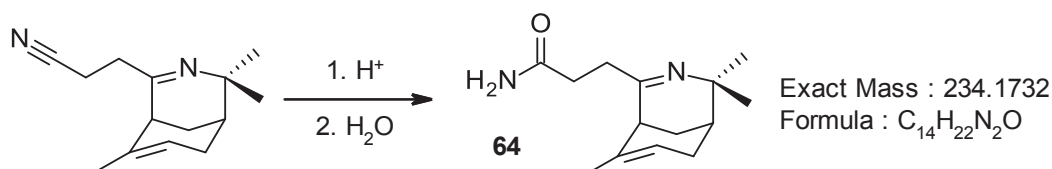
2.3.2.5 Succinonitrile

The bridged Ritter reaction with succinonitrile produced a couple of interesting results. Firstly, and most noticeably, it was another relatively small nitrile to form almost exclusively the imino-alkene product **(-)-60d** with 7% yield (Scheme 2.11). Secondly, the second nitrile in the chain remained unreacted, despite most nitriles undergoing hydrolysis to the corresponding amide during the workup stages of the reaction.



Scheme 2.11 The bridged Ritter reaction between (-)- β -pinene and succinonitrile.

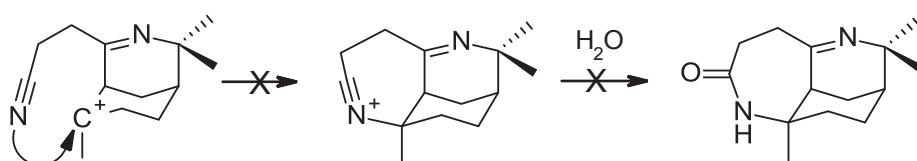
There was a trace amount of the mass expected for the product formed if the nitrile retained after the bridged reaction was converted to an amide **64**, as shown in Scheme 2.12, on the GC-MS, with m/z 234 detected at 7.073 minutes, corresponding to $\text{C}_{14}\text{H}_{22}\text{N}_2\text{O}^+$, however, none of this could be isolated for full characterization. This product may be useful for generating other derivatives and thus is as worthy of exploring in future work continued from this project.



Scheme 2.12 Hydrolysis of (-)-**60d** nitrile to form the amide derivative.

Succinonitrile was also of specific interest due to its hypothesised potential to form a third ring system using the terminal nitrile clipping across to the carbocation remaining at C-6 in an intramolecular fashion, after the formation of the bridged ring, as shown in the proposed mechanism in Scheme 2.13. This product's mass was not detected in the crude product mixture as analysed by GC-MS, so it is unlikely that this type of reaction is possible. This may

be attributed to the way that the nitrile is projected away from the carbocation by the flexibility of the CH₂ groups adjacent to the C-4 imine and hence the lone pair on the nitrogen is never in close enough proximity to form a bond with the C-6 carbocation. It is most likely, however, that the carbocation quickly collapses to irreversibly form the alkene, hindering any further reactivity and making it more likely that the amide **64** will form preferentially to a tricyclic product. If this reaction was possible, it would have been a novel way to introduce a third ring system and generate products that more closely resemble the structure of the *Aristotelia* alkaloids, as mentioned in Section 1.3.1.



Scheme 2.13 Proposed mechanism for the formation of tri-cyclic alkaloid-like products from the intramolecular cyclisation of nitrile and carbocation.

Finally, another interesting outcome of this reaction was the vast range of colours produced during the purification of the crude product. Figure 2.4 displays the colours of the fractions collected that were run off a silica column using 1:3 acetone/*n*-hexane for fractions 1-15 and 1:9 ethanol/DCM thereafter. The purely isolated imino-alkene product **(-)-60d** was collected in fraction four as a deep red coloured oil.



Figure 2.4 Colours obtained from the purification of the crude product of the bridged Ritter reaction with succinonitrile.

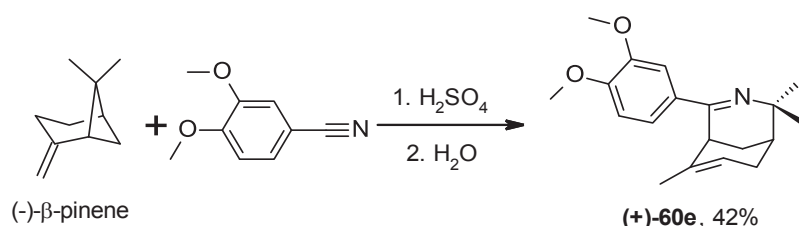
For the imino-alkene **(-)-60d**, the presence of the quaternary nitrile carbon was assigned in the ¹³C NMR spectrum at δ 120.66 ppm. The two C-4 CH₂ groups adjacent to the imine were assigned in the ¹H NMR spectrum as multiplets at δ 2.72-2.65 and 2.64-2.55 ppm, while the broad singlets resulting from the C-5 bridgehead and C-7 alkene protons were

assigned at δ 2.44 and 5.36 ppm respectively. The specific rotation was found to be $[\alpha]_D^{20} - 45.28$ (c 1.00, CHCl_3) and the $[\text{M}+\text{H}]^+$ exact mass was 217.1705, corresponding to the molecular formula $\text{C}_{14}\text{H}_{20}\text{N}_2$.

A similar attempt was made with phthathanonitrile to test if the rigid planar structure of the aromatic ring could provide fewer degrees of bond rotation, hence increasing the proximity of the second nitrile to the C-6 carbocation. These attempts were unsuccessful and returned a complex mixture that could not be purified or characterised, yet future work should investigate the use of longer or shorter dinitriles for this purpose.

2.3.2.6 3,4-Dimethoxybenzonitrile

The bridged Ritter reaction with 3,4-dimethoxybenzonitrile gave a moderate yield of the imino-alkene **(+)-60e** at 42% (Scheme 2.14). This alkene had a thick waxy consistency of pale yellow colour. It is believed that the amide was not formed due to the relatively large size of the nitrile hindering the second addition to the C-6 carbocation. The ^1H NMR spectrum of **(+)-60e** showed the Ar-4 α f aromatic proton at δ 7.24 ppm as a doublet of doublets ($J = 2.0, 8.5$ Hz), Ar-4 α b at 6.88 ppm as a doublet ($J = 2.0$ Hz) and Ar-4 α e at 6.87 ppm as a doublet ($J = 2.0$ Hz). The methoxy peaks were assigned as broad singlets at δ 3.96 and 3.94 ppm in the ^1H spectrum and at 56.42 and 56.41 ppm in the ^{13}C spectrum. The functionality of substituents provided by the nitrile, in conjunction with the characteristic peaks of the core structure, such as the ^1H spectrum peaks for the C-7 alkene showing as a broad singlet at δ 7.51 and the C-5 bridgehead at 4.40 ppm, confirms the successful formation of the bridged product. The specific rotation was found to be $[\alpha]_D^{21} + 66.64$ (c 1.00, CHCl_3) and the $[\text{M}+\text{H}]^+$ exact mass was 300.1963, corresponding to the molecular formula $\text{C}_{19}\text{H}_{25}\text{NO}_2$.

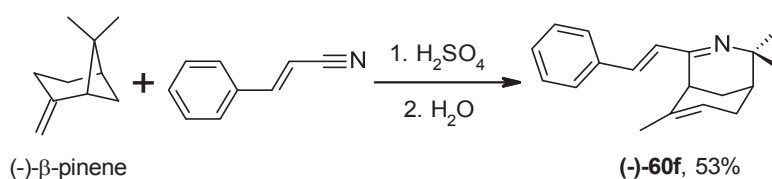


Scheme 2.14 The bridged Ritter reaction between (-)-β-pinene and 3,4-dimethoxybenzonitrile.

2.3.2.7 Cinnamionitrile

The bridged Ritter reaction with cinnamionitrile gave the imino-alkene **(-)-60f** with a 53% yield (Scheme 2.15). Interestingly, this alkene was a honey coloured wax that retained the aroma of cinnamon. The aromatic region of the ^1H NMR spectrum showed the expected three environments due to the plane of symmetry through the system, a doublet at δ 7.51 and two triplets at 7.34 and 7.28 ppm. The cinnamo-alkene functionality is assigned as two doublets (J

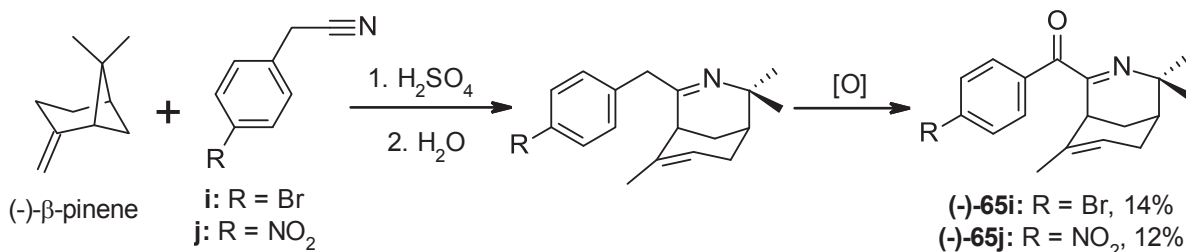
= 15.0 Hz) at δ 7.16 and 6.88 ppm, corresponding to the CH adjacent to the phenyl and the CH adjacent to the imine respectively. The coupling constant of these protons also dictates that the alkene retained the *trans*-configuration. The C-7 alkene was assigned at δ 5.38 and the C-5 bridgehead proton at 3.19 ppm. The specific rotation was found to be $[\alpha]_D^{18} - 35.11$ (c 0.23, CHCl_3) and the $[\text{M}+\text{H}]^+$ exact mass was 266.1901, corresponding to the molecular formula $\text{C}_{19}\text{H}_{23}\text{N}$. No imino-amide was detected to have formed, as determined by GC-MS and ^1H NMR analysis of the crude product.



Scheme 2.15 The bridged Ritter reaction between (-)- β -pinene and cinnamionitrile.

2.3.2.8 4-Bromophenylacetonitrile, 4-Nitrophenylacetonitrile and the Autoxidation of Benzylic Nitrile Products

The reaction of benzyl cyanides (entry **i** and **j**) with (-)- β -pinene, yielded the additional oxidised products (-)-**65i** and (-)-**65j**, with 14 and 12% yield respectively (Scheme 2.16). The oxidation of benzylic CH_2 is well established in the literature and it has been reported that the use of benzyl cyanides under Ritter reaction conditions gave products that underwent spontaneous oxidation to give benzoyl products.^[129] Initial evidence for the formation of (-)-**65i** was derived from its molecular weight observed in the crude GC-MS analysis, which showed a product 14 units higher than that of the expected corresponding imine-alkene **65i**. The IR spectrum presented a band at 1665 cm^{-1} , corresponding to a conjugated ketone carbonyl group. It was further confirmed by the ^{13}C NMR spectrum of (-)-**65i**, which showed a resonance at δ 193.19 ppm, corresponding to the quaternary $\text{C}=\text{O}$ carbon.

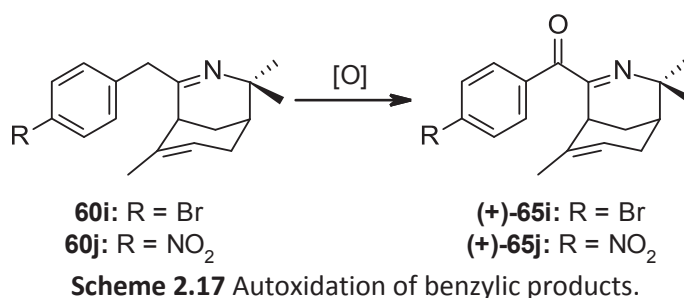


Scheme 2.16 The bridged Ritter reaction between (-)- β -pinene and benzyl cyanides 4-bromophenylacetonitrile and 4-nitrophenylacetonitrile.

Compound (-)-**60j** was also initially noted in the crude mixture. Overtime, (-)-**65j** underwent air-oxidation at the benzylic carbon (C-4 α) to provide (-)-**65j** as assigned in ^1H NMR

by the disappearance of the benzylic protons resonance at δ 3.71 ppm. The formation of (-)-**65j** from **60j** was confirmed by the GC-MS of the crude showing the m/z of 298 for the non-oxidised product at 8.48 minutes, while the oxidised product was observed with m/z 312 at 8.43 minutes. IR spectroscopy indicates the presence of the ketone carbonyl stretch at 1672 cm^{-1} . The HRMS showed the $[M+H]^+$ exact mass of compound (-)-**65j** to be 313.1554, corresponding to the molecular formula $C_{18}H_{21}N_2O_3$. The specific rotation of was found to be $[\alpha]_D^{23} - 34.77$ (c 1.04, $CHCl_3$).

The slow air oxidation of the benzylic carbon made isolation *via* column chromatography for **60i** and **60j**, from their corresponding oxidised products, challenging. Despite this challenge, the benzoyl products (-)-**65i** and (-)-**65j** were obtained and characterised, after the full conversion had occurred. Attempts were made to increase the yield of the benzoyl products by forcing the oxidation by bubbling air through the reaction mixture. It was found, however, that this was unable to accelerate the reaction and the same crude products containing the benzylic alkenes were obtained.

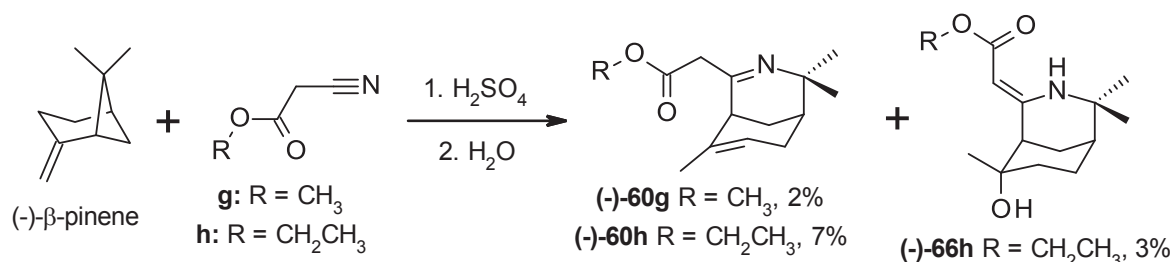


For compound (-)-**65i**, IR spectroscopy indicated the presence of the ketone carbonyl stretch at 1665 cm^{-1} and the ^{13}C NMR carbonyl resonance was assigned at δ 193.19 ppm. The standard characteristic peaks of the bridged imino-alkene products were assigned in the 1H spectrum, such as the broad singlet of the C-7 alkene at δ 5.43 and the C-5 bridgehead at 3.45 ppm. The specific rotation was found to be $[\alpha]_D^{22} - 31.48$ (c 1.00, $CHCl_3$) and the $[M+H]^+$ exact mass was 346.0803, corresponding to the molecular formula $C_{18}H_{20}Br^{79}NO$.

2.3.2.9 Methyl Cyanoacetate, Ethyl Cyanoacetate and Cyanoacetate Rearrangement

Two cyanoacetate nitriles, namely methyl and ethyl (entry **g** and **h**), were used with the bridged Ritter reaction. The products obtained from these nitriles were low yielding with (-)-**60h** obtained with 7% yield after isolation by preparative TLC, while (-)-**60g** was obtained with 2% yield after column chromatography (Scheme 2.18). Both of these alkenes exist in the keto and enol form in solution (Scheme 2.19), as shown by the additional resonances in the

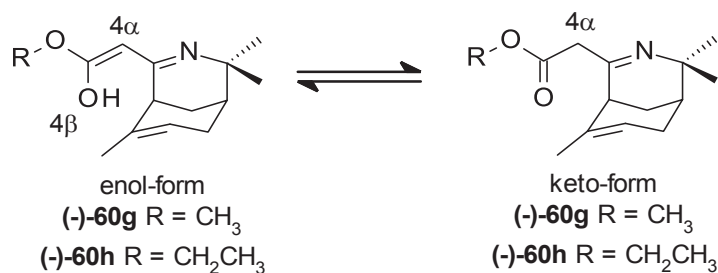
NMR spectra. Using the integral values of the ^1H NMR resonances, it was determined that the ratio of enol to keto form for both (-)-60h and (-)-60g was 1:2.



Scheme 2.18 The bridged Ritter reaction between (-)- β -pinene and methyl cyanoacetate and ethyl cyanoacetate.

In the ^1H NMR spectrum of (-)-60h, the $4\beta\text{-OH}$ and $4\alpha\text{-CH}$ resonances were assigned at δ 8.28 and 4.38 ppm, respectively, for the enol form, while the $4\alpha\text{-CH}_2$ of the keto form occurred as singlets at 4.73 and 4.63 ppm. In the ^{13}C NMR spectrum of (-)-60h, the enol $4\alpha\text{-CH}$ was assigned at δ 80.0 ppm while the keto $4\alpha\text{-CH}_2$ was assigned at 108.2 ppm. The ethoxy group was assigned as a triplet ($J = 7.5$ Hz) at δ 1.25 and a multiplet at 4.08 ppm and confirmed by COSY experiments. Other key peaks of (-)-60h included the C-7 alkene at δ 5.40 and the C-5 bridgehead at 2.46 ppm. IR spectroscopy indicated the presence of both the alcohol at 3261 cm^{-1} and ketone carbonyl stretch at 1647 cm^{-1} . The specific rotation was found to be $[\alpha]_{\text{D}}^{22} - 123.92$ (c 1.00, CHCl_3) and the $[\text{M}+\text{H}]^+$ exact mass was 250.1805, corresponding to the molecular formula $\text{C}_{15}\text{H}_{23}\text{NO}_2$.

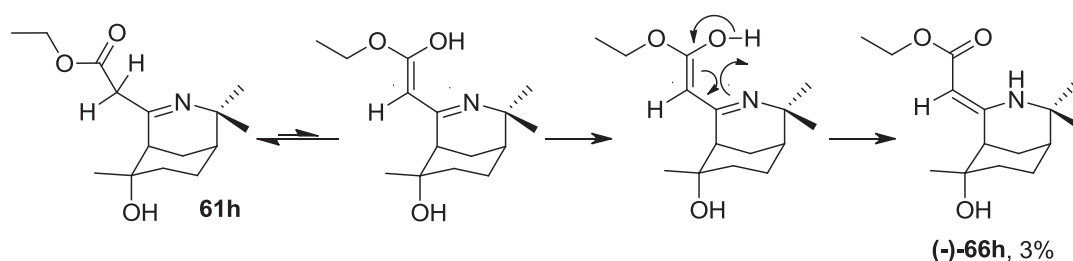
For (-)-60g, the ^1H NMR spectrum showed the $4\beta\text{-OH}$ as a singlet at δ 8.51, the $4\alpha\text{-CH}$ as a singlet at 4.38 and the $4\alpha\text{-CH}_2$ as two singlets at 4.75 and 4.64 ppm. The corresponding resonances on the ^{13}C spectrum were the quaternary alcohol/carbonyl at δ 163.4 ppm, the $4\alpha\text{-CH}$ at 82.91 and the $4\alpha\text{-CH}_2$ at 108.3 ppm. Meanwhile, the methoxy signal was assigned as a singlet at δ 3.63 ppm. Other key peaks of (-)-60g included the C-7 alkene at δ 5.41 and the C-5 bridgehead at 2.47 ppm. IR spectroscopy indicated the presence of both the alcohol at 3259 cm^{-1} and ketone carbonyl stretch at 1649 cm^{-1} . The specific rotation was found to be $[\alpha]_{\text{D}}^{21} - 42.38$ (c 1.00, CHCl_3) and the $[\text{M}+\text{H}]^+$ exact mass was 236.1639, corresponding to the molecular formula $\text{C}_{14}\text{H}_{21}\text{NO}_2$.



Scheme 2.19 Interconversion of the enol and keto forms of **(-)-60g** and **(-)-60h**.

The ethyl cyanoacetate also resulted in an unexpected amino-alcohol product **(-)-66h**, which was isolated in only the β -unsaturated carbonyl (keto) form with 3% yield (Scheme 2.18). A proposed mechanism for the rearrangement of the cyanoacetate that resulted in this structure is seen in Scheme 2.20. It is believed that **(-)-66h** exists only in the keto-form due hydrogen bonding between the carbonyl oxygen and amino hydrogen, stabilising this conformation. This bonding was seen in the X-ray structure obtained from suitable single crystals of **(-)-66h**, which were grown from CH₂Cl₂/hexane. The X-ray structure also showed that the C4 to C4 α double bond adopts the Z-conformation. The Z-conformation is favoured by the intramolecular H-bonding between NH---O=C (Figure 2.5).

The 4 α alkene CH was assigned in the ¹H NMR spectrum at δ 4.35, which is slightly upfield from the expected region of vinylic protons due to the shielding nature of possible resonance of the β -unsaturated carbonyl system. The same can be seen for the CH ¹³C resonance, which exists at δ 83.0. Characteristic absorbance peaks were also observed in the IR spectrum, notably, those corresponding to the C-6 alcohol, amine and carbonyl functionality stretches at 3470, 3287 and 1625 cm⁻¹ respectively. The high-resolution mass spectrometry (HRMS) showed the [M+H]⁺ exact mass of compound **(-)-66h** to be 268.1898, corresponding to the molecular formula C₁₅H₂₆NO₃ and the specific rotation was found to be $[\alpha]_D^{20}$ – 33.26 (c 1.00, CHCl₃).



Scheme 2.20 A possible mechanism for the rearrangement of cyanoacetate product **(-)-66h**.

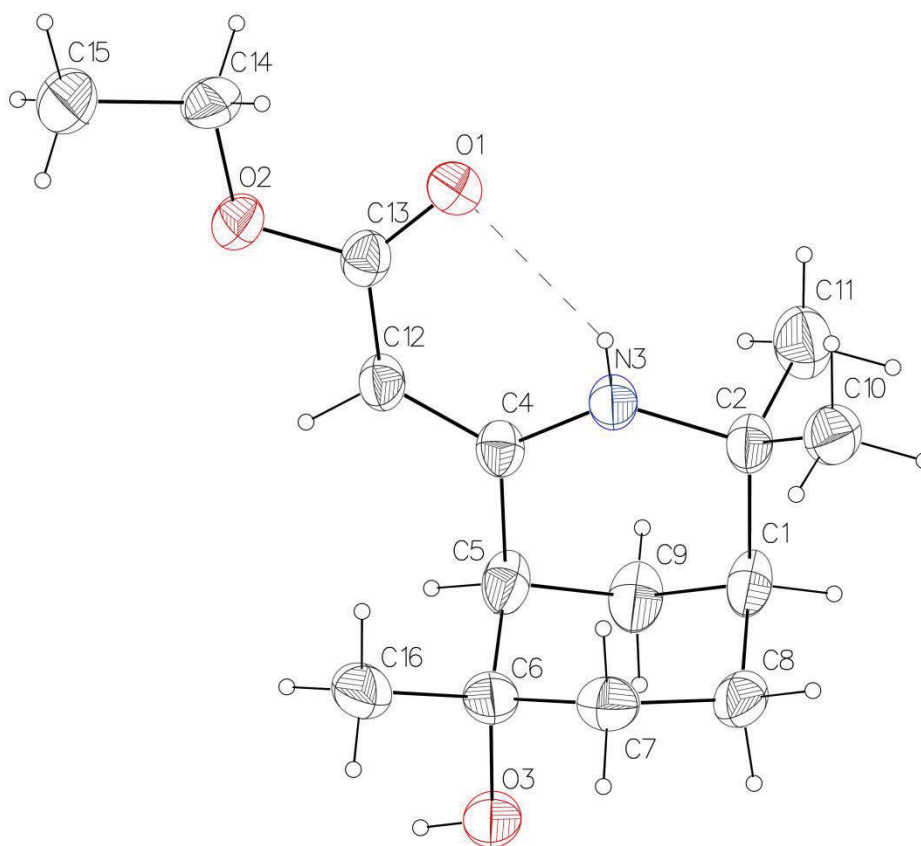


Figure 2.5 ORTEP diagram of **(-)-66h** molecule in the crystal structure of racemic, showing the intramolecular H-bonding between NH---O=C.

The crystal structure of **66h** was found to be in the *Cc* space group, having four symmetry operations, as this crystal contains the **(-)-66h** (*1R, 5S, 8S*) and **(+)-66h** (*1S, 5R, 8R*) enantiomers (Figure 2.6). Compounds **(-)-66h** and **(+)-66h** are coloured in grey and magenta, respectively, according to their symmetry operation. This result was unexpected, because the bridged Ritter reaction is asymmetric and should generate optically pure products from chiral starting materials such as (-)- β -pinene.

The presence of both enantiomers in the crystal packing was a result of trace impurities of (+)- β -pinene in the starting material. The (-)- β -pinene used for the reaction was sourced from Sigma-Aldrich, who reported that the product had a 97% enantiomeric excess and a specific rotation of $[\alpha]_D^{25} - 22$ (neat). The optical rotation of the product was measured to be $[\alpha]_D^{22} - 18.85$ (neat). The trace amounts of **(+)-66h** in the crude product would have favoured the co-crystallisation of the enantiomers in the sample taken from the crude and recrystallised, while the purified sample of **(-)-66h** was isolated and characterised.

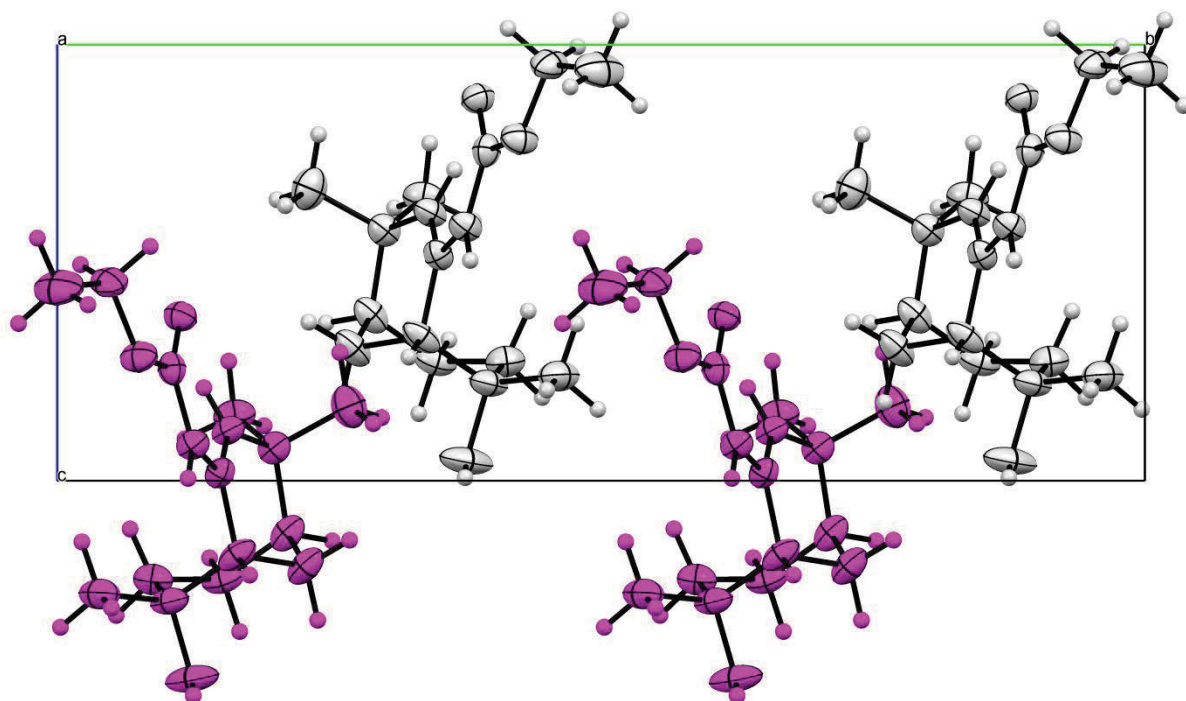


Figure 2.6 Enantiomers of **(-)-66h** (grey) and **(+)-66h** (magenta, glide plane related) in the unit cell looking down the *a* axis.

2.3.3 Preparation of 3-Azabicyclo[3.3.1]non-3-en-6-yl) acetate Products

The mild bridged Ritter reaction conditions, utilising acetic acid in place of the benzene solvent, were used for acetonitrile, propionitrile and potassium cyanide. With the exception of the unique structure obtained from potassium cyanide (discussed in Section 2.3.3.1), these conditions resulted in isolatable quantities of the corresponding imino-alkenes **(-)-60b** and **(+)-60l**, the imino-amides **(+)-59b** and **(+)-59l** as well as the formation of the additional imino-acetate products **(+)-63b** and **(+)-63l** (as presented earlier in Scheme 2.6). The acetate products **63** were unexpected but investigated after the occurrence of the detection of additional products in the GC chromatogram, with a mass 1 AMU higher than that of the expected corresponding imino-amide product **59**. The use of the polar solvent, however, did not increase the yield, in comparison to the standard conditions used. For acetonitrile, the ratio of the amide to the alkene to acetate was determined to be 1:0.81:0.72. The reduction in overall yield may result as the carbocation does not form as readily in comparison to the standard conditions. This observation concurred with those reported by Benson *et al.*,^[110] in which dilution of the Ritter reaction with high quantities of solvent result in some cases where the reaction does not proceed.

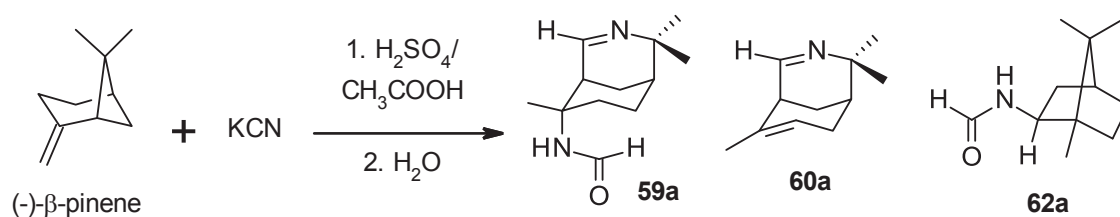
The yields obtained for purely isolated **(+)-63l** and **(+)-63b** were 9% and 4%, respectively. These yields are not an accurate representation of the overall crude quantities, as the oily consistency and similarity in polarity between the imino-alkene **60** and imino-acetates

63 meant they were mutually soluble and, therefore, challenging to separate in large quantities by column chromatography. As a result, preparative TLC had to be used on fractions of the crude previously obtained from column chromatography. Separation was optimised by removal of most of the imino-amide prior to separation method development *via* precipitation of the amide in a DCM/diethyl ether mixture.

For **(+)-63I**, the ^{13}C NMR reveals a downfield shift of C-6 by 22 ppm compared to the equivalent amide structure, due to being adjacent to the oxygen atom. The formation of acetate **(+)-63I** was confirmed by HRMS to have an exact mass of 238.1805, corresponding to $\text{C}_{14}\text{H}_{24}\text{NO}_2^+$. The specific rotation of **(+)-63I** was found to be $[\alpha]_{\text{D}}^{20} + 72.64$ (c 1.00, CHCl_3). For **(+)-63b**, the $[\text{M}+\text{H}]^+$ exact mass was found to be 252.1956 corresponding to $\text{C}_{15}\text{H}_{26}\text{NO}_2$, with a specific rotation of $[\alpha]_{\text{D}}^{22} + 35.72$ (c 1.00, CHCl_3).

2.3.3.1 Unexpected Acetate Crystal Structure

Using the toxic and low boiling hydrogen cyanide is a safety limitation when performing the Ritter reaction, however alternative approaches that avoid this dangerous substance are now available.^[130] The resulting *N*-alkylformamides reported from these methods can be hydrolysed relatively easily, thereby providing an important synthetic route to the corresponding *N*-alkylamines.^[131] Unfortunately, these alternative procedures are not applicable to the bridged-Ritter reaction. In fact, clipping H–CN (or its chemical equivalent) across an unsaturated carbenium ion intermediate has not been previously reported. The polar reaction conditions were used with potassium cyanide as a safe way to generate hydrogen cyanide *in situ*, in order to form the 3-azabicyclo[3.3.1]non-3-ene products containing hydrogen as the –R substituent at C-4 (Scheme 2.21).



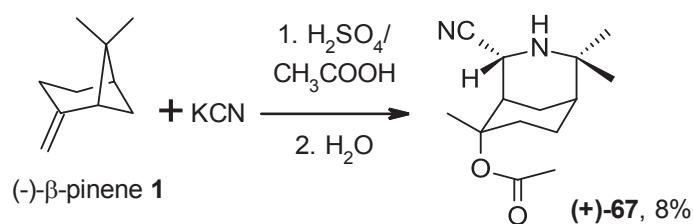
Scheme 2.21 Expected outcome from the bridged Ritter reaction between (-)-β-pinene and potassium cyanide.

The crude reaction mixture was analysed by GC-MS which identified the expected imino-alkene (m/z 163, $R_t = 11.32$ minutes) and imino-acetate (m/z 223, $R_t = 14.72$ minutes) products. Purification was attempted using hexane to ethyl acetate gradient mobile phase on silica stationary phase. The purification was unsuccessful due to the co-elution of products in

the collected fractions, yet single crystals were grown in these fractions and isolated for analysis. Additionally, initial analysis by HRMS gave the $[M+H]^+$ exact mass as 224.1644, corresponding to formula $C_{13}H_{22}NO_2$, suggesting that the product was (1*S*,5*R*,6*S*)-2,2,6-trimethyl-3-aza-bicyclo[3.3.1]non-3-en-6-yl acetate. This, however, did not correspond to the pure NMR data collected for the crystals.

The IR spectrum of this unexpected product revealed bands at 2220, 1720, 1220 and 1017 cm^{-1} corresponding to CN, C=O and C-O stretches that are indicative of cyano and ester functional groups, respectively. ^{13}C NMR showed two resonances at δ 170.7 and 123.1 ppm that confirmed the presence of C=O and CN functional groups. The lacking of the imine carbon (\approx 166 ppm) and the presence of an additional CH at 45.7 ppm, further suggests that the imine functionality is no longer present within the structure.

The compound was recrystallised from benzene and analysed by X-ray crystallography to unequivocally give the unexpected (1*S*,4*R*,5*R*,6*S*)-4-cyano-2,2,6-trimethyl-3-azabicyclo[3.3.1]nonan-6-yl acetate product **(+)-67** (Figure 2.7) with 8% yield (Scheme 2.22). This agreed with the ^{13}C NMR data above, while the position 4 CH was assigned at δ 4.10 in the 1H NMR. HRMS of the compound was reassessed using neutral conditions, to find the molecular ion of m/z 251.1754 $[M+H]^+$ which corresponds to the correct formula for **(+)-67**, $C_{14}H_{22}N_2O_2$. The specific rotation was found to be $[\alpha]_D^{20} + 9.76$ (c 1.00, $CHCl_3$).



Scheme 2.22 Actual outcome from the bridged Ritter reaction between (-)-β-pinene and potassium cyanide.

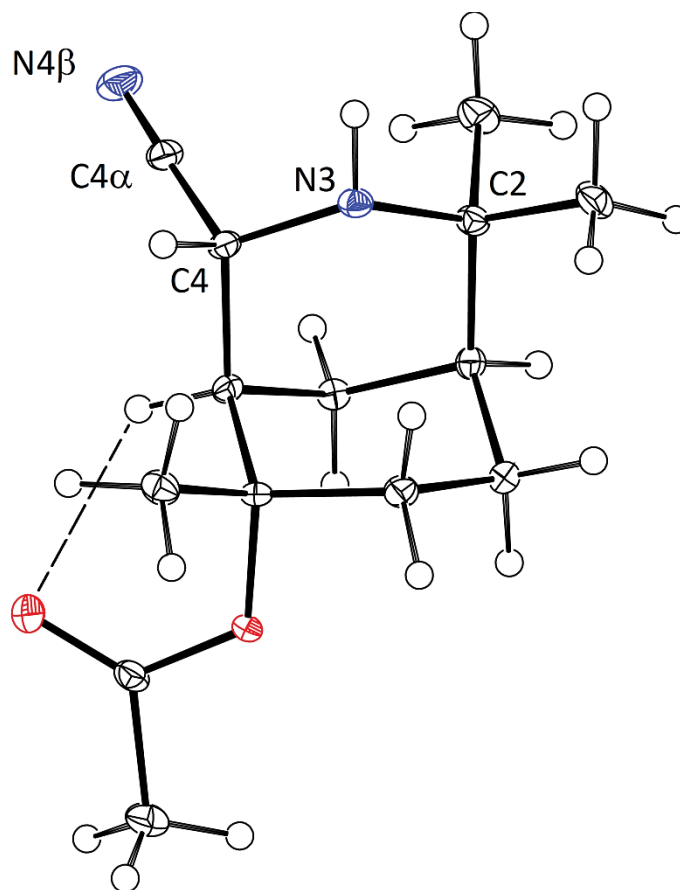
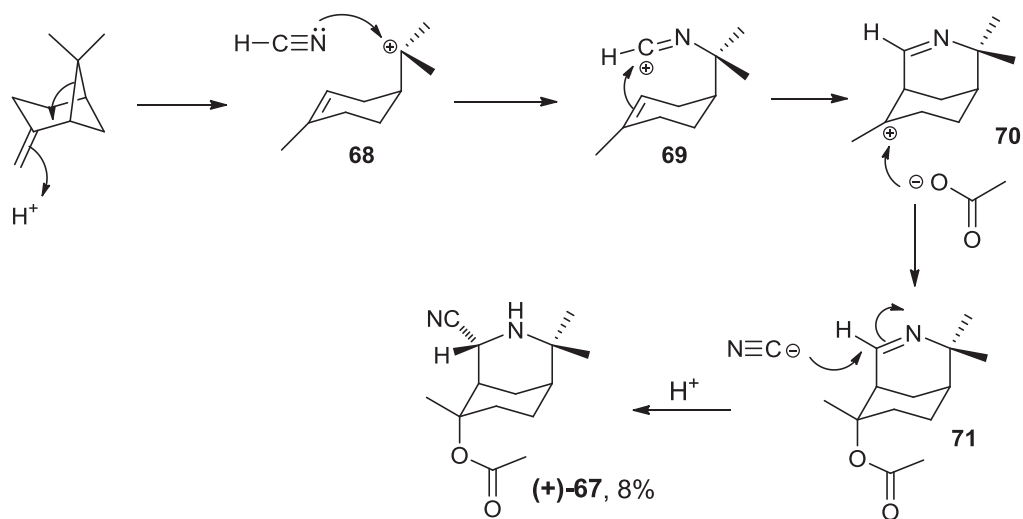


Figure 2.7 ORTEP diagram for the compound **(+)-67**.

Compound **(+)-67** crystallised in the monoclinic $P2_1$ space group and adopts a chair-chair conformation. The molecule shows an intramolecular C-H...O interaction in the solid state (Figure 2.7) and the bond lengths within the azabicyclo[3.3.1]nonane core structure show the evidence for the sp^3 hybridisation at C-4. The N3-C4 bond is 1.451 (3) Å, which is very similar in length to that of N3-C2 (1.479 (3) Å). It is expected that the N3-C4 in the imine **71** (Scheme 2.23) would be significantly shorter than N3-C2 (1.479 (3) Å). This is seen in previous work on the azabicyclo[3.3.1]nonene system, which showed the N3-C4 distance in the imine bond to be in the range of 1.274 (4) - 1.259 (11).^{[101],[132]} The presence of cyano group at C-4 is confirmed by the bond lengths of C4-C4 α and N4 β -C4 α to be 1.504 (3) and 1.148 (3) Å, respectively, in addition to the bond angle for N4 β -C4 α -C4 (178.1 (2)°). These distances and angle are in agreement with the generally accepted values for correlated molecules that contain a cyano group.^{[133],[134]} Moreover, the crystal data of **(+)-67** compares well with the results observed in similar azabicyclo[3.3.1]nonane systems found in the literature.^{[135],[136]} Crystal and refinement data of **(+)-67** are given in Table 9.4 of Chapter 9.

Due to the unique and unexpected nature of this product, a proposed mechanism for its formation was postulated. As seen in Scheme 2.23, KCN reacts with H_2SO_4 to generate HCN

in situ. HCN then reacted with **68** to give the second carbenium ion intermediate **69**, which undergoes intramolecular cyclisation to provide **70**. The acetate ion adds *via* nucleophilic addition to **70**, to give the imine product **71**. Available CN anions then asymmetrically added to **71** at C-4, from the *Si* face of the imine bond, to give the optically active compound (+)-**67**.



Scheme 2.23 A proposed mechanism for the formation of compound (+)-**67**.

2.3.4 Investigation of Reaction Time

The effect of reaction time was investigated in order to determine the optimum reaction conditions. This was only explored for acetonitrile, for which the length of reaction time was found to influence the product ratio between the imino-amide and imino-alkene. Under the standard reaction time (24 hours), the reaction gave a 2.78:1 ratio of imino-amide to imino-alkene. Only the imino-amide was formed when the reaction time was shortened to four hours. On the other hand, when the reaction time was extended to 96 hours, the ratio became 1:3. It appears that the longer reaction times led to greater formation of the alkene product.

2.3.5 Influence of the Nitriles

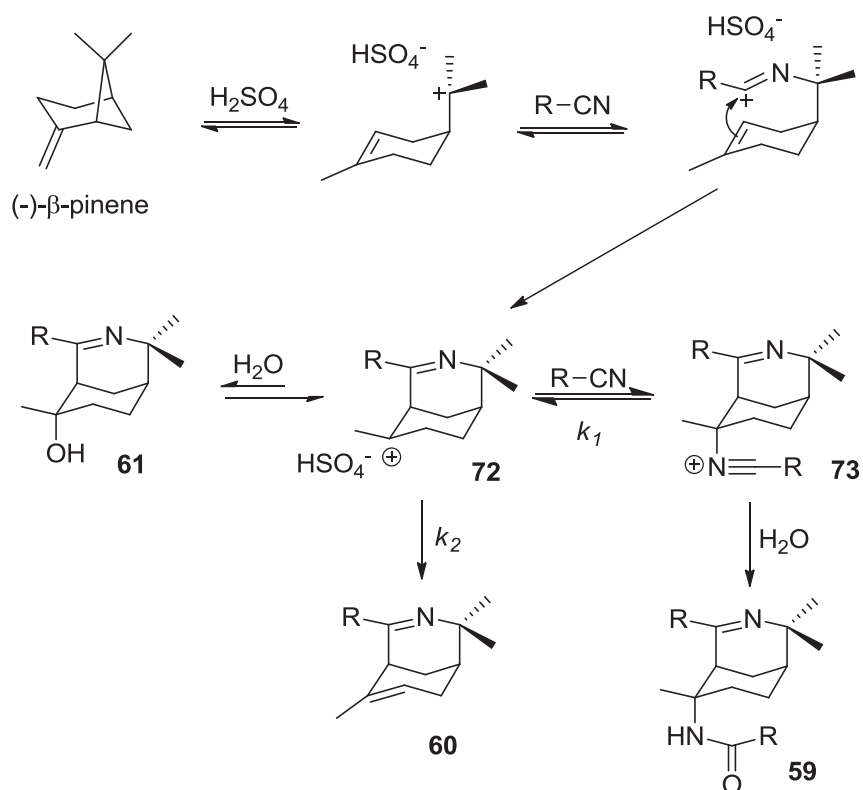
The results of early work by our research team with acetonitrile (**l**) and benzonitrile (**e**) revealed the formation of **59** and **60** in the ratios of 2.78:1 and 1.75:1, respectively.^[126] From the results reported above, there is a clear trend which correlates to the properties of the nitriles used. Notably, the size of the nitrile imposes a steric factor where the bulky nitriles tend to favour the formation of imine-alkenes **60**. When benzonitrile was used, however, it provided both **59** and **60**, despite its relative bulkiness. This suggests that the nucleophilicity of the nitrile has a strong influence on the selectivity of these cyclic imines.^[137] Attack of the C-6 carbocation intermediate **72** by a strongly nucleophilic nitrile would eventually favour the

formation of the imine-amides **(+)-59**, as described in the proposed mechanism in Section 2.3.6.

Depending on the nitrile, several side reactions could also occur under the bridged Ritter reaction conditions used. For instance, the nitriles would react with water upon quenching to form the corresponding amide. This effect was more pronounced for aromatic nitriles such as benzonitrile, cinnamitrile and 3,4-dimethoxybenzonitrile, although it also produced isolatable quantities from propionitrile and chloroacetonitrile, which was undesirable due to increasing the complexity of the purification required. This problem was overcome by extracting the acidic quenched reaction mixture before the solution was basified and extracted again to isolate the products. This pre-extraction reduced the yield and made purification significantly easier as it also removed any unreacted starting material.

2.3.6 Proposed Mechanism for the Bridged Ritter Reaction with (-)- β -pinene

The results from varying the reaction time, or solvent polarity, has allowed for a potential reaction mechanism to be proposed. This is seen in Scheme 2.24, where each of the imino products forms through the intermediate **72**. The nitrile used also had a significant influence on the reaction outcome, including the steric factor imposed by the size of the nitrile and its nucleophilicity, as has been previously reported to influence reactivity.^[137] In general, bulky nitriles favour the formation of the imino-alkenes, however attacking of the C-6 carbocation intermediate by a strongly nucleophilic nitrile would preferentially favour the formation of the imino-amides as the short reaction times formed almost exclusively amide, while more alkene was obtained from longer reaction times. Where the imino-amides **59** are the major product, the data suggests that the transformation of **72** into **59** is controlled by the rate k_1 , which is influenced by the nucleophilicity of the nitrile. The reaction of **72** with another mole of R-CN forms **73** and eventually **59** upon quenching with water. Alkene is slowly continuously formed from the collapsing of carbocation **72** that remains after the maximum amount of **73** has formed. It appears that the longer reaction times led to greater formation of the alkene product. This suggests that in the proposed mechanism (Scheme 2.24), the reaction of **72** to **73** is an equilibrium process or could result if carbocation **72** remaining after the maximum amount of **73** has formed collapses slowly to the alkene **60**.

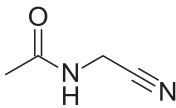
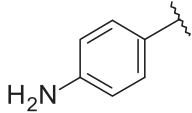
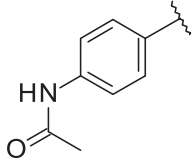


Scheme 2.24 Proposed mechanism for the bridged Ritter reaction with (-)- β -pinene.

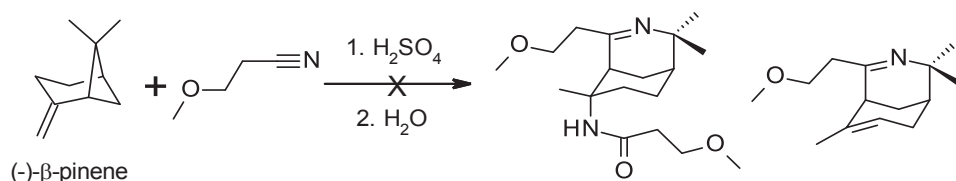
2.3.7 Attempted Bridged Ritter Reactions

The following outlines the attempted, unsuccessful synthesis of novel 3-azabicyclo[3.3.1]non-3-ene alkaloid-like molecules. Each of these reactions appears to be unsuccessful due to the properties of the nitriles used and, despite several attempts to explore and interpret the reaction outcomes, only postulations can be made as to the reason why the bridged Ritter reaction did not work with the nitriles listed in Table 2.2.

Table 2.2 List of nitriles unsuccessfully used for the bridged Ritter reaction and the hypothesised reasons.

Entry	Nitrile	-R	Reason
1	3-Methoxypropionitrile	CH ₃ OCH ₂ CH ₂ -	Unstable – undergoes side reactions
2	Aminoacetonitrile hydrogensulfate	NH ₂ CH ₂ -	Unstable – undergoes side reactions
3	<i>N</i> -(Cyanomethyl)acetamide		Acetamide cleaved under reaction
4	4-Aminobenzonitrile		Poor nucleophile as ammonium ion formed is electron withdrawing
5	<i>N</i> -(4-Cyanophenyl)acetamide		Acetamide cleaved under reaction conditions to give amine
6	3-Chloropropionitrile	ClCH ₂ CH ₂ -	Reactivity of alkyl halide
7	4-Chlorobutyronitrile	ClCH ₂ CH ₂ CH ₂ -	Poor nucleophile
8	5-Chlorovaleronitrile	ClCH ₂ CH ₂ CH ₂ CH ₂ -	Poor nucleophile
9	Bromoacetonitrile	BrCH ₂ -	Reactivity of alkyl halide

The bridged Ritter reaction was attempted with 3-methoxypropionitrile in order to mimic the interactions of the recrystallization artefact ligand 2-[2-[2-(2-hydroxyethoxy)ethoxy]ethoxy]ethanol seen residing in the AChE gorge of the 1DX6 protein file, as shown in Figure 2.8. The artefact is coloured pink, while the Galantamine in the active site is coloured red. It was hypothesised that a compound with similar functionality at -R would interact in a similar way and hence would result in increased favourable interactions with the AChE gorge and hence produce a more potent inhibitor. A similar rational design approach is discussed in more depth in Chapters 3 and 7. This reaction was unsuccessful at forming the desired products and no other unexpected products were isolated (Scheme 2.25).



Scheme 2.25 Attempted bridged Ritter reaction between (-)-β-pinene and 3-methoxypropionitrile.

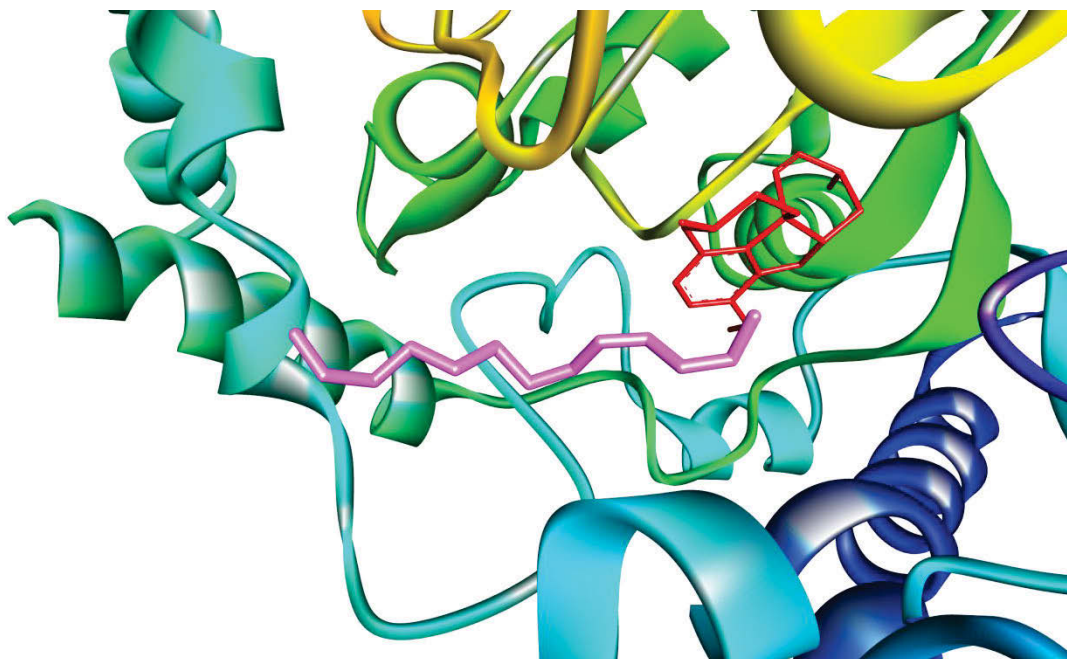
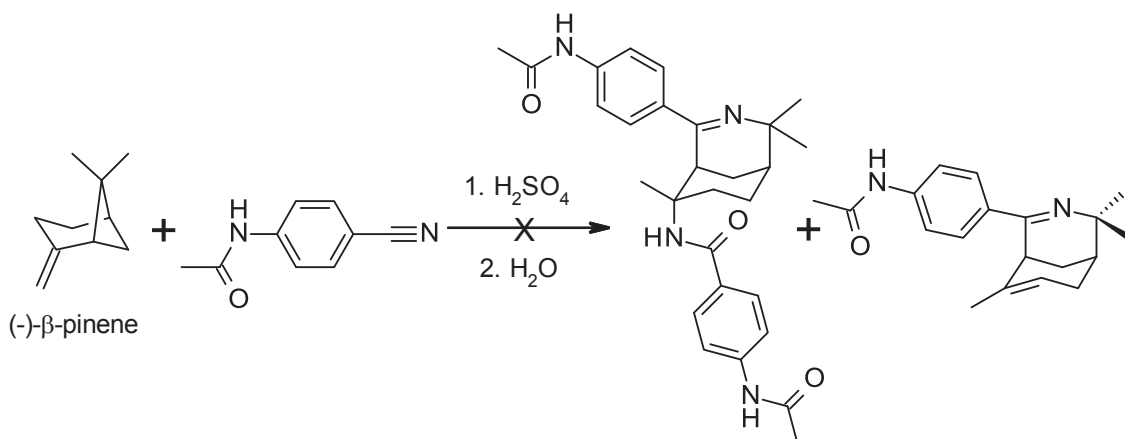


Figure 2.8 AChE protein file 1DX6 containing 2-[2-[2-(2-hydroxyethoxy)ethoxy]ethoxy]ethanol (pink) in the gorge leading down to the active site where Galantamine (red) interacts.

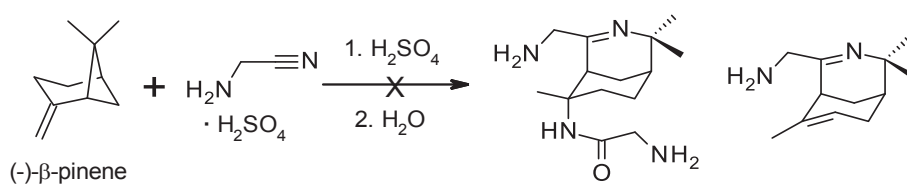
It was expected that the reactions with the nitriles containing amines might not proceed due to the precipitation of salts under acidic conditions. To overcome this, the amine groups were also protected with acetic anhydride.

When the bridged Ritter reaction was attempted with 4-aminobenzonitrile, the order of addition of the reaction reagents was changed to avoid the formation of the amino salt. After our previous work had revealed that the bridged Ritter reaction occurs almost instantaneously,^[126] it was assumed that the formation of the bridged product could be prioritised by acidifying the reaction solution containing all of the components, as opposed to adding the (-)-β-pinene to the already acidified reaction solution (Scheme 2.26). This failed to provide the expected products and the starting material was recovered.

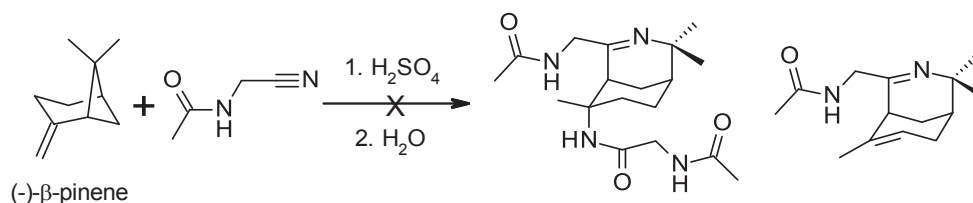


Scheme 2.28 Attempted bridged Ritter reaction between (-)-β-pinene and *N*-(4-cyanophenyl)acetamide.

The aminoacetonitrile used was the hydrogensulfate salt, allowing it to be soluble in the reaction conditions. Despite initial observations based on the standard colour changes observed with each bridged Ritter reaction, the bridged Ritter reaction did not occur as the expected products could not be detected when analysed by GC-MS and ^1H NMR (Scheme 2.29). It appears that the aminoacetonitrile undergoes side reactions, such as hydrolysis to form glycine. This was outlined by Moser and Mathews,^[138] who also state that α -amino nitriles, such as aminoacetonitrile, are “among the most unstable nitriles known”. The aminoacetonitrile was also protected to *N*-(cyanomethyl)acetamide and the bridged Ritter reaction performed using it, but the acetamide was cleaved under the reaction conditions (Scheme 2.30).

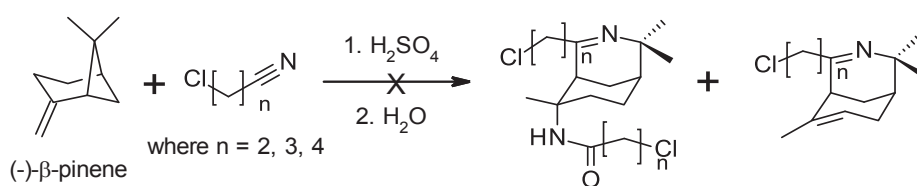


Scheme 2.29 Attempted bridged Ritter reaction between (-)-β-pinene and aminoacetonitrile hydrogen sulfate.



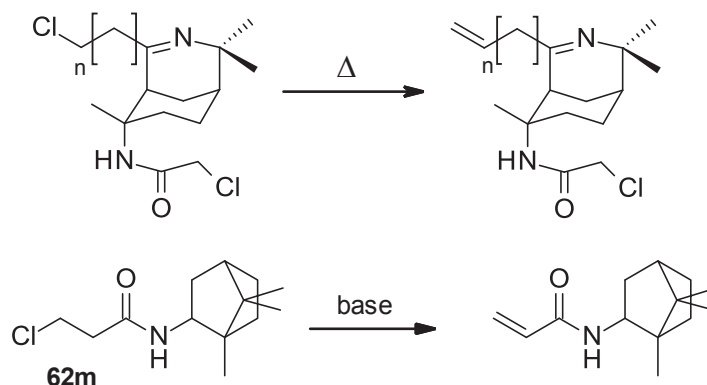
Scheme 2.30 Attempted bridged Ritter reaction between (-)-β-pinene and *N*-(cyanomethyl)acetamide.

The crude product from the reaction with 3-chloropropanenitrile (Scheme 2.31 where $n = 2$) was analysed by GC-MS and ^1H NMR. No evidence of the desired products was observed, but the MS data provides support for the formation of the *N*-isobornylamide **62m** with molecular ion peaks at m/z 243, corresponding to $[\text{C}_{13}\text{H}_{22}\text{ClNO}]^+$. Purification of this product was attempted by recrystallization from DCM/hexane, but the samples obtained were of insufficient purity. This is most likely attributed to the reactive behaviour of the alkyl halide functionality, as they have a good ability to act as a leaving group, resulting in side reactions under the conditions used. One reaction, for example, could be the elimination of the alkyl halide to give an alkene, as shown in Scheme 2.32. The crude product was analysed for these by-products, although none of the products derived from the expected products were identified. It is possible that these alkenes are capable of undergoing further reactions under the acidic reactions used, whereby another carbocation is generated and reacts further. This would explain the polymer-like appearance of the ^1H NMR spectrum of the crude product.

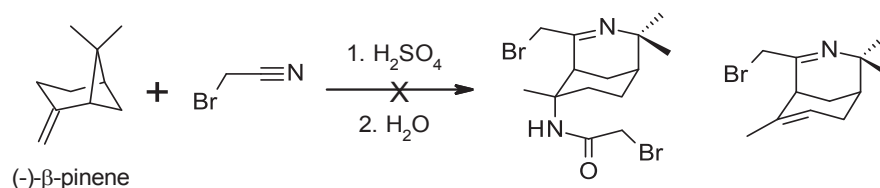


Scheme 2.31 General scheme for attempted bridged Ritter reactions between (-)- β -pinene and terminal chloronitrile's where chain length = n .

This elimination was, however, observed for the *N*-isobornylamide product when it was treated with a base such as sodium hydroxide (Scheme 2.32). Monitoring a crude sample of **62m** with ^1H NMR before and after treatment with sodium hydroxide, revealed the introduction of new peaks at δ 3.80 and 4.05 ppm, presumably corresponding to the alkene. Full characterisation was attempted but unsuccessful due to the constant decomposition of reactive components present. The same could be said for the bromoacetonitrile (Scheme 2.33), which displayed a similar impurity profile in the ^1H NMR analysis (entry 9 in Table 2.2).

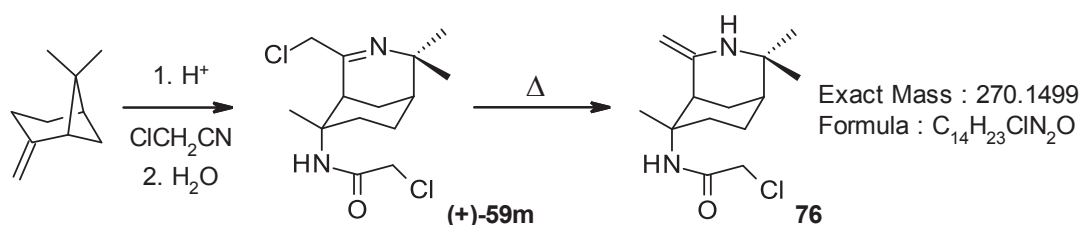


Scheme 2.32 Halide elimination of the bridged Ritter reaction product and *N*-isobornylamides.



Scheme 2.33 Attempted bridged Ritter reaction between (-)-β-pinene and bromoacetonitrile.

Evidence of this phenomenon was also seen for the bridged Ritter reaction with chloroacetonitrile, reported previously. GC-MS analysis of the crude product shows trace amounts of product **76**, corresponding to the elimination product seen in Scheme 2.34, which has a m/z of 270 at 18.13 minutes corresponding to $[C_{14}H_{23}ClN_2O]^+$.



Scheme 2.34 Halide elimination of (+)-59m to give the alkene product.

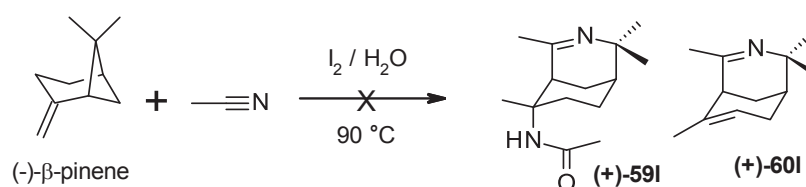
When the reaction was attempted with 4-chlorobutyronitrile and 5-chlorovaleronitrile (Scheme 2.31 where $n = 3$ and 4 respectively), none of the impurities were observed in the 1H NMR spectra of the crude products, as were none of the expected products. In both cases, the reactions were unsuccessful and the nitrile was recovered. This suggests that these nitriles are unreactive due to their poor nucleophilic nature.

2.3.8 Alternative Bridged Ritter Reaction Catalysis

Several alternative conditions for generating the carbocation in the Ritter reaction have been reported.^[130] A few of these alternatives were explored to find an optimised or more mild set of conditions that could be applied to the bridged Ritter reaction, in particular to the sensitive and low yielding nitriles used. To test the viability of performing the bridged

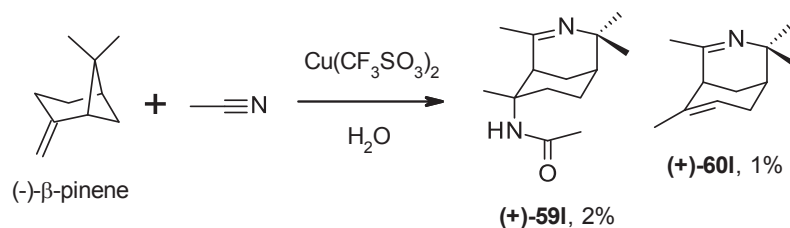
Ritter reaction with these conditions, the reaction with acetonitrile and (-)- β -pinene was attempted using both iodine and copper and zinc trifluoromethanesulfonate (triflate) as the catalyst to replace sulfuric acid.

The bridged Ritter reaction with I_2 was adapted from Hanzawa *et al.*^[139] who reported the synthesis of *N*-isobornylamides from camphene and various nitriles in addition to several pinene isomers which they only reported to produce ‘complex mixtures’. The conditions used, therefore, were applied to the reaction of (-)- β -pinene and acetonitrile but no bridged products were obtained (Scheme 2.35). Trace amounts of the corresponding *N*-isobornylamide **62I** were detected when analysing the crude product by GC-MS, with molecular ion peaks at m/z 195 found at 15.00 minutes, corresponding to $[C_{12}H_{21}NO]^+$.

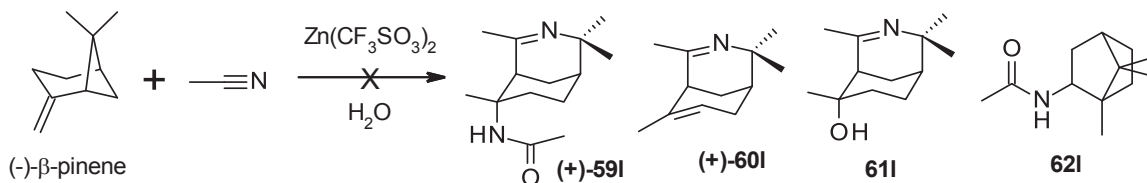


Scheme 2.35 Attempted bridged Ritter reaction between (-)- β -pinene and acetonitrile with I_2 catalyst.

The bridged Ritter reaction was attempted using the Lewis acid copper triflate as a substitute for sulfuric acid, using a method adapted by Callens *et al.*^[140] Although there are many reports of various metal triflates being used to perform the classical Ritter reactions, with much effort going into finding the optimum condition for these reactions,^[141] no incidence of using triflates to perform the bridged Ritter reaction have been found. This method provides an alternative setting under which to achieve the intramolecular cyclisation. Initial analysis of the crude product by GC-MS did show that the bridged Ritter products **(+)-59I** and **(+)-60I** had in fact formed in 2 and 1% of the crude mass, respectively, as confirmed by matching retention times and mass spectra from those previously isolated under standard conditions (Scheme 2.36). Unfortunately, these products only formed in quantities of impractical yield for isolation, hence this method was deemed an unviable alternative. The reaction was then attempted using zinc triflate which was also unsuccessful (Scheme 2.37), with none of the expected products being detected in the analysis of the crude product by GC-MS, amidst the mix of rearranged (-)- β -pinene impurities. Future work could investigate the use of stronger Lewis acid, after the signs of potential shown by copper triflate.



Scheme 2.36 The bridged Ritter reaction between (-)-β-pinene and acetonitrile with copper triflate catalyst.

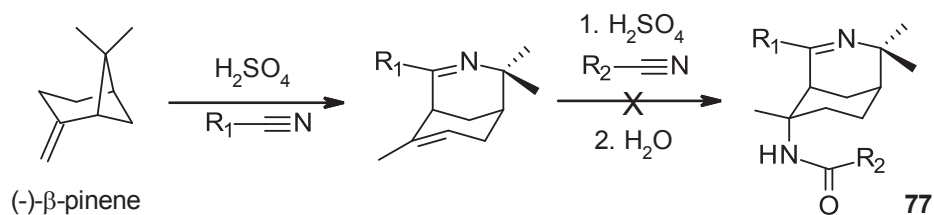


Scheme 2.37 The bridged Ritter reaction between (-)-β-pinene and acetonitrile with zinc triflate catalyst.

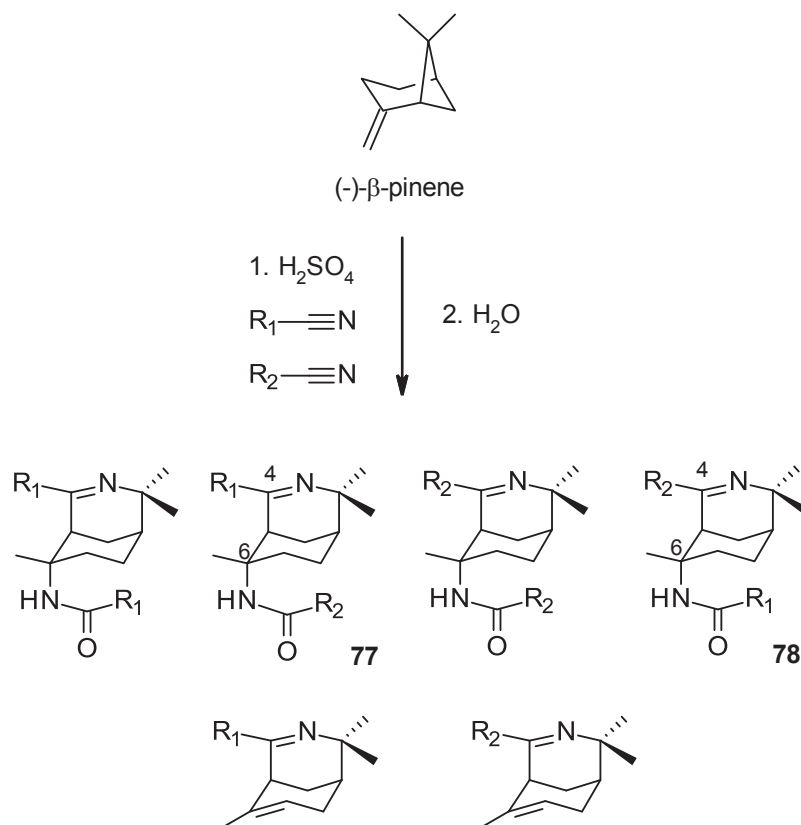
Despite the success of alternative catalysts used for the Ritter reaction, it appears that the strong sulfuric acid conditions is the most effective catalyst for the bridged Ritter reaction. This highlights the importance of the activation of the nitrile *via* increasing its nucleophilicity with polar environments, as outlined in Section 2.2.2.1.

2.4 Mixed Bridged Ritter Reactions

To increase the versatility and range of products that could be obtained from the bridged Ritter reaction, two sets of variations to the reaction were made. The first set will herein be referred to as the 'controlled mixed Ritter reaction' and it aimed to perform a standard Ritter reaction on the alkenes isolated from the bridged Ritter reaction to selectively introduce functionality from an alternative nitrile through the formation of the amide (Scheme 2.38). The second set is a one-pot mixed Ritter reaction, where the reaction is performed using a mixture of two nitriles instead of one, leading to the possibility of a mixture of products containing not only the bridged products from the individual nitriles but also alternative combinations of the products that result from the two nitriles. This can be seen in Scheme 2.39, where positions 4 and 6 are either both -R₁, both -R₂, -R₁ and -R₂ respectively **77**, or *vice versa* **78**. In addition, the outcomes of these reactions can further increase the understanding of the nitrile reactivity and hence the kinetics of the proposed mechanism for the bridged Ritter reaction.



Scheme 2.38 General reaction scheme for a controlled mixed Ritter reaction.



Scheme 2.39 General reaction scheme for a one-pot mixed Ritter reaction.

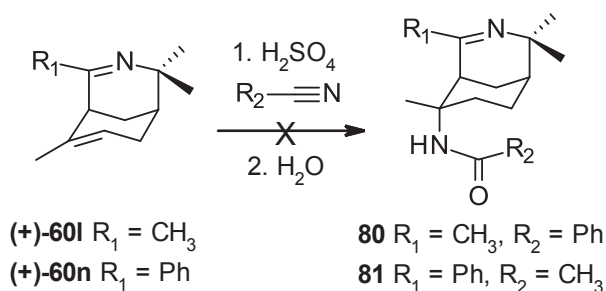
The variation in functionality at these two positions is a critical point to be considered when designing synthetic pathways to a target compound that can allow for more diverse structural modification, as discussed further in Chapter 3. The following mixed Ritter reactions were a synthetic effort driven by the results of molecular modelling docking studies performed on the library of compounds formed from the standard bridged Ritter reaction, as discussed in depth in Chapter 7. This highlighted the way that greater control over the R₁ and R₂ functionality could be utilised to design more potent AChE inhibitors.

Only one instance of this type of one-pot mixed Ritter reaction has been reported by Samanieg *et al.*^[142] with the reaction of (-)-β-pinene with acetonitrile and benzonitrile. Although the reaction was reported to be successful, the characterisation data reported was ambiguous and only one product, with the phenyl group at C-4 and acetamide at C-6, was

isolated. This method also used perchloric acid and as such, it is worth investigating the reaction outcome using sulfuric acid.

2.4.1 Outcomes of the Controlled Mixed Ritter Reaction

The controlled mixed Ritter reaction was attempted, starting from the methyl-imino-alkene **(+)-60l** and the phenyl-imino-alkene **(+)-60n**, with benzonitrile and acetonitrile, respectively, as shown in Scheme 2.40. Theoretically, the acidic conditions should re-generate the carbocation **72** seen in the proposed mechanism in Scheme 2.24, however, it is unclear if this happens at all. Upon workup of these reactions, only the starting material was recovered. It, therefore, seems unfeasible to use a controlled mixed Ritter type reaction to selectively introduce $-R_2$ functionality through the addition of an amide to C-6 of the imino-alkene scaffolds.



Scheme 2.40 Attempted controlled mixed Ritter reactions.

2.4.2 Outcomes of the One-Pot Mixed Ritter Reaction

The one-pot mixed Ritter reaction was first attempted with acetonitrile and benzonitrile using the standard bridged Ritter reaction conditions, with the only adjustment being the molar ratio of nitrile to (-)- β -pinene. For the bridged Ritter reaction with a single nitrile, a seven mole equivalent excess of nitrile to (-)- β -pinene was used and for the reactions containing two nitriles, the ratio for each nitrile was three and a half times the mole equivalent of (-)- β -pinene, keeping the total nitrile to (-)- β -pinene ratio the same. GC-MS analysis of the crude products identified the formation of each of the expected products, based on known retention time and m/z , from either nitrile as determined from the standard bridged Ritter reaction, as well as two additional products. These additional products had the expected m/z and fragment patterns of the mixed products.

For the acetonitrile and benzonitrile mixture, the m/z 298 was found at 22.526 and 22.937 minutes, corresponding to the molecular formula $[\text{C}_{19}\text{H}_{26}\text{N}_2\text{O}]^+$. Each of these products was isolated using silica column chromatography, with the mobile phase used favouring the mixed Ritter products, as the others had already been characterised. Compound **(+)-79**

contained $-\text{CH}_3$ at the C-4 substituent and $-\text{Ph}$ at the C-6 amide substituent, of which 122 mg was isolated, a total yield of 6%. This product was then characterised by ^1H and ^{13}C NMR and the HRMS showed the $[\text{M}+\text{H}]^+$ exact mass of compound **(+)-79** to be 299.2119, corresponding to the molecular formula $\text{C}_{19}\text{H}_{26}\text{N}_2\text{O}$. The opposite mixed product, compound **(+)-80**, with $-\text{Ph}$ at the C-4 substituent and $-\text{CH}_3$ at the C-6 amide substituent, was isolated with 133 mg, 7% total yield. This product was characterised by ^1H and ^{13}C NMR and the HRMS showed the $[\text{M}+\text{H}]^+$ exact mass of compound **(+)-79** to be 299.2118, corresponding to the molecular formula $\text{C}_{19}\text{H}_{26}\text{N}_2\text{O}$. In addition, analysis by X-ray crystallography was carried out, after suitable single crystals were grown from ethyl acetate/hexane. The X-ray structure of **(+)-80** can be seen in Figure 2.9. The isolation of both mixed Ritter products suggests that the sulfuric acid conditions used are relatively more ideal for the formation of mixed Ritter products than that using perchloric acid as reported by Samanieg *et al.*^[142]

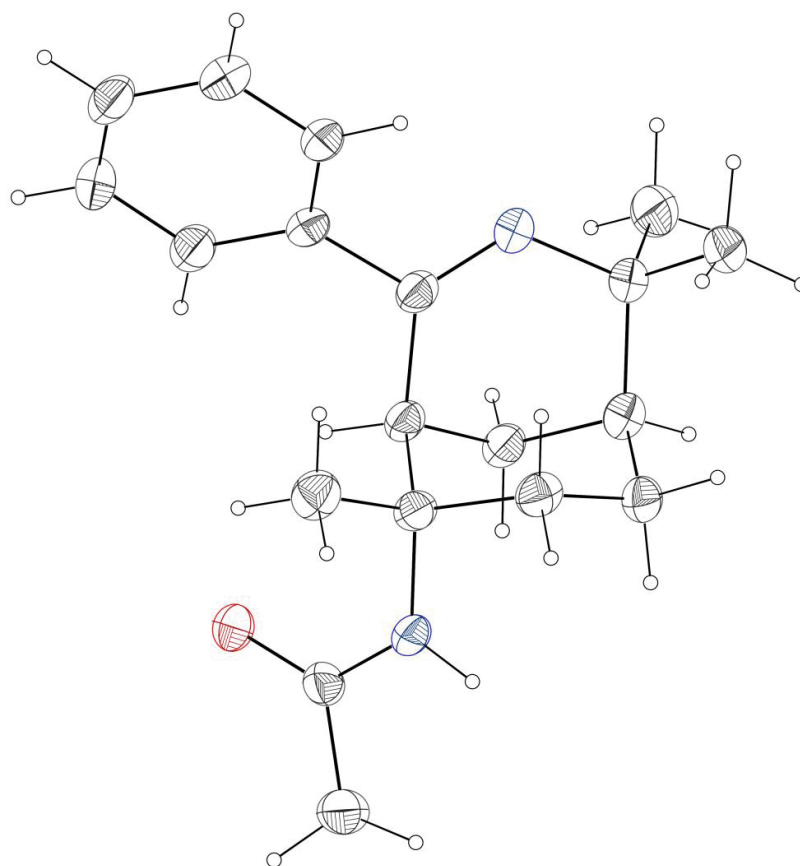


Figure 2.9 ORTEP diagram of the crystal structure of compound **(+)-80**.

The second one-pot mixed Ritter reaction was attempted using propionitrile and benzonitrile. This reaction was also successful at generating the mixed bridged Ritter products as identified by the m/z 312 corresponding to $[\text{C}_{20}\text{H}_{28}\text{N}_2\text{O}]^+$ as detected at 23.027 and 23.246 minutes by GC-MS analysis. Purification of these products was more challenging than that of

the reaction with acetonitrile and benzonitrile and only mixed product **81** was able to be isolated of sufficient purity for characterisation by ^1H NMR, ^{13}C NMR and HRMS. Purification was made significantly more challenging due to the presence of benzamide in the sample, despite efforts to remove this impurity *via* recrystallization, extraction and flash chromatography. Even when the molar ratio of nitrile used was lowered to 2.1 mole equivalent of (-)- β -pinene, to avoid the reaction occurring with the remaining excess nitrile, the hydrolysis of benzonitrile to benzamide remained the dominant reaction. The mixed product **82** was able to be partially characterised by characteristic features identified in the ^1H NMR spectrum, such as the aromatic peaks at δ 7.83 and 7.37-7.35 ppm, the amide NH singlet at 5.37 ppm, the C-5 bridge-head singlet at 4.34 ppm and the ethyl CH_3 triplet ($J = 7.5$ Hz) at 1.18 ppm. The C-1 and C-5 CH peaks could also be identified in the ^{13}C NMR spectrum at δ 34.5 and 34.1 ppm, respectively. The HRMS showed the $[\text{M}+\text{H}]^+$ exact mass of compound **82** to be 313.2274, corresponding to the molecular formula $\text{C}_{20}\text{H}_{28}\text{N}_2\text{O}$.

The ^1H NMR spectrum showed that the sample of compound **82** isolated contained significant quantities of its opposite corresponding mixed product **81**, even after multiple attempts to purify the product. The similarity in retention factors that resulted in co-elution could be due to these isomers having the same theoretical polar surface area. The complex nature of these mixtures and resulting challenging purification required, led to the crude samples of all the one-pot mixed Ritter reactions attempted after being analysed to determine if it would be feasible to separate and isolate the mixed bridged Ritter products. Table 2.3 lists all of the nitrile combinations performed with the one-pot mixed bridged Ritter reaction.

Each of the reaction's crude samples were analysed by GC-MS and GC-FID to detect the formation of the mixed products to determine the percentage composition of the crude mass of each of the products, respectively. Despite having the same molecular weight and hence m/z , the mixed products could be identified by their fragmentation patterns. Most significantly, the fragment resulting from the cleaving of the C-N bond of the amide at C-6 leaves the core structure with the mass of the alkene corresponding to the nitrile giving the C-4 functionality. This was used to determine the order of elution from the GC column.

The mixed bridged Ritter reaction outcome of acetonitrile and benzonitrile is shown below as an example of how the constitutional isomers were identified and differentiated. Figure 2.10 shows the mass fragment pattern for the GC elution detected at 22.562 minutes (Figure 2.12). This was identified as compound **(+)-80** by the molecular ion m/z 298 and the fragment m/z 239, corresponding to the mass of the fragment containing the phenyl group at

C-4, that occurs when the amide bond is cleaved (Figure 2.10). The opposite is seen for the GC elution detected at 22.937 minutes, which was identified as compound **(+)-79**, where the molecular ion m/z 298 is present and so is the fragment m/z 177, corresponding to the mass of the fragment with $-CH_3$ functionality at C-4 (Figure 2.11).

Abundance

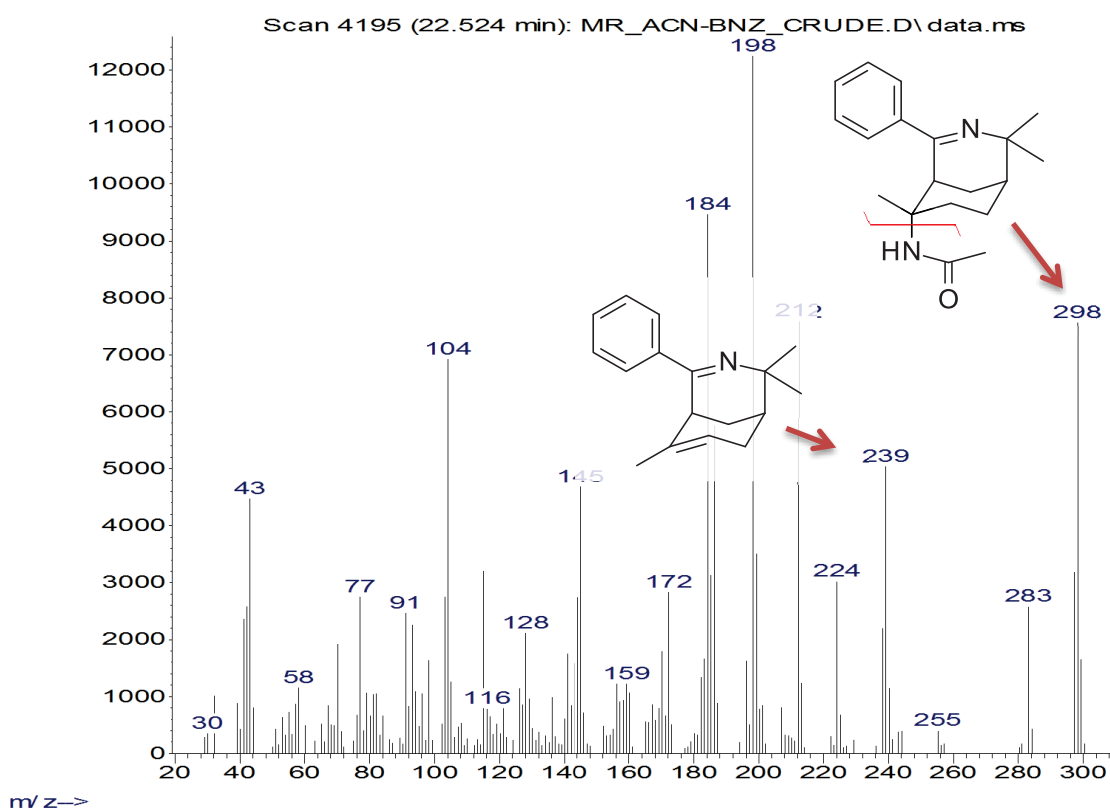


Figure 2.10 Mass spectrum for the mixed product **(+)-80**, showing the identifying fragment.

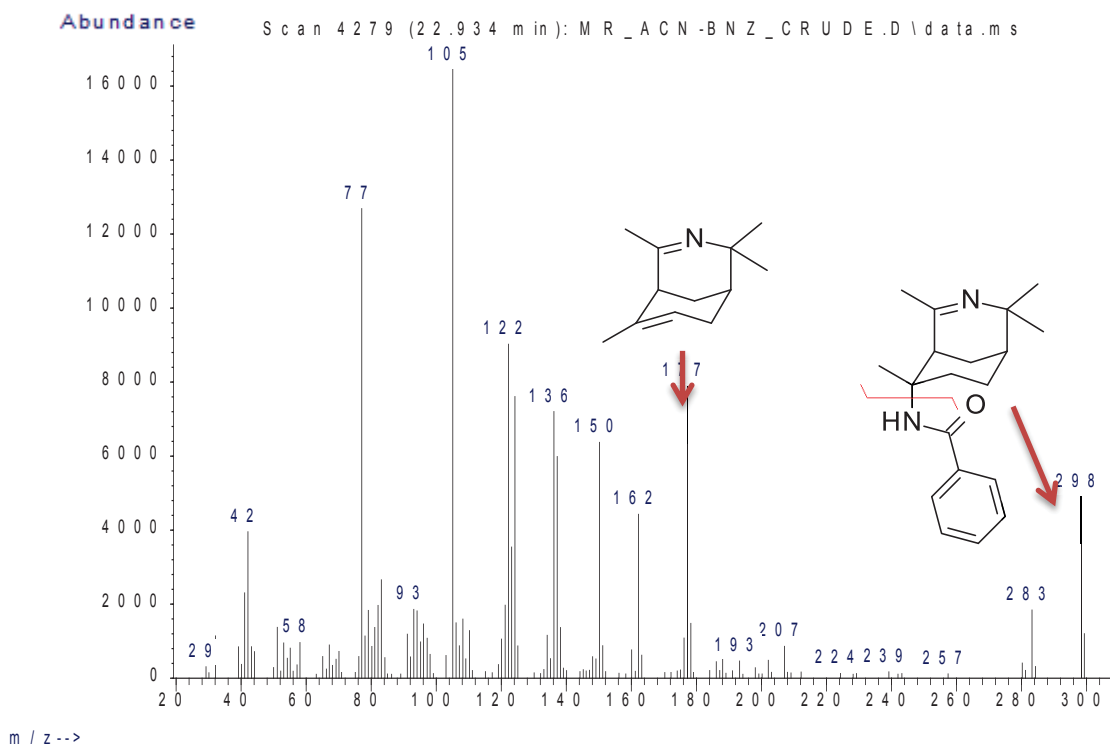


Figure 2.11 Mass spectrum for the mixed product (+)-79, showing the identifying fragment.

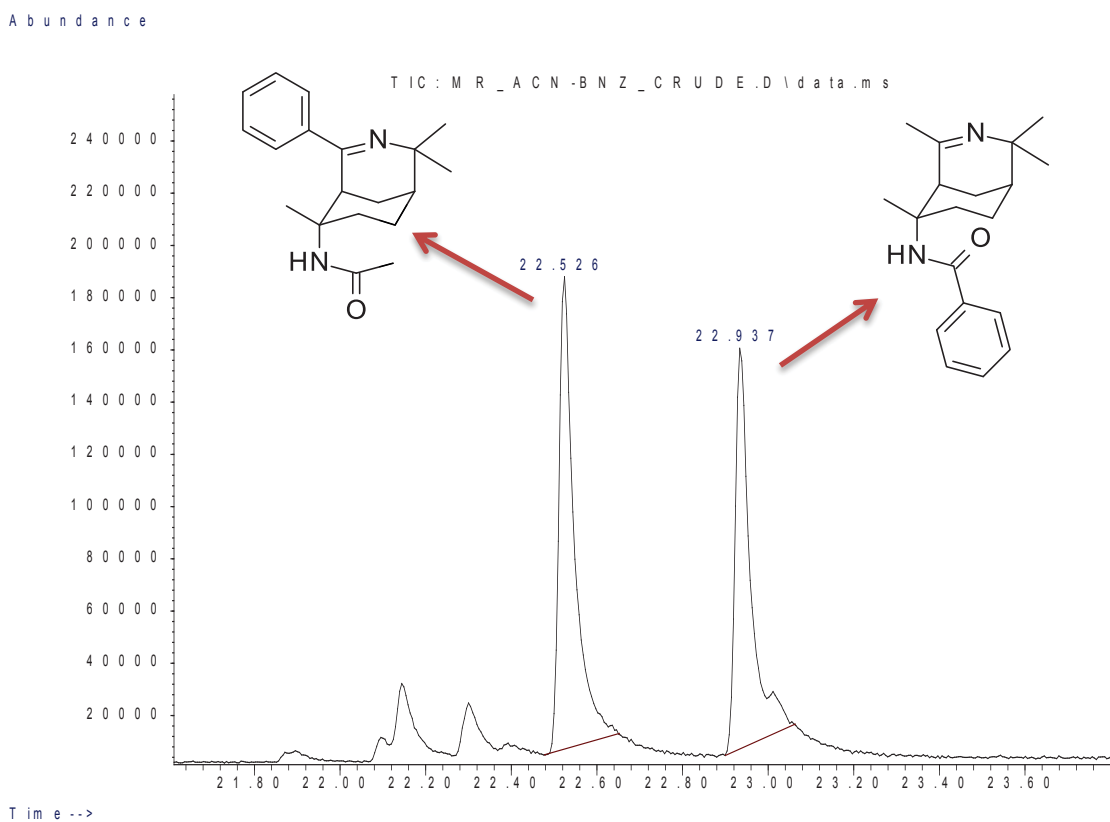
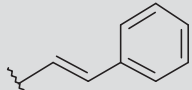
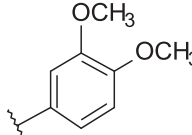
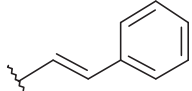


Figure 2.12 TIC chromatogram for the mixed bridged Ritter products of acetonitrile and benzonitrile.

As can be seen in Table 2.3, the mixed bridged Ritter products were detected and identified by their mass spectrum. Each of these products made up less than 10% of the crude mixture, with the exception of those formed from acetonitrile and propionitrile, with which a maximum of 15% observed for compound **83**. This analysis showed that all of these reactions resulted in a similar composition of mixed bridged Ritter products to those which had already been attempted to be purified, so the purification was deemed unsuitable due to the time constraints of this project. This could be investigated in future studies if the reactions could be optimised, as well as revisiting the reaction condition used by Samanieg *et al.*^[142] It was evident, however, that it is possible to form mixed Ritter products and utilise them for generating a diverse number of derivatives, as will be discussed in Chapter 3.

The results obtained from the analysis of these crude reaction mixtures also provided information about the behaviour of nitriles. Although further work would be required to confirm the trends, it appears that the larger bulky nitriles can react to give the corresponding C-6 amides when paired with a small nitrile at C-4. The formation of C-6 amides with cinnamitrile and 3,4-dimethoxybenzotrile was not observed when used as the sole nitrile in the bridged Ritter reaction with (-)- β -pinene.

Table 2.3 Nitrile combinations attempted with the one-pot mixed bridged Ritter reaction.

Reaction nitriles	Crude mass (g)	R ₁	R ₂	P4	P6	Comp. no	% of crude
Acetonitrile / Benzonitrile	1.5319	-CH ₃	-Ph	R ₁	R ₂	(+)-79	6.4
				R ₂	R ₁	(+)-80	6.7
Acetonitrile / Propionitrile	1.4524	-CH ₃	-CH ₂ CH ₃	R ₁	R ₂	84	10.3
				R ₂	R ₁	83	15.1
Acetonitrile / Chloroacetonitrile	0.7854	-CH ₃	-CH ₂ Cl	R ₁	R ₂	85	5.0
				R ₂	R ₁	86	6.0
Acetonitrile / Valeronitrile	1.5227	-CH ₃	-CH ₂ CH ₂ CH ₂ CH ₃	R ₁	R ₂	87	6.1
				R ₂	R ₁	88	5.6
Acetonitrile / Cinnamonitrile	0.6348	-CH ₃		R ₁	R ₂	89	7.2
				R ₂	R ₁	90	2.3
Acetonitrile / 3,4-Dimethoxybenzonitrile	1.8897	-CH ₃		R ₁	R ₂	91	7.2
				R ₂	R ₁	92	8.1
Propionitrile / Benzonitrile	1.8341	-CH ₂ CH ₃	-Ph	R ₁	R ₂	82	8.8
				R ₂	R ₁	81	7.6
Propionitrile / Chloroacetonitrile	0.7222	-CH ₂ CH ₃	-CH ₂ Cl	R ₁	R ₂	93	9.7
				R ₂	R ₁	94	2.9
Propionitrile / Valeronitrile	1.7537	-CH ₂ CH ₃	-CH ₂ CH ₂ CH ₂ CH ₃	R ₁	R ₂	95	7.0
				R ₂	R ₁	96	9.1
Propionitrile / Cinnamonitrile	0.4675	-CH ₂ CH ₃		R ₁	R ₂	97	2.3
				R ₂	R ₁	98	1.7
Benzonitrile / Chloroacetonitrile	2.3937	-Ph	-CH ₂ Cl	R ₁	R ₂	99	1.5
				R ₂	R ₁	100	4.8

2.5 Conclusions and Future Directions

In summary, the bridged Ritter reaction is a viable method for generating a chemically diverse library of optically pure alkaloid-like molecules. The nitriles used have the greatest influence on the outcome of the reaction and scaffold type obtained, as well as providing a versatile range of functional groups containing the 3-azabicyclo[3.3.1]non-3-ene core. Most notably, the more electron donating the nature of the group adjacent to the nitrile, the higher the yields. The increase in nucleophilicity of the nitrile favours the affinity towards the carbocation reaction intermediate, leading to imino-amide products. When nitriles larger than benzonitrile are used, steric hindrance tends to favour the formation of the imino-alkene

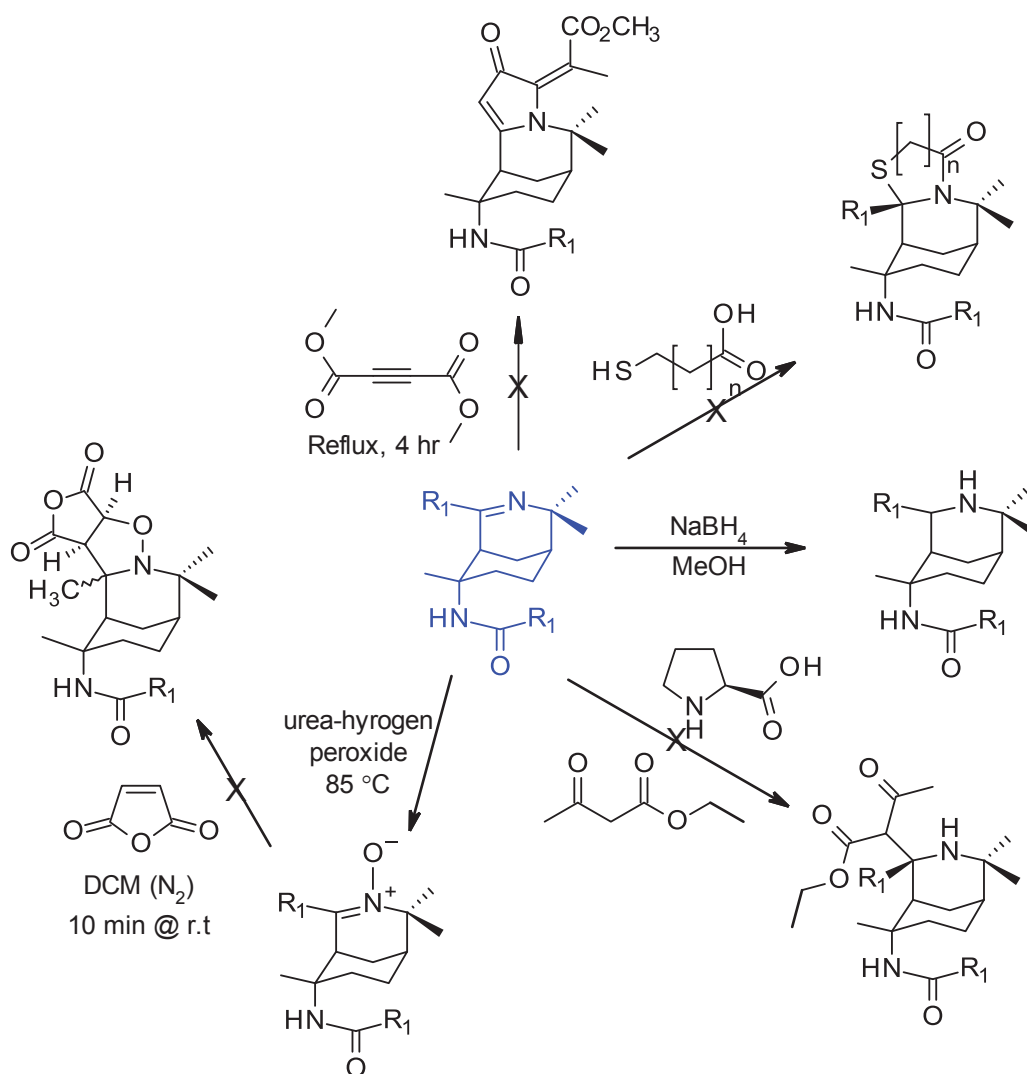
products. The conformation of the scaffold must also provide a steric hindrance effect by decreasing the ability of the nitrile to attack the carbocation.

Although additional structural diversity can be obtained by using two nitriles simultaneously in the bridged Ritter reaction, the yields of the mixed Ritter products are too low to obtain viable quantities of material for further investigation. This is, however, something that could be investigated in future work through the use of optimised purification techniques, such as preparative HPLC or preparative column chromatography, as well as through the exploration of alternative catalysts for the bridged Ritter reaction. This study has determined that the standard conditions reported are at this point the most optimum reaction conditions. For this reason, the nature of these alkaloid-like molecules can be explored in more depth through derivatisation of the 3-azabicyclo[3.3.1]non-3-ene core structure, as described in Chapter 3.

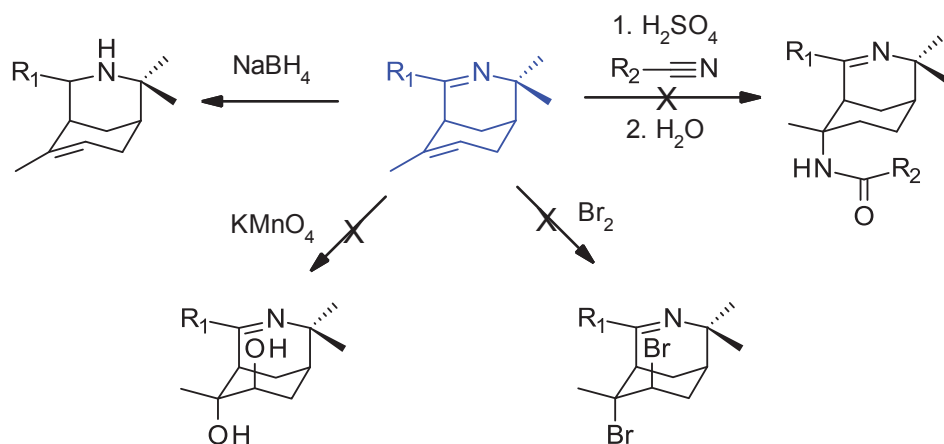
CHAPTER 3: Synthesis of Alkaloid-like Molecules *via* Derivatisation of 3-azabicyclo[3.3.1]non-3-enes

3.1 General Introduction

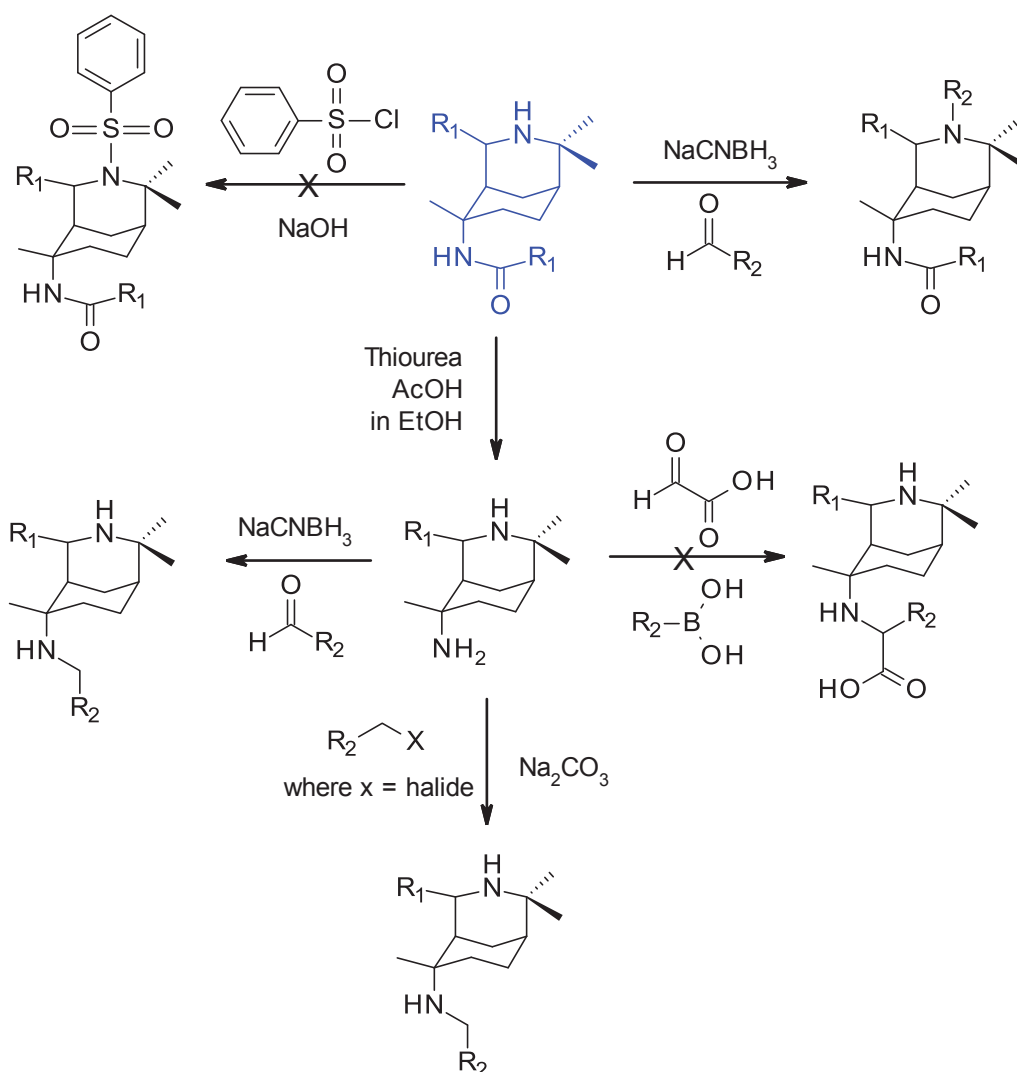
The 3-azabicyclo[3.3.1]non-3-enes products described in Chapter 2 contain functional groups that are capable of a wide range of reactions. This chapter describes several reactions for the derivatisation of the products obtained from the bridged Ritter reaction and the alkaloid-like molecules that were formed. Scheme 3.1 represents a range of reactions attempted *via* the imine functionality, while Scheme 3.2 summarises reactions attempted *via* the alkene functionality. Several secondary synthetic pathways were also explored *via* the corresponding amine scaffolds, as shown in Scheme 3.3.



Scheme 3.1 Scaffold derivatisation *via* the imine functionality.



Scheme 3.2 Scaffold derivatisation *via* the alkene functionality.

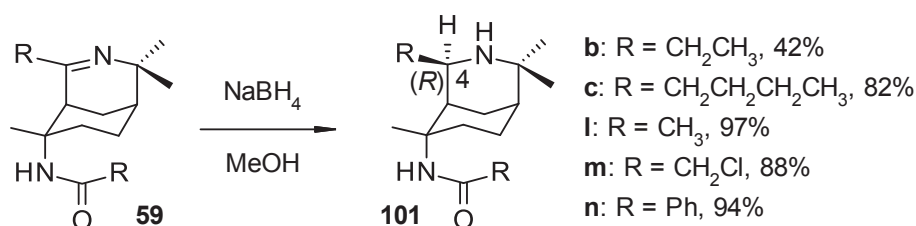


Scheme 3.3 Scaffold derivatisation *via* the amine functionality.

3.2 Reduction of Cyclic Imines

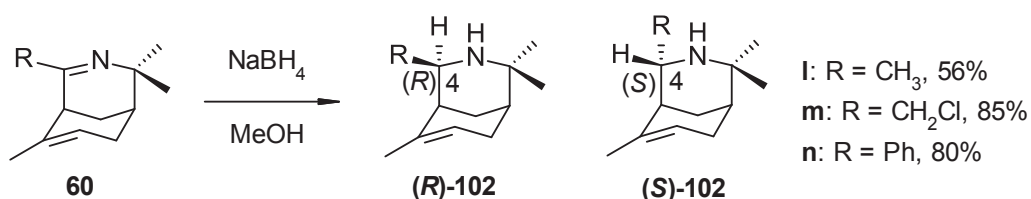
Both imino-amide (Scheme 3.4) and imino-alkene (Scheme 3.5) products prepared *via* the bridged Ritter reaction were reduced to the corresponding amine structures, using

NaBH₄.^[143] The imine bond of the imino-amides was reduced asymmetrically to give the (*R*)-stereocenter exclusively at C-4, with the substituent from the nitrile projecting forward from the *Re* face, as depicted for **101** in Scheme 3.4 and determined in each case by NOE NMR and optical rotation. This stereoselective outcome resulted from the imine bond being hindered by the cyclohexane ring that projects out from the *Re* face of the imine, only allowing for the hydride ion to approach from the *Si* face side. The amine compounds retain their optical activity, as indicated by the reported optical rotations.



Scheme 3.4 Reduction of imino-amide scaffolds to amino-amides.

Reduction of the imino-alkene (+)-**60l** resulted in a mixture of diastereoisomers. This non-facial selectivity of the hydride attack at C-4 was only observed, however, when the -R group was methyl. In this case, the (*R*)-diastereoisomer (-)-**102l** was the major product and the only isolated diastereoisomer. The presence of the (*S*)-diastereoisomer was observed in the GC-MS and NMR analysis of the crude product, in which the ratio between (*R*) and (*S*) was 4.5:1, with GC retention times of 11.1 and 10.7 minutes, respectively. The formation of the (*S*)-isomer was perhaps assisted by alkene-directed hydride reduction from the *Re* face of the imine bond.



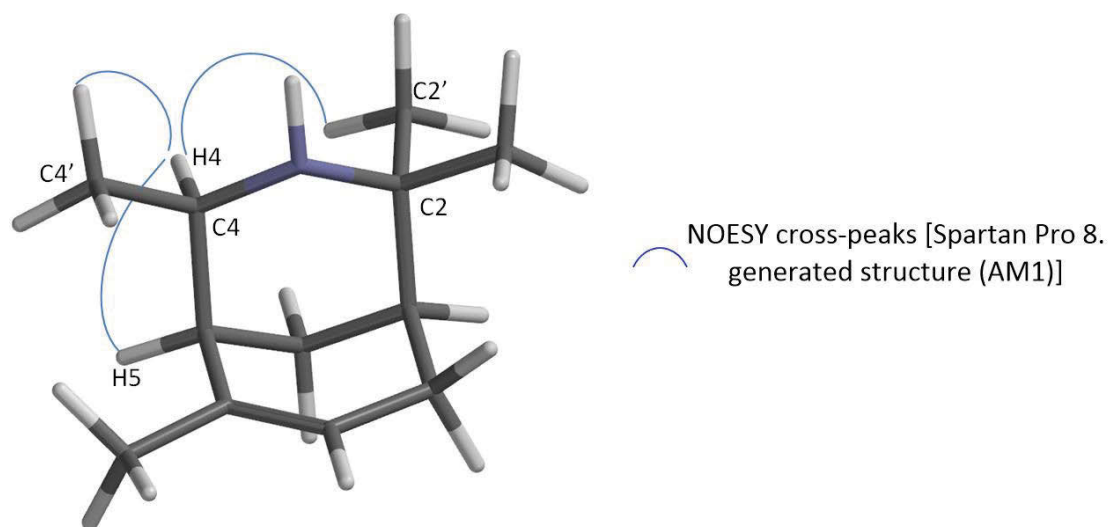
Scheme 3.5 Reduction of imino-alkene scaffolds to amino-alkenes.

Table 3.1 lists the corresponding amino-amides (**101**) and amino-alkenes (**102**) that were obtained stereospecifically, *via* hydride reduction using NaBH₄, with (*R*)-stereocentres at the C-4 position.

Table 3.1 Yields of amine-scaffolds obtained from the reduction of corresponding imines.

Entry	Imine Used	Amine Product	Yield (%)
1	(+)-59l	(+)-101l	97
2	(+)-60l	(-)-102l	56
3	(+)-59b	(+)-101b	42
4	(+)-59c	(+)-101c	82
5	(+)-59m	(+)-101m	88
6	(+)-60m	(-)-102m	85
7	(+)-59n	(+)-101n	94
8	(+)-60n	(-)-102n	80

^1H NMR showed two new resonances due to the formation of NH and H-4. For the new proton at H-4, proton resonance splitting depends on the R substituent, where consistency between the amide and alkene scaffolds is seen for the corresponding R group. For **(+)-101l** and **(-)-102l** (R = CH_3), the H-4 resonance is a quartet of doublets. For **(+)-101m** and **(-)-102m** (R = CH_2Cl), the H-4 resonance is a doublet of triplets. ^{13}C NMR showed the presence of an additional CH resonance, resulting from the conversion of C-4 from a quaternary to a tertiary carbon. The stereochemistry at C-4 was confirmed by 1D NOESY (Nuclear Overhauser Effect Spectroscopy) experiments, where the orientation of H-4 was determined by observing the resonance alteration caused by the NOE (Nuclear Overhauser Effect) when irradiated. Cross-peaks are observed between the H-4 and H-5 resonances and the H-4 and $\text{CH}_3\text{-}2\alpha$ resonances, indicating their spatial proximity of less than 3 Å and confirming that H-4 and H-5 are in the *syn* orientation, consistent with the molecular model of **(-)-102l** calculated using Spartan molecular modelling software (Figure 3.1). The spectral analysis of **(+)-101l** and **(+)-101b** and their respective single crystal X-ray structures (grown from $\text{CH}_2\text{Cl}_2/\text{hexane}$), unequivocally confirmed that C-4 is the (*R*)-stereocentre, with the hydrogen projecting away from the *Re* face of the ring and the substituent forward (Figure 3.2).

**Figure 3.1** NOESY correlations for compound **(-)-102l** generated by Spartan Pro 8. (AM1).

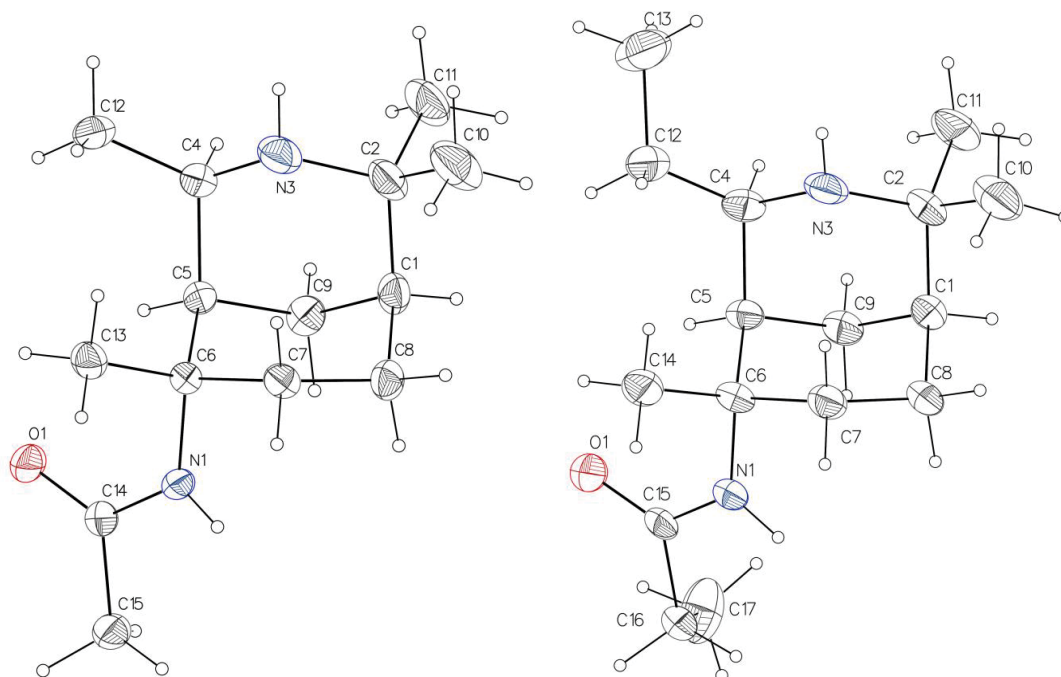


Figure 3.2 ORTEP diagram of **(+)-101I** (left) and **(+)-101b** (right), showing the configuration of stereocenter at C-4.

3.2.1 Crystal Packing of **(+)-101I** and **(+)-101b**

The X-ray analysis of compounds **(+)-101I** and **(+)-101b** revealed a remarkable similarity in the interactions involved in the packing of the molecules in crystals. Between the 2_1 screw related molecules, intermolecular hydrogen bonding was observed between the NH and C=O functionality of the amide groups at position 6 (N1-H1...O1) and two C-H...O contacts (one inter and one intra) between C=O and CH of either the amide CH₃ for **(+)-101I** or CH₂ for **(+)-101b** (Figure 3.3 (I) and (b), respectively). The geometry parameters of the H-bonding interactions are given in Table 3.2 and Table 3.3. It should be noted that no hydrogen bonding is observed from the amine NH (N3-H3), this can be accounted for by the methyl substituents on the adjacent carbons are crowding the nitrogen and hindering any possible interactions. This can clearly be seen in the space filling diagrams for **(+)-101I** and **(+)-101b** in Figure 3.4.

Table 3.2 Hydrogen-bond geometry for **(+)-101I**

<i>D</i> —H... <i>A</i>	<i>D</i> —H (Å)	H... <i>A</i> (Å)	<i>D</i> ... <i>A</i> (Å)	<i>D</i> —H... <i>A</i> (°)
N1—H1...O1'	0.88	2.13	2.973 (4)	161
C5—H5...O1	1.00	2.43	3.105 (5)	125
C16—H16B...O1'	0.99	2.37	3.280 (5)	152

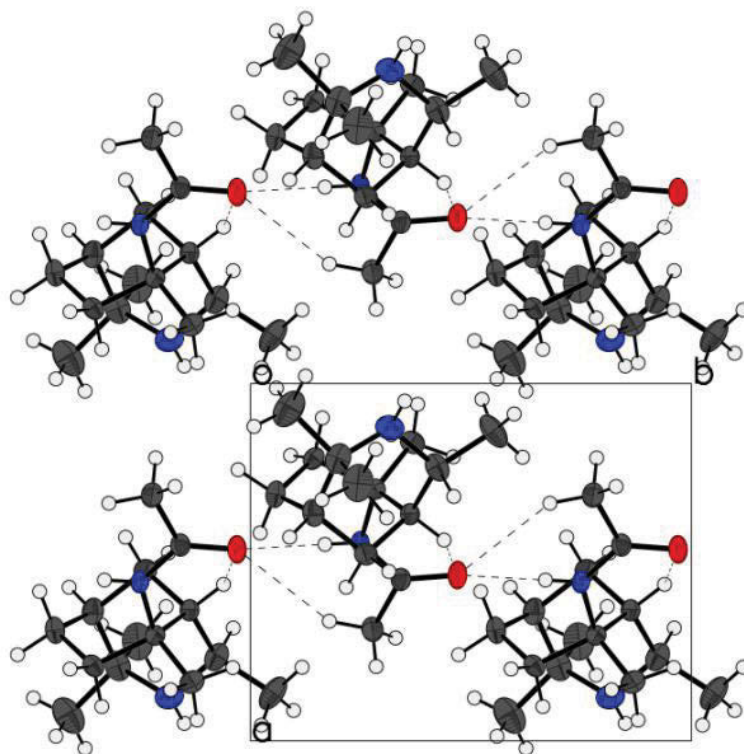
Symmetry codes: (i) $-x+2, y+1/2, -z+3$

Table 3.3 Hydrogen-bond geometry for (+)-101b

<i>D</i> —H··· <i>A</i>	<i>D</i> —H (Å)	H··· <i>A</i> (Å)	<i>D</i> ··· <i>A</i> (Å)	<i>D</i> —H··· <i>A</i> (°)
N1—H1···O1'	0.81 (3)	2.22 (2)	3.0097 (18)	166 (2)
C5—H5···O1	0.98 (2)	2.45 (2)	3.1140 (18)	124.8 (17)
C15—H15B···O1'	0.97 (3)	2.55 (3)	3.414 (2)	147.9 (19)

Symmetry codes: (i) $-x+1, y-1/2, -z+1$.

a)



b)

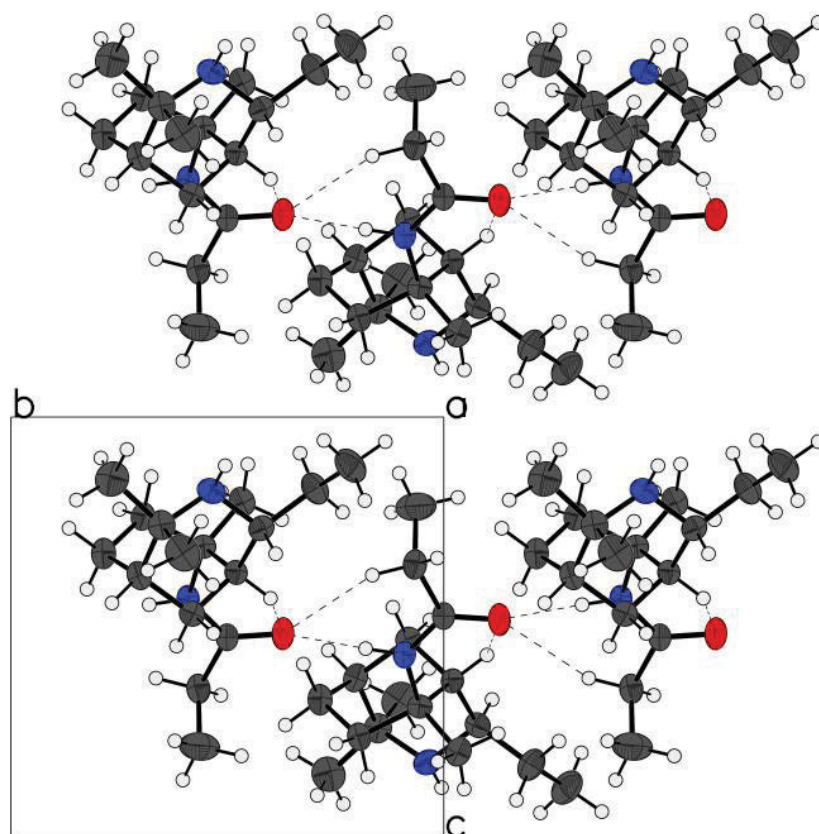


Figure 3.3 The NH----O=C and CH---O=C hydrogen bonding observed in the crystal structures of **a**, compound (+)-101a and **b**, compound (+)-101b.

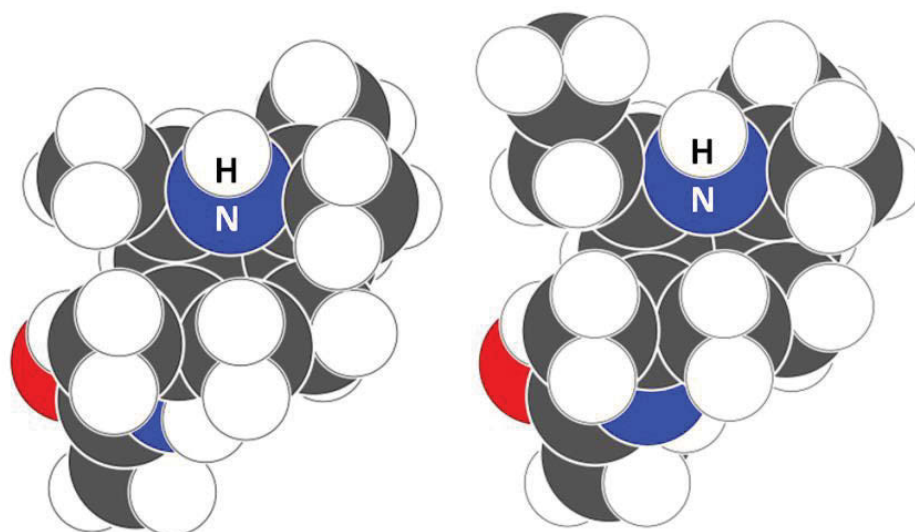
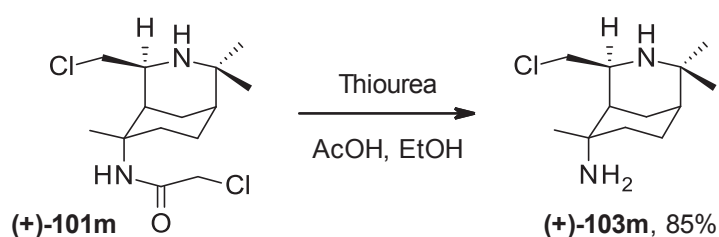


Figure 3.4 Space filling diagrams of **(+)-101l** (left) and **(+)-101b** (right), showing the crowding of the amine NH.

3.3 Amide Deprotection of **(+)-102m**

The diamine **(+)-103m** was obtained in one step from the amino-amide **(+)-101m** via amide deprotection (Scheme 3.6). The presence of the chloroacetamide functional group in **(+)-101m** makes the amide bond labile, allowing it to be hydrolysed under mild conditions to **(+)-103m** with 85% yield. The reaction was performed according to the method outlined by Torres *et al.*^[144] The cleavage of the amide bond was confirmed by the absence of the chloroacetamide CH₂ peak in the ¹H NMR spectrum. For compound **(+)-103m**, the HRMS showed the [M+H]⁺ exact mass to be 231.1618, corresponding to C₁₂H₂₄ClN₂ and the specific rotation was found to be $[\alpha]_D^{23} + 18.83$ (c 1.63, MeOH).



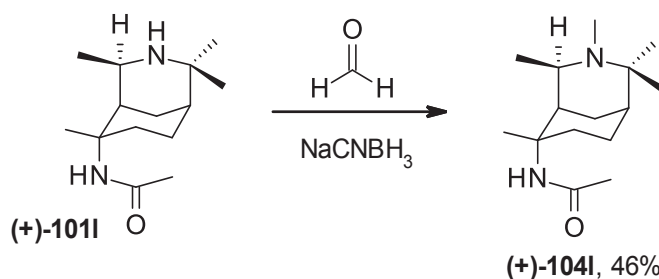
Scheme 3.6 Amide deprotection of amino-amide **(+)-101m** to diamine **(+)-103m**.

3.4 Reductive *N*-Alkylation of *N*-3 Amines

Reductive *N*-methylation was carried out on **(+)-101l** using the method described by Taylor *et al.*^[143] (Scheme 3.7) which gave **(+)-104l** in 46% yield. The reaction with **(+)-101l** was also attempted under the same reaction conditions with propionaldehyde, pentanaldehyde and benzaldehyde, while also attempted using **(-)-102m** and formaldehyde, but none of these reactions were successful and only starting material was recovered. These outcomes highlight the significance of the crowding of the amine at position NH-3 in the scaffold, as contributed by the three adjacent methyl groups, illustrated in the X-ray structures (Figure 3.2). The

hindered nature of NH-3 prevented access of the aldehydes and hence only formaldehyde could successfully react with **(+)-101I** to give **(+)-104I**.

The identity of compound **(+)-104I** was confirmed by NMR analysis. The ^1H NMR spectrum shows the newly formed $N\text{-CH}_3$ as a singlet at δ 2.07 ppm and the ^{13}C NMR shows the $N\text{-CH}_3$ at 33.74 ppm. The rest of the spectral features of **(+)-104I** are very similar to that of **(+)-101I**, with subtle changes in their chemical shifts. Most noticeably, the H-4 proton was shifted slightly upfield, while H-5 and H-1 were both shifted slightly downfield. The HRMS showed the $[\text{M}+\text{H}]^+$ exact mass to be 253.2276 which corresponds to the molecular formula $\text{C}_{15}\text{H}_{29}\text{N}_2\text{O}$. The specific rotation of compound **(+)-104I** was found to be $[\alpha]_{\text{D}}^{25} + 13.89$ (c 0.37, CHCl_3).



Scheme 3.7 Reductive N -methylation of amino-amide **(+)-101I** to **(+)-104I**.

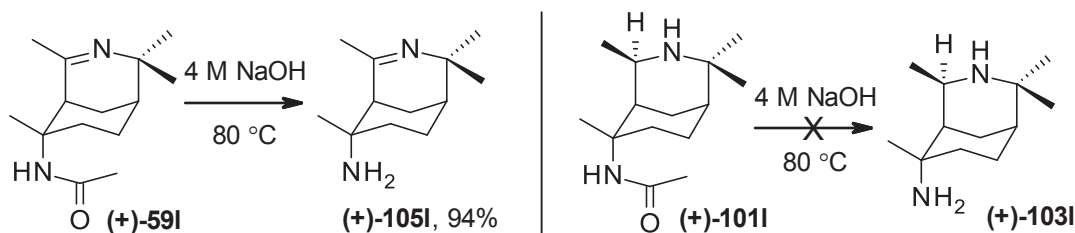
Other potential alternative reactions to alkylate the N-3 nitrogen would include $\text{S}_{\text{N}}2$ reactions with alkyl halides with a base stronger than sodium carbonate, because it was determined that there was no reaction with benzyl bromide and N-3 under the conditions used (Section 3.5.2.3). This was unable to be explored due to time constraints but is something that should be explored in future work.

3.5 Attempted Derivatisation Reactions

3.5.1 Amide Hydrolysis

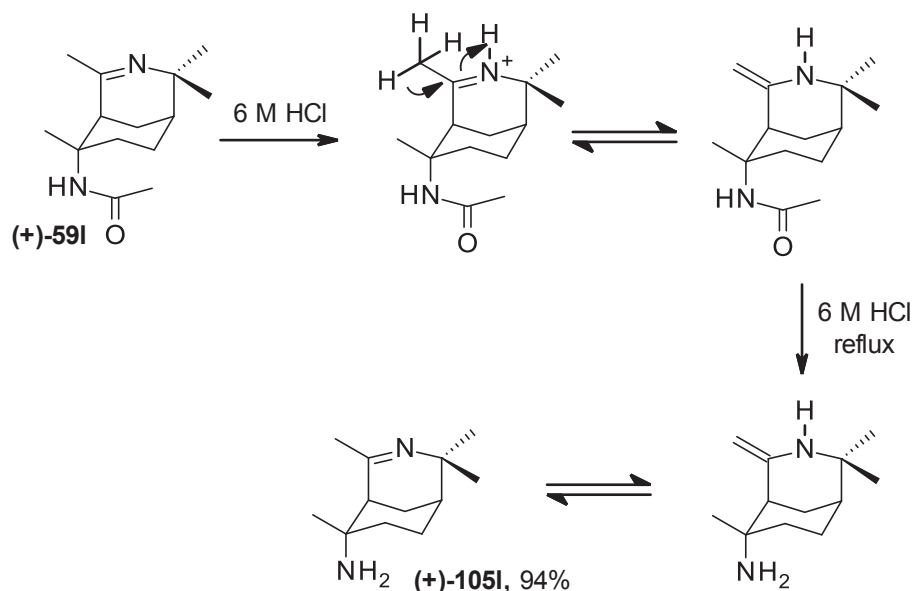
In order to derivatise C-6 of the 3-azabicyclo[3.3.1]non-3-enes scaffolds, the hydrolysis of the amides not containing the chloroacetamide functionality was attempted to give primary amines. Amine functionality at C-6 opens the scaffold up to a wide range of reactions and could be used as a synthetic pathway to structures important for developing a SAR understanding of this type of alkaloid-like compound. Two methods that are commonly reported include hydrolysis in basic NaOH solution^[145] and hydrolysis in acidic HCl solution.^[146]

The reaction under basic conditions was attempted with both **(+)-59I** and **(+)-101I** (Scheme 3.8) by dissolution in iso-butanol and placing in a glass pressure tube with 4 M NaOH at 80 °C where it was stirred for 3 days. For both of these reactions, only starting material was recovered, as confirmed by both ^1H NMR analysis and GC-MS.



Scheme 3.8 Expected outcome of the amide hydrolysis of (+)-59I and (+)-101I by NaOH.

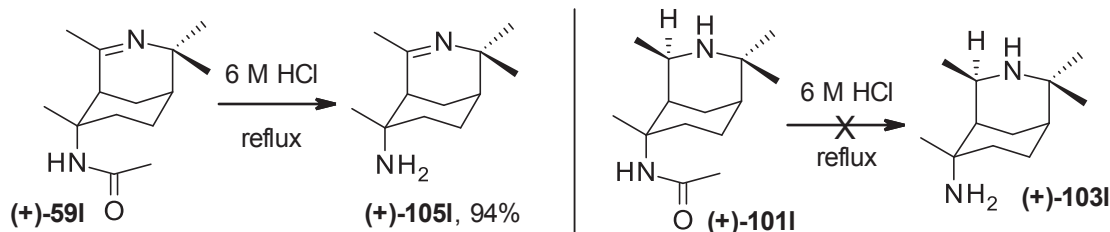
The reaction under acidic conditions was attempted with both (+)-59I and (+)-101I (Scheme 3.10) by heating at reflux in 6 M HCl overnight. The reaction with (+)-59I successfully gave a clean sample of compound (+)-105I as the hydrochloride salt and the free base was recovered in a respectable yield of 62%. The formation of (+)-105I was confirmed by NMR characterisation of the salt in D₂O and the free base in CDCl₃. For the free base, the two NH peaks were assigned as singlets at δ 5.34 and 3.15 ppm. NH stretches were also observed in the IR spectrum at 3362 and 3278 cm⁻¹. The HRMS showed the [M+H]⁺ exact mass to be 195.1859 which corresponds to the molecular formula C₁₂H₂₂N₂. The specific rotation was found to be $[\alpha]_{\text{D}}^{22} + 122.98$ (c 1.58, CHCl₃). It is believed that the imine bond was retained during this process due to the rearrangement that occurs to form the enamine under the acidic conditions (Scheme 3.9). It is commonly reported that this tautomerisation results in resistance to hydrolysis in HCl and boiling water.^{[147],[148]}



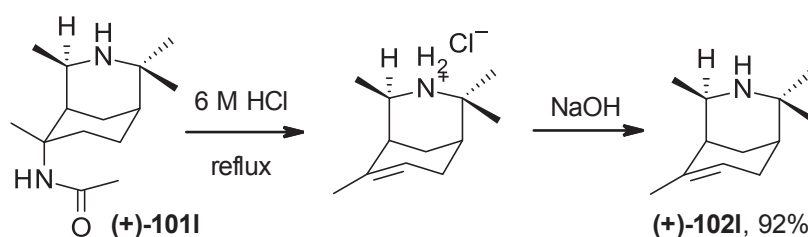
Scheme 3.9 Imine-Enamine tautomerisation that protects the imine from hydrolysis.

The reaction of (+)-101I, however, produced an interesting result and gave the chloride salt of the amino-alkene product (-)-102I instead of the expected di-amine (Scheme 3.11). This was confirmed by analysis with ¹H NMR and GC-MS of the free base (-)-102I, which

showed an identical spectrum and that the compound has the same retention time, 11.09 minutes and m/z at 179, as the (-)-102I obtained from the reduction of (+)-60I. It is possible that the alkene was formed due to *E1* elimination, such as that described by Lacey.^[149]

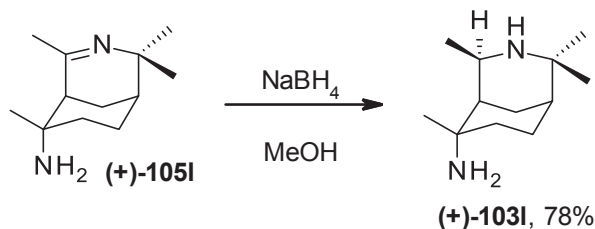


Scheme 3.10 Expected outcome of the amide hydrolysis of (+)-59I and (+)-101I by HCl.



Scheme 3.11 Actual outcome of the amide hydrolysis of (+)-101I by HCl.

Compound (+)-103I was eventually obtained by the hydride reduction of (+)-105I, as shown in Scheme 3.12, using the same method as in Section 3.2. Compound (+)-103I was isolated in a 78% yield. The newly formed CH-4 proton was assigned at δ 3.34 ppm as a characteristic quartet of doublets ($J = 7.5, 1.5$ Hz) in the ^1H spectrum with the corresponding ^{13}C resonance at 52.3 ppm. In the infrared spectrum, NH stretches were observed at 3429 and 3304 cm^{-1} , as was the primary amine NH bending at 1546 cm^{-1} . The HRMS showed the exact mass to be 197.2016 which corresponds to the molecular formula $\text{C}_{12}\text{H}_{25}\text{N}_2$. The specific rotation was found to be $[\alpha]_{\text{D}}^{22} +15.24$ (c 1.00, CHCl_3).



Scheme 3.12 The hydride reduction of (+)-105I to give (+)-103I.

3.5.2 N-6 Amine Derivatisation and Rational Drug Design

The N-6 amine is a useful synthetic handle for extension of the 3-azabicyclo[3.3.1]non-3-ane structure and is a primary point of rational drug development, mediated by molecular modeling, as outlined in Chapter 7. With the aim of introducing aromatic functionality capable

of interacting with the aromatic gorge of AChE, several aromatic aldehydes were investigated for their AChE docking affinity. The following section outlines several reactions attempted to investigate the validity of the compounds proposed and evaluated for their AChE docking properties in Chapter 7.

The amines **(+)-105l** and **(+)-103m** were used as a proof of concept for the reactions chosen for this derivatisation because they were relatively easy to obtain. This was attributed to quick isolation of the precursor amides *via* recrystallisation. Compound **(+)-105l** is more advantageous to use as it can be formed in two steps, as opposed to **(+)-103m** which requires three steps and therefore has a lower overall yield. The reactions used for the extension of the amine were reductive *N*-alkylation and the Petasis reaction.

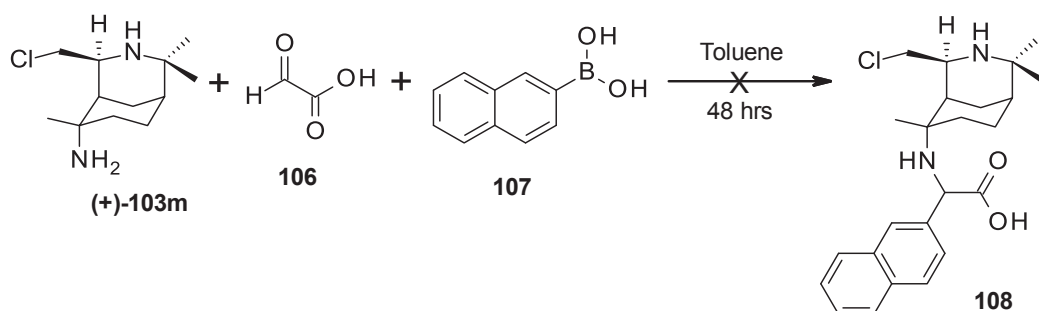
3.5.2.1 Petasis-Borono Mannich Multicomponent Reaction of **(+)-103m**

The Petasis reaction is a carbon efficient method of introducing the functionality from a boronic acid to an amine, linked *via* either an aldehyde or glyoxylic acid. This reaction was used to extend the functionality of the 3-azabicyclo[3.3.1]non-3-ene scaffold at the C-6 primary amine. Molecular modelling docking studies of the synthesised compounds listed in Chapter 2 showed that the N-3 region of the ring system pointed down into the catalytic triad of the AChE active site, while the C-6 substituent region points towards the gorge that leads into the active site.

As a result of this orientation, the primary amine functionality at C-6 allows for derivatisation whereby the scaffold is extended into the gorge providing improved interactions, as outlined in the molecular modelling Chapter 7. The Petasis reaction can utilise either glyoxylic acid or an aldehyde as a linker between the amine and boronic acid functionality so both scenarios were assessed. The molecular modeling docking studies identified that the structures obtained from using glyoxylic acid **106** yielded structures with better theoretical interaction scores than those from the aldehydes. For simplicity, only formaldehyde was considered as the linker carbon because the resulting product would have a CH₂ linker, as opposed to a chiral center. The smallest aldehyde would also provide the highest accessibility for reaction with the somewhat hindered C-6 amines. Another consideration for the Petasis reaction is the activation of the boronic acids based on the aromatic substituents because this will also affect the viability of products that can be formed.

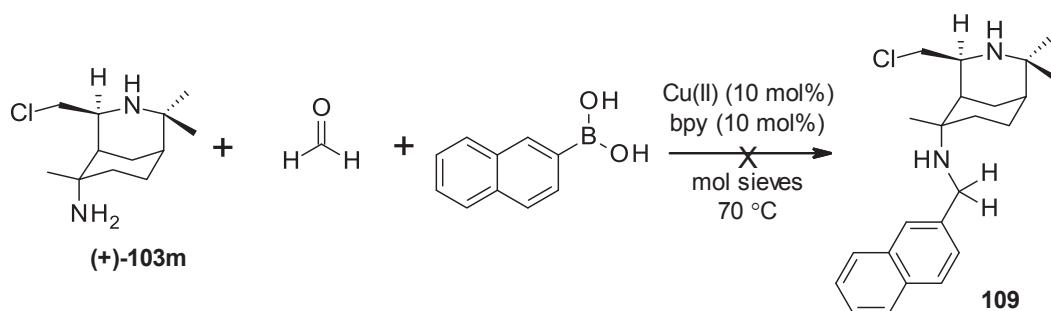
Docking was used to identify which of the boronic acids available in-house would give the best interactions. This was found to be 2-naphthylboronic acid **107** and, therefore, the

reaction was attempted between compound **(+)-103m**, glyoxylic acid and 2-naphthylboronic acid to give **108**, as shown in Scheme 3.13.



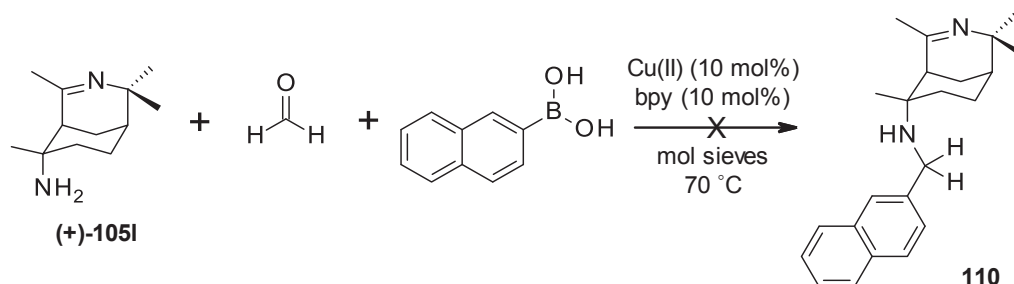
Scheme 3.13 Attempted Petasis reaction of **(+)-103m** with glyoxylic acid and 2-naphthylboronic acid.

Initially, the reaction was attempted using the conditions reported by Petasis *et al.*^[150] Upon workup, however, it was found that the reaction was unsuccessful and the starting material **(+)-103m** was recovered. The same reaction was attempted a second time using 4-biphenyl boronic acid, the second highest scoring compound with respect to the docking studies. Unfortunately, this reaction was unsuccessful and the starting material was recovered. For this reason, another attempt at the Petasis reaction was made, again using 2-naphthylboronic but with alternative reaction conditions, involving formaldehyde instead of glyoxylic acid, to give **109** as shown in Scheme 3.14. This reaction was unsuccessful and the starting material was recovered



Scheme 3.14 Petasis reaction of **(+)-103m** with formaldehyde and 2-naphthylboronic acid.

This method varied greatly from the glyoxylic acid method as it employed the use of copper (I or II) salts and 2,2'-bipyridine (bpy) as catalysts for the reaction, as outlined by Frauenlob *et al.*^[151] Unfortunately, this reaction was unsuccessful at forming the desired product. One last attempt at the Petasis reaction was made using the amine **(+)-105I** to give **110** (Scheme 3.15), but this proved unsuccessful and the starting material was recovered.

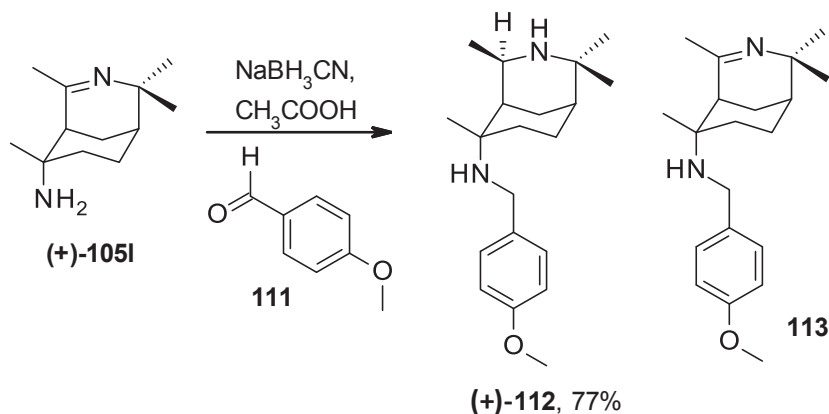


Scheme 3.15 Petasis reaction of **(+)-105I** with formaldehyde and 2-naphthylboronic acid.

3.5.2.2 Reductive *N*-alkylation of **(+)-105I** with *p*-anisaldehyde

A set of proposed compounds that would result from the alkylation of amines **(+)-105I** and **(+)-103m** with the aldehydes that were available in-house were docked. Of this set, *p*-anisaldehyde **111** was one of the aldehydes that resulted in the highest scoring product when used to alkylate **(+)-105I**. The alkylation was therefore performed using **(+)-103I** with the same reductive alkylation conditions as described in Section 3.4. This is expected to give compound **(+)-112**, as shown in Scheme 3.16. In practice, it was found that after leaving the reaction overnight both imino-amine **113** and amino-amine **(+)-112** in Scheme 3.16 were formed. This is attributed to the weakly reductive nature of the sodium cyanoborohydride which only partially reduced the N-3 imine. The use of different reaction times or molar ratios of reducing agents could be investigated in future work in order to determine the reduction reaction kinetics and to obtain a crude reaction mixture with different ratios of imine to amine products. Varying the ratios of imine to amine products would be very difficult to control but would yield useful results, as the retention of the N-3 imine is also desirable, as shown by the docking score of compound **113** listed in Chapter 7 in Table 7.4. Furthermore, it would also allow for a greater understanding of the SAR properties to be developed.

Although this reaction was investigated for the derivatisation of the N-6 amine, the N-3 amine formed under the reductive conditions was not expected to also be alkylated after previous attempts at this in Section 3.4 were shown to be unsuccessful. This was confirmed to be the case as only **(+)-112** and **113** were obtained. The bulky nature of the benzylic secondary amine formed also provides steric hindrance that favours only mono-alkylation of the primary amine.

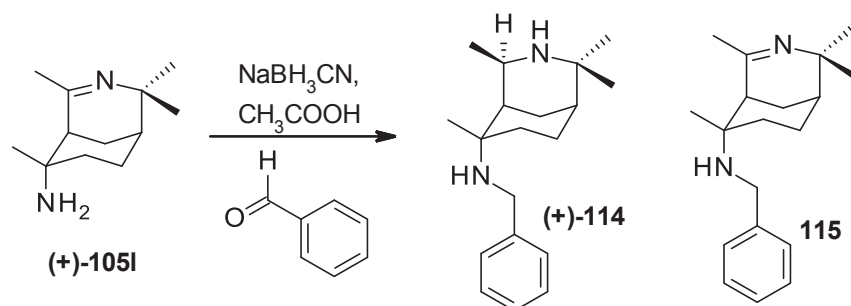


Scheme 3.16 Reductive *N*-alkylation of 6-*N* amine **(+)-105I** with *p*-anisaldehyde.

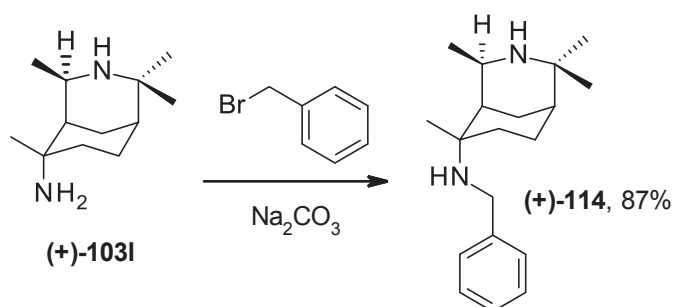
As expected, compound **(+)-112** was the major and only product that was able to be isolated, although **113** was detected in trace amounts in the crude product by analysis with GC-MS, eluting at 24.362 minutes with m/z 314. Compound **(+)-112** eluted from the GC at 24.074 minutes (m/z 316) and was isolated from column chromatography with a 77% yield. Spectroscopic analysis confirmed the identity of **(+)-112**, with the ¹H NMR spectrum showing the characteristic quartet of doublets splitting ($J = 7.0$ and 2.5 Hz) of the C-4 proton at δ 3.51 ppm, indicating the reduction of the imine to the N-3 amine. New resonances were also assigned, firstly doublets ($J = 8.5$ Hz) at δ 7.28 and 6.86 ppm for the aromatic hydrogens, secondly the benzylic CH₂ as a doublet of doublets ($J = 8.5$ and 12.0 Hz) at 3.58 ppm and lastly the methoxy CH₃ as a singlet at 3.80 ppm. The HRMS showed the $[M+H]^+$ exact mass to be 317.2587 which corresponds to the molecular formula C₂₀H₃₃N₂O. The specific rotation was found to be $[\alpha]_D^{22} +7.64$ (c 1.00, CHCl₃).

3.5.2.3 Reductive *N*-alkylation of **(+)-105I** with Benzaldehyde

Compound **(+)-105I** was reacted with benzaldehyde to give the expected product diamine **(+)-114**. The same reaction time and mole ratio of **(+)-105I** to sodium cyanoborohydride, as was used for the reaction with *p*-anisaldehyde, was attempted. It was again found that the imine product **115** was also formed but in a higher ratio to its counterpart **113** (Scheme 3.17). In comparison, **113** was formed in only trace amounts, while the ratio of **115** to **(+)-114** was determined to be 1:2 as shown by analysis of the crude product by GC-MS where **115** eluted at 7.984 minutes, with m/z 284, while compound **(+)-114** was eluted at 7.884 minutes, with m/z 286. Exact masses were also confirmed with HRMS. Unfortunately, these compounds were unable to be isolated by chromatography. A direct method *via* S_N2 *N*-alkylation of **(+)-103I** was therefore used as an alternative approach to selectively obtain **(+)-114**, as shown in Scheme 3.18.

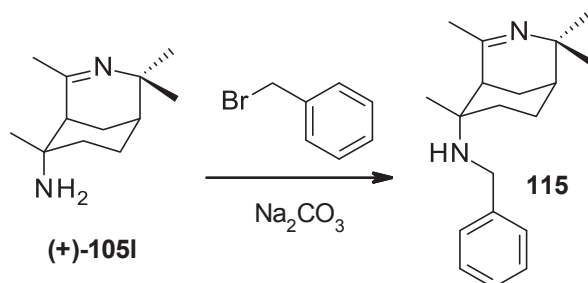


Scheme 3.17 Reductive N-alkylation of 6-N amine (+)-105I with benzaldehyde.



Scheme 3.18 Reaction of (+)-103I with benzyl bromide.

Compound (+)-114 was synthesised and purified to give an isolated yield of 87% as a light brown wax. The newly formed benzylic CH₂ peaks were assigned at δ 3.70 ppm as a doublet ($J = 12.0$ Hz) in the ¹H NMR spectrum, while the corresponding ¹³C peak was assigned at 46.0 ppm. The HRMS showed the [M+H]⁺ exact mass to be 287.2491 which corresponds to the molecular formula C₁₉H₃₁N₂. The specific rotation was found to be $[\alpha]_D^{22} + 15.90$ (c 1.58, CHCl₃). This type of reaction also provides a synthetic pathway to selectively provide the corresponding imine product 115, as shown in Scheme 3.19, but due to time constraints, this reaction will need to be investigated further in future work.



Scheme 3.19 Potential proposed reaction of (+)-105I with benzyl bromide.

The C-6 amines synthesised were considerably challenging to characterise due to the doubling of certain NMR resonances that result from the enantiomers of the nitrogen chirality that occurs in solution as a result of nitrogen inversion.^[152]

3.5.3 Alkene Reactions

As outlined in Section 2.4.1, attempts to react isolated alkenes with a second alternative nitrile under the standard bridged Ritter reaction conditions were unsuccessful. The alkene was also unreactive towards bromination and hydrolysis. The stable nature of the alkene supports the mechanism suggested (Scheme 2.24) for its increase in yield with longer reaction times. It may also indicate that there is a degree of hindrance of the alkene bond, making it less susceptible to electrophilic addition or dihydroxylation.

It was hypothesised that these alkenes are significantly stable due to a resonance stabilised-like phenomenon where the double bond π -electrons are distributed across the carbons from C-6 α to C-7. A similar observation was described in the work of Mirand *et al.*,^[29] where these bonds are in fact represented as resonance bonds, as shown in Figure 3.5 for **(+)-60l**. Interestingly, all of the imino alkenes synthesised, with the exception of **(+)-60m**, were observed to exist only as the internal alkene, as characterised by the C-6 α CH₃ and C-7 CH resonances in the NMR spectra. In the case of **(+)-60m**, resonances for the terminal 'external' alkene **117**, as well as the internal alkene **(+)-60m** (Scheme 3.20), can be seen in the hydrogen NMR. The ¹H NMR spectrum of the terminal alkene C-6 α CH₂ resonances were assigned as two triplets ($J = 2.0$ Hz) at δ 4.84 and 4.75 ppm, while the internal alkene C-7 CH resonance was assigned as a singlet at 5.37 ppm.

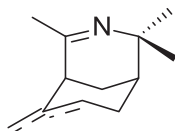
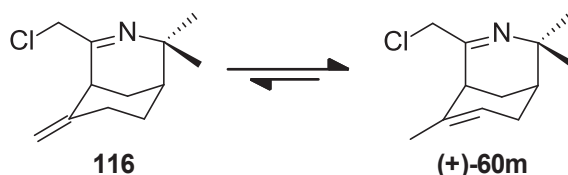


Figure 3.5 Imino-alkene **(+)-60l** with the alkene bond represented as a resonance stabilised structure.

In the case of **(+)-60m**, it was found that the external alkene is converted to the internal alkene over time and most probably exists as an equilibrium that favours the energetically stable internal alkene isomer, as shown in Scheme 3.20. This is in agreement with the hypothesis that there may be some degree of resonance effect occurring. This was also shown by energy calculations performed using the software Spartan'08 V1.0.0 (WAVEFUNCTION INC), which calculated the enthalpy of formation (ΔH_f) for the internal and external alkenes to be 17.16 and -4.00 kJ/mol respectively. It is assumed that this is only observed for **(+)-60m** due to the electronegative nature of the chloromethyl substituent.

Further investigation as to whether the rate or direction of this conversion could be controlled by temperature was carried out using variable temperature proton NMR

experiments. No measurable difference in the integral values was observed at each temperature within the tested range. This is depicted in Figure 3.6, where the ratio of the two isomers at each temperature was 9:1, internal to external alkene, as determined by the integral data.



Scheme 3.20 Conversion of the internal alkene **116** into the internal alkene **(+)-60m**.

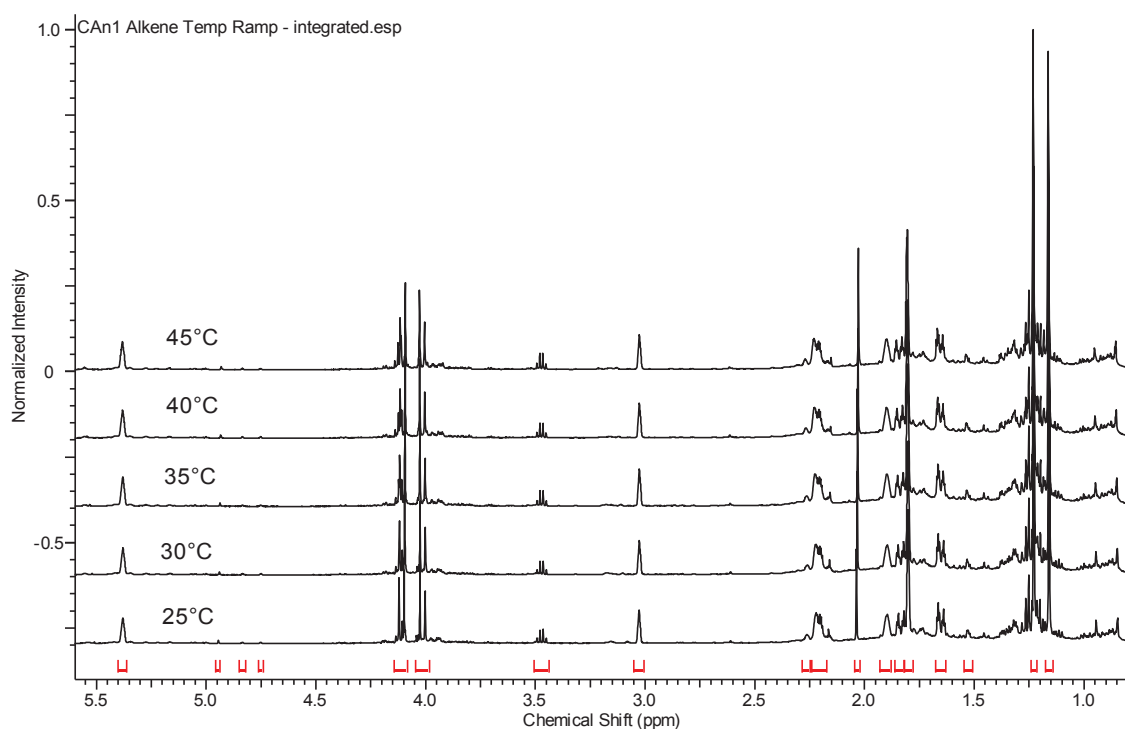
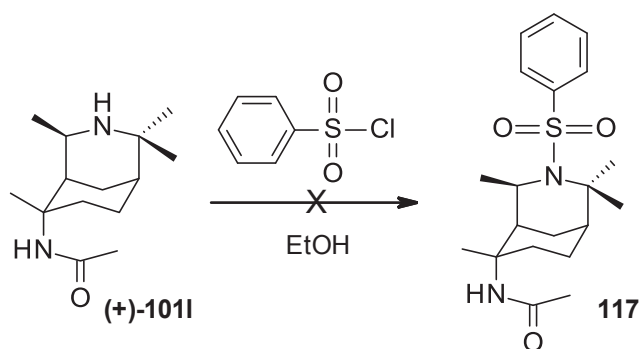


Figure 3.6 Overlaid ^1H NMR spectra of **(+)-60m** at 5 °C temperature intervals to observe a change in integral values of the C-7 CH and C-6 α CH $_2$ resonances.

3.5.4 Reaction of **(+)-101I** with Benzenesulfonyl Chloride

The reaction of **(+)-101I** with benzenesulfonyl chloride was attempted using the method by Jafarpour *et al.*,^[153] as shown in Scheme 3.21, to give **117**. The interest in using this reaction stems from the pronounced biological activities reported for sulphonamides, particularly as anticancer, anti-inflammatory and antiviral compounds.^[154] The introduction of the sulphonamide functionality was investigated to explore the SAR properties of the core 3-azabicyclo[3.3.1]non-3-ene scaffold.



Scheme 3.21 The attempted reaction of **(+)-101I** with benzenesulfonyl chloride.

After performing the reaction using the method by Jafarpour *et al.*,^[153] analysis of the crude product by GC-MS revealed that the reaction had not occurred and the starting material was recovered. The reaction was repeated, extending the reaction time from 3 hours to overnight, after which an aliquot of the reaction was removed for analysis showing the reaction was still not proceeding. After this, an alternative method was used, as outlined by Thuan *et al.*,^[155] where the starting material was dissolved in *N,N*-dimethyl formamide (DMF) instead of ethanol, and catalysed by the inclusion of the organic base, triethylamine. Under these new conditions, the reaction did not occur and the starting material was once again recovered.

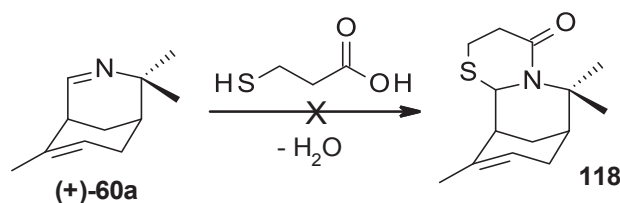
The inability for compound **(+)-101I** to undergo such a commonly reported, straightforward and high-yielding reaction must be accounted for by the steric crowding by the three adjacent methyl groups. These findings reiterate the results described earlier for the reductive *N*-alkylation of **(+)-101I** in Section 3.4.

3.5.5 Imine Reactions with **(+)-60a**

Previous work showed that compound **(+)-59I** was unable to react with the thiols 3-mercaptopropionic acid and mercaptoacetic acid, ethyl acetoacetate and maleic anhydride, despite these reactions being previously reported for similar systems by Lin *et al.*,^[156] Monaco *et al.*^[125] and Ali *et al.*,^[157] respectively. After consideration of the 3D X-ray structure of the crystallised lattice for compounds **(+)-101I** and **(+)-101b** in Section 3.2, and the hypothesis that the unreactive nature of the N-3 imines and amines was a result of their protection by steric bulk, the reactions were re-attempted with the compound **(+)-60a**. As the C-4 substituent in **(+)-60a** is hydrogen, as opposed to a methyl group in **(+)-59I**, the nitrogen is less hindered and may allow access for the reactions to occur.

4.3.1.1 Reaction of (+)-60a with 3-mercaptopropionic Acid

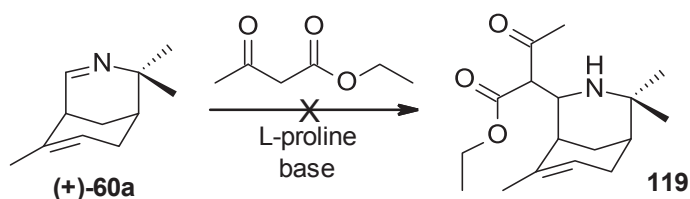
Compound **(+)-60a** was attempted to be reacted with 3-mercaptopropionic acid by heating at reflux in toluene in a Dean-Stark apparatus for 24 hours with *p*-toluenesulfonic acid, as shown in Scheme 3.22, to give **118**. Despite the less hindered nature of **(+)-60a** compared to that of **(+)-59I**, with which the reaction was previously attempted, the reaction was still unsuccessful. Analysis of the crude product by ^1H NMR and GC-MS showed the starting material and none of the expected product.



Scheme 3.22 Reaction of **(+)-60a** with 3-mercaptopropionic acid.

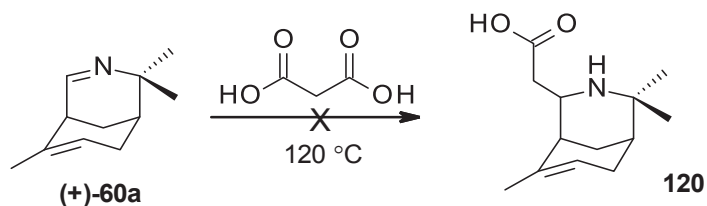
4.3.1.2 Mannich Reaction of (+)-60a with Ethyl Acetoacetate and Malonic Acid

The Mannich reaction was attempted on **(+)-60a** with ethyl acetoacetate and malonic acid in hope to obtain **119** (Scheme 3.23) and **120** (Scheme 3.24), respectively. The method employed by Monaco *et al.*^[125] used L-proline to direct the nucleophile and a base to activate the nucleophilic nature of the ethyl acetoacetate, making it capable of attacking the susceptible C-4 imine carbon. The bases triethylamine and sodium hydroxide were used in separate attempts. This reaction proved to be unsuccessful and the starting material was recovered after GC-MS and ^1H NMR analysis indicated none of the expected product had formed. This reaction was reattempted in the absence of L-proline, in case it was hindering the accessibility to the imine, however, this made no difference.



Scheme 3.23 Attempted reaction of **(+)-60a** with ethyl acetoacetate.

The reaction with malonic acid was attempted using an alternative set of conditions by Pelletier *et al.*,^[158] with the expected outcome to result in the addition of the acid functionality to give **121** as shown in Scheme 3.24. This reaction was unsuccessful, as analysis by GC-MS and ^1H NMR did not show any of the expected products and the starting material was recovered.

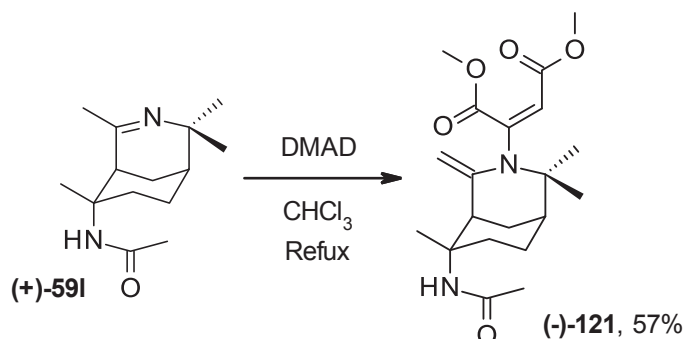


Scheme 3.24 Attempted reaction of **(+)-60a** with malonic acid.

3.6 Reaction of **(+)-59I** with DMAD

The reaction of compound **(+)-59I** with DMAD was performed by adapting the method published by Ung *et al.*^[100] to afford **(-)-121** in 57% yield. HRMS showed the $[M+H]^+$ exact mass to be 379.2229, corresponding to $C_{20}H_{31}N_2O_5$. This compound showed a surprisingly high specific rotation of $[\alpha]_D^{25} - 464.17$ (*c* 1.02, $CHCl_3$), in comparison to that of its precursor **(+)-59I**. The 1H NMR spectrum showed new peaks corresponding to functionality added to the scaffold through the amine nitrogen at N-3 and these include the singlet at δ 5.58 ppm due to the alkene C-H ($C=CHCO_2Me$). Two new CH_3 resonances were also assigned as singlets at δ 3.73 and 3.70 ppm corresponding to the two methoxy groups. Where there was previously a singlet from the C-4 CH_3 , two singlets were assigned for each of the CH_2 protons, occurring at 4.61 and 4.44 ppm. The HSQC experiment confirmed the protons as bonded to the same carbon. The ^{13}C NMR spectrum revealed the new carbonyl carbons at δ 167.1 and 166.4 ppm as well as the new quaternary carbon at 146.8 ppm.

The orientation of the two CO_2Me groups was confirmed by 1D NOESY experiments. Upon irradiating the proton ($C=CHCO_2Me$) at δ 5.58 ppm, two significant cross-peaks with the two CH_3 groups (1.45 and 1.39 ppm) at C-2 (Figure 2.7) were observed. These peaks indicate that the groups are within 3 Å proximity to each other in space, and the two CO_2Me groups must be in *cis*-orientation as shown in Scheme 3.25.



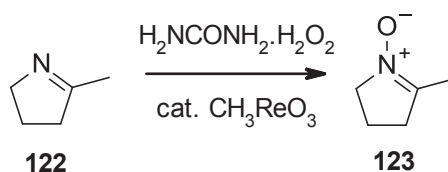
Scheme 3.25 The reaction of **(+)-59I** with DMAD to give **(-)-121**.

It was expected that compound **(-)-121** could be cyclised through the C-4 CH_2 and the formed amine, as previously reported by Lin *et al.*^[159] This intermediate adduct product,

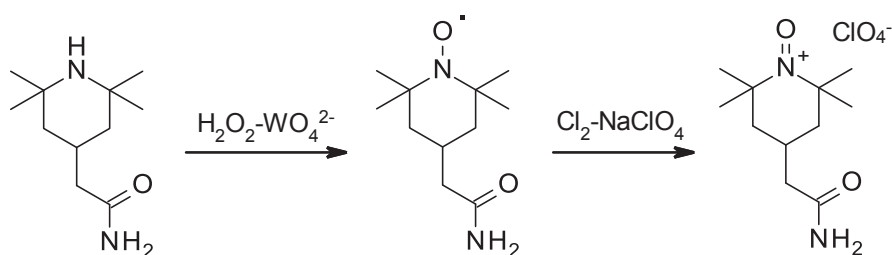
however, was unable to cyclise due to the highly hindered nature of the N-3 nitrogen, as outlined in Sections 3.4. In addition, the adsorption of (-)-**121** to silica gel did not result in cyclisation, as reported in a follow-up paper by Lin *et al.*^[156] on the reactivity of a related adduct. It is likely that for the tricyclic scaffolds previously reported by Lin *et al.*, the nitrogen is relatively less hindered due to the constraints of the ring pulling the carbon adjacent to C-4 away from it.

3.7 Conversion of Imine to Nitron and Subsequent 1,3-Dipolar Cycloaddition of Maleic Anhydride

After past unsuccessful efforts to introduce a third ring system to the 3-azabicyclo[3.3.1]non-3-ene scaffold due to steric factors, another synthetic approach was explored. Work by Soldaini *et al.*^[160] has shown the successful synthesis of the cyclic nitron **122** from the imine **123** (5-methyl-3,4-dihydro-2H-pyrrole) (Scheme 3.26), in one step using urea hydrogen peroxide catalysed by methyltrioxorhenium (MTO). Similarly, if not more, crowded piperidine structures have also been converted from amines to nitrones as shown by Sen *et al.*,^[161] using tungstate catalysed oxidation with hydrogen peroxide (Scheme 3.27).

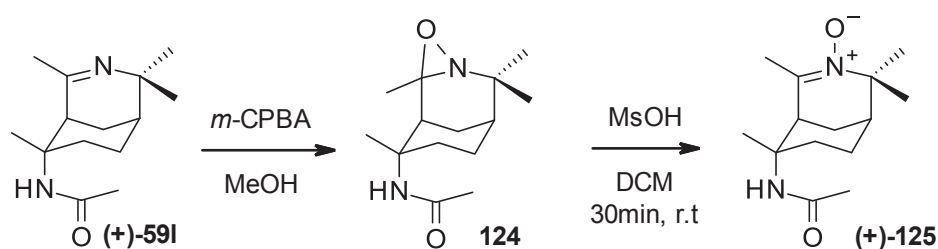


Scheme 3.26 Imine to nitron conversion by methyltrioxorhenium catalysed urea hydrogen peroxide.^[160]



Scheme 3.27 Tungstate catalysed oxidation of structurally similar amines with hydrogen peroxide.^[161]

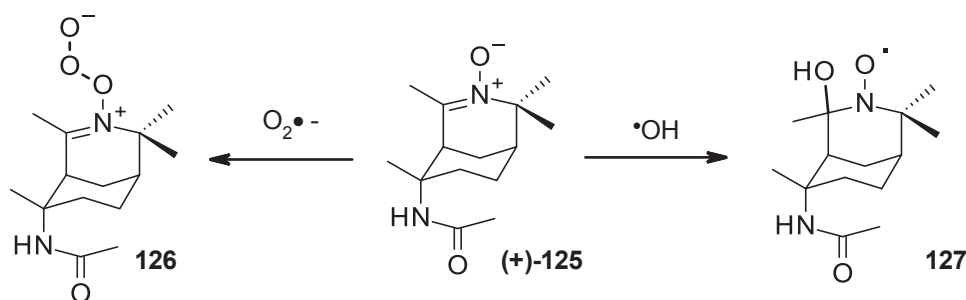
Several other methods have been reported for converting imines to their *N*-oxidised nitrones, with most of them progressing through an oxaziridine precursor. The method published by Kammoun *et al.*^[162] was adapted and used, whereby the oxaziridine **124** was generated from reaction with *meta*-chloroperoxybenzoic acid (*m*-CPBA), before converting to the nitron (+)-**125** using acidic conditions, as shown in Scheme 3.28.



Scheme 3.28 Synthesis of nitrone **(+)-125** via oxaziridine **124** from reacting **(+)-59I** with *m*-CPBA.

These nitrones make useful reactive intermediates, such as for 1,3-dipolar cycloaddition (Section 3.8), as well as having other useful practical applications in their own right. One application includes use as spin traps for detecting free radicals with electron paramagnetic resonance (EPR) spectroscopy^[163] or as therapeutic antioxidants.^[164] Nitroxides have also been shown to be useful for the controlled destruction or penetration of biofilms for improved antibiotic treatments.^[165]

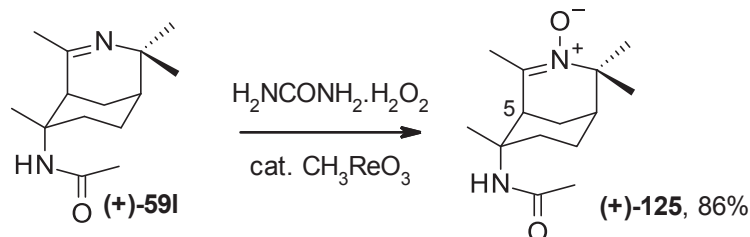
The method reported by Kammoun *et al.*^[162] was successful at converting **(+)-59I** into the nitrone **(+)-125**, however only in low quantities, as revealed by ¹H NMR analysis, which showed the dominant presence of the starting material. Increasing the mole ratio of *m*-CPBA from one to three equivalence, completely converted the starting material, although the excess of *m*-CPBA appeared to have led to the oxidation of **(+)-59I** to the trioxide **126** with *m/z* 284. A similar outcome was reported by Suarez-Bertoa *et al.*^[166] Alternatively, **(+)-125** may also be acting as a spin trap for oxygen or hydroxide radicals during the aqueous work-up, resulting in the products **126** or **127**, where **127** was detected in the GC-MS with *m/z* 269 (Scheme 3.29). The presence of the trioxide **126** was supported by HRMS data, whereby the [M+H]⁺ exact mass was 285.1816, corresponding to C₁₄H₂₆N₂O₄. This could be confirmed by electron paramagnetic resonance spectroscopy, however no access to this equipment was available.



Scheme 3.29 Formation of **126** and **127** from *N*-oxide **(+)-125**.

The method reported by Soldaini *et al.*^[160] was attempted to avoid the same workup procedure, as shown in Scheme 3.30. This method was more reliable at providing high yields of

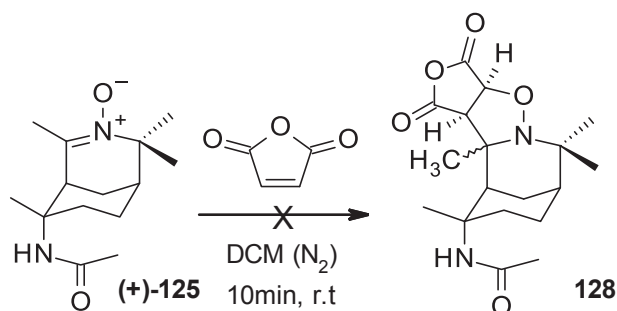
the nitrone **(+)-125** at 86%, when compared to the method using *m*-CPBA. Work up was also a more simple process, as the urea could be removed by precipitation when the crude product was re-dissolved in dichloromethane after removal of the reaction solvent. For the nitrone **(+)-125**, the N-O stretch being observed in the infrared spectrum at 1531 cm⁻¹. The HRMS showed the [M+H]⁺ exact mass to be 253.1912 which corresponds to the molecular formula C₁₄H₂₅N₂O₂ and the specific rotation was [α]_D²² +5.08 (*c* 1.00, CHCl₃). The *N*-oxide functionality also resulted in some interesting splitting in the ¹H NMR spectrum, with CH-5 now occurring as a doublet of doublets at δ 3.74 ppm (*J* = 3.5 & 12.5 Hz).



Scheme 3.30 Synthesis of nitrone **(+)-125** using the method by Soldaini *et al.*^[160]

3.8 1,3-Dipolar Cycloaddition of Cyclic Nitrones with Maleic Anhydride

The 1,3-dipolar cycloaddition reaction was attempted with the nitrone **(+)-125** and maleic anhydride, and was expected to give **128** as shown in Scheme 3.31, using the method outlined by Ali *et al.*^[157] This product would have produced an interesting new structure with an additional ring system, however, product **128** failed to form. These reaction conditions returned the nitrone **(+)-125** to its precursor **(+)-59b**, as determined by ¹H NMR and GC-MS analysis of the crude product. Future work could investigate the possibility of this reaction occurring for with the less hindered *N*-oxide of **(+)-60a**.



Scheme 3.31 Attempted 1,3-dipolar cycloaddition of maleic anhydride to **(+)-125**.

3.9 Conclusions and Future Directions

The reactions attempted with the 3-azabicyclo[3.3.1]non-3-ene core provided by the bridged Ritter reaction highlight several interesting factors about the chemistry of these alkaloid-like compounds. Firstly, reduction of the imine allowed secondary amines to be

generated with stereospecific outcomes. The hindered nature of these amines, however, only allowed for the generation of tertiary amines *via* alkylation with formaldehyde. The hindrance resulting from the crowding of the position 3 nitrogen is also observed in the X-ray crystal structures.

Secondly, the alkene products were extremely stable towards electrophilic addition. This led to the conclusion that the C-6 alkenes are not a suitable group for derivatisation. Chloroacetonitrile, however, did provide a labile amide which was readily hydrolysed under mild conditions to give the amine functionality at C-6, which could be further functionalised. An equally efficient route for obtaining amine functionality at C-6 was *via* hydrolysis with 6 M HCl. These amines provide a diverse synthetic handle and the most viable synthetic route for the extension of this core scaffold. This should be investigated further in future work for a wider range of derivatisation reactions, in particular, S_N2 reactions with a variety of electrophiles, as shown possible by the reactions performed with benzyl bromide.

Several of the derivatisation reactions were able to provide increased diversity to the library of 3-azabicyclo[3.3.1]non-3-ene compounds obtained from the bridged Ritter reaction and hence provide useful information about the structure-activity relationships for this class of alkaloid-like compounds. This is explored *via* the biological testing of these compounds in Chapters 4, 5 and 6, as well as the *in silico* assessment of drug-likeness and ADMET properties in Chapter 7.

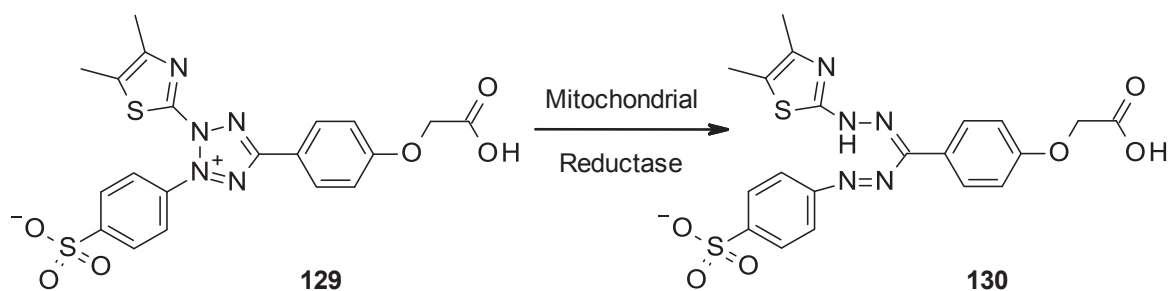
CHAPTER 4: Anticancer Biological Results

4.1 General Introduction to Assessment of Cytotoxicity

Alkaloids are predominant in the chemical space of chemotherapies, as outlined in Chapter 1. In particular, alkaloid-like compounds, similar to those synthesised, have shown cytotoxicity against the MCF-7 breast cancer cell line in unpublished work performed by our research group. Twenty eight of the synthesised alkaloid-like compounds were investigated for potential cytotoxicity by in-house anticancer screening using the MTS assay for the MDA-MB-231 cell line. The assay was used to identify active compounds based on their percentage inhibition of cell proliferation and to determine the IC₅₀ values for the active compounds. A few compounds were also screened externally by BIOTECH, Thailand,^[167] against two cancerous cell lines, namely KB and MCF-7, as well as the healthy mammalian cell line, Vero, an African green monkey kidney cell line. This data was used to provide an understanding of the SAR of the screened compounds.

4.1.1 MTS Assay

The MTS assay is a simple colorimetric method for determination of a compound's cytotoxicity *via* establishing the number of viable cells remaining in a culture that has been treated with the tested compound.^[168] The assay was performed using the commercially available CellTiter 96® AQ_{UEOUS} One Solution Reagent, which contains the tetrazolium salt 3-(4,5-dimethylthiazol-2-yl)-5-(3-carboxymethoxyphenyl)-2-(4-sulfophenyl)-2H-tetrazolium **129** (MTS), and the electron coupling reagent, phenazine ethosulfate (PES). The MTS is cleaved by NADH and NADPH-dependant dehydrogenase enzymes found in the mitochondria of cells that are metabolically active,^[169] where cell viability is defined as a cell that is metabolically active. For this reason, the MTS assay does not differentiate between the loss of viable cells resulting from apoptosis or cytostasis that is caused by the tested compound. The cleaving of MTS forms a formazan **130** (Scheme 4.1), which has a dark red colour and therefore has a measurable absorbance at 490-500 nm, where the absorbance is directly proportional to the number of viable cells in the culture. Cultures treated with the synthesised compounds in 96 well plates were analysed with a spectrophotometer after addition of the MTS reagent and 4 hours of incubation.



Scheme 4.1 Mitochondrial cleavage of MTS **129** to formazan **130**.

For each of the compounds tested, stock samples were prepared in DMSO and then diluted to the working concentration in media. The viability percentage was calculated by normalising the average of triplicate sample absorbance values, to the average of the triplicate control absorbance values. Control cells were treated with the highest concentration of DMSO that was present in any of the drugged cells (0.1% v/v). The results of the MTS cell proliferation assay, as described above for compounds listed in Table 4.1, are outlined in the following sub-sections. The initial screening data is summarised in Figure 4.1 and listed in Table 4.1. For the identified cytotoxic compounds, the concentration at which 50% of the cells remain viable (IC_{50}) is reported in Table 4.2.

4.1.2 Screening for Cytotoxicity

Table 4.1 displays the results obtained from the cytotoxic screening of the MTS assay for the compounds synthesised in Chapters 2-3. Each of the compounds were assessed as replicates (technical triplicate), run on different plates and different days. For each replicate, the absorbance was measured from three triplicate wells for each tested concentration (biological triplicate), the average of which was used to calculate the percentage viability. The three replicate percentage viability values obtained for each concentration were analysed with One-way ANOVA tests and Dunnett's multiple comparisons test using GraphPad Prims 6.07. Statistical significance was determined according to a decrease in drugged cell viability when compared to the control. The average percent viability values are listed in Table 4.1.

Based on this initial screening assay, three compounds showed statistically significant cytotoxic activity against the MDA-MB-231 cell line, at the highest tested concentration of 50 μ M. These compounds were **(+)-59m**, **(+)-60m** and **(+)-101m** shown in Table 4.1 and Figure 4.1 where statistical significance is indicated by the following; * ($P \leq 0.05$), ** ($P \leq 0.01$), *** ($P \leq 0.001$), **** ($P \leq 0.0001$) and unlabelled values are of no significance ($P > 0.05$). The remaining compounds were found to be inactive, as they showed no significant decrease in

cell proliferation against the MDA-MB-231 cell line at 50 μ M, as judged by One-way ANOVA tests and Dunnett's multiple comparisons test.

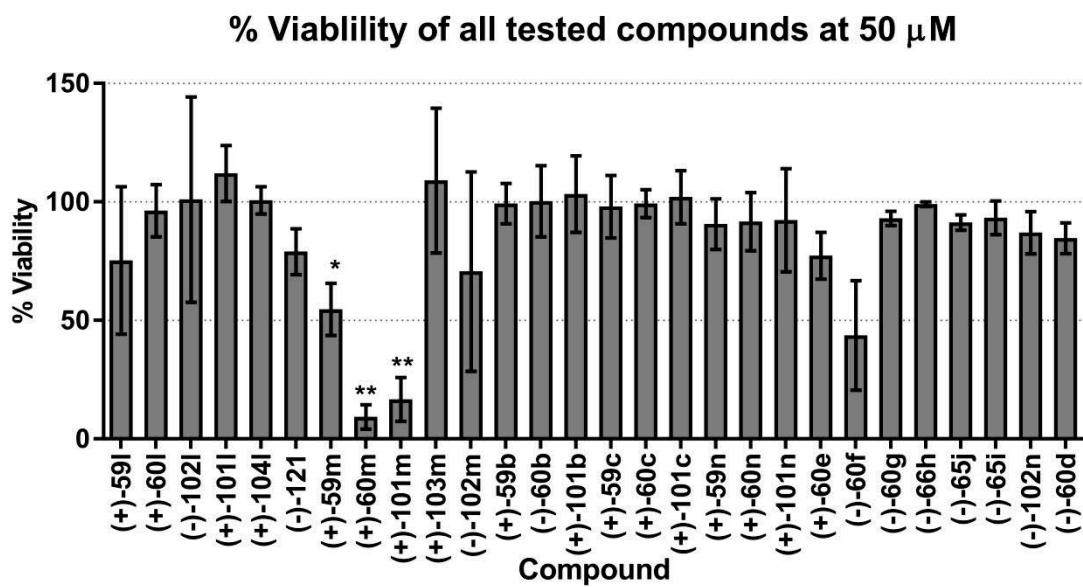


Figure 4.1 All compounds % viability at 50 μ M. Data represented is the mean of replicate \pm SD.

Table 4.1 MDA-MB-231 MTS screening results as % viability normalised to control.

Entry	Compound	% Viability at concentration (μM)			
		1	10	25	50
1	(+)-59l	96	90	109	75
2	(+)-60l	115	95	104	96
3	(-)-102l	100	107	115	101
4	(+)-101l	109	109	108	112
5	(+)-104l	100	104	109	101
6	(-)-121	95	92	88*	79
7	(+)-59m	96	103	84	55*
8	(+)-60m	91	40****	11**	9**
9	(+)-101m	111	84	40	17**
10	(+)-103m	111	119	114	109
11	(-)-102m	106	103	101	71
12	(+)-59b	94	99	98	99
13	(-)-60b	100	88	95	100
14	(+)-101b	98	96	101	103
15	(+)-59c	89	98	109	98
16	(+)-60c	102	102	104	99
17	(+)-101c	101	103	98	102
18	(+)-59n	100	102	99	91
19	(+)-60n	102	102	101	92
20	(+)-101n	104	103	97	92
21	(+)-60e	89	88	81	77
22	(-)-60f	91	89	76	44
23	(-)-60g	97	97	96	93
24	(-)-66h	100	99	101	99
25	(-)-65j	98	93	92	91
26	(-)-65i	94	94	92	93
27	(-)-102n	92	97	93	87
28	(-)-60d	88	92	79	85

Note: statistical significance is indicated by the following; * ($P \leq 0.05$), ** ($P \leq 0.01$), *** ($P \leq 0.001$), **** ($P \leq 0.0001$) and unlabelled values are of no significance ($P > 0.05$).

4.1.3 Dose-response analysis of cytotoxicity

For the three compounds ((+)-59m, (+)-60m and (+)-101m) which were deemed to be active, the cytotoxicity was reassessed by repeating the assay with several testing concentrations. This was performed to determine the IC_{50} values, as a more accurate representation of each of the compound's relative potencies. New concentrations were chosen specifically to fall on either side of an estimated IC_{50} value that was calculated from the screening data. For (+)-59m, the concentrations used were 30, 35, 40, 45, 50, 55, 60 and 65 μM ; for (+)-60m, 2, 4, 6, 7, 10, 12, 14 and 16 μM were used; for (+)-101m, 5, 10, 15, 20, 25, 30,

35 and 40 μM were used. The IC_{50} results obtained are listed in Table 4.2 and the dose response curves for each **(+)-59m**, **(+)-60m** and **(+)-101m** are seen in Figure 4.3, Figure 4.4 and Figure 4.5, respectively. These figures only show a narrow portion of the dose response curve and show that in future, a wider concentration range should be used for the analysis of the IC_{50} .

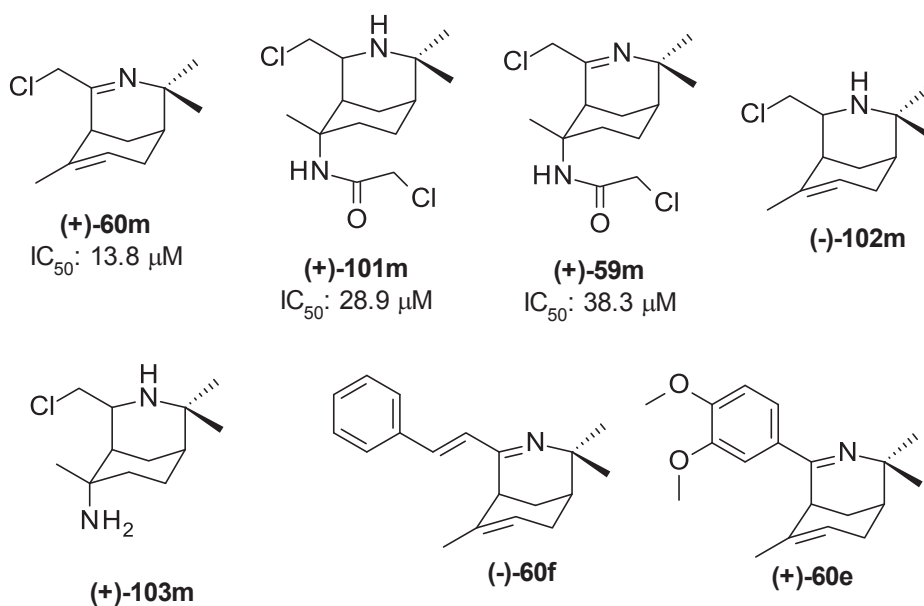


Figure 4.2 The structures of compounds for visual comparison of SAR properties.

Table 4.2 MTS assay IC_{50} results with the standard errors.

Entry	Compound	IC_{50} (μM)	+ SD	- SD
1	(+)-59m	38.27	2.42	2.58
2	(+)-60m	13.83	2.36	2.85
3	(+)-101m	28.87	4.64	5.53

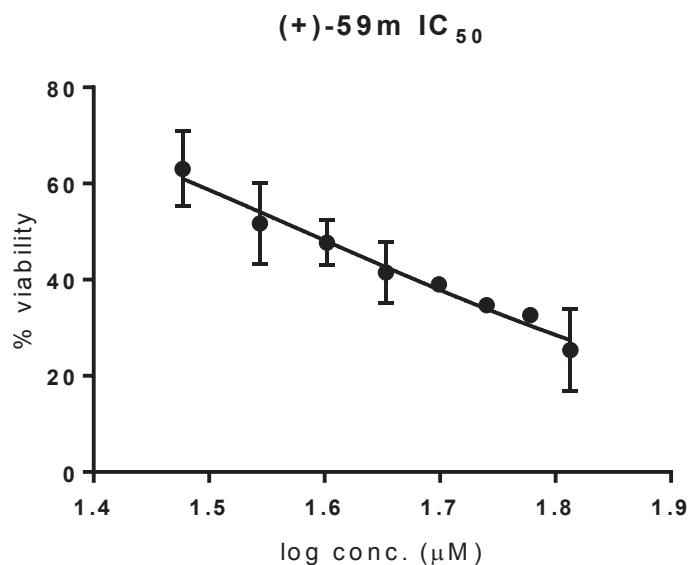


Figure 4.3 MDA-MB-231 cytotoxicity dose-response curve for **(+)-59m**.

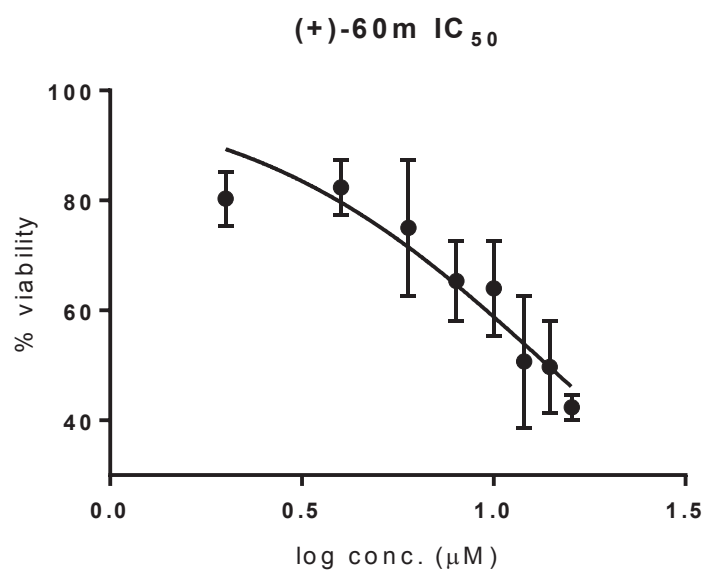


Figure 4.4 MDA-MB-231 cytotoxicity dose-response curve for **(+)-60m**.

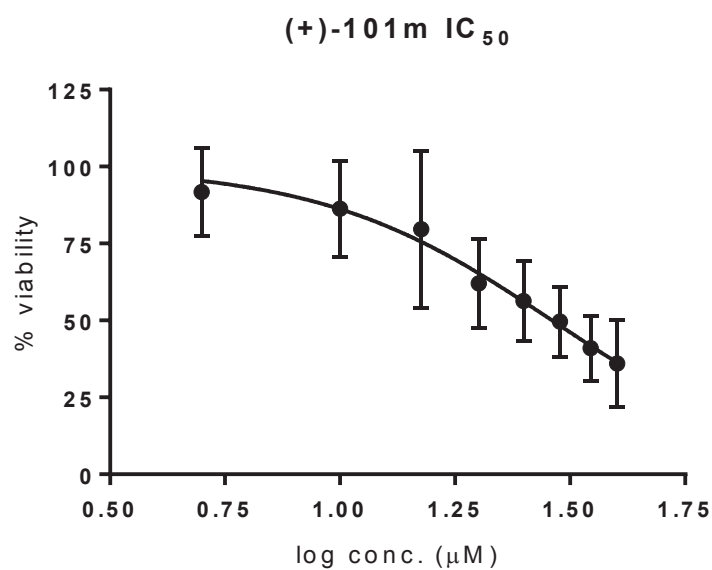


Figure 4.5 MDA-MB-231 cytotoxicity dose-response curve for **(+)-101m**.

As seen in Table 4.2, compound **(+)-60m** shows the most potent cytotoxicity against MDA-MB-231, followed by **(+)-101m** and then **(+)-59m**. The effects of **(+)-60m** on the cell line can be seen in Figure 4.6, where cells treated with **(+)-60m** at 50 μM appear to have lost adherence (A), compared to the mixture of healthy and apoptotic cells at 10 μM (B), and the healthy control cells (C).

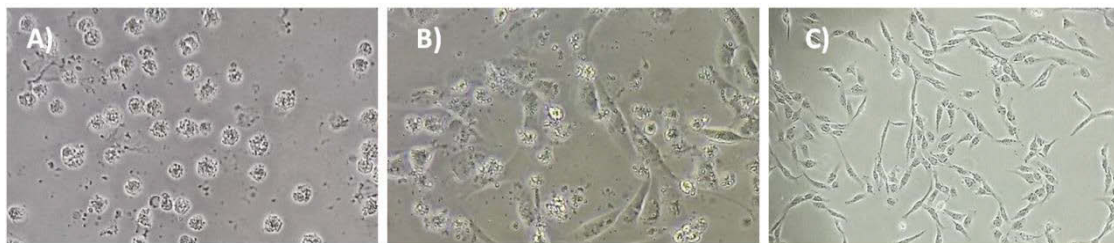


Figure 4.6 The effects of **(+)-60m** on MDA-MB-231 cells after 48 hours. Images were viewed at 10 x magnification using light microscopy. **A)** **(+)-60m** at 50 μM ; **B)** **(+)-60m** at 10 μM ; **C)** healthy untreated control cells.

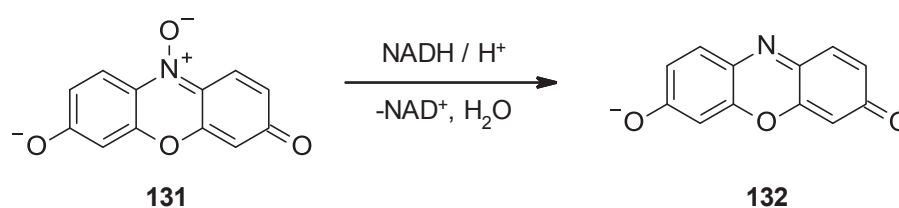
4.1.4 SAR of Cytotoxic Activity Against MDA-MB-231

Although few compounds showed significant cytotoxic activity against MDA-MB-231, some SAR information can be conferred from these results. Most notably, the presence of the chloromethyl ($-\text{CH}_2\text{Cl}$) substituent at the C-4 position inferred activity, because three of the six compounds containing this functionality displayed a significant reduction in cell viability. Of those six, compound **(+)-103m** showed a consistent decrease in viability (71%) but was deemed not significantly cytotoxic due to the large standard error in the measurement. Of the three significantly active compounds, two contained the imine functionality at N-3 (**(+)-59m**, **(+)-60m**), while the other contained amino-functionality at N-3 (**(+)-101m**). In the case of the corresponding N-3 imino-amide and amino-amide pair, **(+)-59m** and **(+)-101m**, the observed activity increased for the amine, while the reverse effect is observed for the corresponding N-3 imino-alkene and amino-alkene pair, **(+)-60m** and **(+)-103m**. In combination with the imine functionality, the alkene at position C-6 gives rise to the strongest cytotoxic activity, suggesting the alkene functionality assists in achieving higher potency. Comparing the alkene and the amide functionality at C-6 reveals that cytotoxicity is relatively reduced with the presence of the amide. The activity was markedly reduced when the amide functionality was replaced with a primary amine, as observed for **(+)-103m**. Of the compounds that did not contain the chloromethyl functionality, the imino-alkenes **(+)-60e** and **(-)-60f** did show a reduction in cell viability, at 77 and 44% viability, respectively, but this was not of statistical significance. The structures of the discussed compounds are shown in Figure 4.2.

These results suggest that the chloromethyl and alkene pharmacophores are necessary for potent cytotoxic activity and therefore the compounds containing these groups are worth investigating further. Future work may develop a deeper understanding of these compounds potential as anticancer agents through mechanistic experiments to determine potential molecular targets or cell cycle functions affected by the treatment of cells with these compounds, as well as resistance studies.

4.2 External Screening of Cytotoxicity

The external screening was carried out on three additional cell lines using the services of the Bioassay Laboratory Bioresources Technology Unit, Thailand (BIOTEC).^[167] The compounds **(+)-59l**, **(+)-60l**, **(+)-101l**, **(+)-104l**, **(-)-122**, **(+)-59m**, **(+)-60m**, **(+)-101m**, **(+)-103m** and **(+)-102m** were investigated for their cell growth inhibition against human epidermoid carcinoma of oral cavity cell line (KB), the ER-positive human breast adenocarcinoma cell line MCF-7 and for their toxicity against healthy mammalian cells using the African green monkey kidney (Vero) cells. The assays were performed employing the Resazurin Microplate assay (REAM) as described by O'Brien *et al.*,^[170] where ellipticine and doxorubicin were used as positive controls and 0.5% DMSO and water were used as negative controls. Cell viability was determined by measuring fluorescence at 590 nm after the cells were treated with resazurin **131**, which is reduced by NADH to resorufin **132** in the mitochondria of living cells (Scheme 4.2).^{[171],[172]}



Scheme 4.2 Reduction of resazurin **134** to resorufin **135** by NADH.

The results from this assay are reported as a percentage inhibition of cell growth, as shown in Table 4.3. These values were calculated using Equation 4.1, where FUT is the mean fluorescent unit from the drug-treated cells and FUC is the mean fluorescent unit from untreated control cells.

Table 4.3 Cytotoxicity results from external screening performed at BIOTEC.

Entry	Compound	Concentration (mM)	% Inhibition of cell line		
			KB	MCF-7	Vero
1	(+)-60m	0.165	99.62	95.28	64.87
2	(+)-59m	0.164	83.35	99.09	83.03
3	(+)-101m	0.163	93.13	-8.9	88.35
4	(-)-121	0.132	53.46	-16.66	81.83
5	(-)-102m	0.235	-1.88	98.44	37.81
6	(+)-103m	0.217	-5.38	7.73	55.11
7	(+)-60l	0.282	5.06	-9.72	75.42
8	(+)-104l	0.198	0.14	-11.92	19.52
9	(+)-101l	0.21	-1.81	-11.04	16.42
10	(+)-59l	0.212	2.17	-5.19	-12.42

Equation 4.1 Fluorescent assay percent inhibition calculation

$$\% \text{ Inhibition} = \left[1 - \left(\frac{\text{FUT}}{\text{FUC}} \right) \right] \times 100$$

From the external screening results against the MCF-7 breast cancer cell line, the cytotoxicity, or lack of, was compared with the internally screened MDA-MB-231 breast cancer cell line for the compounds listed in Table 4.1. This allowed for the investigation of variations in activity for different sub-types of breast cancer. The uses of the epidermoid carcinoma and healthy mammalian cells determined any specificity of the compounds across each of the tested cell lines.

Compound **(+)-102m** showed the most selective activity, with no significant activity against MDA-MB-231 and KB, while close to 100% inhibition of MCF-7 and less than the accepted 50% threshold for activity against the Vero cell line at 0.235 mM. Compound **(+)-101m** displayed specificity towards the KB cell line over MCF-7, yet was also above the accepted threshold for Vero cell activity at 0.163 mM. Compounds **(+)-59m** and **(+)-60m** both showed low selectivity, as they displayed strong activity against all of the tested cell lines at 0.164 and 0.165 mM, respectively. Compound **(+)-103m** showed activity against the Vero cells and negligible activity against KB and MCF-7 cell lines at 0.217 mM.

4.3 Conclusions and Future Directions

External screening confirmed the in-house cytotoxicity screen, which identified the significance of the activity provided when the chloromethyl functionality is part of the 3-azabicyclo[3.3.1]nonane core structure. Both sets of results also demonstrate the influence of a third ring system on cytotoxic activity. This is observed for a related series of compounds, such as compound **52** without the chloromethyl motif (Chapter 1), which was reported by others in our research group, as this compound and the *Aristolelia* alkaloids do show activity. It can be concluded that the activity of these compounds arises from a mechanism not specific to any of the cell lines and therefore warrants the investigation of future work into determining the mechanism. For the compounds which showed no anticancer activity, there is the potential to be investigated for other biological properties, such as AChE inhibition activity, as assessed in Chapter 5. Those that showed unselective cytotoxicity are unlikely to be suitable for use as a drug against any other target.

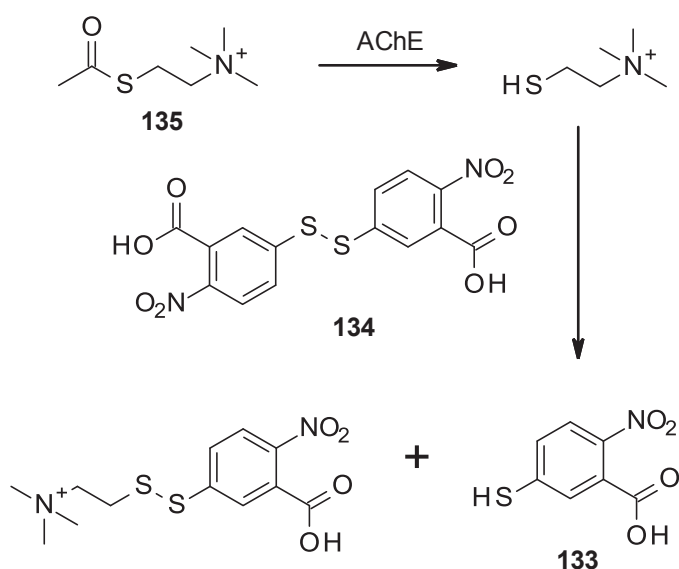
CHAPTER 5: AChE inhibition biological results

5.1 Introduction to Alzheimer's Disease and AChE inhibition

The most commonly reported method for measuring the AChE inhibition activity of novel compounds is the spectroscopic assay is the Ellman method. This method, in addition to the complimentary screening bioautograph TLC method, was used to assess the inhibition activity of the synthesised library's activity against eeAChE (EC 3.1.1.7). The results were then analysed to derive possible structural activity relationships.

5.1.1 Ellman Assays

There are various published methods for determining the inhibition of AChE by novel compounds. The Ellman method was developed by Ellman *et al.*^[173] in 1961 and is a photometric analysis that employs a spectrophotometer to measure the absorbance of light at 412 nm, resulting from the formation of yellow 2-nitro-5-sulfanyl-benzoic acid (TNB) **133**. TNB is formed when the colour reagent 5,5'-dithiobis-(2-nitrobenzoic acid) (DTNB) **134** reacts with thiocholine that is formed by enzymatic hydrolysis of the substrate acetylthiocholine (ATCh) **135** by AChE, as seen in Scheme 5.1. As such, the absorbance measured is proportional to the extent by which this reaction has occurred. ATCh is used as a substitute for the natural analogue acetylcholine which yields similar results regarding the enzyme kinetics. In the presence of an AChE inhibitor, there will be a consequential reduction in the formation of TNB and hence a lower absorbance measured at 412 nm for the assay solution. Subsequently, measuring this inhibition at several concentrations allows a concentration-response curve to be used to determine the inhibitors IC₅₀.

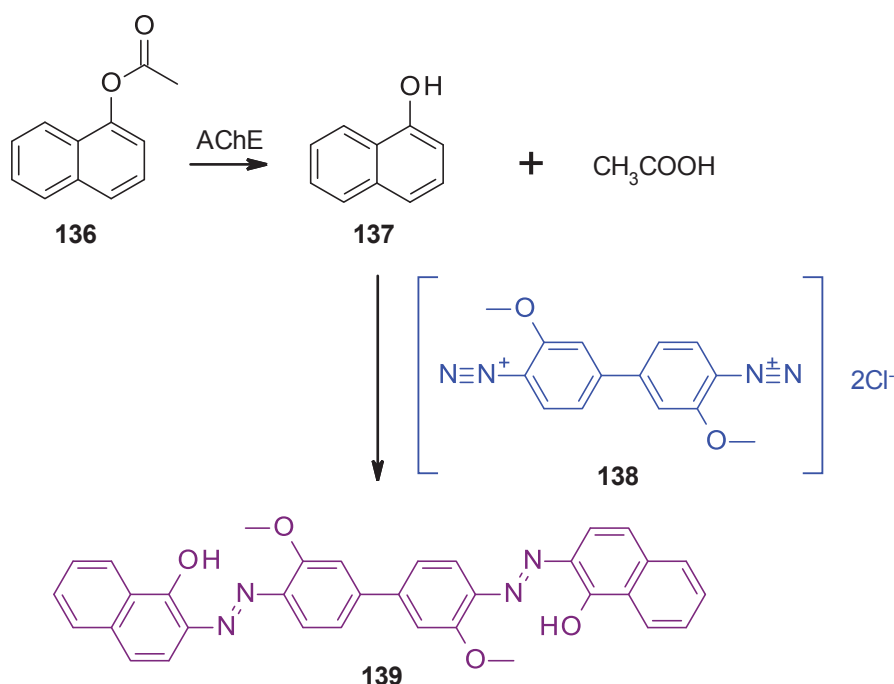


Scheme 5.1 Hydrolysis of ATCh by AChE and the subsequent formation of yellow TNB (**133**).

One of the limitations of this method occurs when using coloured inhibitors that absorb light in the same region as TNB, because this results in false-negative results. On the other hand, false-positive results can be avoided by performing parallel tests where the DTNB is omitted, which determines whether the compounds tested react with the thiocholine formed. Many other methods have been developed in an attempt to overcome these limitations. Other methods include fluorimetric flow assays,^[174] capillary electrophoresis, UPLC-MS assays,^[175] and TLC bioautographs. The Ellman method, however, remains the most accessible method.

5.1.2 TLC Bioautographic Method

The TLC bioautographic method developed by Hostettmann *et al.*^[176] is a useful method for rapid screening of novel inhibitors. It works similarly to the Ellman method whereby a colour change occurs to give a visual representation of inhibition. In the TLC bioautographic method, the ester naphthyl acetate **136** is used as the substitute for acetylcholine and is hydrolysed by AChE into α -naphthol **137**. This then reacts in the presence of Fast Blue B salt **138** to give a purple diazonium dye **139**, as seen in Scheme 5.2. The inhibition of AChE prevents the formation of the azo dye and hence a white region remains on the TLC plates, while regions of no inhibition turn purple with the rest of the untreated area of the plate. This is seen for the Galantamine control for each of the tested concentrations in Figure 5.1.



Scheme 5.2 Hydrolysis of naphthyl acetate by AChE and the subsequent formation of the purple dye in the TLC bioautographic assay.

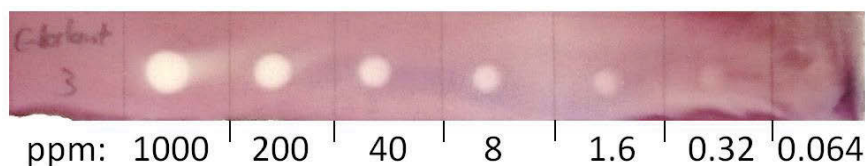


Figure 5.1 Example of the TLC bioautographic with the Galantamine control.

5.1.3 Other AChE Inhibition Methods

Several other methods have also been reported for determining the inhibition of AChE but were not used in the project. A recent report by Marcelo *et al.*^[177] has employed the use of STD NMR as a screening method because it accelerates the process of obtaining SAR information regarding the binding of inhibitors to the enzyme. STD NMR has great significance as a complementary technique in AChE inhibitor discovery.

Liu *et al.*^[175] developed a method employing UPLC-MS to monitor inhibition. This method appears to be the best of the mentioned methods because it can directly detect the enzyme reaction product choline and hence any decrease in its formation from the inhibition of AChE, removing the possibility of false-positive results. It is also more sensitive, accurate, and reproducible than the other methods mentioned. Furthermore, it has a low running cost, because only small total volumes are used and it has short analysis times, making the method suitable for high-throughput screening. Using this approach, Liu and co-workers were also able to show that there was no distinct influence on the enzymatic activity when varying the assay temperature between 25-40 °C - a significant factor to consider when performing any of the AChE inhibition assays. The downfall of this method is the requirement of access to equipment that was not available for this project.

5.2 Review and Validation of Ellman Methods

Review of the literature revealed no two methods with the same experimental procedure for performing the Ellman assay, each of which references the method to be adapted from Ellman's original paper.^[173] Due to this, each enzymatic reaction has different kinetic parameters and as a result, the reported IC₅₀ values cannot be compared across methods. Instead, K_i (the equilibrium constant for the binding of the substrate with the active site) should be used to accurately represent inhibition potency because as by definition, it remains constant, independent of the conditions. If kinetic parameters across experiments are kept the same, however, IC₅₀ values should be comparable and thus this was the approach undertaken. The method by Sastraruji^[178] was initially attempted, using Galantamine as a control to test the comparability of IC₅₀ values obtained.

Upon attempting the assay using Galantamine as a control, the reported IC_{50} of $0.9 \mu\text{M}$ against eeAChE could not be reproduced because the triplicate repeats did not show consistency in the percentage inhibition values obtained. As a result, an average IC_{50} of $14.1 \mu\text{M}$ was obtained. The method was therefore assessed for its validity by undertaking kinetics experiments, where the assay is performed with several concentrations of substrate $[S]$, both in the presence and absence of inhibitor. The Michaelis constant (K_m) and maximum velocity (V_{max}) can be determined for the consumption of the substrate by AChE using a Lineweaver-Burk Plot, where the inverse of the reaction velocity ($1/V$) is plotted against the inverse substrate concentration ($1/[S]$). The plot should also validate the type of inhibition. In the case of a reversible competitive inhibitor such as Galantamine, the trend lines from the reaction in the presence and absence of inhibitor should both intersect the y-axis. This point is $1/V_{max}$, as seen in the example Lineweaver-Burk Plot, Figure 5.2.

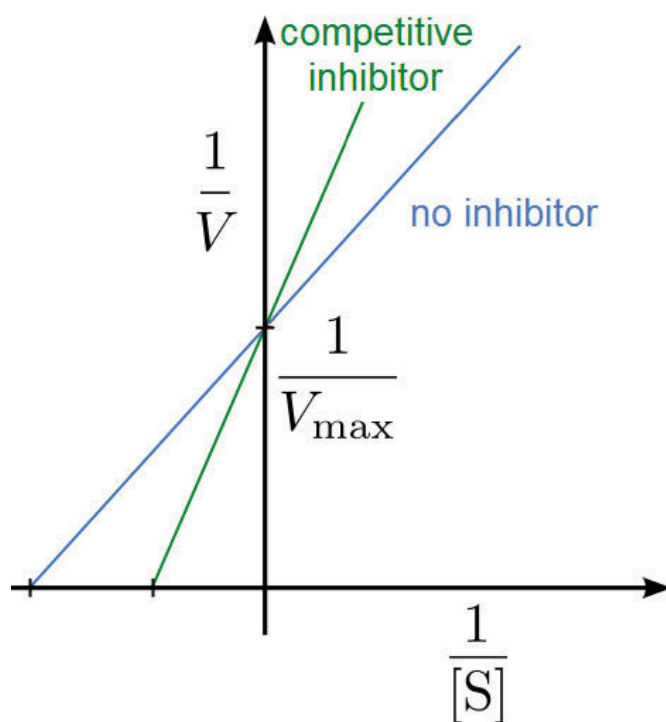


Figure 5.2 Example Lineweaver-Burk Plot for competitive inhibitors.

The following parameters were used for the method validation kinetics experiments. The concentration of Galantamine used was $0.8 \mu\text{M}$, while the concentrations of acetylthiocholine iodide were 9.46, 7.10, 4.73, 3.54, 2.37, 1.18, 0.59, 0.47 mM for the assay run in the presence of inhibitor and 9.46, 7.10, 4.73, 1.18, 0.47 mM without. At each concentration, velocity (V) was determined to be the gradient of average absorbance (of the biological triplicates) versus time. The reciprocals of velocity and substrate concentration were calculated and respectively plotted against each other to give the Lineweaver-Burk Plot seen in

Figure 5.3. As previously stated, $1/V_{\max}$ should be the same with and without the presence of inhibitor. For this method, $1/V_{\max}$ was determined to be 11577 in the presence of Galantamine, while it was 372 without. As the trend lines did not intersect at the y-axis, this method did not produce results that follow the inhibition model. A Michaelis-Menten plot, Figure 5.4, was also generated from the kinetics experiment data seen in Table 5.1 and validates the enzyme kinetics model.

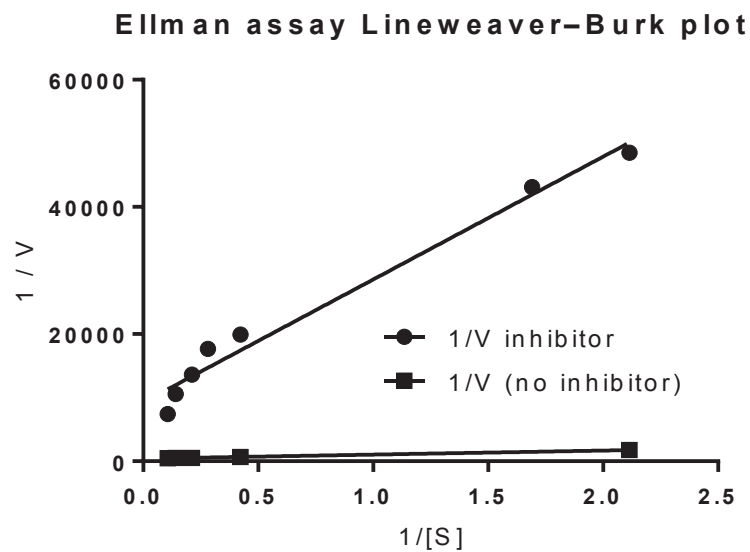


Figure 5.3 Lineweaver-Burk plot of the Ellman assay kinetics experiment data.

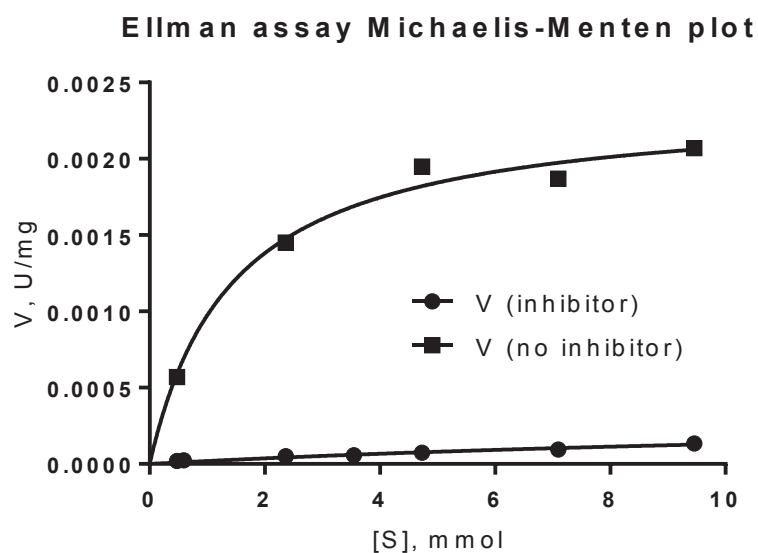


Figure 5.4 Michaelis-Menten plot of the Ellman assay kinetics experiment data.

Table 5.1 Ellman assay kinetics experiment data.

[S] (mM)	1/[S] (mM ⁻¹)	V (mM/s) x10 ⁻⁴	1/V (sec/mM) inhibitor	1/V (sec/mM) no inhibitor
9.46	0.106	1.35	7413	483
7.10	0.141	0.947	10560	535
4.73	0.211	0.733	13643	513
3.55	0.282	0.566	17683	-
2.37	0.423	0.502	19940	-
1.18	0.846	0.210	47642	690
0.591	1.69	0.232	43122	-
0.473	2.11	0.206	48497	1754

Note: [S] = acetylthiocholine iodide concentration, V = velocity

After many unsuccessful attempts to determine why the method by Sastraruji^[178] did not produce results consistent with the inhibition model, an alternative method was developed, based primarily on that used by Ingkaninan *et al.*,^[179] because it was the easiest method that could be adapted to the resources available and sample preparation and data analysis previously used. Ingkaninan *et al.*^[179] report the IC₅₀ of Galantamine to be 1.44 μM under their assay conditions which are outlined in detail in the experimental data in Section 9.6.7 of Chapter 9. The new assay method was attempted with Galantamine as a control and an IC₅₀ of 1.43 μM was obtained, validating these alternative conditions. Furthermore, the method was reproducible and therefore the synthesised compounds were prepared and analysed using this method.

The other methods reviewed varied greatly, not only in the concentration of key components used (as highlighted by the summary of the following data in Table 5.2) but also in volumes used, buffers used, inhibitor solvent and assay reading times. The following briefly outlines these differences corresponding to the entries of Table 5.2:

Table 5.2 Summary of differences in Ellman methods reported.

Entry	Method by	AChE (U/mL)	DTNB conc. (mM)	Acetylcholine conc. (mM)
1	Perry <i>et al.</i>	0.39	10	0.03 - 0.5
2	Ingkaninan <i>et al.</i>	0.28	3	14
3	Bruhlmann <i>et al.</i>	0.5	0.15	0.056 - 0.67
4	Özkay and Özkay	2.5	10	unspecified
5	Lee <i>et al.</i>	0.10	0.2	0.200
6	Sastraruji	0.75	3.15	4.73

Note: U = Enzyme unit

- **Entry 1:** Perry *et al.*^[180] used 50 μL of 0.39 U/mL hAChE (from human erythrocytes) in pH 8 buffer, 20 μL of inhibitor between 0.09 and 9.4 mM in 96% ethanol, 20 μL of 10 mM DTNB in pH 7 buffer and 20 μL of 0.03 to 0.5 mM acetylcholine in water. Absorbance

was read over six minutes. Interestingly, they report that β -pinene shows 68% inhibition at 4.7 mM.

- **Entry 2:** Ingkaninan *et al.*^[179] used 24 μ L of 0.28 U/mL eeAChE in buffer containing 0.1% bovine serum albumin, 25 μ L of 0.1 mg/mL inhibitor in buffer with up to 10% methanol, 125 μ L of 3 mM DTNB dissolved in buffer containing 0.1M NaCl and 0.02 M MgCl₂, 25 μ L of 14 mM acetylthiocholine iodide in water and 50 μ L of 50 mM Tris-HCl buffer at pH 8.0.
- **Entry 3:** Bruhlmann *et al.*^[181] used 20 μ L of 0.5 U/mL eeAChE in pH 7.4 buffer, 20 μ L of inhibitor at 0.5 mM in methanol (working concentration of 37 μ M), 200 μ L of 0.15 mM DTNB in pH 7.4 buffer and 30 μ L of 0.056 to 0.67 mM acetylcholine in water. Absorbance was read over three minutes. Controls were prepared by replacing inhibitor with methanol.
- **Entry 4:** Özkay and Özkay^[182] used 2.5 U/mL eeAChE in a 1% gelatin solution, 50 μ L of inhibitor at 0.1 and 1.0 mM in 2% DMSO, 50 μ L of 10 mM DTNB, 10 μ L of an unspecified concentration of acetylcholine solution and 3 mL of pH 8 phosphate buffer. Absorbance was read over 10 minutes. The % inhibition was calculated with Equation 5.1.
- **Entry 5:** Lee *et al.*^[183] used a 100 mU/mL eeAChE in 0.1% bovine serum albumin solution, inhibitor between 0 and 100 μ M, a 200 μ M solution of DTNB and 50 μ L of 200 μ M acetylcholine. Absorbance was read every 50 seconds for 20 minutes.
- **Entry 6:** Sastraruji^[178] used 20 μ L of 0.75 U/mL eeAChE in pH 7 buffer, 20 μ L of inhibitor in DMSO, 20 μ L of 3.15 mM DTNB in pH 7 buffer, 20 μ L of 5.73 mM acetylcholine iodide in buffer and 120 μ L of buffer. Absorbance was read every 15 seconds over 30 minutes.

Equation 5.1 Ellman assay percent inhibition calculation; Subscript C = control, B = blank and I = inhibitor

$$\% \text{ Inhibition} = \frac{(Abs_C - Abs_B) - (Abs_I - Abs_B)}{(Abs_C - Abs_B)} \times 100$$

5.3 AChE Inhibition Results

The library of compounds was tested for its AChE inhibition activity using both the TLC bioautographic method and the spectroscopic Ellman method reported by Ingkaninan *et al.*^[179] (Entry 2 of Table 5.2). Although the TLC method is intended as a quick screening method, all of the compounds were also tested with the Ellman method to rule out the possibility of false-negative results. Of the 27 compounds tested, eight showed activity with the TLC bioautographic method and seven with the spectroscopic method. Encouragingly, all the compounds shown to be active by the Ellman method were also active on TLC method. This

agreement confirms the activity of the compounds and validates the results of both methods. The results of the TLC assay are represented in Table 5.3.

Table 5.3 TLC bioautographic AChE inhibition assay results.

Entry	Compound	Minimum inhibitory requirements (MIR)	
		ng	nmol
1	(+)-60l	1000	5.65
2	(-)-60b	1000	5.18
3	(+)-60m	1000	4.74
4	(+)-60c	1000	4.56
5	(+)-60n	1000	4.18
6	(-)-60f	1000	3.77
7	(+)-101b	1000	3.76
8	(+)-59m	1000	3.29
9	(+)-101c	1000	-
10	(+)-59l	> 1000	-
11	(-)-102l	> 1000	-
12	(+)-101l	> 1000	-
13	(+)-104l	> 1000	-
14	(-)-121	> 1000	-
15	(+)-101m	> 1000	-
16	(+)-103m	> 1000	-
17	(+)-103m	> 1000	-
18	(+)-59b	> 1000	-
19	(+)-59c	> 1000	-
20	(+)-59n	> 1000	-
21	(+)-101n	> 1000	-
22	(+)-60e	> 1000	-
23	(-)-60g	> 1000	-
24	(-)-66h	> 1000	-
25	(-)-65j	> 1000	-
26	(-)-65i	> 1000	-
27	(+)-67	> 1000	-
28	Galantamine	1.6	4.35x10 ⁻³

The TLC bioautographic method suggests that the compounds are weak inhibitors, because all the activity occurs at the highest concentration tested (1000 ng/mL). This value was converted into the nanomole minimum inhibitory requirement for each compound, which is also reported in Table 5.3. It is possible that some of the compounds tested would show activity above this concentration, however concentrations above this would not make viable drug candidates. Even 1000 ng/mL is much higher than that of currently employed AChE

inhibitors, such as Galantamine which is active at 1.6 ng/mL. These results do allow an understanding of the SAR to be developed.

For a small target based library such as this, the relatively narrow concentration testing range used for both the TLC and Ellman assay, is considered as the 'hit' compound range and is used to accelerate development towards more lead-like compounds through SAR based optimisation. The downfall is that for compounds that are only weakly active, there is a larger degree of uncertainty in values used for calculation of the compound's dose-response properties, as can be seen in the measured IC₅₀ values.

5.3.1 Ellman Assay Results

For the Ellman method, a high degree of uncertainty in the results stemmed from the absorbance being measured for weak inhibition activity. This is attributed to the absorbance values being only slightly different to those obtained where no inhibition occurs. Additionally, a large degree of standard deviation was already observed for readings with no activity, highlighting the sensitive nature of this assay. As a consequence, for compounds that showed activity simply at their higher concentrations, only a fraction of the overall response was measured. In these cases, the response for the concentration range required to calculate the IC₅₀ value was extrapolated by the data processing performed by GraphPad Prism.

The result of this is that the dose response curves for the active compounds have large error bars and, consequently, the 95% confidence intervals for the IC₅₀ values are relatively wide when compared to that measured for the known inhibitor Galantamine. Where the 95% confidence interval range for Galantamine was 1.019 to 2.008 µM, the lowest range for any of the synthesised compounds tested was 0.1636 to 6.199 µM for **(+)-101b**, followed by 8.329 to 69.35 µM for **(+)-60l**. For compounds deemed inactive, the curve fitting calculation used by GraphPad gave the output 'not converged', because the data did not follow the sigmoidal trend resulting from inhibition. Compounds **(+)-59l**, **(-)-102l**, **(+)-101l**, **(+)-104l**, **(-)-121**, **(+)-101m**, **(+)-103m**, **(-)-102m**, **(+)-59b**, **(-)-60b**, **(+)-59c**, **(+)-101c**, **(+)-59n**, **(+)-60n**, **(+)-60e**, **(-)-66h**, **(-)-65j** & **(+)-67** were found to be inactive beyond the testing limits and hence no IC₅₀ values could be determined.

The Ellman method determined the best AChE inhibitor to be **(+)-101b**, with an IC₅₀ value of 1.01 µM. Although this value is lower than Galantamine, the range of the confidence interval is relatively larger, owing to the higher degree of standard deviation in the triplicate measurements. All of the other compounds have significantly higher IC₅₀ values than Galantamine and even wider confidence interval ranges. Comparison of the dose-response

curves from the calculated percentage inhibition for each of the active compounds can be seen in Figure 5.5.

Table 5.4 Ellman assay AChE inhibition results.

Entry	Compound	IC ₅₀ (μM)	95 % Confidence Interval
1	(+)-101b	1.007	0.1636 to 6.199
2	(+)-60l	24.03	8.329 to 69.35
3	(+)-60c	34.77	7.668 to 157.7
4	(+)-59m	131.8	10.81 to 1608
5	(-)-60g	162.5	78.31 to 337.2
6	(+)-60m	364.7	97.40 to 1365
7	(-)-60f	437.5	52.92 to 3616
8	Galantamine	1.430	1.019 to 2.008

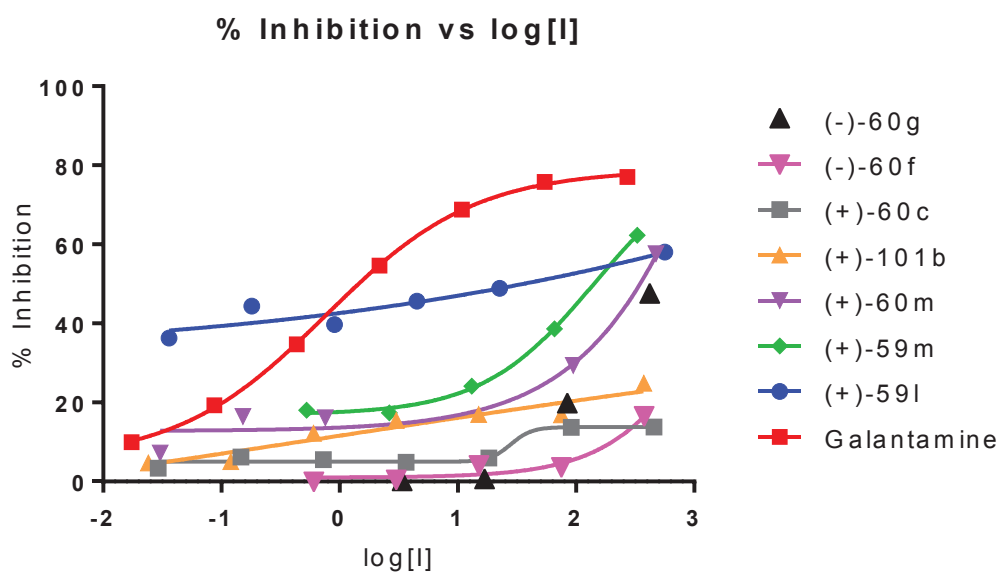


Figure 5.5 Dose-response curves for the % inhibition of active compounds.

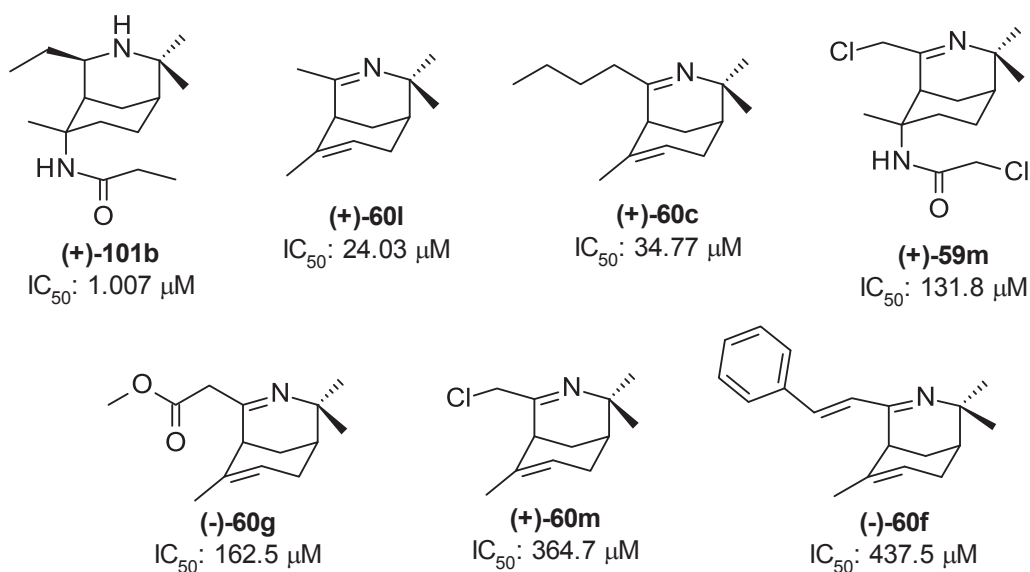


Figure 5.6 Structures of compounds that showed AChE inhibition with the Ellman assay.

There were only a limited number of compounds that showed weak activity so the SAR data is relatively inconclusive, though some trends were noticed. The most notable trend was that the scaffolds containing both the imine and alkene functionality show the highest proportion of active compounds. Eight of the nine compounds tested with this functionality showed AChE inhibition activity. This is compared to the scaffolds that contain imine and amide functionality, of which only one of six compounds showed activity. These comparisons are summarised in Table 5.5. Although this sample size is small, it is interesting to note that removal of the imine functionality is associated with a reduction in alkene activity, because none of the three scaffolds with amine and alkene functionality showed any activity.

Table 5.5 Comparison of functionality on AChE inhibitors.

	C-6 Amide	C-6 Alkene
N-3 Imine	(+)-59m (1/6)	(+)-60l, (-)-60g, (+)-60m, (+)-60c, (+)-60n, (+)-60e, (-)-60f, (-)-65i (8/9)
N-3 Amine	(+)-101n, (+)-101b (2/6)	(0/3)

The influence on activity that results from the functionality provided by the nitrile reagents (at C-4 for the alkene scaffolds and C-4, as well as the C-6 amide substituent in the amide containing scaffolds) was less distinguishable, with no clear or observable trends in the data. Other than the smallest functionality at C-4 (-CH₃) on the alkenes giving the best IC₅₀, the variability in functionality makes it difficult to choose a property that corresponds to the activity.

These results show that this library of compounds has the potential to be developed into more potent inhibitors despite none of the compounds presenting precise AChE inhibition potency close to that of Galantamine. Development of a more potent inhibitor was explored through the use of molecular modelling in Chapter 7. Future work may include the use of STD NMR to investigate the potential enzyme-inhibitor interactions for these weak inhibitors and also determine if they do in fact compete for the same active site as Galantamine.

5.4 Assessment of Rationally Designed AChE Inhibitors

After the molecular modeling guided synthesis of compounds **(+)-112** and **(+)-114** (Figure 5.7), these compounds were evaluated for their AChE inhibition properties with both the TLC bioautographic and Ellman assay methods. The results from these assays can be seen in Table 5.6. Although the TLC bioautographic assay did not show any significant inhibition, with only the 1000 ppm samples displaying weak signs of inhibition, the Ellman Assay proved that these compounds did, in fact, inhibit AChE. Compound **(+)-112** was found to inhibit AChE

with an IC_{50} value of 43.46 μ M, while **(+)-114** was found to have an IC_{50} value of 87.82 μ M. Interestingly, these activities followed the trend of docking scores determined by the molecular modeling. These values are also significant improvements from the inactivity of the compounds they were derived from.

Although these values are not lower than the compounds **(+)-60l**, **(+)-101b** and **(+)-60c**, they show a higher level of confidence in their inhibition results, as seen by the reduced range of the IC_{50} value confidence intervals and smaller error in the triplicate measurements, seen in the dose-response curves (Figure 5.8 and Figure 5.9 for **(+)-112** and **(+)-114**, respectively). These results also show that the 3-aza-bicyclo[3.3.1]nonane scaffold retains activity when the C-6 amine is introduced, despite no longer containing C-6 alkene or N-3 imine functionality, as previously shown to result in reduced activity. This validates the results of the rational drug design outlined in Chapter 3, as guided by the molecular modeling data obtained in Chapter 7. It also highlights the scaffold's potential to be developed further into a more potent inhibitor. This may be investigated in future work, in particular, using lead optimisation *via de novo* or fragment based scaffold extension at the C-6 amine.

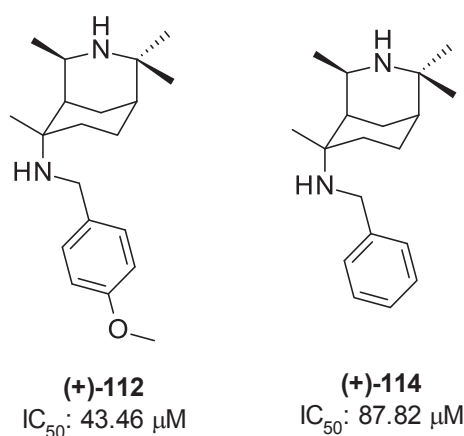


Figure 5.7 Molecular modeling guided rational drug designed compounds **(+)-112** and **(+)-114** and Ellman assay AChE inhibition IC_{50} values.

Table 5.6 AChE inhibition properties of **(+)-112** and **(+)-114**, from the TLC bioautographic and Ellman assays.

Entry	Compound	Ellman Assay results		TLC bioautographic MIR results	
		IC_{50} (μ M)	95% Confidence Interval	ng	nmol
1	(+)-112	43.46	34.86 to 54.12	1000	3.165
2	(+)-114	87.82	40.98 to 192.6	1000	3.497

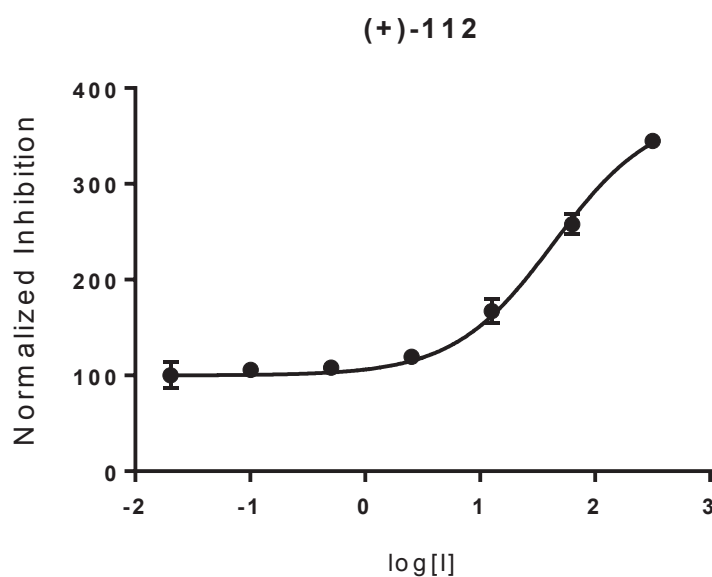


Figure 5.8 Dose-response curve for the IC_{50} value calculated for **(+)-112**.

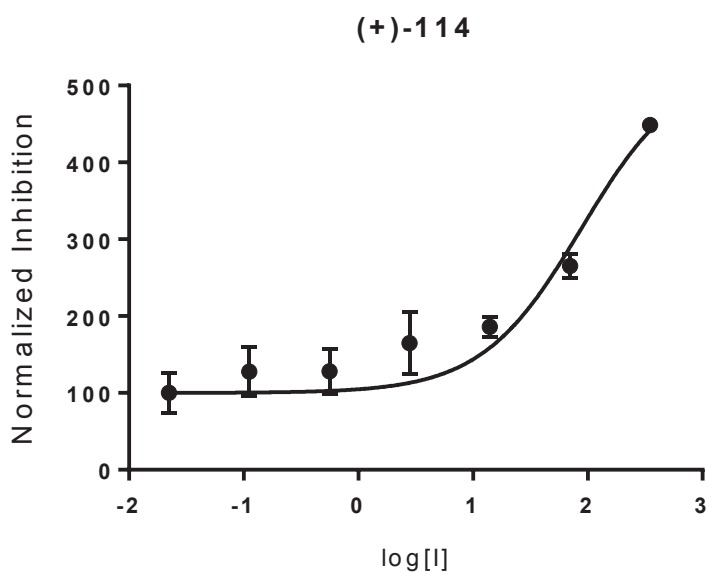


Figure 5.9 Dose-response curve for the IC_{50} value calculated for **(+)-114**.

5.5 Conclusions and Future Directions

The results from both the TLC bioautographic and Ellman methods of determining the AChE inhibition activity of the alkaloid-like compounds synthesised showed that the active compounds only had weak activity. Although several compounds show activity, no real SAR data could be confirmed due to the limited sample size. The assay data in combination with docking results outline in Chapter 7 did, however, guide the design and synthesis of a set of compounds with improved activity. Most notably, modeling predicted the general orientation of the alkaloid-like compounds within the AChE active site, which highlights the possibility of

utilising the C-6 location in the scaffold to increase interactions with the aromatic gorge leading into the active site.

Due to only two of the compounds being successfully made and tested, these are preliminary results in confirming the hypothesis that extending the scaffold with aromatic functionality in the C-6 location of the scaffold would increase the protein interactions with the AChE active site gorge and hence increase inhibition activity. Further work would be required to synthesise and test more compounds to confirm that this is indeed a viable way to increase the activity of compounds with the 3-aza-bicyclo[3.3.1]nonane scaffold. In particular, future work should utilise *De Novo* or fragment based scaffold extension, to hypothesise a set of compounds that fit the gorge more precisely than those compounds proposed based on the aldehydes available in-house. If this were to be successful, other studies, such as STD NMR or 3D HSQC NMR could also be used to confirm the proposed binding orientation of the compounds and gain more understanding about the binding epitopes.

It is interesting to note that of the three compounds that were active in the MTS assay in Chapter 4, two were also identified as active AChE inhibitors. This is a good result to show that this class of compounds does have the potential for broad range biological activity, hence validating the usefulness of the broad screening of the compounds discussed in Chapter 6. Future work could screen these compounds against the NMDA and histamine H₃ receptors for dual action mechanisms, as mentioned in Chapter 1. The compounds deemed to be inactive against AChE are definitely worth investigating for other biological activity and hence are still submitted for broad screening as outlined in Chapter 6.

CHAPTER 6: External Broad Screening

6.1 General Introduction

The pharmaceutical company Eli Lilly offers an open innovation drug discovery (OIDD) program, whereby a selection of the synthesised library is undergoing broad screening for their biological properties. Compounds submitted to the OIDD are assessed with several processes. Firstly, *in silico* screening is used to computationally evaluate the molecules for any pharmaceutically undesirable motifs^[184] or to determine if they have a high similarity to controlled substances, known drugs and compounds already in the Lilly or PubChem databases. Compounds that show more than 85% similarity are disregarded. The compounds that pass this initial screen will then be analysed, using the Blaze method,^[185] to determine if they have a tendency to bind to specific biological targets. For compounds that pass the *in silico* screening, samples can be submitted for *in vitro* screening.

6.2 The *In Vitro* Screening Process

The OIDD program uses a screening panel that is comprised of ‘a series of assays modules’. These screening modules use both target-based and phenotypic assays and are broken down into primary, secondary and confirmatory assays, where a compound only proceeds to the next assay based on the preceding result. The primary screen is performed at a single concentration (or single point/SP) and reported as a percentage of the maximum inhibition or stimulation response at a given concentration. For most assays, a 50% activity threshold is implemented to determine if the compound will be tested in the second primary assay, where the same assay is repeated at increasing concentrations to give a concentration response curve. Secondary assays are used to profile the activity of biochemical and cell-based assays before the final mode of action type assay is performed to confirm the biology.

6.2.1 *In Silico* Screening Results

Of the 31 compounds submitted for *in silico* screening, 16 passed and were submitted for *in vitro* screening. Table 6.1 lists the compounds that failed the OIDD *in silico* screening and the corresponding reason. With the exception of the compounds that were considered to be too similar to others already existing in the databases (as denoted by “insufficient novelty”), most compounds were failed as they contained undesirable motifs including alkyl halides, enamines, esters, weakly reactive compounds with electron donating groups (michael_demerited), monohalo methyl ketones and halogens that are adjacent to aliphatic carbons. The structures of the compounds that passed the *in silico* screen, and as such were submitted for *in vitro* screening, can be seen in Figure 6.1, on the other hand, those that failed the *in silico* screening are shown in Figure 6.2.

Table 6.1 List of compounds that did not pass *in silico* screening.

Entry	Compound	Reason
1	(+)-59b	Insufficient novelty
2	(-)-121	Ester, michael_demerited, enamine_2
3	(-)-102l	Insufficient novelty
4	(+)-101m	Alkyl_Halide, Halogens_to_multiple_aliphatic_C, monohalo_methyl_ketone
5	(+)-103m	Alkyl_Halide
6	(+)-67	Cyano_methyl_amine, ester
7	(+)-59m	Alkyl_Halide, Halogens_to_multiple_aliphatic_C
8	(+)-60m	Alkyl_Halide
9	(+)-103m	Alkyl_Halide
10	(-)-60b	Insufficient novelty
11	(+)-60n	Insufficient novelty
12	(-)-102n	Insufficient novelty
13	(-)-66h	Hemiacetal_acyclic, enamine_2
14	(-)-65j	Keto_carbonyl, nitro
15	(-)-65i	Keto_carbonyl, bromine

Compounds undergoing *in vitro* screening

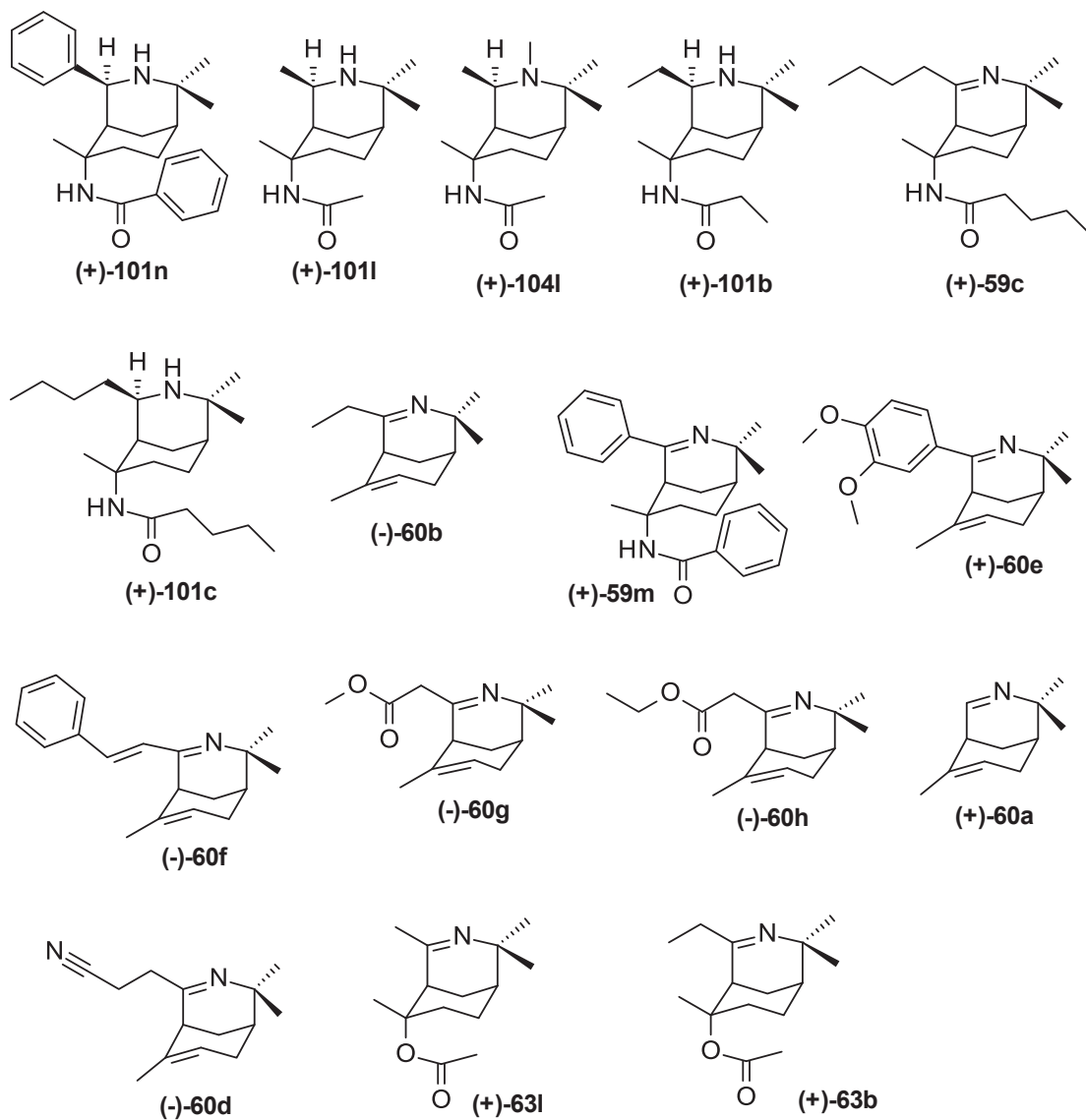


Figure 6.1 Compounds submitted to OIDD program that are undergoing *in vitro* screening.

Compounds that failed *in silico* screening

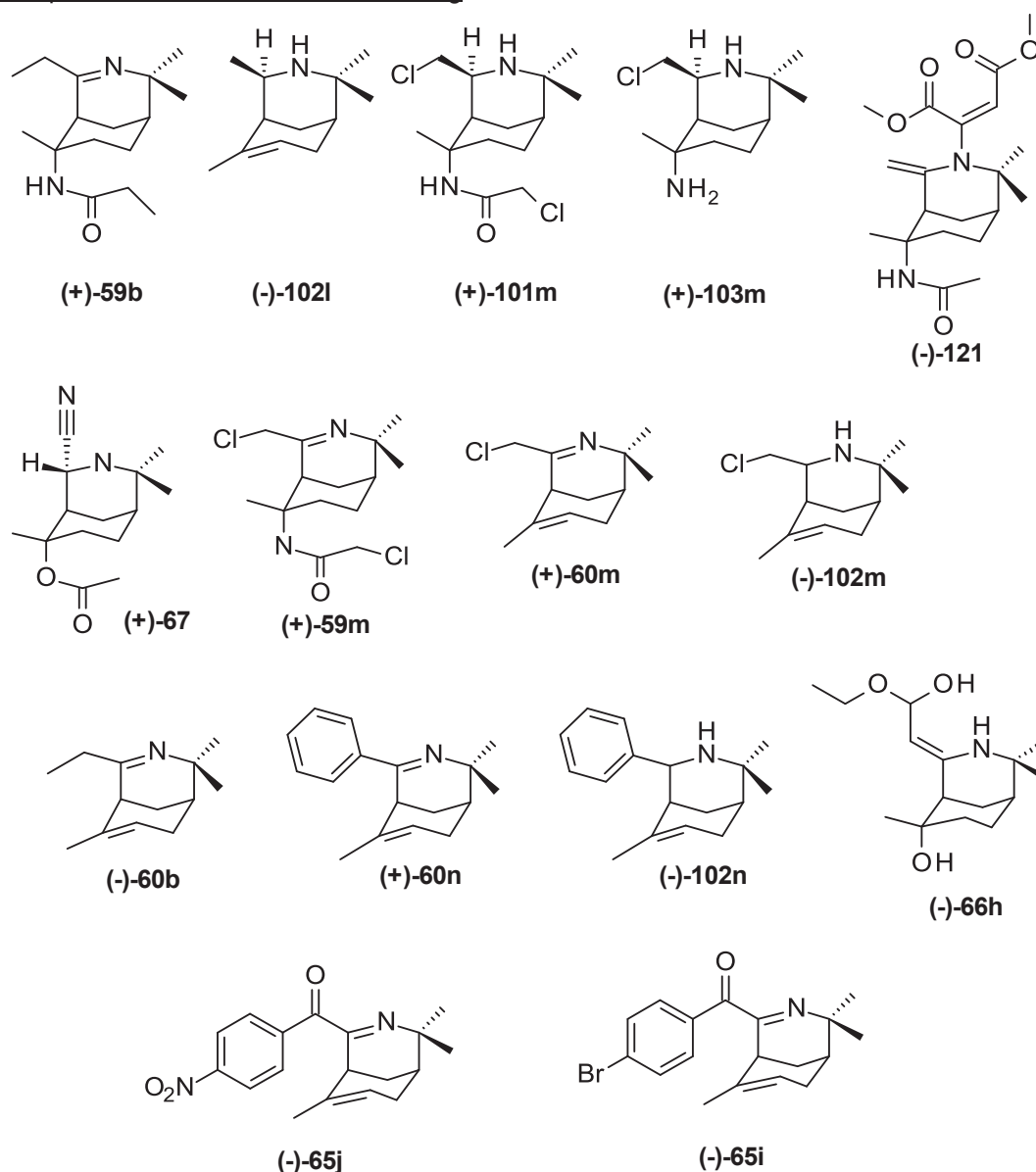


Figure 6.2 Compounds submitted to OIDD program that failed *in silico* screening.

6.2.2 Therapeutic Screening Targets and Results

The therapeutic target areas that are assessed by the OIDD program include oncology, neuroscience, endocrine and cardiovascular, diabetes, immunology and musculoskeletal, as well as any other emerging markets that Lilly deems of interest at the time of screening. The observation of activity towards any of the biological targets associated with these areas would warrant the potential for further investigation of these properties for the active compound.

The *in vitro* screening of the submitted compounds is an ongoing process and, unfortunately, we are still waiting on results for most of the compounds submitted. For the five compounds that have been screened so far, the primary single point screening results obtained are tabulated in the section corresponding to each target. In these tables, the

negative results have been coloured red, while those over the 50% activity threshold have been coloured green and the positive results below the threshold are black. The type of assay used is coloured blue.

6.2.2.1 Endocrine and Cardiovascular

The first of the endocrine and cardiovascular targets is a protein involved in the regulation of cholesterol called proprotein convertase subtilisin kexin type 9 (PCSK9).^[186] Inhibition of PCSK9 synthesis has been associated with protection against coronary artery disease and the lowering of low-density lipoproteins associated with cholesterol.^[187] Primary screening assay results for PCSK9 can be seen in entries one and two of Table 6.2.

The second set of endocrine and cardiovascular targets includes Glucagon-like peptide-1 (GLP-1) and its receptor (GLP-1R). Although there are several complementary mechanisms for treatments involving GLP-1, it has been noted that GLP-1 secretion is decreased in people with type 2 diabetes.^[188] Regulation of GLP-1 secretion is, therefore, a target in the treatment of type 2 diabetes. The peptide is a potent anti-hyperglycemic hormone that induces glucose-dependent insulin secretion and suppresses glucagon secretion, in turn promoting the sensitivity of insulin, making it more effective in cases of reduced efficacy. In addition to a phenotypic screen of a compound's ability to stimulate secretion, the OIDD program investigates the enhancement of glucose-dependant insulin secretion through activation of the GLP-1 receptor *via* positive allosteric modulation.^[189] This assay uses oxyntomodulin, which is a low-affinity agonist used to test for selective modulation of the receptor *via* competition binding and signal transduction studies.^[190] The primary screening assay results for GLP-1 and GLP-1R can be seen in entries 3 through 6 of Table 6.2.

The last endocrine and cardiovascular target is free fatty acid receptor 4 (FFAR4, also known as GPR120). As the name suggests, it is a receptor for long-chain fatty acids, such as Omega-3, and is found to be expressed in the pancreas, adipose tissue, the gastrointestinal tract and pituitary gland. Activation of this receptor is required for the regulation of body weight and glucose homeostasis and, therefore, is a drug target for metabolic disease and diabetes,^[191] with therapeutic benefit already seen in the treatment of obese mice.^[192] Primary screening assay results for GPR120 can be seen in entry 7 of Table 6.2.

Table 6.2 Summary of primary screening results for OIDD endocrine & cardiovascular targets.

Entry	Target / assay used (test conc.)	Compound primary screen results %				
		(+)-101l	(+)-104l	(+)-101b	(+)-101c	(+)-101n
<i>Endocrine/cardiovascular</i>						
1	PKS9 AlphaLisa Huh7 (inhibition at 5 μ M)	18.42	21.06	2.923	-9.893	26.62
2	PCSK9 Huh7 Viability CellTiter- Glo (inhibition at 5 μ M)	7.121	10.37	-8.353	-0.3945	13.58
3	GLP-1 Secretion mSTC-1 GLP1 Sec (stimulation at 2 μ M)	5.257	-0.6343	1.251	2.628	-0.9143
4	GLP-1 Secretion mSTC-1 GLP1 Sec (stimulation at 20 μ M)	7.929	-1.208	-0.0128	1.666	-2.36
5	GLP-1R PAM hGLP1R HiR cAMP HEK293 GLP(9-36) (stimulation at 20 μ M)	0.1956	0.03445	0.2965	0.2065	-0.5628
6	GLP-1R PAM hGLP1R cAMP HTRF ST HEK293 OXM (stimulation at 20 μ M)	-0.9226	3.41	-4.561	-11.35	-16.07
7	GPR120 Agonist (Stimulation at 30 μ M)	-0.2123	-0.315	-0.2362	0.08097	-0.5249

6.2.2.2 Neuroscience

One of the neuroscience targets is the Nav1.7 voltage-gated sodium ion channel, which is a potential target for therapeutic pain relief. Primarily found in the peripheral nervous system and sympathetic ganglia, it is involved in generating action potentials and the propagation or release of neurotransmitters. There is strong evidence that Nav1.7 inhibitors could be used to treat chronic pain without the side effects and efficacy issues associated with currently used non-selective sodium channel inhibitors.^[193] Primary screening assay results for Nav1.7 can be seen in entry 1 of Table 6.3.

Another neuroscience target is *O*-linked *N*-acetyl glucosamine hydrolase (OGA). It is a protein which, when inhibited, reduces the aggregation of tau protein^[194] into the insoluble hyperphosphorylated forms associated with Alzheimer's disease, as outlined in Section 1.7. This reduction of aggregation results from an increase in tau modification by *O*-linked *N*-acetyl glucosamine (*O*-GlcNAc) associated with OGA inhibition.^[195] Primary screening assay results for OGA can be seen in entry 2 of Table 6.3.

Table 6.3 Summary of primary screening results for OIDD neuroscience targets.

Entry	Target / assay used (test conc.)	Compound primary screen results %				
		(+)-101l	(+)-104l	(+)-101b	(+)-101c	(+)-101n
<i>Neuroscience</i>						
1	Nav1.7 Antagonist (inhibition at 3 μ M)	5.806	-3.843	-6.408	18.45	8.359
2	OGA hOGA1 Quench 0.3 DMDS 384 (inhibition at 30 μ M)	-	-12.2	-17.22	-0.0616	-1.494

6.2.2.3 Autoimmune

The autoimmune target investigated is Interleukin 17 (IL-17). IL-17 is a protein essential in the pathology of autoimmune diseases such as multiple sclerosis, psoriasis, psoriatic and rheumatoid arthritis and inflammatory bowel disease.^[196] The IL-17A homodimer is suggested to have roles in neutrophil homeostasis (regulation of white blood cells), the pathogenesis of inflammation and natural defences against extracellular bacteria and fungi.^[197] This results from IL-17 stimulating the release of cytokines and chemokines that direct memory T cells and neutrophils to the site of injury or inflammation associated with the listed autoimmune diseases. Primary screening phenotypically identifies compounds that inhibit the secretion of IL-17, or identify compounds that disrupt IL-17A protein-protein interactions. Primary screening assay results for IL-17 and IL-17A can be seen in Table 6.4.

Table 6.4 Summary of primary screening results for OIDD autoimmune targets.

Entry	Target / assay used (test conc.)	Compound primary screen results %				
		(+)-101l	(+)-104l	(+)-101b	(+)-101c	(+)-101n
<i>Autoimmune</i>						
1	IL-17 secretion antiCD3/antiCD28/IL23_PBMC ELISA IL-17 sec (inhibition at 10 µM)	9.871	8.031	2.584	-5.366	8.958
2	IL-17 secretion antiCD3/antiCD28/IL23_PBMC ELISA IL-5 sec (inhibition at 10 µM)	-73.24	2.69	24.75	33.41	72.63
3	IL-17A PPI AlphaLisa (inhibition at 100 µM)	-2.565	-1.295	-6.202	-2.565	3.188
4	IL-17 secretion antiCD3/antiCD28/IL- 23_PBMC Cytotoxicity (stimulation at 10 µM)	0.8799	-8.631	-2.936	-6.1	8.809

6.2.2.4 Oncology

Oncology screening is performed on the Cluster of Differentiation 73 (CD73) enzyme, which catalyses one of the steps involved in converting ATP to adenosine in cancers. Adenosine generated by CD73 is immunosuppressive, causing impaired antitumor immune responses and thus results in tumour progression and metastases.^[198] Compounds that target and inhibit CD73 may, therefore, make a novel immune therapy pathway for protecting against the development of cancer. Primary screening assay results for CD73 can be seen in Table 6.5.

Table 6.5 Summary of primary screening results for OIDD oncology target.

Entry	Target / assay used (test conc.)	Compound primary screen results %				
		(+)-101l	(+)-104l	(+)-101b	(+)-101c	(+)-101n
<i>Oncology</i>						
1	CD73 MassSpec (inhibition at 50 μ M)	4.422	0.16	8.163	-	7.823

6.2.2.5 Tuberculosis

Tuberculosis (TB) is an infectious disease caused by the bacterial species *Mycobacterium tuberculosis*. It is responsible for millions of deaths worldwide and continues to be a problem due to the development of drug-resistant strains.^[199] The OIDD program screens compounds for any capacity to inhibit the growth of the virulent H37Rv strain using phenotypic cellular assays. Primary screening assay results for TB can be seen in Table 6.6.

Table 6.6 Summary of primary screening results for OIDD tuberculosis target.

Entry	Target / assay used (test conc.)	Compound primary screen results %				
		(+)-101l	(+)-104l	(+)-101b	(+)-101c	(+)-101n
<i>Tuberculosis</i>						
1	Tuberculosis MIC SP IDRI (inhibition at 20 μ M)	7.4	9.1	-14.8	9.2	1.7

6.2.2.6 Malaria

Malaria is an infectious disease where *Plasmodium* parasites are transferred from the saliva of female *Anopheles* mosquitoes to a bitten person's blood. When this happens, the sporozite form of the parasite reaches the liver, where they can mature and result in liver infection, causing damage to blood cells.^[200] Malaria is a global problem, estimated to have caused 214 million deaths in 2015.^[201] The OIDD program screens compounds for activity against different stages of the *Plasmodium berghei* (Pb) strain, found in the liver. This is done by measuring the cell viability of sporozite infection and another developmental form of the parasite known as schizonts. It also screens for inhibition of parasite growth for the *Plasmodium falciparum* (DD2) strain found in the blood. Within the same screening module, compounds are tested for their non-specific cytotoxic properties against the human liver cancer cell line Hep G2. The results of the screening are shown in Table 6.7.

Table 6.7 Summary of primary screening results for OIDD malaria target.

Entry	Target / assay used (test conc.)	Compound primary screen results %				
		(+)-101l	(+)-104l	(+)-101b	(+)-101c	(+)-101n
<i>Malaria</i>						
1	<i>Plasmodium falciparum</i> DD2 (inhibition at 12.5 μ M)	-	59.69	-	25.75	40.93

6.3 Summary and Conclusion of Broad Screening Results

From the results returned by the OIDD *in vitro* screening so far, two compounds show a response above the 50% activity threshold. These include the inhibition of IL-17 secretion by 72.63% by compound **(+)-101n** at 10 μ M and the inhibition of DD2 growth at 59.69% by **(+)-104l** at 12.5 μ M. It must be noted that compounds **(+)-101c** and **(+)-101n** also showed activity close to the activity threshold for DD2 growth at 25.75 and 40.93%, respectively, inferring that there may be some correlation between activity and the 3-azabicyclo[3.3.1]non-3-ene core structure. For ease of interpretation, the positive result data from each of the tables in Section 6.2.2 has also been represented as a 3D graph in Figure 6.3.

The limited activity across all of the targets also allows the deduction that the compounds show some level of target selectivity, a positive to consider in the future development of these compounds. Due to the limited number of compounds screened so far by *in vitro* testing, it is not possible to determine any significant trends in activity or a SAR across the variation in functionality. As most of the results for the compounds tested so far were below the 50% activity threshold, these compounds will not be assessed by the concentration response primary assay or secondary assays.

All positive OIDD results

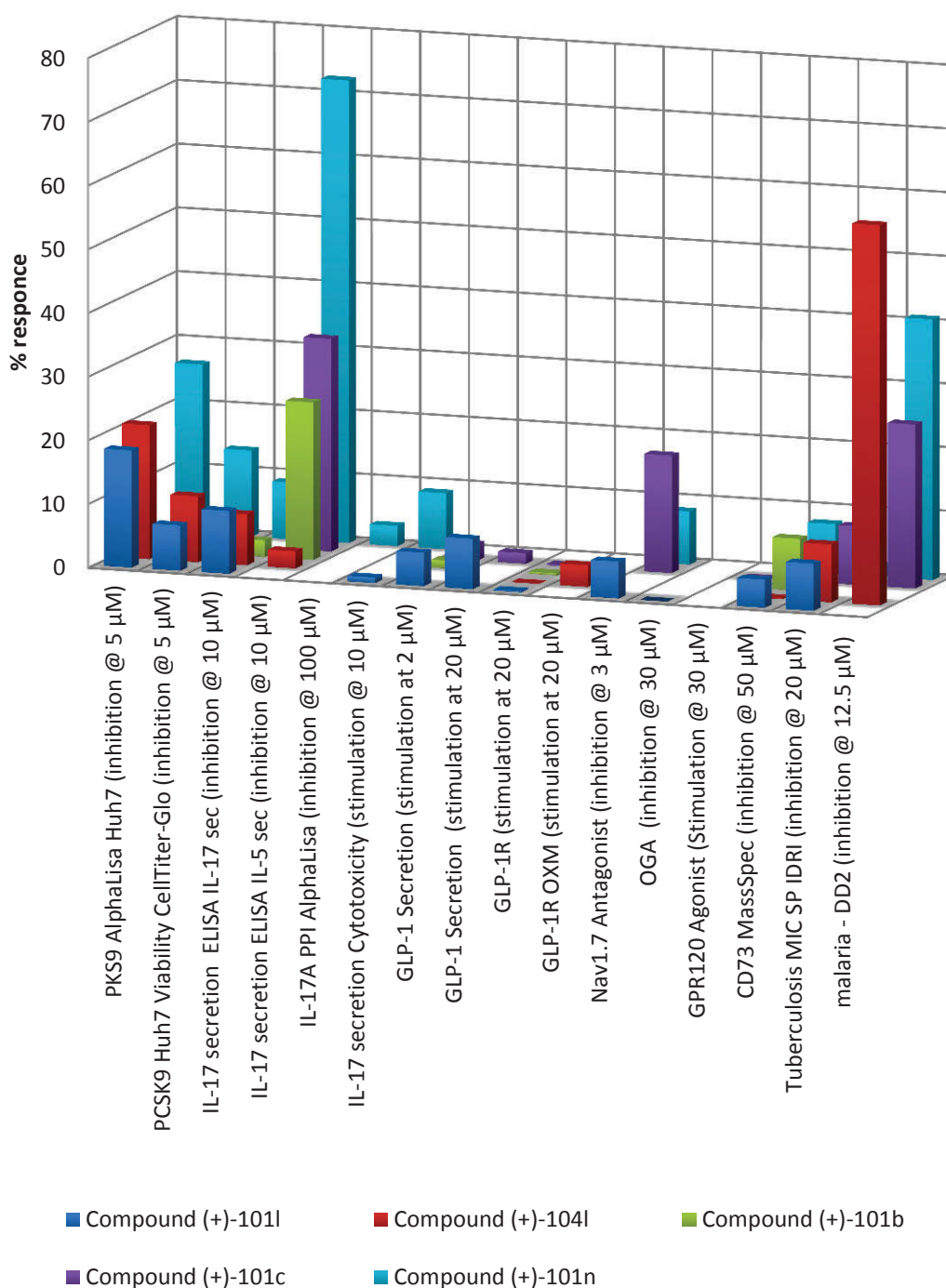


Figure 6.3 3D representation of OIDD primary screening results for each compound and corresponding assay.

CHAPTER 7: Computer-Aided Molecular Modeling

7.1 General Introduction

Molecular modeling has become a powerful tool for accelerating the drug discovery and development timeline. Computer-aided drug design (CADD) aims to reduce the time it takes to develop the potency, efficiency and bioavailability of drug candidates, while also minimising their potential toxicity. Molecular modeling is generally implemented in the lead identification and optimisation phases of a standard discovery pipeline, such as that summarised in Figure 7.1.

Lead compounds can be identified and optimised using modeling results from *de novo* or docking studies. They can then direct rational structure-based drug design (SBDD), when the structure of the biological target is known, such as for AChE in this project (Sections 7.3 and 7.4). If the biological target is unknown, then pharmacophore and QSAR models for ligand-based drug design (LBDD) are used to facilitate the phenotypic cell assays, such as those used in this project, or to predict potential targets.

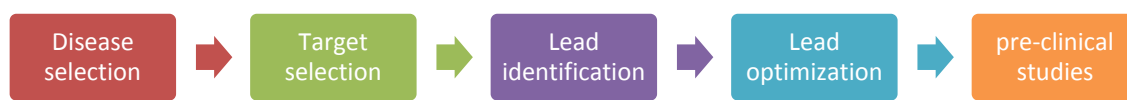


Figure 7.1 Summary of a standard drug discovery pipeline.

Molecular modeling is also often used to predict potential drug candidate's physicochemical properties, which have been identified to be significant for the compound to be considered within the drug-like chemical space. An example of this is Lipinski's rule of five, which is outlined in Chapter 1 and, furthermore, the corresponding properties are discussed in Section 7.2. These methods can be used to screen libraries of compounds and filter out undesirable compounds that fall outside these constraints. Of course, not all compounds developed this way eventuate with improved properties. Modeling data can, however, help assist in the prioritisation of chemical synthesis during the design stages to accelerate the labour-intensive laboratory work. Biological testing is still necessary to evaluate the *in vitro* activity, toxicity and pharmacokinetics before they become lead compounds. All of the modeling calculations performed in this chapter were done using Discovery Studio 4.5, Client v17.1.0.16143 (Dassault Systèmes Biovia Corp).^[202] All of the calculation parameters used are listed in the Appendices, Chapter 10.

7.2 Evaluation of Drug-Like Properties

As part of the rational drug design process, properties such as molecular weight (MW), logP and polar surface area (PSA) are important when considering a drug's solubility and bio-

availability. Properties such as the number of hydrogen bond donors (HBD) and acceptors (HBA), as well as the number of rotatable bonds, are important with regard to the number of and types of interactions a compound could make and hence its target selectivity. These properties are listed in Table 7.1 for all of the synthesised, isolated and characterised compounds.

Table 7.1 List of physicochemical properties corresponding to each compound made.

Compound	MW	LogP	PSA	HBD	HBA	Rotatable bonds
(+)-59l	236.36	1.151	41.46	1	2	1
(+)-102l	179.31	2.386	12.03	1	1	0
(+)-101l	238.38	1.090	41.13	2	2	1
(+)-104l	252.40	1.625	32.34	1	2	1
(-)-121	380.49	1.567	84.94	1	6	6
(+)-59m	305.25	2.217	41.46	1	2	3
(+)-60m	211.74	2.851	12.36	0	1	1
(+)-101m	307.27	1.939	41.13	2	2	3
(+)-103m	230.78	1.385	38.04	2	2	1
(-)-102m	213.75	2.702	12.03	1	1	1
(+)-59b	264.41	2.485	41.46	1	2	3
(+)-101b	266.43	2.280	41.13	2	2	3
(+)-59c	320.52	4.310	41.46	1	2	7
(+)-60c	219.37	3.898	12.36	0	1	3
(+)-101c	322.54	4.105	41.13	2	2	7
(+)-59n	360.50	4.490	41.46	1	2	3
(+)-60n	239.36	3.992	12.36	0	1	1
(+)-101n	362.52	3.989	41.13	2	2	3
(+)-60e	299.42	3.959	30.82	0	3	3
(-)-60f	265.40	4.450	12.36	0	1	2
(-)-60g	235.33	2.354	38.65	0	3	3
(-)-66h	269.39	0.959	61.72	3	4	3
(-)-65j	312.37	3.763	75.25	0	4	3
(-)-65i	346.27	4.617	29.43	0	2	2
(+)-67	250.34	1.225	62.12	1	4	2
(+)-60a	163.26	2.240	12.36	0	1	0
(-)-60d	216.33	2.413	36.15	0	2	2
(+)-63l	237.35	1.799	38.65	0	3	2
(+)-63b	265.40	3.133	38.65	0	3	4
(-)-60h	249.36	2.703	38.65	0	3	4
(-)-102n	241.38	3.621	12.03	1	1	1
(+)-60l	177.29	2.318	12.36	0	1	0
(-)-60b	191.32	2.985	12.36	0	1	1
(+)-105l	194.32	1.130	38.37	1	2	0

As can be seen from Table 7.1, none of the compounds listed violate any of Lipinski's rules and therefore have potential to be orally administered drugs. The good drug-like properties that this library of alkaloid-like compounds shows can be attributed to their resemblance to natural products and the result of using a natural product starting material.

To recap Section 1.2, Lipinski's rule-of-five states that for small molecules intended to be administered orally, the molecular mass should be less than 500 Da, there should be less than five hydrogen-bond donors and less than 10 hydrogen bond acceptors, and the logP (calculated octanol-water partition coefficient) should be less than five.

7.2.1 Evaluation of ADMET Descriptors

ADMET is an abbreviation for Absorption, Distribution, Metabolism, Excretion and Toxicity. These are pharmacokinetic properties that are important to consider when developing drugs. Assessing and optimising these properties during the drug discovery process lowers the chance of developing compounds with undesirable pharmacokinetics, which would make them poor drug candidates and cause them to be discarded at later stages of the drug development pipeline.

The ADMET descriptors calculated by Discovery Studio 4.5 include aqueous solubility, blood-brain barrier (BBB) penetration, CYP2D6 binding, hepatotoxicity, intestinal absorptivity and plasma protein binding (PPB). Each of these models were developed using training sets of compounds to cover a range of prediction levels under which the analysed compounds fall. The intestinal absorption model was developed by Egan *et al.*^[203] and Egan and Lauri,^[204] as was the blood-brain barrier penetration model. The aqueous solubility model was developed by Cheng and Merz,^[204] the cytochrome P450 2D6 (or CYP2D6 binding) and hepatotoxicity models were developed by Susnow and Dixon,^[205] before an alternative method by Xia *et al.*^[206] was applied and used for compound assessment, as was that used for the plasma protein binding model, with the addition of work by Votano *et al.*^[207] The results of the ADMET calculations are summarised in Table 7.2.

Table 7.2 ADMET results of the alkaloid-like library.

Compound	Aqueous solubility	BBB penetration	CYP2D6 binding	Hepatotoxicity	Intestinal absorption	PPB
(+)-59l	3	2	FALSE	TRUE	0	FALSE
(+)-102l	3	1	FALSE	FALSE	0	FALSE
(+)-101l	3	2	FALSE	FALSE	0	FALSE
(+)-104l	3	2	FALSE	FALSE	0	FALSE
(-)-121	3	3	FALSE	FALSE	0	FALSE
(+)-59m	3	2	FALSE	TRUE	0	TRUE
(+)-60m	3	1	FALSE	TRUE	0	TRUE
(+)-101m	3	2	FALSE	FALSE	0	FALSE
(+)-103m	3	2	FALSE	FALSE	0	FALSE
(-)-102m	3	1	FALSE	FALSE	0	TRUE
(+)-59b	3	2	FALSE	TRUE	0	TRUE
(+)-101b	3	2	FALSE	FALSE	0	FALSE
(+)-59c	2	1	FALSE	FALSE	0	TRUE
(+)-60c	2	0	FALSE	FALSE	0	TRUE
(+)-101c	2	1	FALSE	FALSE	0	FALSE
(+)-59n	2	1	FALSE	TRUE	0	TRUE
(+)-60n	2	0	FALSE	FALSE	0	TRUE
(+)-101n	2	1	FALSE	FALSE	0	TRUE
(+)-60e	2	1	FALSE	FALSE	0	TRUE
(-)-60f	2	0	FALSE	FALSE	0	TRUE
(-)-60g	3	2	FALSE	FALSE	0	TRUE
(-)-66h	4	3	FALSE	FALSE	0	FALSE
(-)-65j	2	2	FALSE	TRUE	0	TRUE
(-)-65i	2	0	FALSE	TRUE	0	TRUE
(+)-67	3	3	FALSE	FALSE	0	FALSE
(+)-60a	3	1	FALSE	FALSE	0	TRUE
(-)-60d	3	1	FALSE	TRUE	0	TRUE
(+)-63l	3	2	FALSE	FALSE	0	FALSE
(+)-63b	2	1	FALSE	FALSE	0	TRUE
(-)-60h	3	1	FALSE	FALSE	0	TRUE
(-)-102n	2	0	TRUE	FALSE	0	TRUE
(+)-60l	3	1	FALSE	FALSE	0	TRUE
(-)-60b	3	1	FALSE	FALSE	0	TRUE
(+)-105l	3	2	FALSE	FALSE	0	FALSE

7.2.1.1 Aqueous Solubility

Aqueous solubility is used to assess a compound's drug-likeness and, hence, solubility in blood. This prediction uses a linear regression model to predict the solubility of compounds in water with a pH of seven at 25 °C. The following solubility level scores correspond to the predicted solubility and drug-likeness:

- 0 = Extremely low
- 1 = No, very low, but possible
- 2 = Yes, low
- 3 = Yes, good
- 4 = Yes, optimal
- 5 = No, too soluble

As can be seen in Table 7.2, most of the compounds were predicted to be drug-like and soluble and scored two or three, with compound **(-)-66h** having an optimal score of four.

7.2.1.2 Blood-Brain Barrier Penetration

This model predicts the concentration of an orally administered drug that passes from the blood into the brain tissue *via* the blood-brain barrier. The following prediction levels are used for blood-brain barrier penetration:

- 0 = Very high penetrant
- 1 = High
- 2 = Medium
- 3 = Low
- 4 = Undefined – if prediction falls outside 95% and 99% confidence range

As can be seen in Table 7.2, most of the compounds show very high to medium penetration, with only two compounds (**(-)-121** and **(-)-66h**) showing a low prediction. This prediction is of significant importance for drugs, such as AChE inhibitors, that are required to reach the brain. It is also important to note that it is desirable that compounds that do not target the brain do not pass the blood-brain barrier.

7.2.1.3 Human Intestinal Absorption

The following model predicts the level of intestinal absorption of a compound after it has been administered orally. This is important when considering how much of an administered dose will enter the blood stream. For humans, a compound that is well-absorbed is said to absorb by at least 90%. The following prediction scores are used for intestinal absorption levels:

- 0 = Good adsorption
- 1 = Moderate adsorption
- 2 = Poor adsorption
- 3 = Very poor adsorption

As can be seen in Table 7.2, all of the compounds analysed have a predicted score of zero and hence are predicted to show good intestinal absorption in humans.

7.2.1.4 CYP2D6 Binding

CYP2D6 is the human gene that encodes the cytochrome P450 2D6 enzyme. This enzyme is expressed in the liver and is responsible for the metabolism of a high portion of clinically administered drugs. For this reason, if a compound binds to and inhibits the function of this enzyme, the metabolism of other drugs in the body may be altered, a result called drug-drug interactions.^[208] As this is undesirable for maintaining the correct therapeutic dose of administered drug in the blood stream, testing for CYP2D6 inhibition is a fundamental

requirement in drug discovery and the development of regulations. Different drug outcomes may be the result of genetic variation amongst different people and this is often determined during clinical trials.^[209]

Discovery Studio 4.5 scores compounds screened by this module according to how well they fit the model. This score is used to classify a compound as a CYP2D6 inhibitor based on a score cut-off threshold. The prediction is either 'TRUE' if inhibition is calculated, or 'FALSE' if no inhibition is calculated. Only compound **(-)-102n** was predicted to show any inhibition of CYP2D6, as shown in Table 7.2.

7.2.1.5 Hepatotoxicity

Hepatotoxicity involves any damage to the liver cells caused by drugs. It can lead to liver failure and, as a result, reduced drug clearance from the body. Many drugs have been withdrawn from the market after cases of hepatotoxicity were discovered. It is, therefore, imperative that hepatotoxicity is identified during the drug discovery and development stages. Again, compounds are scored against a model and a cut-off is used to predict either 'TRUE' if hepatotoxicity is predicted or 'FALSE' if it is not. As shown in Table 7.2, eight compounds (**(+)-59l**, **(+)-59m**, **(+)-60m**, **(+)-59b**, **(+)-59n**, **(-)-65j**, **(-)-65i** and **(-)-60d**) are predicted to be hepatotoxic.

7.2.1.6 Plasma Protein Binding

The binding of drugs to carrier proteins in blood plasma plays a significant role in drug pharmacokinetics. Changes in drug efficacy can result from drugs being protected from metabolism, as well as having no pharmacological effect against the intended target while bound to plasma proteins. Although this circumstance is not necessarily a disadvantage, it is important when considering the drug's therapeutic dosing window between pharmacological effect and toxicity.

Discovery Studio 4.5 predicts the likelihood of a compound to be highly bound to plasma proteins, where a high prediction is that bound by greater than or equal to 90%. This prediction is based on a scoring threshold, to result 'TRUE' for highly bound or 'FALSE' for not highly bound compounds. Table 7.2 shows that 21 of the 35 analysed compounds from the alkaloid-like library are predicted to have high plasma protein binding.

7.2.1.7 Summary of Alkaloid-like Library ADMET Results

Based on the results outlined in Table 7.2, the following compounds are unlikely to make good drug candidates, according to Discovery Studio's ADMET predictions: **(-)-102n**, **(+)-59l**, **(+)-59m**, **(+)-60m**, **(+)-59b**, **(+)-59n**, **(-)-65j**, **(-)-65i** and **(-)-60d**. Despite this, it is still

possible that these compounds could be modified to optimise either their activity, or pharmacokinetic properties, to result in desirable properties. Modified compounds would also need to be assessed individually.

It is interesting to note that despite compounds **(+)-102l**, **(-)-121**, **(+)-101m**, **(+)-103m**, **(-)-66h** and **(+)-67**, showing good ADMET properties as predicted by Discovery Studio 4.5, these compounds were rejected by the Lilly *in Silico* screening (Section 6.2.1) on the grounds of toxicity or instability. This highlights that these predictions are only a rough guide that can be used to accelerate decisions for drug development and that more in-depth studies of a potential lead compound's ADMET properties should be explored by experimentation.

7.2.1.8 ADMET Plots

ADMET plots are used to assess the confidence in the calculations utilised to predict the properties of the compounds tested. Figure 7.2 below shows the ADMET plot for the compounds listed in Table 7.1. In this figure, the calculated logP is plotted against the calculated PSA, where each of the dark blue spots represents one of the compounds. There are also two sets of two confidence ellipses, the **red** and **green** representing the human intestinal absorption model of calculation confidence space at 95 and 99%, respectively, while the **magenta** and **cyan** represent the blood brain barrier penetration model of calculation confidence space at 95 and 99%, respectively. If any of the blue compound points fall outside of these ellipses then the calculations for predicting the ADMET properties are considered to be unreliable. As can be seen from Figure 7.2, all the compounds fall within all of the ellipses.

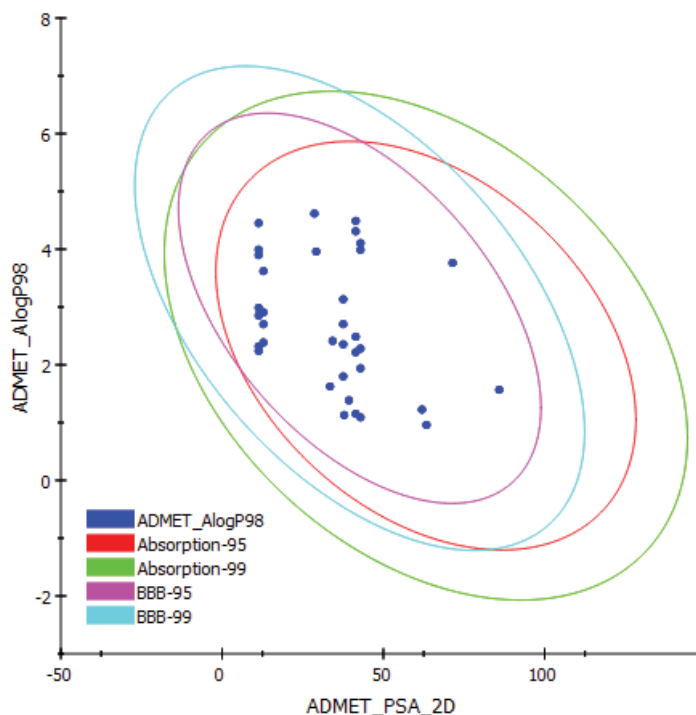


Figure 7.2 ADMET plot of alkaloid-like molecules synthesised.

7.3 Ligand Docking and Interactions

Docking is a computational process whereby potential poses or binding modes for a set of ligands against a specific target receptor are identified. Once ligands are docked, further calculations can be employed to predict the binding affinity of each pose and hence evaluate the relative energy of any potential biological interactions. For the purpose of this research, the docking between the alkaloid-like compounds synthesised and AChE was investigated to evaluate their potential as AChE inhibitors. The PDB protein file 1DX6^[210] was used, which contains the structure of *Tetronarce californica* acetylcholinesterase complexed with Galantamine at 2.3 Å resolution.

7.3.1 Preparing for Docking

Several procedures were carried out in order to obtain worthy docking data. The procedures followed were adapted from work by Kumari *et al.*^[211] The protein file was first prepared to ensure any missing residues from the protein are filled in and all hydrogens are added. Any ligands that are associated with the protein file were removed and the protonation of all the amino acids was adjusted to a set pH (for this purpose, 7.4 was used). The protein was then minimised to the lowest energy state. After this preparation was complete, the binding site within which compounds will be docked was defined. There are several ways in which this can be done in Discovery Studio 4.5. Firstly, potential binding sites can be predicted based on protein cavities within a specific size threshold. Secondly, the protein file may come

with pre-defined sites. Lastly, binding sites can be generated based on a selection of either amino acid residues or ligands within the protein. The residues in the AChE active site are well known, so the binding site was defined by selection of these residues. Any binding sites generated were assigned a set of coordinates within the file and have a set radius, which encompasses the residues where the binding interactions were calculated.

Ligand preparation and minimization calculations were used to ensure that each of the compounds docked are in their most likely confirmation and lowest energy state, contain all hydrogens and are protonated according to the predicted ionisation for the defined pH (7.4 was used to match the protein conditions). Preparation also corrected any valency issues and generated any possible isomers and tautomeric forms of each compound.

Once both the protein and ligands were prepared, the ligands were docked. Discovery Studio 4.5 has the option of using several different algorithms to perform the docking, but CDOCKER^[212] was the protocol chosen for this project. The docking calculations resulted in the output of a protein-ligand complex, which contained the predicted binding mode that result from the most favourable interactions between the residues in the binding site and the input ligand. Once a compound is docked, *in situ* minimization was required to find the lowest energy conformation of the binding mode. These calculations allowed the receptor to be flexible around the ligand, giving a confirmation from which the binding energy of the pose was calculated and a corresponding docking score assigned. Furthermore, because docking scores are a representation of binding energy, they are related to the binding affinity of the equilibrium process of the interaction between the active site and ligand.^[213] This is shown by the expression for the binding energy (ΔG) and binding affinity (K_A) in Equation 7.1 and Equation 7.2, respectively, for the equilibrium $[E] + [L] \leftrightarrow [EL]$, where E represents the enzyme, L represents the ligand and EL is the enzyme-ligand complex.

Equation 7.1 Expression for the binding energy.

$$\Delta G = -RT \ln K_A$$

Equation 7.2 Expression for the binding affinity.

$$K_A = \frac{[EL]}{[E][L]}$$

The order of the protocols used during docking is summarised in Figure 7.3. The parameters used for each of these calculations can be found in the Appendices (Chapter 10). The Ludi_3 scores have been reported and used to evaluate the relative strengths of the

binding interactions, where a higher score represents more favourable interaction between the ligand and protein for the ligand-protein complex generated by the docking. The Ludi scoring function was created by Böhm^[214] and was further developed to provide the most accurate estimate of the binding energy.^[215] The Ludi₃ score is a sum of the energy contributions from the following receptor-ligand complex interactions: hydrogen bonding, ionic, lipophilic, aromatic-aromatic, when the internal degrees of freedom of the ligand are reduced, and when the translational and rotational entropy is lost.



Figure 7.3 Summarised outline of the protocols used for docking in Discovery Studio 4.5.

7.3.2 Docking and Scoring Method Validation

To validate the method for docking ligands, a comparison was made between the interactions of AChE and Galantamine within the crystallised structure in the protein file (PDB: 1DX6)^[210] and those obtained from docking Galantamine in the active site, using the same procedure for docking the library of alkaloid-like compounds. The Ludi₃ score was also obtained as a reference from which to compare the scores generated for the docking of the library of alkaloid-like compounds.

Figure 7.4 shows a 2D representation of the interactions made between Galantamine and the amino acid residues in the AChE active site when co-crystallised with the protein (1DX6). Note that in Figure 7.4, in the interactions key, 'Pi-Pi T-shaped' refers to π - π edge-face interactions. These interactions can be compared to those formed by docking Galantamine in the active site, as seen in Figure 7.5. This shows that the *in silico* docking interactions predicted are very similar to the interactions achieved *in vitro*, whereby the residues GLU199, TRP84, HIS440 and ASP72 are all interacting with the same parts of Galantamine in both scenarios. There were also some differences in the interactions predicted. For instance, the π - π aromatic interaction between the docked Galantamine and PHE331 was absent, while new van der Waal's interactions were formed with SER122 and ASP72, which are not seen in the X-ray structure. This is to be expected yet should not detract from the model. Despite this, Figure 7.6 shows the 3D representation of the two scenarios superimposed, to show the similarity in the poses, where the Galantamine from the X-ray structure is coloured green and the docked pose is coloured blue. The overlay RMS for these poses was calculated to be 0.850. This result validates the docking model for use with the library of alkaloid-like compounds synthesised to

evaluate their potential for interacting with the AChE binding site and hence as AChE inhibitors. The Ludi_3 score calculated for the docked Galantamine was 653.

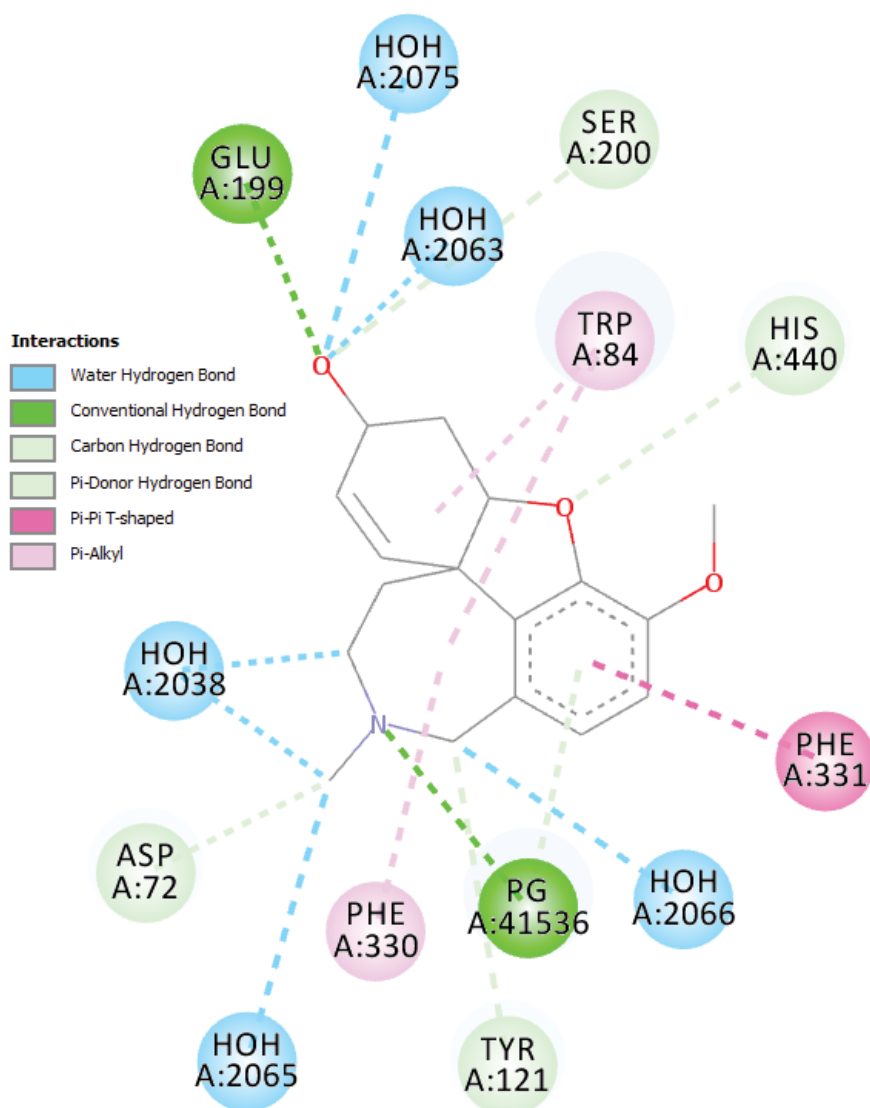


Figure 7.4 Crystal structure binding interactions of Galantamine in the AChE active site for protein file PDB: 1DX6.

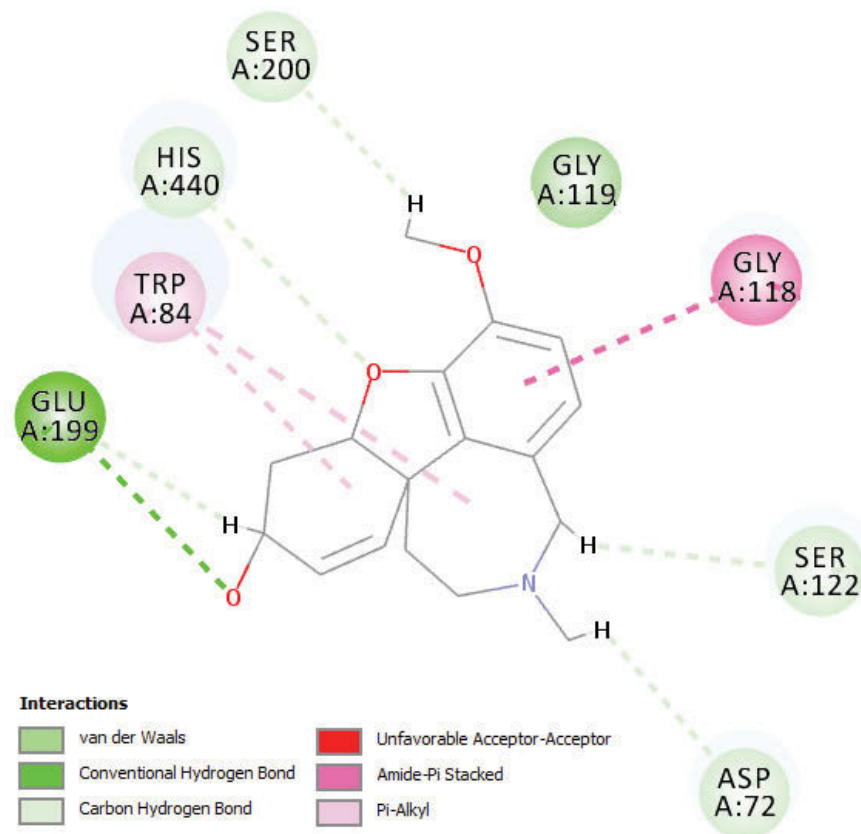


Figure 7.5 Binding interactions for docked of Galantamine in the AChE active site for protein file PDB: 1DX6.

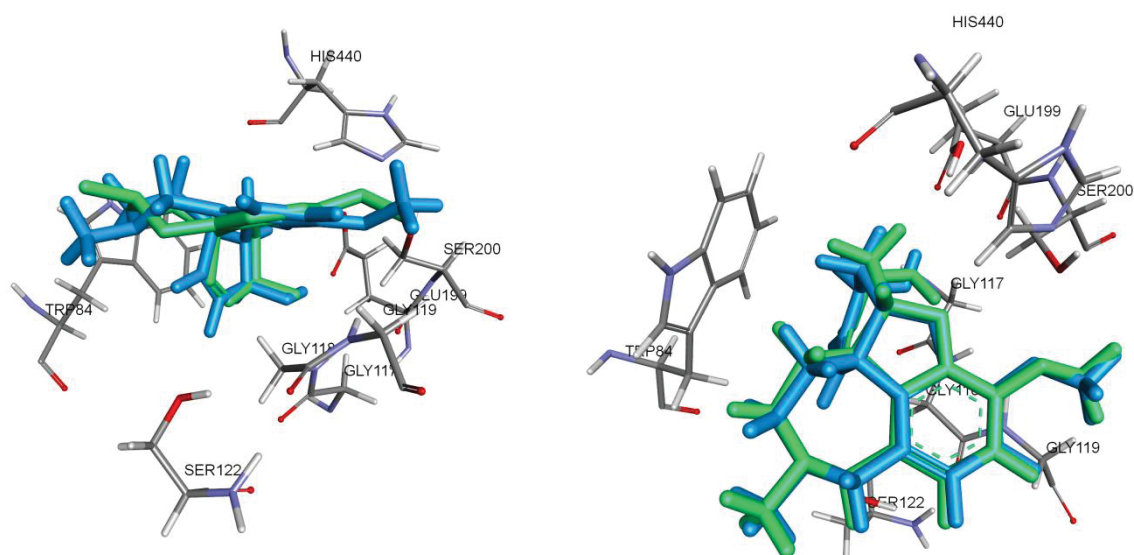


Figure 7.6 Superimposed Galantamine from the x-ray structure (green) and docked (blue).

Note that in the 2D figures of the docking interactions, the grey sphere around some of the residues represents its solvent accessible surface, where the diameter is proportional to that surface.

7.3.3 Alkaloid-like Library AChE Docking Results

Table 7.3 shows the Ludi_3 scores calculated for each of the compounds docked, ordered from highest score to lowest. As can be seen, each compound was successfully docked, three of which had scores higher than Galantamine, namely, **(+)-60n**, **(+)-59n** and **(-)-65j**. Unfortunately, no correlation between the docking scores and the results of the *in vitro* AChE inhibition assays discussed in Chapter 5 was observed. As the bio-assay data concluded that the compounds in this library are only weak inhibitors, if at all, it is no surprise that most of the docking scores fall below that of Galantamine.

Table 7.3 Ludi_3 scores for the docked pose for each of the compounds synthesised.

Compound	Ludi_3 score
(+)-60n	716
(+)-59n	707
(-)-65j	692
Galantamine	653
(-)-60h	611
(-)-60f	595
(+)-101n	590
(-)-65i	559
(+)-60e	543
(+)-60a	515
(-)-60g	488
(-)-102n	480
(+)-60m	475
(+)-60c	459
(+)-59l	440
(-)-60d	428
(+)-59m	423
(-)-60b	410
(+)-59c	403
(+)-63l	389
(-)-102m	377
(+)-102b	377
(-)-66h	362
(-)-121	346
(-)-103m	332
(+)-104l	328
(+)-101l	317
(+)-101b	317
(+)-63b	310
(+)-101c	288
(+)-59b	283
(+)-67	256
(+)-101m	228
(+)-60l	209
(-)-102l	208

Upon visual inspection of the poses for the three top scoring compounds (each of which are displayed in Figure 7.7, Figure 7.8 and Figure 7.9, respectively), it can be seen that favourable π -cation and π - π stacked interactions are made with TRP84 (for **(-)-65j** and **(+)-59n**) or salt bridge interactions with ASP72 (for **(+)-60n**). Both of the residues are at the bottom of the gorge, orientating the compounds to have the N-3 ring system facing down into the active site and the functionality at C-6 pointing up and out towards the gorge leading into the active site, as shown in Figure 7.10 and Figure 7.11. In these two figures, the 3D surface representation of the protein is shown, as is the docked pose of **(-)-65j**. These poses show potential for developing this library of compounds into more potent inhibitors through various rational drug design processes, such as variation at the C-6 region of the scaffold which will result in more favourable interactions.

These docking results highlight the importance of the ability of the imine nitrogen to become protonated at biological pH in order to achieve the interactions mentioned above. It also shows the significance of aromatic substituents that are capable of undergoing π - π interactions with the aromatic residues of the AChE active site and gorge. These are points to consider in the design approach of a better inhibitor.

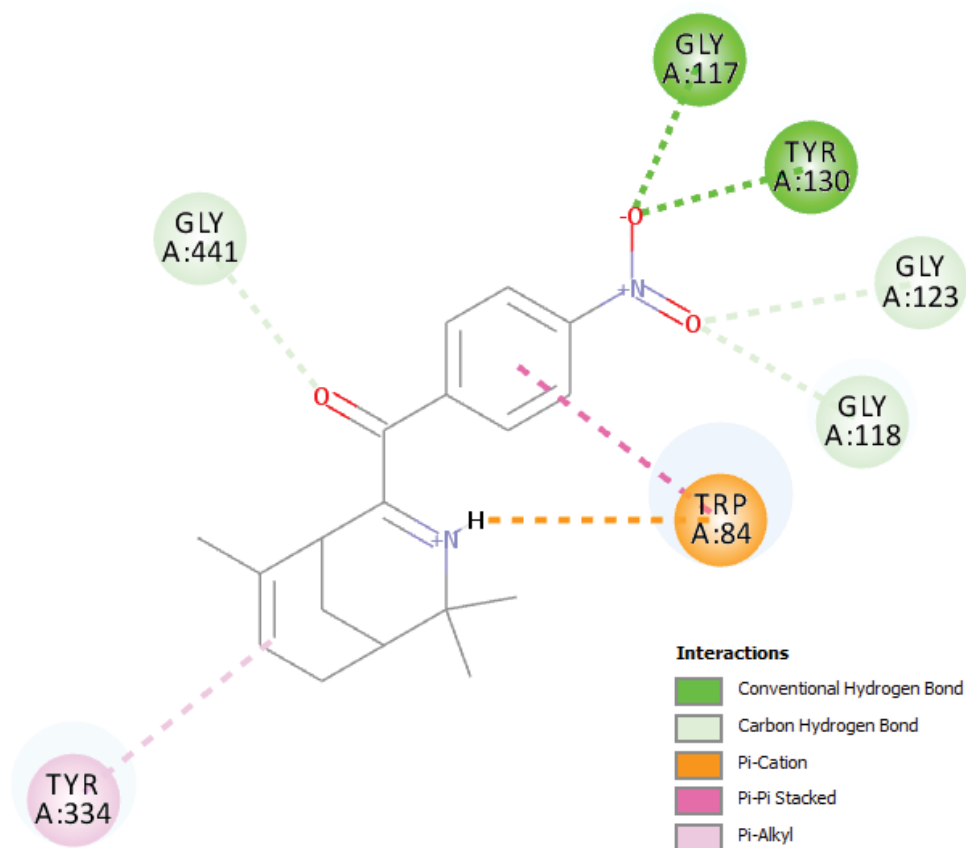


Figure 7.7 2D representation of the binding pose for **(-)-65j** in the AChE active site.

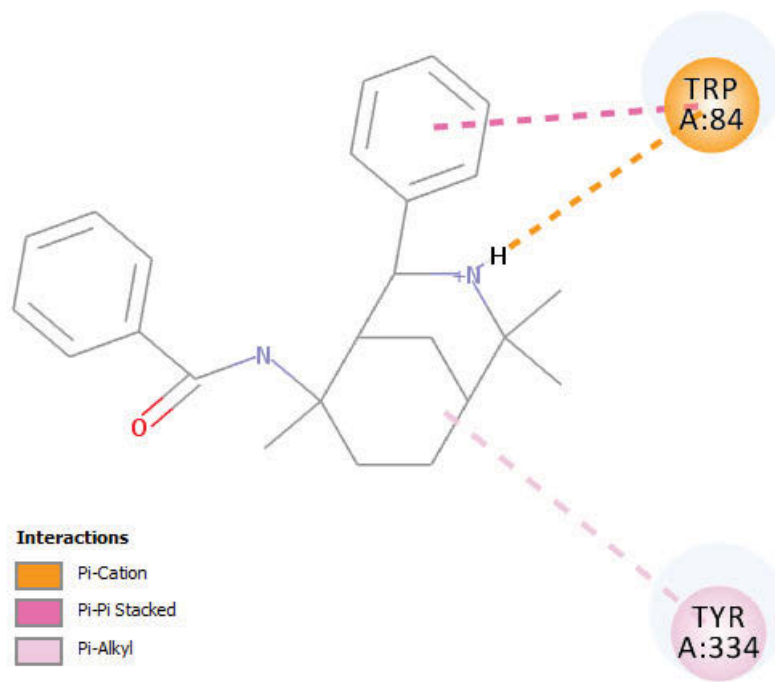


Figure 7.8 2D representation of the binding pose for **(+)-59n** in the AChE active site.

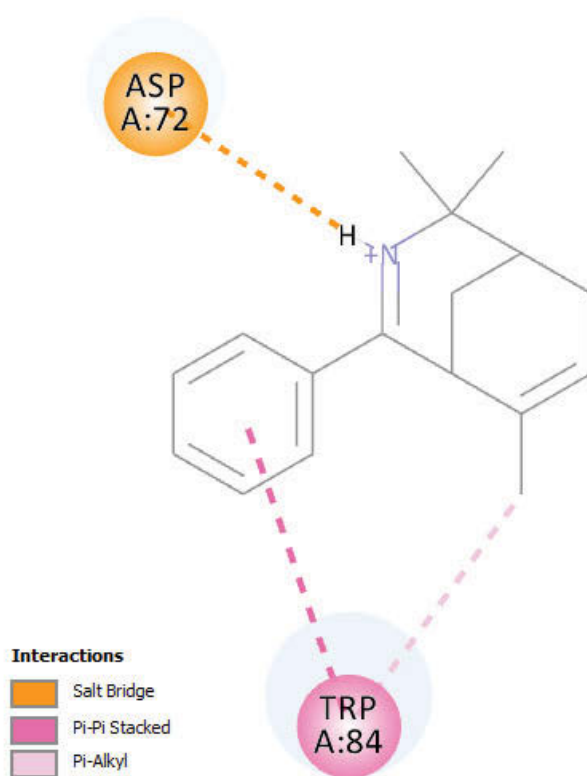


Figure 7.9 2D representation of the binding pose for **(+)-60n** in the AChE active site.

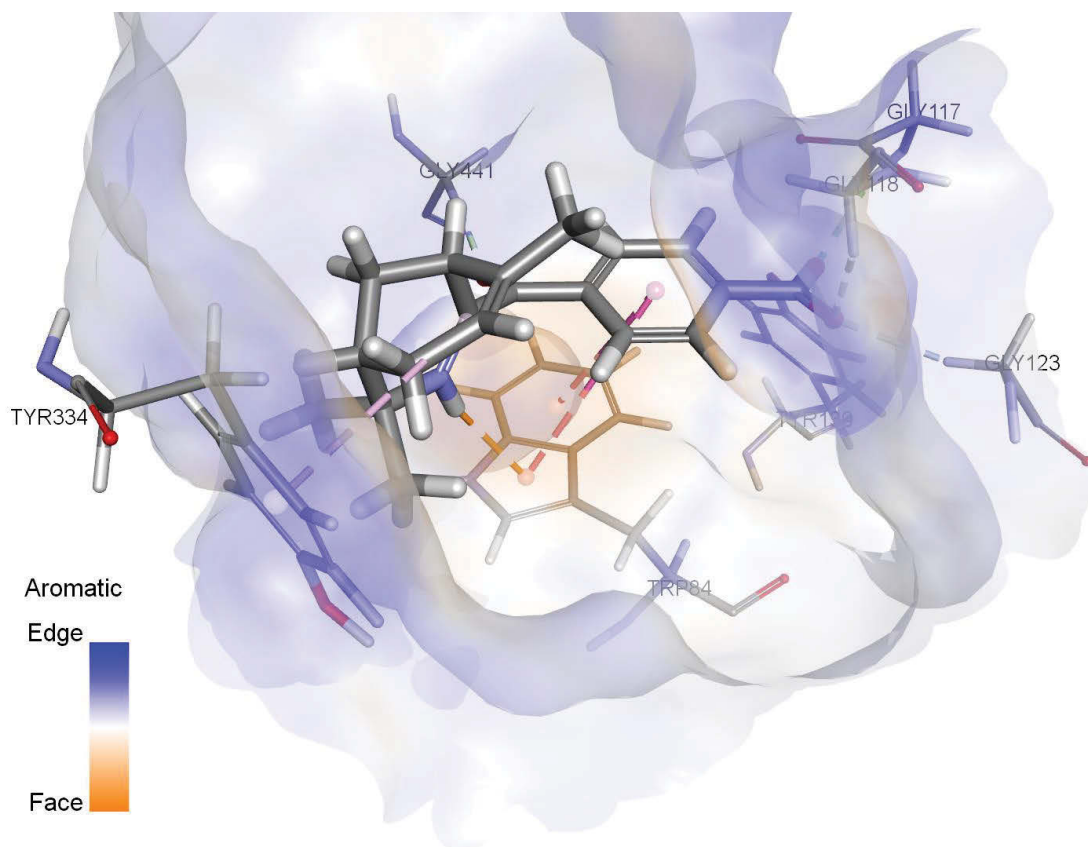


Figure 7.10 3D surface representation of the protein and the docked pose of (-)-65j, looking down the gorge from the top of the entrance.

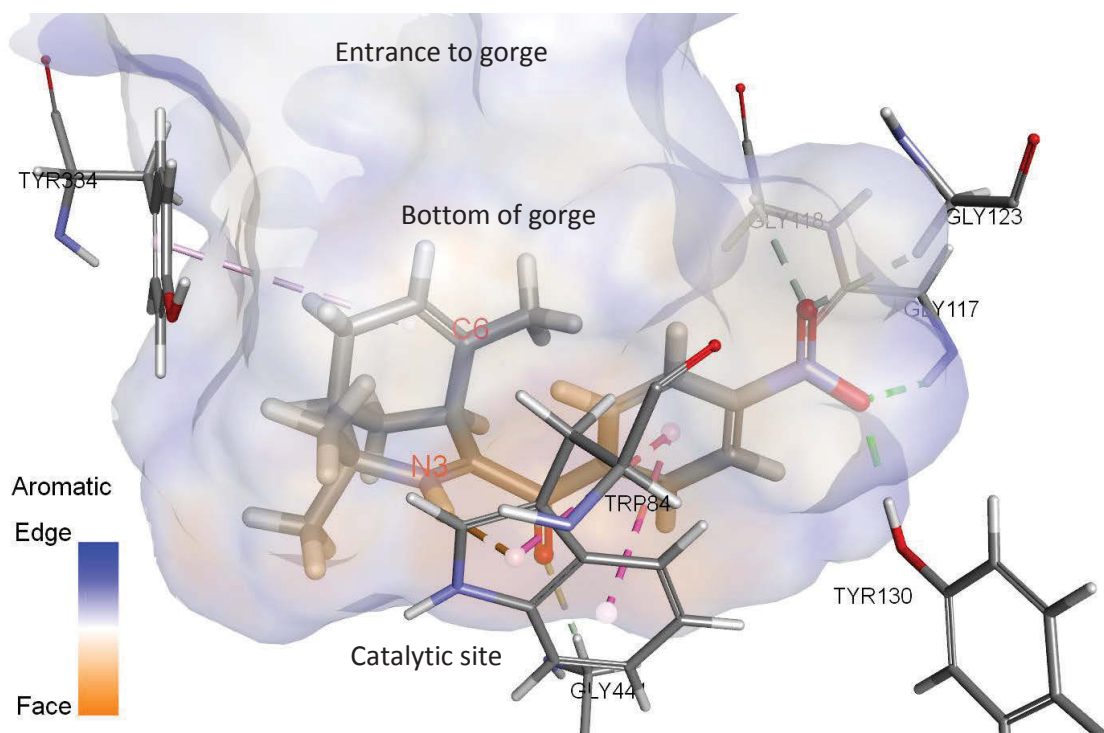
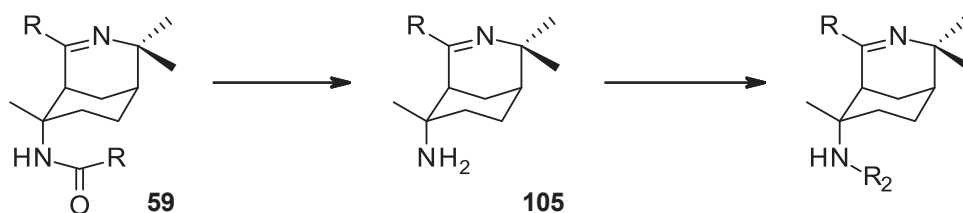


Figure 7.11 3D surface representation of the protein and the docked pose of (-)-65j, looking side-on at the gorge with N3 and C6 labelled.

7.4 Docking Result Directed Rational Drug Design of a Better AChE Inhibitor

As outlined above, the bottom half, or C-6 region, of the 3-aza-bicyclo[3.3.1]nonane scaffold appears the most logical location to derivatise. This will ensure the favourable interactions that occur within the top half, or N-3 region, of the scaffold are maintained, while new interactions are introduced to further improve the potential binding of the ligand-enzyme complex.

It was determined in Chapters 2 and 3 that the alkene scaffolds are not able to be functionalised through the alkene. The low yielding nature of the C-6 alcohol or acetate products leaves the amide as the remaining viable option. The most suitable reaction pathway to functionalise C-6 was *via* the amine **105** obtained from the amide **59**, as outlined in Scheme 7.1. The C-6 amine can undergo a variety of reactions, but firstly the viability of synthesising an amine at C-6 had to be determined. This synthesis can be achieved *via* amines **(+)-105l** and **(+)-103m**, as outlined in detail in Sections 3.3 and 3.5 of Chapter 3.

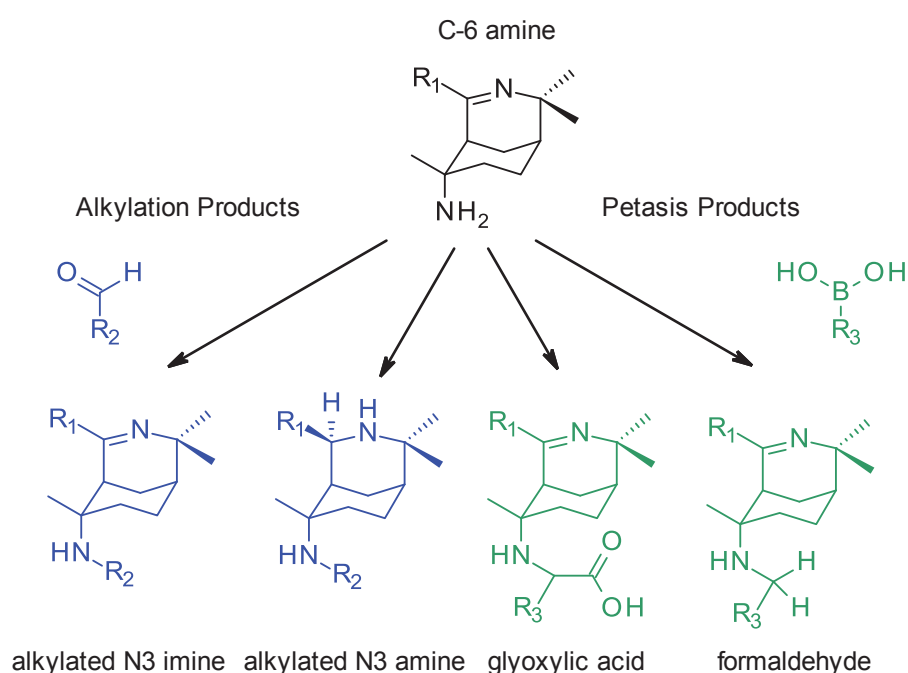


Scheme 7.1 Reaction pathway to functionalise C-6 through amine **105**.

The products that could be obtained from the reaction of each of the boronic acids available in house with **(+)-105l** and **(+)-103m** were drawn and docked to evaluate which would give the best interactions, before the synthesis performed in Chapter 3 was attempted. The same was done with the alkylation product from each aldehyde, yet was repeated to include not only the N-3 amino products but also the N-3 imine products after synthesis had determined it was possible to generate both products, as outlined in Chapter 3.

It must be noted that the proposed di-alkylated products were considered and evaluated, yet have been excluded from the results table as only the non-aromatic aldehydes were considered viable di-alkylation reaction products. This is due to the steric constraints of the hindered amine and bulky aromatic functionality. Each of the non-aromatic di-alkylated products had lower scores than the top scoring mono-alkylated aromatic compounds. Alkylation of the N-3 amines was not considered as the previous attempts have indicated the hindered and unreactive nature of this site, as outlined in Section 3.4 of Chapter 3.

As a consequence of the considerations mentioned above and results from Chapter 3, there are four different possible compounds that could be derived from **(+)-105I** by functionalisation of the C-6 amine *via* either the Petasis reaction or *N*-alkylation. There are three possibilities for **(+)-103I** and **(+)-103m**, due to the exclusion of the imine, and this is outlined in Scheme 7.2. Each of these proposed products were assessed for their possible interaction with the AChE active site using docking and Ludi_3 pose scoring. The scores for the Petasis reaction products are shown in Table 7.4, while the scores for the reductive *N*-alkylation products are shown in Table 7.5. The highest scoring compounds from these tables are indicated by green text, while no score is reported for compounds that failed to dock.



Scheme 7.2 The four different possible compounds that could be formed by derivatising the C-6 amine *via* either the Petasis reaction, shown in green, or reductive *N*-alkylation, shown in blue.

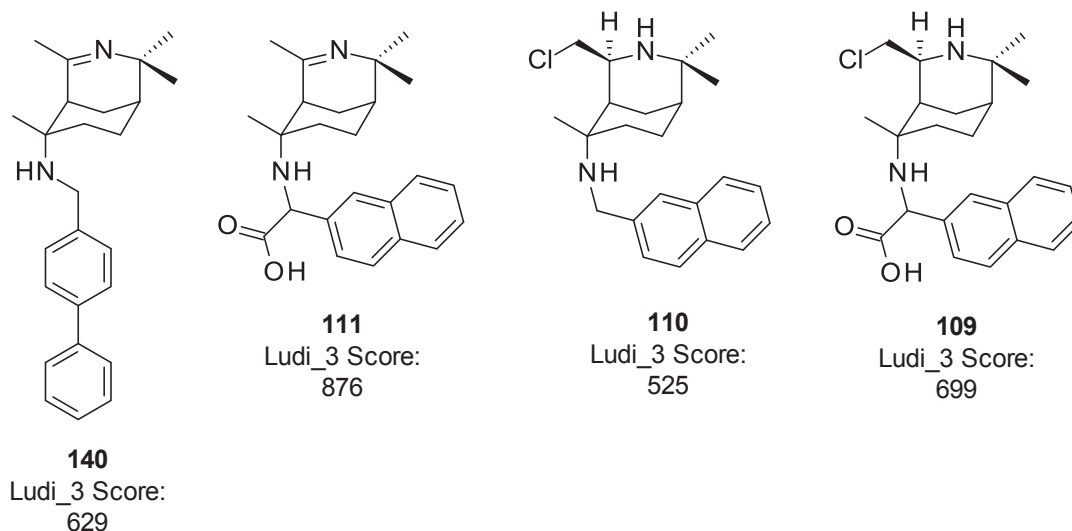
Table 7.4 List of docking scores for hypothetical products of the Petasis reaction.

	Petasis products Ludi_3 docking score			
	Product with (+)-105I		Product with (+)-103m	
Boronic acid:	Aldehyde	Acid	Aldehyde	Acid
• 4-(Trifluoromethyl)phenyl	513	610	412	494
• 4-Biphenyl	629	703	489	611
• 4-Cyanophenyl	490	438	402	441
• 4-Tert-Butylphenyl	582	426	462	338
• 4-(Dimethylcarbamoyl)phenyl	377	453	511	628
• 4-Benzyloxy-3-fluorophenyl	638	449	515	529
• 2-Naphthyl	605	876	525	699

Table 7.5 List of docking scores for hypothetical products of reductive *N*-alkylation.

Aldehyde:	Alkylation products Ludi_3 docking score		
	(+)-105l	(+)-103l	(+)-103m
• Formaldehyde	377	337	260
• Propanal	342	283	321
• Butanal	-	-	362
• Pentanal	279	411	226
• Benzaldehyde	410	480	463
• 4-Dimethylaminobenzaldehyde	571	431	436
• Cinnamaldehyde	403	476	579
• 3-Nitrobenzaldehyde	505	424	-
• <i>p</i> -Anisaldehyde	445	499	444
• <i>m</i> -Anisaldehyde	415	467	470
• Furfural	311	273	572

As can be seen from the scores of the docking results above, most of the proposed compounds show a higher Ludi_3 score than those of the initial library of alkaloid-like compounds listed in Table 7.3, and hence would have greater interactions with the AChE active site, potentially making them better inhibitors. There were, however, two compounds which scored better than Galantamine and one which was better than (+)-60n, as previously identified to have the highest docking score. The structures for each of the best scoring compounds and their score, from each scenario of the Petasis reaction, are shown in Figure 7.12, while those from the *N*-alkylation are shown in Figure 7.13.

**Figure 7.12** Best theoretical docking products of the Petasis reaction.

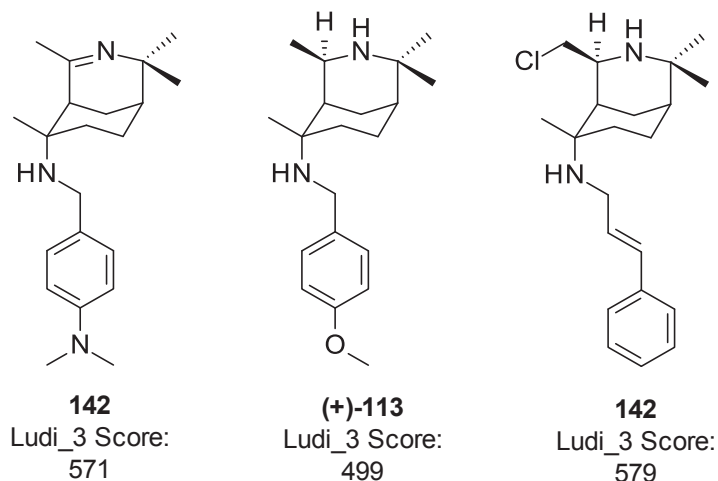


Figure 7.13 Best theoretical docking products from *N*-alkylation.

In most cases, the Petasis products that could be synthesised using a glyoxylic acid linker, performed better in the docking than the equivalent formaldehyde linked product, where the boronic acid functionality is the same. Inspection of the docking poses indicates that this may result from the strong hydrogen bonding that the acid functionality is capable of participating in, as well as how those interactions may orientate the docking pose in a favourable manner. This comparison is displayed in Figure 7.14 and Figure 7.15, for the docking interactions of the **(+)-105I** and 2-naphthylboronic acid products from the acid and aldehyde linkers, respectively. Figure 7.14 also shows the docked pose for the compound with the highest docking score for the Petasis products (**111**). It should be noted that the 2-naphthyl functionality at C-6 gave the best docking scores for three of the four scenarios, most likely due to the favourable π - π interactions with the aromatic residues, as originally hypothesised.

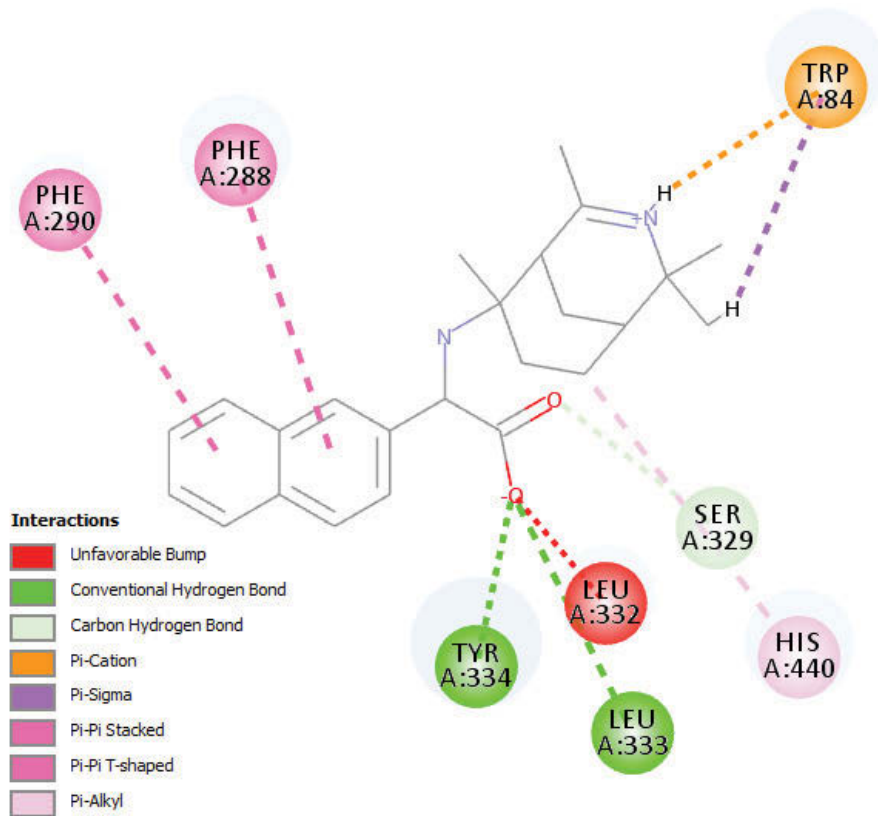


Figure 7.14 2D docking pose of 2-naphthylboronic acid, glyoxylic acid and 111.

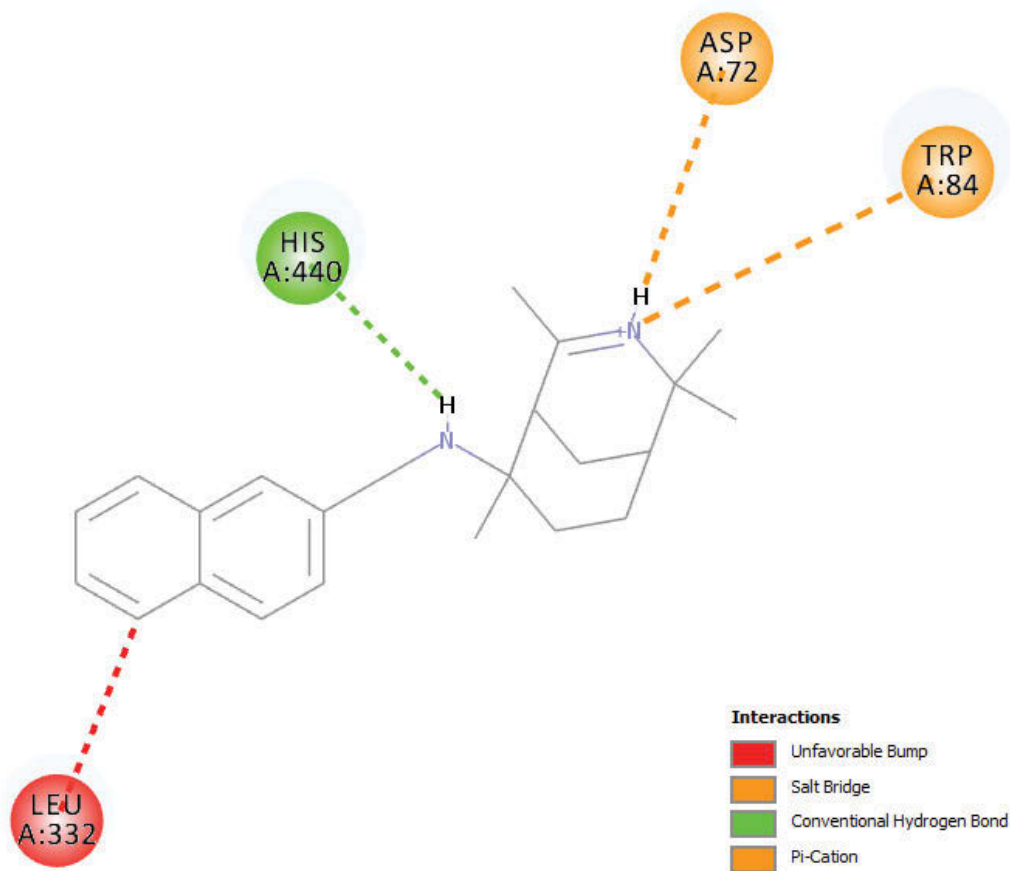


Figure 7.15 2D docking pose of 2-naphthylboronic acid, formaldehyde and 110.

The results of the docking and scoring of the proposed compounds that would result from the *N*-alkylation of the C-6 amine, highlights that none of the compounds score as well as the Petasis reaction products. There was also no consistency in the scores to indicate a single best aldehyde, most likely due to the influence of the N-3 and C-4 functionality, although the aromatic aldehydes all gave better scores than the non-aromatic aldehydes.

As previously mentioned, **(+)-105l** and **(+)-103m** were chosen as proof of concept compounds for docking due to their synthetic ease to obtain. Due to the docking results from the synthesised library showing that the best scores resulted from those compounds with aromatic functionality at C-4, such derivatives should also be considered. For this reason, the hypothetical compound with the best docking score (that shown in Figure 7.14) was modified to include phenyl functionality at C-4. This compound was docked and scored, with the 2D binding pose seen in Figure 7.16. The Ludi_3 score for this compound was 832, which is a relatively good score when compared to most of the scores calculated. It was, however, slightly lower than the 876 obtained for the compound with the C-4 methyl functionality. Inspection of the interactions would suggest that the presence of the phenyl obscures the compound from orientating in a pose where the acid is capable of forming interactions and, therefore, the overall binding energy is lower despite the addition of π - π interactions between the C-4 phenyl and TRP84. The same analysis was then done for all the synthesised imino amides that could be potentially converted to the corresponding amine, but none showed an improved score compared to the C-4 methyl functionality.

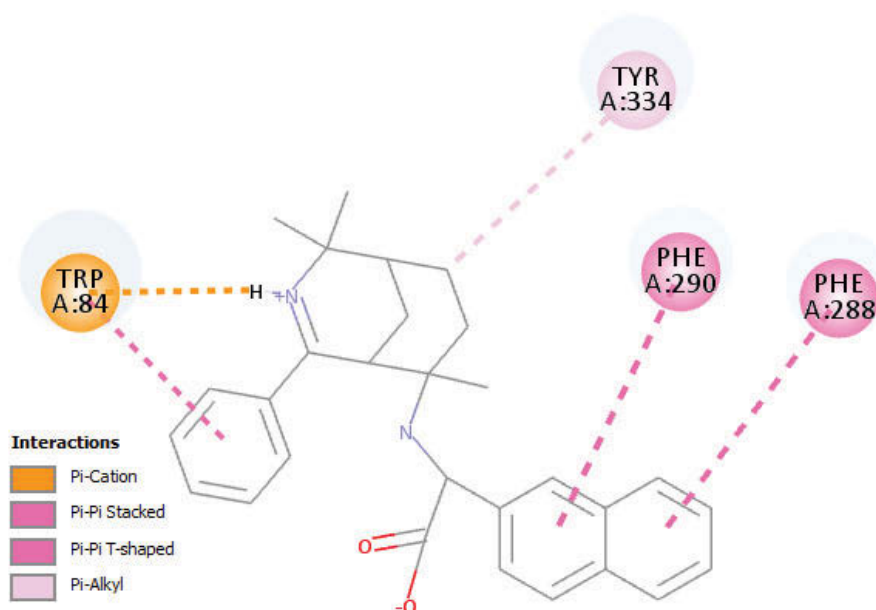


Figure 7.16 2D docking pose of 2-naphthylboronic acid, formaldehyde and **105n** Petasis Product

As outlined in Chapter 4, the compounds with the chloromethyl motif had the most potent biological activity. Although *in silico* docking interaction results indicate that the C-4 methyl compounds derived from **(+)-105I** show better interactions over the C-4 chloromethyl compounds derived from **(+)-103m**, only *in vitro* assays would determine with certainty which compound would make the best inhibitor. For this reason, the compounds with the best docking scores were attempted to be synthesised and evaluated for their *in vitro* activity to confirm this hypothesis.

Before any of the proposed compounds were attempted to be synthesised and subsequently assessed for their *in vitro* activity, they were also screened based on their drug-like properties and ADMET descriptors, as was the originally synthesised library. Performing this analysis revealed that none of the hypothesised compounds showed any violation of Lipinski's rule of five. Figure 7.17 shows the ADMET plot for all of the proposed compounds docked. On this plot, three of the compounds fall outside the ellipses, but all of the best scoring compounds are inside, as indicated by the yellow points. These compounds highlighted in yellow are those that were prioritised for synthesis.

From this analysis, only the best scoring compounds have their ADMET descriptors listed in Table 7.6, because they are the main compounds of synthetic interest. This table shows that **110** has the most optimal properties. Compound **111**, on the other hand, was predicted to show CYP2D6 binding. From this rational drug design and evaluation, it was decided that compounds **140**, **111**, **110**, **109** and **(+)-113** should be synthesised, the results of which were outlined in Chapter 3.

Table 7.6 Evaluation of the best docking compounds ADMET descriptors.

Compound	Aqueous solubility	BBB penetration	CYP2D6 binding	Hepatotoxicity	Intestinal absorption	PPB
140	2	0	TRUE	TRUE	0	TRUE
111	2	2	TRUE	FALSE	0	TRUE
110	2	1	FALSE	FALSE	0	FALSE
109	1	0	TRUE	TRUE	0	TRUE
141	2	1	FALSE	TRUE	0	TRUE
113	2	1	FALSE	FALSE	0	TRUE
142	2	1	FALSE	FALSE	0	TRUE

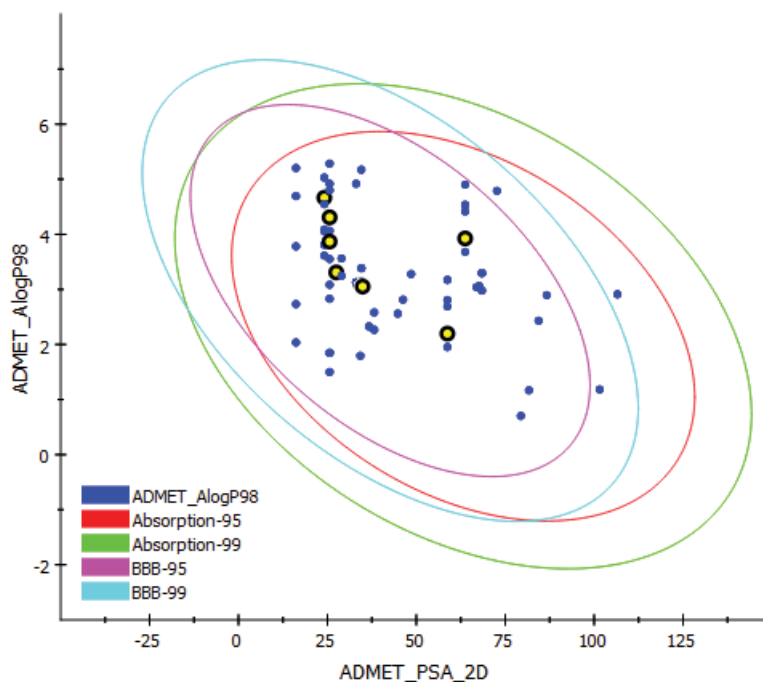


Figure 7.17 ADMET plot for the proposed docked compounds, with the best scoring compounds listed in Table 7.6 highlighted in yellow.

7.5 Conclusion

Although there was no direct correlation observed between the docking scores calculated for the compounds binding to AChE and the *in vitro* assay results, the binding poses generated did highlight possible interactions that could be utilised in the design of a more potent inhibitor. Preliminary results show that this is a viable hypothesis, yet more work is required to confirm. As such, the methods used above will definitely aid in the acceleration of the drug development process.

CHAPTER 8: Conclusion and Future Directions

8.1 Chemical Synthesis Conclusions

In summary, the bridged Ritter reaction is a viable method for generating a chemically diverse library of optically pure alkaloid-like molecules. The 3-azabicyclo[3.3.1]non-3-ene core was synthesised using (-)- β -pinene with the bridged Ritter reaction and was decorated with various functionality provided by the nitrile used, in the C-4 and C-6 locations. The nitriles used have the greatest influence on the outcome of the reaction and scaffold type obtained. These reactions successfully gave several imino-amides **59**, imino-alkenes **60**, an amino-alcohol **(-)-66h** and two imino-acetates **63**. The imino-alkenes were the most common reaction outcome, as highlighted in Chapter 2. Several interesting outcomes were found as a result of the chemistry utilised to generate the library of compounds. This highlighted the influence of the structural features of the 3-azabicyclo[3.3.1]non-3-ene scaffolds and most significantly the selective nature of the synthetic outcomes.

The C-6 amine functionality provided useful synthetic pathways to further analogues of this structure. The viability of this was confirmed through both reductive *N*-alkylation and S_N2 alkylation reactions. Although the imino-alkenes were the most commonly obtained scaffold type, they were not useful precursors for the synthesis of additional alkaloid-like derivatives because the N-3 nitrogen was the only region able to be manipulated, as outlined in Chapter 3. The C-6 alcohol and acetate products were low yielding and, hence, deprotecting the C-6 amide products, in order to give C-6 amines, was the most viable pathway for further derivatisation.

While attempting to derivatise the core scaffold, an in depth understanding of the scaffold was developed. Key observations included the inert nature of the cyclic imines towards hydrolysis in strong acidic conditions, and the stable and unreactive nature of the C-6 alkenes. When the N-3 imines were reduced to secondary amines (amino-amides **101** and amino-alkenes **102**), the products were stereospecific due to the hindered nature of the scaffold only allowing stereospecific attack by the hydride ion. This hindrance was also deemed to be the cause of the N-3 imine's limited reactivity, as highlighted by the X-ray crystallography results obtained. The limited reactivity reduced the possibility of introducing a third ring system to the scaffold through this location, also shown by the lack of success for the cyclisation reactions attempted.

8.2 Biological Assays Conclusions

For the compounds that were successfully synthesised, purified and characterised, the broad range of biological properties were explored *via* several methods. Firstly, the compounds' potential as anticancer drugs was assessed by investigating their cytotoxicity against a number of cancerous cell lines in Chapter 4. The breast cancer cell line MDA-MB-231 was tested in house, against which **(+)-59m**, **(+)-60m** and **(+)-101m** showed antiproliferation activity with IC₅₀ values of 38.27, 13.83 and 28.87 μ M, respectively. These compounds also showed activity against the cancerous human cell lines, MCF-7 and KB, and the healthy mammalian Vero cell line in the external screening. These results highlight how these compounds are not selective towards any particular cell type and most likely have a general toxicity, as contributed by the chloromethyl functionality at C-4. This should be confirmed in future work but was outside of the timeframe of this thesis. Of the additional seven compounds screened against MCF-7, KB and Vero cells externally, compound **(-)-102m** showed the most promise with 98% inhibition of MCF-7 growth at 0.235 mM, yet no significant activity against any of the other cell lines.

The preliminary screens for cytotoxicity highlighted that the 3-azabicyclo[3.3.1]non-3-ene core must not have any significant contribution to the anticancer properties of the *Aristolelia* alkaloids or the alkaloid-like compounds derived with the same core. Moreover, the indole motif is most likely the key contributing factor, highlighting the significance of privileged structures. It was unfortunately not possible to introduce a third ring system into the 3-azabicyclo[3.3.1]non-3-ene core generated by the bridged Ritter reaction to mimic the heterocyclic nature of the *Aristolelia* alkaloids. For this reason, the library of alkaloid-like compounds listed in Chapter 4 were deemed as not suitable anticancer agents, within the scope and time constraints of this project, due to the limited ability to vary the scaffold to improve the activity and toxicity against healthy cells.

As a consequence of these results, more focus was placed on developing the AChE inhibition activity of the synthesised library. Molecular modeling showed the potential of the 3-azabicyclo[3.3.1]non-3-ene core to be derivatised in a manner that could improve the potency of the synthesised library by introducing additional favourable interactions with the gorge that leads into the active site of AChE. All of the compounds also showed good drug-like properties when assessed for the corresponding descriptors, as shown in Chapter 7.

The initially synthesised alkaloid-like compounds were evaluated for their AChE inhibition properties with the TLC bioautographic and Ellman methods in Chapter 5. It was

determined that there was potential for development of a potent AChE inhibitor, because seven of the 27 compounds tested showed activity across both assays. An additional set of compounds was designed based on molecular modeling results, where an improved docking score with the 1DX6 protein file was achieved. Despite having a new set of proposed compounds with better docking scores than the previously synthesised compounds and Galantamine, not all of the proposed compounds were able to be synthesised, as outlined in Chapter 3. Of those that were synthesised, compounds **(+)-112** and **(+)-114** were assessed for their AChE inhibition properties with the same assays. This determined that compounds **(+)-112** and **(+)-114** were active at 43.46 and 87.82 μM , respectively, and despite not being particularly low values when compared to Galantamine, the error in the results suggested that these compounds showed more reliable activity than those compounds previously assessed. It also demonstrated that these compounds do have the potential to be developed further into better inhibitors, which should be confirmed by further investigation in future studies.

As the molecular modeling showed the 'drug-likeness' of all the compounds synthesised, it was deemed that all were appropriate for broad screening of their biological properties through the Lilly OIDD program. Although the broad screening results are only obtained progressively as the assessments are performed, based on the current data returned, several useful conclusions could be made. Firstly, the compounds showed little activity against all of the targets screened and hence when activity is found, the compound demonstrated a very selective nature towards that target. This selectivity is a greatly desired property and, as such, these compounds have the potential to be repurposed towards one of these targets that has not been investigated in depth in-house. This is the case for compound **(+)-101n** which showed good L-17 secretion inhibition activity. Understanding this activity is an area that could be investigated in future work.

8.3 Future Directions

Based on the results of this thesis, numerous areas could be explored in future work in addition to those areas already mentioned above. The opposite enantiomers of all of the compounds discussed in this thesis could be investigated to determine if there are biological properties that are stereospecific towards either enantiomer. This could be achieved through repeating the same reactions but using (*R*)-limonene as the starting material.

It would also be interesting to convert more of these compounds to the *N*-oxides and then assess them for their biofilm inhibition properties.^[165] If then linked to a potential

antimicrobial, these hypothetical compounds should also be screened against other targets, for example through the Community for Open Antimicrobial Drug Discovery (CO-ADD) service.

CHAPTER 9: Experimental

9.1 General Experimental

9.1.1 Nuclear Magnetic Resonance (NMR) Spectroscopy

9.1.1.1 Proton (^1H) NMR Spectra

^1H NMR spectra were recorded on an Agilent 500 MHz spectrometer in deuterated chloroform (CDCl_3) containing 0.03% v/v tetramethylsilane (TMS), unless otherwise specified. All samples were referenced relative to the TMS chemical shift at 0 ppm. Proton resonances were assigned as: chemical shift (multiplicity, coupling constant(s), the number of protons, proton assignment). Multiplicities are reported as: m (multiplet), s (singlet), br s (broad singlet), d (doublet), t (triplet), q (quartet), qin (quintet), n (nonet), dd (doublet of doublets), dt (doublet of triplets), td (triplet of doublets), qd, (quartet of doublets), qt (quartet of triplets), dsex (doublet of sextets), dsep (doublet of septets) and ddd (doublet of doublets of doublets). NMR assignments were based on COSY, NOESY, HSQC and DEPT experiments and are numbered according to the systematic name.

9.1.1.2 Carbon (^{13}C) NMR Spectra

^{13}C NMR spectra were recorded on an Agilent 125 MHz spectrometer in deuterated chloroform (CDCl_3) containing 0.03% v/v tetramethylsilane (TMS), unless otherwise specified. All samples were referenced relative to the CDCl_3 chemical shift at 77.36 ppm. Carbon resonances were assigned as chemical shift (carbon assignment). NMR assignments were based on COSY, NOESY, HSQC and DEPT experiments and are numbered according to the systematic name.

9.1.2 Mass Spectrometry (MS)

9.1.2.1 Low -Resolution (LRMS)

Low-resolution mass spectra were obtained on either an Agilent 6890GC fitted with a 5% polysilphenylene, 95% polydimethylsiloxane column and an Agilent 5973n mass spectrometer with electron-ionization ion source or a Thermo Scientific Trace 1310 CG fitted with a (5%-Phenyl)-methylpolysiloxane column and Thermo Scientific ISQ LT mass spectrometer with electron impact ionization ion source. Samples were prepared in either acetone or methanol.

9.1.2.2 High-Resolution (HRMS)

High-resolution mass spectra were obtained on an Agilent 6510 Accurate-Mass Q-TOF Mass Spectrometer, equipped with an electrospray ionisation source using an acetonitrile-

water (70:30) solvent system with 0.1% v/v formic acid. HRMS were obtained *in lieu* of elemental analysis, with NMR used to determine purity.

9.1.3 Chromatography

9.1.3.1 Column Chromatography

Compounds were purified by column chromatography using either Merck flash neutral alumina or silica gel (40 – 63 μm) packed as a slurry in the eluent. Separations were performed using a 35 mm diameter column and the stated solvent system, either by gravity or elution by compressed air.

9.1.3.2 Thin Layer Chromatography (TLC)

TLC analysis was performed using aluminium backed Merck 60 GF₂₅₄ silica gel or Merck 60 GF₂₅₄ neutral alumina gel TLC plates. The progress of reactions was monitored and separation methods were developed with the stated chromatography solvent system. UV detection at 254 nm and I₂ atmosphere staining was used to develop the plates.

9.1.3.3 Preparative TLC

Compounds were purified by preparative TLC using Chem-Supply 20 X 20 cm glass backed Silica 60 F₂₅₄, 2000 micron thick. Plates were developed with the stated chromatography solvent system and UV detection at 254 nm was used to identify bands. Bands were scraped off the glass backing, extracted with ethanol and filtered before the solvent was removed under vacuum.

9.1.4 Infrared Spectroscopy

Infrared spectra were collected using an Agilent Cary 630 FTIR spectrometer.

9.1.5 Melting Points

Melting points were measured on a Gallenkamp Melting Point Apparatus and were uncorrected.

9.1.6 Optical Rotation

Optical rotation was measured using a Jasco P-2000 polarimeter.

9.1.7 Plate Readers for Bio-Assays

For the Ellman assay, absorbance was read with a BIO-TEK Synergy HT plate reader using Falcon Polystyrene 96-well Flat-bottom plates. For the MTS assay, absorbance was read with a Tecan Infinite M1000 PRO plate reader using Falcon Polystyrene 96-well Flat-bottom plates.

9.1.8 Reagents and Solvents

Reagents and analytical grade solvents were purchased from either Sigma-Aldrich or Chem-Supply without further purification.

9.1.9 Partial Characterisation

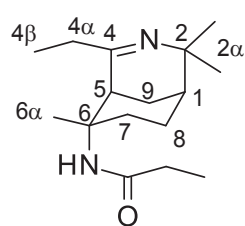
For compounds that were unable to be fully characterised, the beginning of the compound name has been denoted with an asterisk (*). This was the case where products could still be identified, even though there was not enough quantity to be used for all analytical techniques, or the purity of the product was low. This could be rectified by future work related to this project.

9.2 General Chemical Reaction Methods

9.2.1 Standard Bridged Ritter Reaction Conditions

Sulfuric acid (18 M, 2 mL) was stirred in a flask fitted with a reflux condenser and a drying tube at 0 °C. To the reaction flask, the nitrile (53.4 mmol, 7 mol equiv. of (-)- β -pinene) was added. A solution of (-)- β -pinene (1.2 mL, 7.62 mmol) in benzene (5 mL) was added dropwise to the reaction mixture, *via* the condenser. A further 0.50 mL of benzene was used to wash all traces of (-)- β -pinene into the reaction flask. After 30 min the reaction was allowed to reach room temperature and left to stir for 24 h. The reaction was then quenched by the addition of water (30 mL). The mixture was then basified with 4 M NaOH (until pH > 10). The reaction mix was then extracted with CHCl₃ (2 X 15 mL) and dried with Na₂CO₃. Note: if the nitrile used was solid, it was dissolved in 20 mL benzene before addition to sulfuric acid.

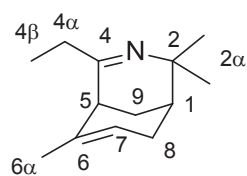
N-(4-Ethyl-2,2,6-trimethyl-3-azabicyclo[3.3.1]non-3-en-6-yl)propanamidyl (+)-59b



(512 mg, 1.94 mmol, 25%) white solid; m.p. 96-97 °C, *R_f* (ethyl acetate) 0.69; $[\alpha]_D^{18} +125.95$ (*c* 0.95, CHCl₃); ν_{\max} (neat) 3278, 3080, 2972, 2946, 2872, 1637, 1555, 1451, 1348, 1285, 1235, 1110, 955 cm⁻¹; ¹H NMR (500 MHz, CDCl₃) δ 5.35 (br s, NH), 3.27 (br s, 1H, CH-5), 2.31 (dt, *J* = 7.5, 6.0 Hz, 1H, CH₂-4 α), 2.27 (dt, *J* = 7.5, 6.0 Hz, 1H, CH₂-4 α b), 2.21 (qt, *J* = 7.5, 2.0 Hz, 2H, COCH₂CH₃), 1.80-1.83 (m, 1H, CH₂-9 α), 1.76 (dt, *J* = 13.0, 2.0 Hz, 1H, CH₂-8 α), 1.66-1.63 (m, 2H, CH₂-8 β & CH-1), 1.56 (tt, *J* = 13.5, 4.5 Hz, 1H, CH₂-9 β), 1.46-1.36 (m, 2H, CH₂-7), 1.42 (br s, 3H, CH₃-6 α), 1.28 (br s, 3H, CH₃-2 α), 1.16 (t, *J* = 7.5 Hz, 3H, COCH₂CH₃), 1.12 (br s, 3H, CH₃-2 α), 1.09 (t, *J* = 7.5 Hz, 3H, CH₃-4 β); ¹³C NMR (125 MHz, CDCl₃) δ 173.7 (C-4), 171.7 (C=O), 58.1 (C-6), 56.0 (C-2), 38.3 (CH-5), 36.7 (CH₂-4 α), 34.5 (CH-1), 33.6 (CH₂-7), 32.1 (CH₃-2 α), 31.0 (COCH₂CH₃), 27.4 (CH₃-6 α), 26.3 (CH₃-2 α), 25.1 (CH₂-9), 24.9 (CH₂-8), 13.0 (CH₃-4 β), 12.3 (COCH₂CH₃); GC-MS *R_t* = 18.74 min, *m/z* 264 (72 M⁺), 249 (27), 191 (59), 176 (50), 164 (56), 150

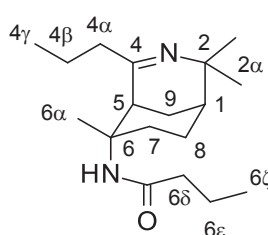
(47), 136 (100), 122 (23), 97 (31), 57 (33%). HRMS (ESI): C₁₆H₂₈N₂O calcd: 265.2275 [M+H]⁺; found: 265.2271 [M+H]⁺.

4-Ethyl-2,2,6-trimethyl-3-azabicyclo[3.3.1]nona-3,6-diene (-)-60b



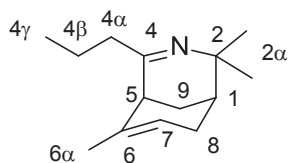
(198 mg, 1.04 mmol, 14%) yellow oil; R_f (1:4 hexane/diethyl ether) 0.6; [α]_D²³ -22.56 (c 1.00, CHCl₃); ν_{max}(neat) 2961, 2927, 2868, 1686, 1662, 1453, 1377, 1356 cm⁻¹; ¹H NMR (500 MHz, CDCl₃) δ 5.34 (br s, 1H, CH-7), 2.60 (br s, 1H, CH-5), 2.27 (q, *J* = 7.5 Hz, 2H, CH₂-4α), 2.25-2.14 (m, 2H, CH₂-9), 1.87 (br s, 1H, CH-1), 1.79-1.77 (m, 4H, CH₃-6α & CH₂-8a), 1.57 (dt, *J* = 12.0, 2.5 Hz, 1H, CH₂-8b), 1.19 (br s, 3H, CH₃-2α), 1.16 (br s, 3H, CH₃-2α), 1.11 (t, *J* = 7.5 Hz, 3H, CH₃-4β); ¹³C NMR (125 MHz, CDCl₃) δ 171.3 (C-4), 135.1 (C-6), 122.5 (CH-7), 58.7 (C-2), 38.5 (CH-5), 34.5 (CH₂-4α), 34.10 (CH-1), 32.2 (CH₃-2α), 29.2 (CH₂-9), 28.2 CH₃-2α), 26.2 (CH₂-8), 24.2 (CH₃-6α), 11.9 (CH₃-4β); GC-MS R_t = 5.431 min, *m/z* 191 (14 M⁺), 176 (5), 136 (23), 121 (11), 93 (100), 77 (14%). HRMS (ESI): C₁₃H₂₁N calcd: 192.1747 [M+H]⁺; found: 192.1751 [M+H]⁺.

N-(2,2,6-Trimethyl-4-propyl-3-azabicyclo[3.3.1]non-3-en-6-yl)butanamide (+)-59k



(219 mg, 0.749 mmol, 10%) yellow oil; R_f (diethyl ether) 0.14; [α]_D²¹ +33.70 (c 1.00, CHCl₃); IR ν_{max} (neat) 3280, 2963, 2931, 2871, 1641, 1541, 1457, 1366, 1207, 1036, 922, 728 cm⁻¹; ¹H NMR (500 MHz, CDCl₃) δ 5.44 (br s, 1H, NH), 3.42 (br s, 1H, CH-5), 2.39-2.33 (m, 2H, CH₂-4β), 2.16 (td, *J* = 14.5, 3.5 Hz, 2H, CH₂-6ε), 1.85-1.79 (m, 2H, CH₂-8a & CH₂-9a), 1.71-1.63 (m, 6H, CH-1, CH₂-8b, CH₂-9b, CH₂-4αα & CH₂-6δ), 1.61-1.54 (m, 1H, CH₂-4ab), 1.52-1.48 (m, 1H, CH₂-7a), 1.43 (s, 3H, CH₃-6α), 1.42-1.36 (m, 1H, CH₂-7b), 1.34 (s, 3H, CH₃-2α), 1.20 (s, 3H, CH₃-2α), 0.98 (t, *J* = 3.5 Hz, 3H, CH₃-6ζ), 0.94 (t, *J* = 4.5 Hz, 3H, CH₃-4γ); ¹³C NMR (125 MHz, CDCl₃) δ 178.0 (C-4), 175.47 (C=O), 61.2 (C-6), 58.4 (C-2), 46.4 (CH₂-4β), 39.9 (CH₂-6ε), 38.9 (CH-5), 34.5 (CH-1), 33.4 (CH₂-7), 31.8 (CH₃-2α), 27.4 (CH₃-6α), 28.5 (CH₃-2α), 24.9 (CH₂-9), 24.4 (CH₂-8), 22.3 (CH₂-4α), 19.5 (CH₂-6δ), 14.2 (CH₃-4γ), 14.1 (CH₃-6ζ); GC-MS R_t = 20.40 min, *m/z* 292 (39 M⁺), 277 (38), 264 (62), 249 (28), 205 (85), 190 (46), 177 (100), 164 (52), 150 (85%). HRMS (ESI): C₁₈H₃₂N₂O calcd: 293.2587 [M+H]⁺; found: 293.2593 [M+H]⁺.

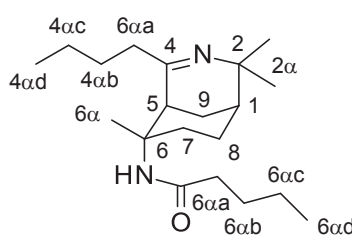
2,2,6-Trimethyl-4-propyl-3-azabicyclo[3.3.1]nona-3,6-diene (-)-60k



(88.2 mg, 0.43 mmol, 6%) pale yellow liquid; R_f (diethyl ether) 0.5; [α]_D²¹ -2.38 (c 1.00, CHCl₃); IR ν_{max} (neat) 2931, 2961, 2834, 1697, 1656, 1449, 1377, 1354, 1203, 1142 900, 799 cm⁻¹; ¹H NMR (500 MHz, CDCl₃) δ 5.34 (br s, 1H, CH-7), 2.58 (br s, 1H, CH-5), 2.31-2.13 (m, 4H, CH₂-8 & CH₂-4α), 1.87-1.86 (m, 1H, CH-1), 1.80-1.77 (m, 4H, CH₃-6α & CH₂-9a), 1.69-

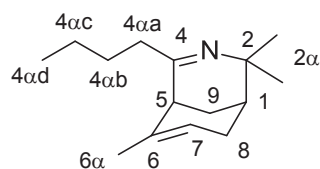
1.62 (m, 1H, CH₂-4βa), 1.59-1.51 (m, 2H, CH₂-9a & CH₂-4βb), 1.19 (s, 3H, CH₃-2α), 1.16 (s, 3H, CH₃-2α), 0.94 (t, *J* = 7.5 Hz, 3H, CH₃-4γ); ¹³C NMR (125 MHz, CDCl₃) δ 17.3 (C-4), 135.0 (C-6), 122.4 (CH-7), 58.7 (C-2), 43.3 (CH₂-8), 38.7 (CH-5), 34.1 (CH-1), 32.3 (CH₃-2α), 29.2 (CH₂-4α), 28.1 (CH₃-2α), 26.1 (CH₂-9), 24.2 (CH₃-6α), 20.2 (CH₂-4β), 14.1 (CH₃-4γ); GC-MS R_t = 13.24 min, *m/z* 205 (11 M⁺), 190 (4), 177 (5), 136 (21), 121 (8), 93 (100%). HRMS (ESI): C₁₄H₂₃N calcd: 206.1903 [M+H]⁺; found: 206.1908 [M+H]⁺.

***N*-(4-Butyl-2,2,6-trimethyl-3-azabicyclo[3.3.1]non-3-en-6-yl)pentanamide (+)-59c**



(298 mg, 0.931 mmol, 12%) yellow oil; R_f (1:3 ethyl acetate/hexane) 0.47; [α]_D²² +81.82 (*c* 1.35, CHCl₃); ν_{max}(neat) 3296, 3071, 2959, 2933, 2874, 1642, 1544, 1458, 1378, 1367, 1272, 1110, 929, 910, 734 cm⁻¹; ¹H NMR (500 MHz, CDCl₃) δ 5.31 (s, 1H, NH), 3.27 (br s, 1H, CH-5), 2.32-2.28 (m, 1H, CH₂-6αc), 2.25-2.20 (m, 1H, CH₂-6αb), 2.17 (td, *J* = 7.5, 3.5 Hz, 2H, CH₂-6αc), 1.84-1.79 (m, 1H, CH₂-8a), 1.74-1.76 (m, 1H, CH₂-9a), 1.75-1.65 (m, 1H, CH₂-9b), 1.63-1.60 (m, 3H, CH-1 & CH₂-4αa), 1.59-1.52 (m, 2H, CH₂-7a & CH₂-8b), 1.45-1.30 (m, 7H, CH₂-7b, CH₂-4αb, CH₂-4αc & CH₂-6αd), 1.42 (br s, 3H, CH₃-2α), 1.28 (br s, 3H, CH₃-2α), 1.12 (br s, 3H, CH₃-6α), 0.94 (t, *J* = 7.5 Hz, 3H, CH₃-4αd), 0.90 (t, *J* = 7.5 Hz, 3H, CH₃-6αd); ¹³C NMR (125 MHz, CDCl₃) δ 173.1 (C-4), 170.9 (C=O), 58.2 (C-6), 56.1 (C-2), 42.7 (CH₂-6αc), 38.7 (CH-5), 37.8 (CH₂-6αb), 34.5 (CH-1), 33.5 (CH₂-4αb), 32.1 (CH₂-6α), 31.2 (CH₂-7), 28.2 (CH₂-4αa), 27.4 (CH₃-2α), 25.1 (CH₂-8), 24.7 (CH₂-9), 23.0 (CH₂-6αa), 22.7 (CH₂-4αc), 14.4 (CH₃-6αd), 14.2 (CH₃-4αd); GC-MS R_t = 21.95 min, *m/z* 320 (1 M⁺), 305 (6), 278 (27), 219 (17), 177 (100), 57 (18%). HRMS (ESI): C₂₀H₃₆N₂O calcd: 321.2900 [M+H]⁺; found: 321.2884 [M+H]⁺.

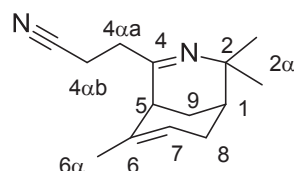
4-Butyl-2,2,6-trimethyl-3-azabicyclo[3.3.1]nona-3,6-diene (+)-60c



(198 mg, 0.903 mmol, 12%) yellow oil; R_f (1:3 ethyl acetate/hexane) 0.97; [α]_D²¹ +9.22 (*c* 1.00, CHCl₃); ν_{max}(neat) 2959, 2931, 2874, 1698, 1655, 1560, 1542, 1458, 1382, 1361, 1331, 1255, 1207, 1173, 980, 804 cm⁻¹; ¹H NMR (500 MHz, CDCl₃) δ 5.34 (br s, 1H, CH-7), 2.59 (br s, 1H, H-5), 2.29-2.26 (m, 2H, CH₂-4αa), 2.25-2.16 (m, 2H, CH₂-8), 1.86 (br s, 1H, H-1), 1.80 (br s, 3H, CH₃-6α), 1.78-1.75 (m, 1H, CH₂-9a), 1.57 (dt, *J* = 3.0, 12.0 Hz, 1H, CH₂-9b), 1.52-1.48 (m, 2H, CH₂-4αb), 1.37-1.32 (m, 2H, CH₂-4αc), 1.19 (br s, 3H, CH₃-2α), 1.16 (br s, 3H, CH₃-2α), 0.93 (t, *J* = 7.0 Hz, 3H, CH₃-4αd); ¹³C NMR (125 MHz, CDCl₃) δ 170.6 (C-4), 135.1 (C-6), 122.5 (CH-7), 58.7 (C-2), 41.3 (CH₂-4αa), 38.7 (CH-5), 34.1 (CH-1), 29.0 (CH₃-2α), 29.8 (CH₂-4αb), 29.3 (CH₂-8), 28.1 (CH₃-2α), 26.1 (CH₂-9), 24.2 (CH₃-6α), 23.0 (CH₂-4αc), 14.4

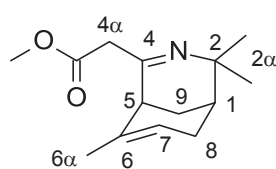
(CH₃-4 α d); GC-MS R_t = 14.26 min, *m/z* 219 (3 M⁺), 204 (3), 190 (4), 177 (31), 162 (8), 136 (9), 121 (9), 93 (100), 77 (12), 41 (12%). HRMS (ESI): C₁₅H₂₅N calcd: 220.2060 [M+H]⁺; found: 220.2048 [M+H]⁺.

3-(2,2,6-Trimethyl-3-azabicyclo[3.3.1]nona-3,6-dien-4-yl)propanenitrile (-)-60d



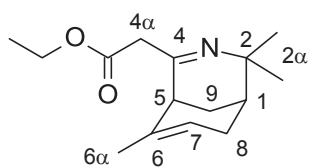
(119 mg, 0.552 mmol, 7%) red oil; R_f (1:3 acetone/hexane) 0.70; [α]_D²⁰ -45.28 (c 1.00, CHCl₃); ν_{max}(neat) 2965, 2932, 2910, 2873, 2836, 1665, 1629, 1450, 1431, 1381, 1359, 1205, 1143, 1114, 894, 798 cm⁻¹; ¹H NMR (500 MHz, CDCl₃) δ 5.36 (br s, 1H, CH-7), 2.72-2.65 (m, 2H, CH₂-4β), 2.64-2.55 (m, 2H, CH₂-4α), 2.44 (br s, 1H, CH-5), 2.20-2.18 (m, 1H, CH₂-9a), 2.16-2.14 (m, 1H, CH₂-9b), 2.90-1.87 (m, 1H, CH-1), 1.81-1.8-1.85 (m, 1H, CH₂-8a), 1.79 (d, *J* = 2.0 Hz, 3H, CH₃-6α), 1.57 (dt, *J* = 12.0, 3.0 Hz, 1H, CH₂-8b), 1.17 (br s, 3H, CH₃-2α), 1.12 (br s, 3H, CH₃-2α); ¹³C NMR (125 MHz, CDCl₃) δ 164.9 (C-4), 134.1 (C-6), 123.0 (CH-7), 120.7 (CN), 51.3 (C-2), 40.3 (CH-5), 35.5 (CH₂-4α), 34.0 (CH-1), 31.9 (CH₃-6α), 29.2 (CH₂-9), 28.0 (CH₃-2α), 25.9 (CH₂-8), 24.2 (CH₃-2α), 13.8 (CH₂-4β); GC-MS R_t = 6.455 min, *m/z* 216 (18 M⁺), 177 (27), 136 (27), 121 (14), 93 (100), 77 (18%). HRMS (ESI): C₁₄H₂₀N₂ calcd: 217.1699 [M+H]⁺; found: 217.1705 [M+H]⁺.

Methyl 2-(2,2,6-Trimethyl-3-azabicyclo[3.3.1]nona-3,6-dien-4-yl)acetate (-)-60g



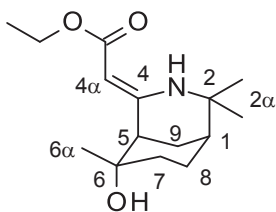
(40.0 mg, 0.17 mmol, 2%) yellow-green oil; R_f (CHCl₃) 0.75; [α]_D²¹ -42.38 (c 1.00, CHCl₃); ν_{max}(neat) 3259, 2960, 2943, 1649, 1595, 1229, 1139, 1049 cm⁻¹; ¹H NMR (500 MHz, CDCl₃) δ 8.51 (s, 1H, OH), 5.41 (s, 1H, CH-7), 4.75 (s, 1H, CH₂-4αa), 4.64 (s, 1H, CH₂-4αb), 4.38 (s, 1H, CH-4α), 3.63 (s, 3H, OCH₃), 2.47 (s, 1H, CH-5), 2.35-2.32 (m, 1H, CH₂-8a), 2.23-2.22 (m, 2H, CH₂-9), 2.10 (dt, *J* = 6.0, 3.0 Hz, 1H, CH₂-8b), 1.94 (s, 1H, CH-1), 1.73 (br s, 3H, CH₃-6α), 1.31 (br s, 3H, CH₃-2α), 1.24 (br s, 3H, CH₃-2α); ¹³C NMR (125 MHz, CDCl₃) δ 171.1 (C=O), 163.4 (C-4), 136.0 (C-6), 121.8 (CH-7), 108.3 (CH₂-4α, keto), 82.9 (CH-4α, enol), 54.9 (C-2), 50.2 (OCH₃), 47.0 (CH-5), 35.5 (CH-1), 33.0 (CH₃-2α), 30.8 (CH₃-2α), 27.7 (CH₃-6α), 24.4 (CH₂-9), 23.5 (CH₂-8); GC-MS R_t = 6.643 min, *m/z* 235 (50 M⁺), 220 (88), 204 (14), 188 (100), 160 (10), 121 (11), 93 (17), 93 (14%). HRMS (ESI): C₁₄H₂₁NO₂ calcd: 236.1645 [M+H]⁺; found: 236.1639 [M+H]⁺.

Ethyl 2-(2,2,6-trimethyl-3-azabicyclo[3.3.1]nona-3,6-dien-4-yl)acetate (-)-60h



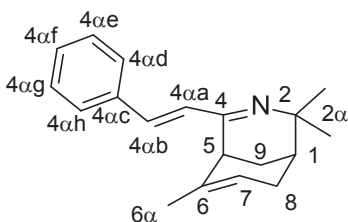
(139 mg, 0.557 mmol, 7%) yellow oil; R_f (1:9 ethyl acetate/dichloromethane) 0.9; $[\alpha]_D^{22} -123.92$ (c 1.00, CHCl_3); $\nu_{\text{max}}(\text{neat})$ 3261, 2963, 2933, 1647, 1599, 1490, 1468, 1293, 1280, 1140, 1051, 782 cm^{-1} ; $^1\text{H NMR}$ (500 MHz, CDCl_3) δ 8.28 (br s, 1H, OH), 5.40 (br s, 1H, CH-7), 4.73 (s, 1H, CH_2 -4 α), 4.63 (s, 1H, CH_2 -4 α b), 4.38 (s, 1H, CH-4 α), 4.11-4.05 (m, 2H, CH_2 -4 γ), 2.46 (br s, 1H, CH-5), 2.35-2.32 (m, 1H, CH_2 -8a), 2.22-2.18 (m, 1H, CH_2 -8b), 2.10 (dt, $J = 12.5, 3.0$ Hz, 1H, CH_2 -9a), 1.93 (br s, 1H, CH-1), 1.81-1.79 (m, 1H, CH_2 -9b), 1.74 (br s, 3H, CH_3 -6 α), 1.30 (br s, 3H, CH_3 -2 α), 1.25 (t, $J = 7.5$ Hz, 3H, CH_3 -4 δ), 1.24 (br s, 3H, CH_3 -2 α); $^{13}\text{C NMR}$ (125 MHz, CDCl_3) δ 170.9 (C=O), 164.2 (C-4), 136.0 (C-6), 121.7 (CH-7), 108.2 (CH_2 -4 α , keto), 80.0 (CH-4 α , enol), 58.6 (CH_2 -4 γ), 55.2 (C-2), 40.1 (CH-5), 35.0 (CH-1), 33.1 (CH_3 -2 α), 28.9 (CH_3 -2 α), 28.6 (CH_2 -8), 25.4 (CH_2 -9), 22.1 (CH_3 -6 α), 15.0 (CH_3 -4 δ); GC-MS $R_t = 17.968$ min, m/z 249 (42 M^+), 234 (78), 204 (17), 188 (100), 162 (11), 93 (21%). HRMS (ESI): $\text{C}_{15}\text{H}_{23}\text{NO}_2$ calcd: 250.1802 $[\text{M}+\text{H}]^+$; found: 250.1805 $[\text{M}+\text{H}]^+$.

(4Z)-4-(2-Ethoxy-2-hydroxy-ethylidene)-2,2,6-trimethyl-3-azabicyclo[3.3.1]nonan-6-ol (-)-66h



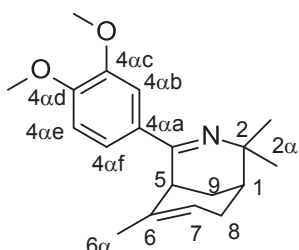
(56.0 mg, 0.21 mmol, 3%) pale red solid; m.p. 92 °C, R_f (1:9 ethyl acetate/dichloromethane) 0.66; $[\alpha]_D^{20} -33.26$ (c 1.00, CHCl_3); $\nu_{\text{max}}(\text{neat})$ 3470, 3287, 2984, 2951, 2912, 2874, 1739, 1625, 1578, 1493, 1454, 1365, 1342, 1330, 1272, 1230, 1145, 1133, 1102, 1052, 1029, 962, 907, 784, 714 cm^{-1} ; $^1\text{H NMR}$ (500 MHz, CDCl_3) δ 8.50 (br s, 1H, OH), 4.35 (s, 1H, CH-4 α), 4.04-4.14 (m, 2H, OCH_2CH_3), 2.24 (dt, $J = 13.0, 3.0$ Hz, 1H, CH_2 -9a), 2.14 (br s, 1H, CH-5), 1.93 (dt, $J = 13.0, 3.0$ Hz, 1H, CH_2 -9b), 1.86-1.82 (m, 2H, CH_2 -8a, CH_2 -7a), 1.79-1.72 (m, 1H, CH_2 -7b), 1.68 (br s, 1H, CH-1), 1.44-1.41 (dt, 1H, CH_2 -8b), 1.29 (br s, 3H, CH_3 -2 α), 1.28 (br s, 3H, CH_3 -2 α), 1.27 (br s, 3H, CH_3 -6 α), 1.26 (br s, 3H, OCH_2CH_3); $^{13}\text{C NMR}$ (125 MHz, CDCl_3) δ 170.5 (C=O), 162.9 (C-4), 83.0 (CH-4 α), 71.5 (C-6), 58.3 (OCH_2CH_3), 54.5 (C-2), 46.6 (CH-5), 35.2 (CH-1), 32.9 (CH_2 -7), 32.6 (CH_3 -6 α), 30.5 (CH_3 -2 α), 27.3 (CH_3 -2 α), 24.1 (CH_2 -8), 23.2 (CH_2 -9), 14.6 (OCH_2CH_3); GC-MS $R_t = 19.42$ min, m/z 267 (52 M^+), 252 (100), 222 (26), 206 (70), 197 (17), 182 (17), 148 (19), 96 (30), 43 (26%). HRMS (ESI): $\text{C}_{15}\text{H}_{25}\text{NO}_3$ calcd: 268.1907 $[\text{M}+\text{H}]^+$; found: 268.1898 $[\text{M}+\text{H}]^+$.

2,2,6-Trimethyl-4-[(E)-styryl]-3-azabicyclo[3.3.1]nona-3,6-diene (-)-60f



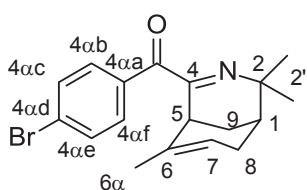
(1.067 g, 4.03 mmol, 53%) yellow wax; R_f (0.5:9.5 ethanol/ethyl acetate) 0.69; $[\alpha]_D^{18} -35.11$ (c 0.23, CHCl_3); $\nu_{\text{max}}(\text{neat})$ 3321, 2965, 2929, 1607, 1451, 1331, 1255, 1212, 1186, 1153, 972, 752, 694 cm^{-1} ; $^1\text{H NMR}$ (500 MHz, CDCl_3) δ 7.51 (d, $J = 7.5$ Hz, 2H, Ar-4 α d & Ar-4 α h), 7.34 (t, $J = 7.5$, 2H, Ar-4 α e & Ar-4 α g), 7.28 (t, $J = 7.5$ Hz, 1H, Ar-4 α f), 7.16 (d, $J = 16.5$ Hz, 1H, CH-4 α b), 6.88 (d, $J = 16.5$ Hz, 1H, CH-4 α a), 5.38 (br s, 1H, CH-7), 3.19 (br s, 1H, CH-5), 2.19-2.30 (m, 2H, CH_2 -8), 1.96 (br s, 1H, CH-1), 1.89 (dt, $J = 2.5, 12.0$ Hz, 1H, CH_2 -9a), 1.78 (br s, 3H, CH_3 -6 α), 1.73 (dt, $J = 2.5, 12.0$ Hz, 1H, CH_2 -9b), 1.28 (br s, 3H, CH_3 -2 α), 1.26 (br s, 3H, CH_3 -2 α); $^{13}\text{C NMR}$ (125 MHz, CDCl_3) δ 166.9 (C-4), 136.7 (C-4 α c), 135.4 (CH-4 α b), 135.1 (C-6), 131.8 (CH-4 α a), 129.0 (CH-4 α d), 128.9 (CH-4 α f), 127.5 (CH-4 α e), 122.8 (CH_2 -8), 59.9 (C-2), 35.8 (CH-5), 34.5 (CH-1), 32.5 (CH_3 -2 α), 29.4 (CH_2 -8), 27.8 (CH_3 -2 α), 25.8 (CH_2 -9), 24.1 (CH_3 -6 α); GC-MS $R_t = 6.10$ min, m/z 265 (50 M^+), 250 (14), 224 (7), 136 (21), 130 (18), 115 (14) 93 (100) 77 (18%). HRMS (ESI): $\text{C}_{19}\text{H}_{23}\text{N}$ calcd: 266.1903 $[\text{M}+\text{H}]^+$; found: 266.1901 $[\text{M}+\text{H}]^+$.

4-(3,4-Dimethoxyphenyl)-2,2,6-trimethyl-3-azabicyclo[3.3.1]nona-3,6-diene (+)-60e



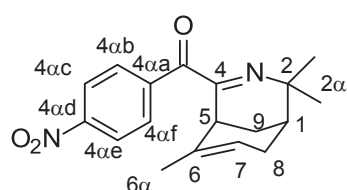
(948 mg, 3.17 mmol, 42%) pale yellow wax; R_f (1:1 ethyl acetate/hexane) 0.46; $[\alpha]_D^{21} +66.64$ (c 1.00, CHCl_3); $\nu_{\text{max}}(\text{neat})$ 2969, 2937, 2838, 1637, 1608, 1585, 1508, 1458, 1270, 1162, 1134, 1028, 916, 771 cm^{-1} ; $^1\text{H NMR}$ (500 MHz, CDCl_3) δ 7.51 (br s, 1H, CH-7), 7.24 (d, $J = 2.0$ Hz, 1H, Ar-4 α f), 6.88 (d, $J = 2.0$ Hz, 1H, Ar-4 α b), 6.87 (d, $J = 2.0$ Hz, 1H, Ar-4 α e), 4.40 (br s, 1H, CH-5), 3.96 (br s, 3H, OCH_3), 3.94 (br s, 3H, OCH_3), 2.01 (dt, $J = 2.5$ Hz, 13.5, 1H, CH_2 -9a), 1.96-1.93 (m, 1H, CH_2 -8a), 1.89-1.87 (m, 1H, CH_2 -9b), 1.77-1.69 (m, 1H, CH-1), 1.72 (dt, $J = 4.5, 14.0$ Hz, 1H, CH_2 -8b), 1.42 (br s, 3H, CH_3 -2 α), 1.28 (br s, 3H, CH_3 -2 α) 1.14 (br s, 3H, CH_3 -6 α); $^{13}\text{C NMR}$ (125 MHz, CDCl_3) δ 167.2 (C-4), 152.1 (C-4 α a), 149.6 (C-4 α c), 149.1 (C-4 α d), 128.6 (C-6), 119.0 (C-4 α f), 110.7 (CH-4 α b), 110.5 (CH-4 α e), 110.3 (CH-7), 56.8 (C-2), 56.4 (OCH_3), 56.4 (OCH_3), 35.9 (CH-5), 34.7 (CH-1), 32.1 (CH_3 -2 α), 27.7 (CH_3 -6 α), 26.9 (CH_3 -2 α), 25.3 (CH_2 -8), 24.6 (CH_2 -9); GC-MS $R_t = 22.22$ min, m/z 299 (46 M^+), 164 (29), 136 (35), 121 (14) 93 (100), 77 (15%). HRMS (ESI): $\text{C}_{19}\text{H}_{25}\text{NO}_2$ calcd: 300.1958 $[\text{M}+\text{H}]^+$; found: 300.1963 $[\text{M}+\text{H}]^+$.

(4-Bromophenyl)-(2,2,6-trimethyl-3-azabicyclo[3.3.1]nona-3,6-dien-4-yl)methanone (-)-65i



(372 mg, 1.08 mmol, 14%) honey colour oil; R_f (1:3 ethyl acetate/hexane) 0.94; $[\alpha]_D^{22} - 31.48$ (c 1.00, CHCl_3); ν_{max} (neat) 2957, 2929, 2870, 1665, 1655, 1587, 1460, 1384, 1272, 1231, 1071, 1013, 899, 810, 756 cm^{-1} ; $^1\text{H NMR}$ (500 MHz, CDCl_3) δ 7.82 (d, $J = 8.5$ Hz, 2H, Ar-4 α b), 7.56 (d, $J = 8.5$ Hz, 2H, Ar-4 α c), 5.43 (br s, 1H, CH-7), 3.45 (br s, 1H, H-5), 2.32-2.25 (m, 2H, CH_2 -8), 1.99-2.00 (m, 1H, H-1), 1.91 (dt, $J = 2.5, 12.0$ Hz, 1H, CH_2 -9a), 1.77 (dt, $J = 2.5, 12.0$ Hz, 1H, CH_2 -9b), 1.52 (br s, 3H, CH_3 -6 α), 1.32 (br s, 3H, CH_3 -2 α), 1.26 (br s, 3H, CH_3 -2 α); $^{13}\text{C NMR}$ (125 MHz, CDCl_3) δ 193.2 (C=O), 166.5 (C-4), 134.9 (C-4 α a), 134.5 (C-4 α d), 132.6 (C-4 α b & C-4 α f), 131.8 (C-4 α c & C-4 α e), 128.8 (C-6), 122.8 (CH-7), 61.3 (C-2), 35.1 (CH-5), 34.5 (CH-1), 31.3 (CH_3 -2 α), 29.3 (CH_2 -8), 27.8 (CH_3 -2 α), 25.3 (CH_2 -9), 23.3 (CH_3 -6 α); GC-MS $R_t = 8.19$ min, m/z 345 (29 M^+), 330 (54), 304 (18), 183 (27), 155 (18), 93 (100), 77 (19%). HRMS (ESI): $\text{C}_{18}\text{H}_{20}^{79}\text{BrNO}$ calcd: 346.0801 $[\text{M}+\text{H}]^+$; found: 346.0803 $[\text{M}+\text{H}]^+$.

(4-Nitrophenyl)-(2,2,6-trimethyl-3-azabicyclo[3.3.1]nona-3,6-dien-4-yl)methanone (-)-65j



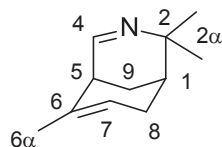
(211 mg, 0.68 mmol, 12%) deep red oil; R_f (1:3 ethyl acetate/hexane) 0.99; $[\alpha]_D^{23} - 34.77$ (c 1.04, CHCl_3); ν_{max} (neat) 2967, 2933, 2870, 1672, 1603, 1525, 1460, 1346, 1272, 1231, 1110, 905, 856, 810, 706 cm^{-1} ; $^1\text{H NMR}$ (500 MHz, CDCl_3) δ 8.25 (dd, $J = 7.0, 7.5$ Hz, 2H, Ar-4 α c & Ar-4 α e), 8.08 (dd, $J = 7.0, 7.5$ Hz, 2H, Ar-4 α b & Ar-4 α f), 5.45 (br s, 1H, H-7), 3.52 (br s, 1H, H-5), 2.31-2.33 (m, 2H, CH_2 -9), 2.01 (s, 1H, H-1), 1.89 (dt, $J = 3.0, 12.5$ Hz, 1H, CH_2 -8a), 1.79 (dt, $J = 3.0, 12.5$ Hz, 1H, CH_2 -8b), 1.57 (br s, 3H, CH_3 -6 α), 1.33 (br s, 3H, CH_3 -2 α) 1.26 (br s, 3H, CH_3 -2 α); $^{13}\text{C NMR}$ (125 MHz, CDCl_3) δ 192.2 (C=O), 166.4 (C-4), 150.3 (C-4 α d), 141.3 (C-4 α a), 134.8 (C-6), 132.1 (CH-4 α b & CH-4 α f), 123.4 (CH-4 α c & CH-4 α e), 123.0 (CH-7), 61.8 (C-2), 34.5 (CH-5), 34.4 (CH-1), 31.3 (CH_3 -2 α), 29.3 (CH_2 -9), 27.7 (CH_3 -2 α), 25.3 (CH_2 -8), 23.3 (CH_3 -6 α); GC-MS $R_t = 23.44$ min, m/z 312 (25 M^+), 297 (50), 271 (24), 150 (24), 120 (25), 93 (100), 77 (23%). HRMS (ESI): $\text{C}_{18}\text{H}_{20}\text{N}_2\text{O}_3$ calcd: 313.1547 $[\text{M}+\text{H}]^+$; found: 313.1554 $[\text{M}+\text{H}]^+$.

9.2.1.1 The Bridged Ritter Reaction with Trimethylsilyl Cyanide

Trimethylsilyl cyanide (6 mL, 47.95 mmol) was added to a sealed round bottom flask with a condenser connected to a gas trap filled with NaOH solution, containing H_2SO_4 (18 M; 2 mL), being stirred at 0 °C. (-)- β -Pinene (1.2 mL, 7.63 mmol) dissolved in dichloromethane (10 mL), was added dropwise *via* syringe through the septum. The reaction was stirred overnight before being quenched with water (20 mL) and basified (until pH > 10) with NaOH solution (4

M). The product was then extracted with chloroform (2 X 30 mL) and the combined extracts were dried over Na₂CO₃ and the solvent removed under reduced pressure to give 0.7128 g of crude product.

2,2,6-Trimethyl-3-azabicyclo[3.3.1]nona-3,6-diene (+)-60a



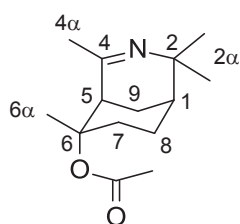
(713 mg, 4.37 mmol, 57%) pale yellow liquid; R_f (diethyl ether) 0.36; $[\alpha]_D^{21} +3.99$ (c 1.00, CHCl₃); IR ν_{\max} (neat) 3339, 2961, 2931, 2907, 2838, 1710, 1459, 1384, 1364, 1248 1090, 1066, 915 cm⁻¹; ¹H NMR (500 MHz, CDCl₃) δ 5.64-5.63 (m, 1H, CH-4), 3.67 (s, 1H, CH-7), 2.47-2.51 (m, 1H, CH₂-9a), 2.28 (br s, 1H, CH-5), 2.22-2.23 (m, 2H, CH₂-8), 1.69-1.74 (m, 1H, CH₂-9b), 1.66-1.67 (m, 3H, CH₃-6 α), 1.57 (m, 1H, CH-1), 1.46 (s, 3H, CH₃-2'), 1.08 (s, 3H, CH₃-2 α); ¹³C NMR (125 MHz, CDCl₃) δ 132.5 (C-6), 125.9 (CH-4), 54.1 (C-2), 47.6 (CH-7), 37.6 (CH-5), 34.3 (CH-1), 30.6 (CH₃-2 α), 28.0 (CH₃-2 α), 27.7 (CH₂-8), 25.4 (CH₂-9), 22.1 (CH₃-6 α); GC-MS R_t = 10.845 min, m/z 163 (50 M⁺), 148 (27), 122 (100), 93 (57), 77 (24%). HRMS (ESI): C₁₁H₁₇N calcd: 164.1434 [M+H]⁺; found 164.1436 [M+H]⁺.

9.2.2 Alternative Condition Bridged Ritter Reactions

9.2.3 Polar Bridged Ritter Reaction Conditions

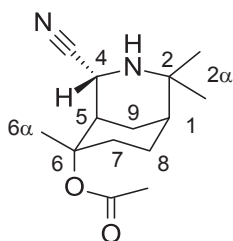
Sulfuric acid (18 M; 2 mL) was stirred in a flask fitted with a reflux condenser and a drying tube at 0 °C. To the reaction flask, the nitrile (53.4 mol, 7 mol equiv. of (-)- β -pinene) was added. A solution of (-)- β -pinene (1.2 mL, 7.62 mmol) in glacial acetic acid (10 mL) was added dropwise to the reaction mixture, *via* the condenser. After 30 min the reaction was allowed to reach room temperature and left to stir for 24 h. The reaction was then quenched by the addition of water (30 mL). The reaction mixture was then washed with dichloromethane to remove any neutral impurities, before it was basified with NaOH solution (4 M) until pH > 10. The reaction mix was then extracted with chloroform (2 X 15 mL) and the combined organic extracts were dried over Na₂CO₃ before the solvent was removed under reduced pressure. 0.6626 g of crude product was obtained from acetonitrile and 0.6919 g of crude product was obtained for propionitrile.

(2,2,4,6-Tetramethyl-3-azabicyclo[3.3.1]non-3-en-6-yl) acetate (+)-63l



(154 mg, 0.649 mmol, 9%) pale yellow oily wax; R_f (1:3 ethyl acetate/hexane) 0.83; $[\alpha]_D^{20} +72.64$ (c 1.00, CHCl₃); ν_{\max} (neat) 2949, 2927, 1732, 1649, 1627, 1458, 1367, 1245, 1220, 1200, 1157, 1099, 1018 cm⁻¹; ¹H NMR (500 MHz, CDCl₃) δ 3.12 (br s, 1H, CH-5), 2.06 (s, 3H, COCH₃),

(1S,4R,5R,6S)-4-Cyano-2,2,6-trimethyl-3-azabicyclo[3.3.1]nonan-6-yl acetate (+)-67



(148 mg, 0.59 mmol, 8%) colourless crystal; m.p = 164 °C; $[\alpha]_D^{20} +9.76$ (c 1.00, CHCl₃). IR (neat, cm⁻¹) 3335, 2985, 2956, 2929, 2899, 2869, 2220, 1720, 1497, 1458, 1380, 1361, 1255, 1210, 1193, 1148, 1118, 1020, 969, 928, 817, 727, 693; ¹H NMR (500 MHz, CDCl₃) δ 4.10 (br s, 1H, CH-4), 2.69 (br s, 1H, CH-5), 2.26-2.30 (m, 1H, CH₂-7a), 2.21-2.26 (m, 1H, CH₂-8a), 2.03 (br s, 3H, OCOCH₃), 1.96-1.95 (m, 1H, CH₂-8b), 1.92-1.82 (m, 1H, CH₂-7b), 1.81 (dq, *J* = 14.0, 4.5 Hz, 1H, H-9a) 1.62-1.65 (m, 1H, CH₂-9b), 1.56 (br s, 3H, CH₃-6α) 1.47-1.46 (m, 1H, CH-1), 1.45 (br s, 3H, CH₃-2α), 1.09 (br. s, 3H, CH₃-2α); ¹³C NMR (125 MHz, CDCl₃) δ 170.7 (C=O), 123.1 (CN), 83.8 (C-6), 53.6 (C-2), 45.7 (CH-4), 38.6 (CH-5), 35.5 (CH-1), 33.2 (CH₂-8), 30.3 (OCOCH₃), 29.1 (CH₃-6α), 24.5 (CH₂-9), 24.3 (CH₃-2α), 23.4 (CH₂-7), 22.8 (CH₃-2α); GC-MS *R*_t = 14.72 min, *m/z* 223 (27 M⁺), 208, (7), 180 (100), 164 (74), 148 (23), 122 (36), 108 (64), 43 (62%). HRMS (ESI): C₁₄H₂₂N₂O₂ calcd: 251.1741 [M+H]⁺; found: 251.1754 [M+H]⁺.

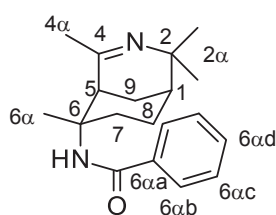
9.2.4 Mixed Ritter Reactions

9.2.4.1 One-Pot Mixed Ritter Reactions

Sulfuric acid (18 M; 2 mL) was stirred in a flask fitted with a reflux condenser and a drying tube at 0 °C. To the reaction flask, both nitriles (26.7 mmol, 3.5 mol equiv. of (-)-β-pinene each) was added. A solution of (-)-β-pinene (1.2 mL, 7.62 mmol) in benzene (5 mL) was added dropwise to the reaction mixture, *via* the condenser. After 30 min, the reaction was allowed to reach room temperature and left to stir for 24 h. The reaction was then quenched by the addition of water (30 mL). The mixture was basified with a solution of NaOH (4 M) until pH > 10. The reaction mix was then extracted with chloroform (2 X 15 mL) and dried over Na₂CO₃ before the solvent was removed under reduced pressure.

For compounds that were unable to be fully characterised, the beginning of the compound name has been denoted with an asterisk (*).

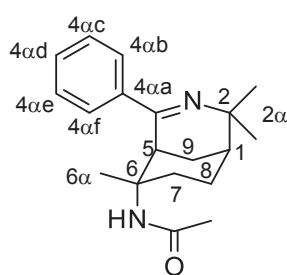
***N*-(2,2,4,6-Tetramethyl-3-azabicyclo[3.3.1]non-3-en-6-yl)benzamide (+)-79**



(122 mg, 0.41 mmol, 6%) pale yellow wax; *R*_f (1:4 EtOAc/hexane) 0.20; $[\alpha]_D^{21} +106.76$ (c 0.98, CHCl₃); *v*_{max}: 3295, 3058, 2933, 1638, 1530, 1453, 1365, 1284, 1164, 1104, 800, 710 cm⁻¹; ¹H NMR (500 MHz, CDCl₃) δ 7.65 (d, *J* = 7.5 Hz, 2H, Ar-CH-6ab & Ar-CH-6af), 7.52 (t, *J* = 7.5 Hz, 1H, Ar-CH-6ad), 7.45 (t, *J* = 7.5 Hz, 2H, Ar-CH-6ac & Ar-CH-6ae), 6.04 (s, 1H, NH), 3.35, (br s, 1H, CH-5), 2.14 (s, 3H, CH₃-4α), 1.87-1.91 (m, 1H, CH₂-9a),

1.83 (dt, $J = 15.0, 2.5$ Hz, 1H, CH₂-7a), 1.73-1.77 (m, 1H, CH₂-9b), 1.63-1.73 (m, 3H, CH₂-8a, CH₂-7b, CH-1), 1.59 (s, 3H, CH₃-6 α), 1.52 (td, $J = 12.0, 4.5$ Hz, 1H, CH₂-8b), 1.31 (s, 3H, CH₃-2 α), 1.17 (s, 3H, CH₃-2 α); ¹³C NMR (125 MHz, CDCl₃) δ 167.0 (C=O), 166.7 (C-4), 135.6 (Ar-C-6 α), 131.4 (Ar-CH-6 α b & Ar-CH-6 α f), 128.6 (Ar-CH-6 α d), 126.6 (2 Ar-CH-6 α c & Ar-CH-6 α e), 58.1 (C-6), 56.0 (C-2), 40.4 (CH-5), 33.9 (CH-1), 33.4 (CH₂-7), 31.7 (CH₃-6 α), 29.8 (CH₃-4 α), 27.3 (CH₃-2 α), 26.3 (CH₃-2 α), 24.8 (CH₂-9), 24.2 (CH₂-8); GC-MS $R_t = 22.937$ min, m/z 298 (42 M⁺), 293 (13), 177 (50), 162 (29), 122 (54), 105 (100), 77 (75%). HRMS (ESI): C₁₉H₂₆N₂O calcd: 299.2118 [M+H]⁺; found: 299.2119 [M+H]⁺.

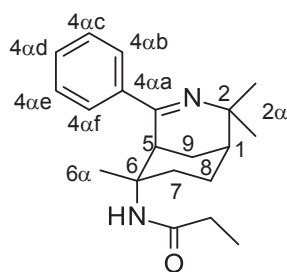
***N*-(2,2,6-Trimethyl-4-phenyl-3-azabicyclo[3.3.1]non-3-en-6-yl)acetamide (+)-80**



(133 mg, 0.45 mmol, 7%) pale yellow wax; R_f (1:4 EtOAc/hexane) 0.33; $[\alpha]_D^{22} +69.18$ (c 1.00, CHCl₃); ν_{max} : 3301, 3059, 2931, 1640, 1544, 1442, 1366, 1281, 1158, 971, 776, 695 cm⁻¹; ¹H NMR (500 MHz, CDCl₃) δ 7.80 (d, $J = 7.5$ Hz, 2H, Ar-CH-4 α b & Ar-CH-4 α f), 7.35 (t, $J = 7.5$ Hz, 3H, Ar-CH-4 α c, Ar-CH-4 α d & Ar-CH-4 α e), 5.37 (s, 1H, NH), 4.22, (br s, 1H, CH-5), 2.01 (s, 3H, CH₃-6 α), 1.95 (dt, $J = 14.0, 3.0$

Hz, 1H, CH₂-9a), 1.85-1.86 (m, 2H, CH₂-9b & CH₂-7a), 1.74-1.75 (m, 1H, CH-1), 1.62-1.65 (m, 2H, CH₂-7b & CH₂-8a), 1.41-1.47 (m, 1H, CH₂-8b) 1.38 (s, 3H, NHCOCH₃), 1.26 (s, 3H, CH₃-2 α), 0.98 (s, 3H, CH₃-2 α); ¹³C NMR (125 MHz, CDCl₃) δ 170.0 (C=O), 166.0 (C-4), 142.2 (Ar-C-4 α a), 129.0 (Ar-CH-4 α b & Ar-CH-4 α f), 128.1 (Ar-CH-4 α d), 127.0 (Ar-CH-4 α c & Ar-CH-4 α e), 58.7 (C-6), 56.2 (C-2), 34.9 (CH-5), 34.2 (CH-1), 33.3 (CH₂-7), 33.6 (CH₃-6 α), 27.4 (CH₃-2 α), 26.5 (CH₃-2 α), 24.5 (CH₂-7), 24.4 (NHCOCH₃), 24.1 (CH₂-8); GC-MS $R_t = 22.526$ min, m/z 298 (67 M⁺), 283 (25), 239 (38), 212 (56), 198 (100), 184 (79), 145 (33), 104 (50%). HRMS (ESI): C₁₉H₂₆N₂O calcd: 299.2118 [M+H]⁺; found: 299.2118 [M+H]⁺.

*** *N*-(2,2,6-Trimethyl-4-phenyl-3-azabicyclo[3.3.1]non-3-en-6-yl)propanamide 81**

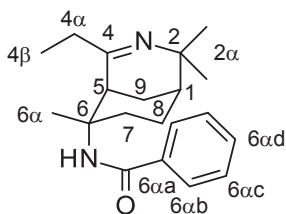


(9.7 mg, 0.031 mmol, 0.4%) yellow semi-solid; R_f (95:5 EtOAc/MeOH) 0.4; ¹H NMR (500 MHz, CDCl₃) δ 7.75 (d, $J = 7.5$ Hz, 2H, Ar-CH-6 α b & Ar-CH-6 α f), 7.52 (t, $J = 7.5$ Hz, 1H, Ar-CH-6 α d), 7.45 (t, $J = 7.5$, 2H, Ar-CH-6 α c & Ar-CH-6 α e), 6.06 (s, 1H, NH), 3.48 (s, 1H, CH-5), 1.86-1.88

(m, 1H, CH₂-9a), 1.72 (s, 1H, CH-1), 1.34 (s, 3H, CH₃-6 α), 1.23 (s, 3H, CH₃-2 α), 1.17 (s, 3H, CH₃-2 α), 1.14 (t, $J = 7.5$ Hz, 3H, CH₃-4 β), 0.78-0.89 (m, 2H, CH₂-4 α); ¹³C NMR (125 MHz, CDCl₃) δ 34.5 (CH-1), 34.1 (CH-5), 30.9 (CH₂-4 α), 27.3 (CH₃- α), 27.0 (CH₃-2 α), 25.2 (CH₃-6 α); GC-MS $R_t = 8.232$ min, m/z 312 (58 M⁺), 297 (22), 239

(49), 224 (24), 212 (60), 198 (100), 184 (70), 145 (30), 104 (45%). HRESIMS: $[M+H]^+$, found 313.2279, $C_{20}H_{28}N_2O$ required 313.2275.

*** *N*-(4-Ethyl-2,2,6-trimethyl-3-azabicyclo[3.3.1]non-3-en-6-yl)benzamide 82**

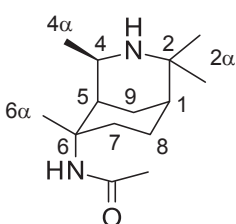


(4.6 mg, 0.015 mmol, 0.2%) yellow semi-solid; R_f (95:5 EtOAc/MeOH) 0.65; 1H NMR (500 MHz, $CDCl_3$) δ 7.83 (d, $J = 7.5$ Hz, 2H, Ar-CH-4 α b & Ar-CH-4 α f), 7.37-7.35 (m, 3H, Ar-CH-4 α c, Ar-CH-4 α d & Ar-CH-4 α e), 5.37 (br s, 1H, NH), 4.34 (br s, 1H, H-5), 2.23 (q, $J = 7.5$ Hz, 2H, $\underline{CH_2}CH_3$), 1.95 (dt, $J = 13.5, 6.0$ Hz, 2H, CH_2 -8), 1.90-1.85 (m, 1H, CH_2 -9a), 1.76 (br s, 1H, H-1), 1.66-1.65 (m, 1H, CH_2 -9b), 1.45-1.44 (m, 1H, CH_2 -7a), 1.42 (s, 3H, CH_3 -6 α), 1.41-1.40 (m, 1H, CH_2 -7b), 1.26 (br s, 3H, CH_3 -2 α), 1.18 (t, $J = 7.5$ Hz, 3H, CH_2CH_3), 0.97 (s, 3H, CH_3 -2 α); ^{13}C NMR (125 MHz, $CDCl_3$) δ 174.0 (C=O), 131.4 (Ar-C-4 α a), 128.8 (Ar-CH-4 α b & Ar-CH-4 α f), 127.7 (Ar-CH-4 α c & Ar-CH-4 α e), 77.6 (C-6), 56.5 (C-2), 35.5 (CH-5), 34.7 (CH-1), 33.9 (CH_2 -7), 30.9 ($\underline{CH_2}CH_3$), 30.4 (CH_3 -2 α), 27.8 (CH_3 -6 α), 26.6 (CH_3 -2 α), 24.9 (CH_2 -9), 24.3 (CH_2 -8), 10.2 ($\underline{CH_2}CH_3$); GC-MS $R_t = 8.319$ min, m/z 312 (43 M^+), 297 (15), 191 (47), 176 (30), 164 (36), 150 (31), 136 (50), 105 (100), 77 (50%). HRMS (ESI): $C_{20}H_{28}N_2O$ calcd 313.2275 $[M+H]^+$; found: 313.2274 $[M+H]^+$.

9.2.5 Hydride Reduction Reactions

Compound (+)-59l (0.20 g, 0.85 mmol) was dissolved in dry methanol (10 mL) in a round-bottom flask and fitted with a rubber septum and needle for ventilation of gases. The mixture was set to stir in an ice bath, to which $NaBH_4$ (224 mg, 5.93 mmol, 7 mol equiv.) was added and left to stir at 0 °C for 30 min before left at room temperature overnight. The reaction was quenched by the addition of water (5 mL), followed by saturated $NaHCO_3$ (15 mL). The product was then extracted with chloroform (2 X 20 mL). The combined extracts were washed with a saturated solution of NaCl (20 mL) before drying over Na_2CO_3 and the solvent removed under reduced pressure. The same procedure was adapted for the reduction of imine-amides (+)-59b, (+)-59c, (+)-59m and (+)-59n and imine-alkenes (+)-60l, (+)-60m and (+)-60n.

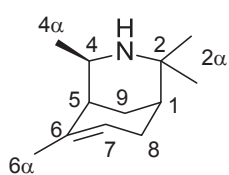
***N*-((1*S*,4*R*,5*R*,6*S*)-2,2,4,6-Tetramethyl-3-azabicyclo[3.3.1]nonan-6-yl)acetamide (+)-101l**



(195 mg, 0.819 mmol, 97%) pale yellow solid; m.p. 100 °C; $[\alpha]_D^{25} +18.30$ (c 1.43, $CHCl_3$); ν_{max} (neat) 3307, 2954, 2932, 1638, 1544, 1439, 1378, 1292, 1261, 1116, 754, 733, 665 cm^{-1} . 1H NMR (500 MHz, $CDCl_3$) δ 5.35 (s, 1H, NH), 3.37 (qd, $J = 2.5, 7.5$ Hz, 1H, CH-4), 2.46 (td, $J = 5.5, 15.5$ Hz,

1H, CH₂-7a), 2.31 (s, 1H, CH-5), 1.94 (s, 3H, COCH₃), 1.90-1.84 (m, 1H, CH₂-8a), 1.82-1.80 (m, 2H, CH₂-9), 1.56-1.54 (m, 2H, CH₂-7a and CH₂-8b), 1.52 (s, 3H, CH₃-6α), 1.30 (s, 1H, CH-1), 1.21 (d, *J* = 7.5 Hz, 3H, CH₃-4α), 1.19 (s, 3H, CH₃-2α), 1.11 (s, 3H, CH₃-2α); ¹³C NMR (125 MHz, CDCl₃) δ 169.0 (C=O), 57.9 (C-6), 53.3 (C-2), 51.3 (CH-4), 39.6 (CH-5), 35.6 (CH-1), 34.3 (CH₂-9), 30.1 (CH₂-7), 29.6 (CH₃-2α), 28.0 (CH₃-6α), 27.4 (CH₃-2α), 24.9 (CH₂-8), 24.8 (COCH₃), 23.1 (CH₃-4α); GC-MS (EI) *R*_f = 12.56 min, *m/z* 238 (20 M⁺), 223 (100), 179 (26), 164 (26), 122 (26), 84 (46%); HRMS (ESI): C₁₂H₂₁N calcd: 239.2118 [M+H]⁺; found: 239.2121 [M+H]⁺.

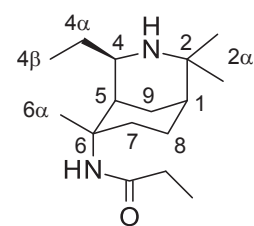
(1S,5S)-2,2,4,6-Tetramethyl-3-azabicyclo[3.3.1]non-6-ene (-)-102l



(125 mg, 0.626 mmol, 56%) red wax; *R*_f (3:7 MeOH/CH₂Cl₂) 0.47; [α]_D²⁵ -15.71 (*c* 0.47, CHCl₃); *v*_{max}(neat) 2957, 2923, 2886, 1734, 1599, 1458, 1379, 1227, 1160, 1126, 1083, 1035, 1011, 918, 824, 800, 751 cm⁻¹.

¹H NMR (500 MHz, CDCl₃) δ 5.57 (s, 1H, CH-7), 3.13 (qd *J* = 7.0, 2.5 Hz, 1H, CH-4), 2.20 -2.17 (m, 1H, CH₂-8s), 2.09-2.07 (m, 2H, CH₂-8b & CH₂-9a), 1.94 (d, *J* = 3.0 Hz, 1H, H-5), 1.71 (s, 3H, CH₃-6α), 1.60 (dt, *J* = 3.5, 9.5 Hz 1H, CH₂-9b), 1.43 (dt, *J* = 6.0, 3.0 Hz, 1H, CH-1), 1.21 (s, 3H, CH₃-2), 1.09 (s, 3H, CH₃-2α), 0.98 (d, *J* = 7.0 Hz, 3H, CH₃-4); ¹³C NMR (125 MHz, CDCl₃) δ 133.4 (C-6), 124.2 (CH-7), 53.6 (C-2) 50.1 (CH-4), 39.7 (CH-5), 34.3 (CH-1), 29.8 (CH₃-2α), 28.9 (CH₂-9), 22.6 (CH₂-8), 25.7 (CH₃-2α), 25.5 (CH₃-6α), 21.7 (CH₃-4α); GC-MS (EI) *R*_f = 11.09 min, *m/z* 179 (62 M⁺), 164 (47), 136 (34), 124 (43), 93 (100), 44 (32%); HRMS (ESI): C₁₂H₂₁N calcd: 180.1747 [M+H]⁺; found: 180.1747 [M+H]⁺.

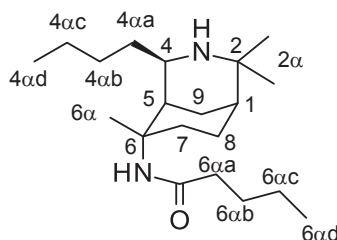
***N*-(4-Ethyl-2,2,6-trimethyl-3-azabicyclo[3.3.1]nonan-6-yl)propanamide (+)-101b**



(257 mg, 0.967 mmol, 42%) white solid; m.p. 103 °C, *R*_f (1:3 ethyl acetate/hexane) 0.13; [α]_D²³ +26.80 (*c* 1.05, CHCl₃); *v*_{max}(neat) 3302, 3069, 2957, 2933, 2877, 1637, 1544, 1460, 1432, 1382, 1361, 1261, 1236, 1119, 1086, 974, 808 cm⁻¹; ¹H NMR (500 MHz, CDCl₃) δ 5.29 (br s, NH), 3.02 (ddd, *J* = 2.0, 7.0, 2.5 Hz, 1H, CH-4), 2.53 (td, *J* = 4.5, 13.5, 1H, CH₂-7a), 2.48 (br s, 1H, CH-5), 2.16 (qd, *J* = 1.0, 7.5 Hz, 2H, COCH₂CH₃), 1.87-1.93 (m, 1H, CH₂-8a), 1.83 (dt, *J* = 3.0, 13.5 Hz, 1H, CH₂-9a), 1.77-1.76 (m, 1H, CH₂-9b), 1.74-1.66 (m, 1H, CH₂-4α), 1.52 (br s, 3H, CH₃-6α), 1.50-1.48 (m, 1H, CH₂-8b), 1.47-1.45 (m, 1H, CH₂-7b), 1.40-1.37 (m, 1H, CH₂-4αb), 1.32-1.31 (m, 1H, CH-1), 1.18 (br s, 3H, CH₃-2α), 1.14 (t, *J* = 7.5 Hz, 3H, COCH₂CH₃), 1.11 (br s, 3H, CH₃-2α), 0.96 (t, *J* = 7.5 Hz, 3H, CH₃-4β); ¹³C NMR (125 MHz, CDCl₃) δ 172.0 (C=O), 59.4 (CH-4), 57.9 (C-2), 53.6 (C-6), 38.1 (CH-5), 36.5 (CH-1), 35.1 (CH₂-7), 31.2 (COCH₂CH₃), 30.7 (CH₂-9), 29.9 (CH₃-2α), 29.7 (CH₂-4α), 27.7 (CH₃-2α), 27.5 (CH₃-6α), 25.4 (CH₂-8), 12.7 (CH₃-4β), 10.5 (COCH₂CH₃); GC-MS *R*_f = 7.22 min, *m/z* 266 (5 M⁺), 251 (25), 237 (100),

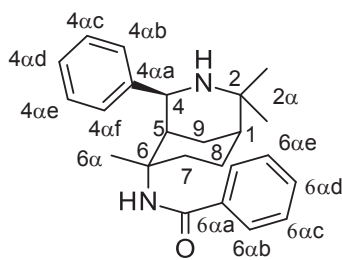
136 (25), 98 (30), 58 (50%). HRMS (ESI): C₁₆H₃₀N₂O calcd: 267.2431 [M+H]⁺; found: 267.2430 [M+H]⁺.

***N*-(4-Butyl-2,2,6-trimethyl-3-azabicyclo[3.3.1]nonan-6-yl)pentanamide (+)-101c**



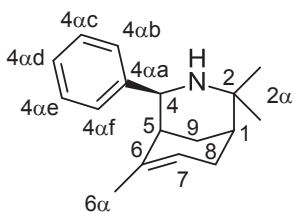
(289 mg, 0.899 mmol, 82%) pale yellow wax; $[\alpha]_D^{19} +13.36$ (c 1.00, CHCl₃); $\nu_{\max}(\text{neat})$ 3325, 3182, 2958, 2931, 2874, 1642, 1541, 1508, 1459, 1438, 1381, 1217, 1118, 752 cm⁻¹; ¹H NMR (500 MHz, CDCl₃) δ 5.29 (s, 1H, NH), 3.12-3.09 (m, 1H, H-4), 2.53 (td, $J = 4.5, 13.5$ Hz, 1H, CH₂-7a), 2.46 (s, 1H, CH-5), 2.13 (t, $J = 7.0$ Hz, 2H, CH₂-6 α a), 1.92-1.89 (m, CH₂-8a), 1.82-1.81 (m, 2H, CH₂-4 α a), 1.69-1.65 (m, 1H, CH₂-9a), 1.65-1.56 (m, 2H, CH₂-6 α b), 1.52 (br s, 3H, CH₃-2 α), 1.51-1.42 (m, 2H, CH₂-8b & CH₂7b), 1.39-1.32 (m, 8H, CH₂-9b, CH-1, CH₂-4 α b, CH₂-4 α c, CH₂-6 α c), 1.18 (br s, 3H, CH₃-2 α), 1.11 (br s, 3H, CH₃-2 α), 0.93 (t, $J = 7.0$ Hz, 3H, CH₃-6 α d), 0.90 (t, $J = 6.5$ Hz, 3H, CH₃-4 α d); ¹³C NMR (125 MHz, CDCl₃) δ 172.4 (C=O), 58.1 (C-2), 57.61 (CH-4), 53.6 (C-6), 38.6 (CH-5), 38.1 (CH₂-6a), 36.8 (CH₂-9), 36.5 (CH-1), 35.1 (CH₂-7), 30.8 (CH₂-4 α a), 30.7 (CH₂-4 α b), 29.9 (CH₃-6), 28.4 (CH₂-6 α b), 27.7 (CH₃-2 α), 25.6 (CH₂-8), 23.2 (CH₂-4 α c), 22.7 (CH₂-6 α c), 14.4 (CH₃-4 α d), 14.2 (CH₃-6 α d); GC-MS $R_t = 22.53$ min, m/z 322 (2 M⁺), 307 (18), 265 (100), 222 (9), 206 (9), 164 (25), 126 (25), 86 (31%). HRMS (ESI): C₂₀H₃₈N₂O calcd: 323.3057 [M+H]⁺; found: 323.3041 [M+H]⁺.

***N*-((1*S*,4*S*,5*R*,6*S*)-2,2,6-Trimethyl-4-phenyl-3-azabicyclo[3.3.1]nonan-6-yl)benzamide (+)-101n**



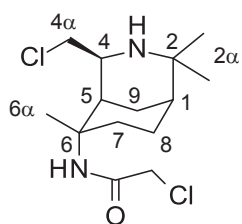
(39 mg, 0.11 mmol, 94%) pale yellow semi-solid; $[\alpha]_D^{20} +73.42$ (c 1.00, CHCl₃); $\nu_{\max}(\text{neat})$ 3337, 2969, 2933, 1709, 1639, 1525 cm⁻¹; ¹H NMR (500 MHz, CDCl₃) δ 7.71 (d, $J = 7.5$ Hz, 2H, Ar-6 γ b & Ar-6 γ f), 7.49 (d, $J = 7.5$ Hz, 2H, Ar-6 γ c & Ar-6 γ e), 7.46 (t, $J = 7.5$ Hz, 1H, Ar-6 γ d), 7.41 (t, $J = 7.5$ Hz, 2H, Ar, Ar-4 α b & Ar-4 α f), 7.32 (t, $J = 7.5$ Hz, 2H, Ar-4 α c & Ar-4 α e), 7.19 (t, $J = 7.5$ Hz, 1H, Ar-4 α d), 5.94 (s, 1H, HNCO), 4.57 (br s, 1H, CH-5), 3.29 (s, 1H, NH), 2.80-2.81 (m, 1H, CH-4), 2.08 (s, 1H, CH-1), 2.05-2.02 (m, 2H, CH₂-7), 1.68-1.61 (m, 2H, CH₂-8), 1.48-1.45 (m, 2H, CH₂-9), 1.27 (s, 6H, 2CH₃-2 α). 0.84 (s, 3H, CH₃-6 α); ¹³C NMR (125 MHz, CDCl₃) δ 167.2 (C=O), 166.4 (C-4 α a), 145.4 (C-6 γ a), 131.5 (2C, CH-6 γ b & CH-6 γ f), 131.0 (CH-4), 129.1 (2C, CH-6 γ c & CH-6 γ e), 128.7 (CH-6 γ d), 128.4 (CH-4 α b & CH-4 α f), 127.1 (CH-4 α c & CH-4 α e), 126.7 (CH-4 α d), 58.8 (C-6), 53.4 (C-2), 36.0 (CH-5), 34.8 (CH-1), 30.0 (CH₂-7), 29.7 (CH₃-6 α), 27.3 (CH₃-2 α), 27.0 (CH₃-2 α), 25.1 (CH₂-9), 24.9 (CH₂-8). GC-MS (EI): $R_t = 27.89$ min, m/z 362 (38 M⁺), 347 (34), 271 (13), 242 (18), 186 (25), 146 (33), 122 (18), 105 (100), 91 (25), 77 (47%); HRMS (ESI): C₂₄H₃₁N₂O calcd: 363.2436 [M+H]⁺; found: 363.2424 [M+H]⁺.

(4S,7S,8S)-2,2,6-Trimethyl-4-phenyl-3-azabicyclo[3.3.1]non-6-ene (-)-102n



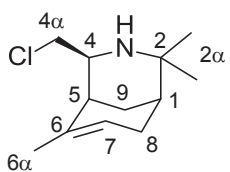
(266 mg, 1.10 mmol, 80%); R_f (5:80:15, MeOH/EtOAc/hexane); $[\alpha]_D^{20}$ -20.84 (c 1.00, CHCl_3); ν_{max} (neat) 2961, 2922, 2883, 2836, 1600, 1439, 1382 cm^{-1} ; $^1\text{H NMR}$ (500 MHz, CDCl_3) δ 7.26 (t, $J = 7.5$ Hz, 2H, Ar-4 α b & Ar-4 α f), 7.21 (d, $J = 7.5$ Hz, 2H, Ar-4 α c & Ar-4 α e), 7.16 (t, $J = 7.5$ Hz, 1H, Ar-4 α d), 5.53 (s, 1H, CH-7), 4.26 (s, 1H, CH-5), 2.35 (d, $J = 3.0$ Hz, 1H, CH-4), 2.31-2.25 (m, 2H, CH_2 -9) 1.71 (dt, $J = 3.0, 12.0$ Hz, 2H, CH_2 -8), 1.64 (s, 1H, NH), 1.51 (t, $J = 3.0$ Hz, 1H, CH-1), 1.30 (s, 3H, CH_3 -2 α), 1.22 (s, 3H, CH_3 -6 α), 0.87 (s, 3H, CH_3 -2 α) ppm; $^{13}\text{C NMR}$ (125 MHz, CDCl_3) δ 143.6 (C-6) 133.4 (C-4 α a), 128.0 (2C, CH-4 α b & CH-4 α f), 126.6 (CH-4 α d), 125.7 (2C, CH-4 α c & CH-4 α e), 124.1 (CH-7), 57.1 (CH-5), 53.8 (C-2), 42.6 (CH-4), 34.4 (CH-1), 30.1 (CH_3 -6 α), 29.4 (CH_2 -9), 27.7 (CH_2 -8), 25.6 (CH_2 -2 α), 24.2 (CH_2 -2 α) ppm. GC-MS (EI): $R_t = 17.75$ min, m/z 241 (59 M^+), 226 (37), 146 (63), 106 (100), 93 (63), 79 (22%). HRMS (ESI): $\text{C}_{17}\text{H}_{24}\text{N}$ calcd: 242.1903 $[\text{M}+\text{H}]^+$; found: 242.1901 $[\text{M}+\text{H}]^+$.

2-Chloro-N-((1S,4S,5R,6S)-4-(chloromethyl)-2,2,6-trimethyl-3-azabicyclo[3.3.1]nonan-6-yl)acetamide (+)-101m



(139 mg, 0.45 mmol, 88%) pale yellow solid; m.p. 88 °C; $[\alpha]_D^{25} +76.42$ (c 0.5, CHCl_3); ν_{max} (neat) 3282, 2987, 2963, 2919, 2899, 2876, 2708, 1673, 1643, 1551, 1458, 1438, 1318, 1251, 1110, 720 cm^{-1} . $^1\text{H NMR}$ (500 MHz, CDCl_3) δ 6.52 (s, 1H, NHCO), 3.97 (s, 2H, COCH_2Cl), 3.78 (dd, $J = 2.5, 10.5$ Hz, 1H, CH_2Cl -4 α a), 3.66 (t, $J = 10.0$, 1H, CH_2Cl -4 α b), 3.46 (dt, $J = 2.5, 10.5$ Hz, 1H, CH-4), 2.65 (td, $J = 5.0, 15.5$ Hz, 1H, CH_2 -7a), 2.54 (br s, 1H, CH-5), 1.98-1.94 (m, 1H, CH_2 -8a), 1.83 (dd, $J = 3.0, 3.0$ Hz, 2H, CH_2 -9), 1.56-1.50 (m, 2H, CH_2 -7b & CH_2 -8b), 1.45 (s, 3H, CH_3 -6 α), 1.38 (t, $J = 3.0$ Hz, 1H, CH-1), 1.21 (s, 3H, CH_3 -2 α), 1.16 (s, 3H, CH_3 -2 α); $^{13}\text{C NMR}$ (125 MHz, CDCl_3) δ 164.4 (C=O), 59.4 (CH-4), 57.5 (C-6), 53.4 (C-2), 50.5 (CH_2Cl -4 α), 43.1 (COCH_2Cl), 38.9 (CH-5), 35.9 (CH-1), 34.2 (CH_2 -7), 30.0 (CH_2 -9), 29.4 (CH_3 -2 α), 27.4 (CH_3 -6 α), 26.9 (CH_3 -2 α), 24.8 (CH_2 -8); GC-MS (EI) $R_t = 21.44$ min, m/z 306 (9 M^+), 291 (100), 271 (81), 257 (29), 121 (32), 58 (41%); HRMS (ESI): $\text{C}_{14}\text{H}_{24}\text{Cl}_2\text{N}_2\text{O}$ calcd: 307.1266 $[\text{M}+\text{H}]^+$; found: 307.1266 $[\text{M}+\text{H}]^+$.

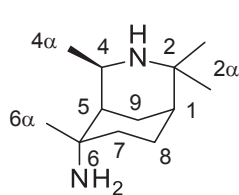
4-(Chloromethyl)-2,2,6-trimethyl-3-azabicyclo[3.3.1]non-6-ene (-)-102m



(45 mg, 0.21 mmol, 85%) yellow waxy liquid; R_f (diethyl ether) 0.98; $[\alpha]_D^{20} -8.63$ (c 0.24, CH_2Cl_2); ν_{max} (neat) 3412, 3309, 2929, 2956, 1665, 1527, 1458, 1384, 1262, 1115, 1091, 1080, 804 cm^{-1} ; $^1\text{H NMR}$ (500 MHz, CDCl_3) δ 5.61 (br s, 1H, CH-7), 3.37 (dd, $J = 7.0, 10.5$ Hz, 1H, CH_2Cl -4 α a), 3.28 (dd, $J = 2.5, 10.5$ Hz, 1H, CH_2Cl -4 α b), 3.23 (td, $J = 2.5, 2.5$ Hz, 1H, CH-4), 2.29 (d, $J = 2.0$ Hz, 1H,

CH-5), 2.28-2.22 (m, 1H, CH₂-9a), 2.10-2.03 (m, 2H, CH₂-9b & CH₂-8a), 1.71 (br s, 3H, CH₃-6α), 1.64 (dt, *J* = 2.5, 12.5 Hz, 1H, CH₂-8b), 1.48-1.46 (m, 1H, CH-1), 1.21 (br s, 3H, CH₃-2α), 1.11 (br s, 3H, CH₃-2α); ¹³C NMR (125 MHz, CDCl₃) δ 164.8 (C-6), 132.5 (C-2), 125.9 (CH-7), 57.1 (CH-4), 48.0 (CH₂Cl-4α), 36.5 (CH-5), 35.2 (CH-1), 30.2 (CH₃-2α), 29.0 (CH₂-8), 28.1 (CH₂-9), 26.1 (CH₃-2α), 25.2 (CH₃-6α); GC-MS *R*_t = 6.10 min, *m/z* 213 (28 M⁺), 198 (66), 178 (43), 164 (25), 118 (50), 93 (100), 84 (31), 77 (18%). HRMS (ESI): C₁₂H₂₀ClN calcd: 214.1357 [M+H]⁺; found: 214.1354 [M+H]⁺.

(4*R*)-2,2,4,6-Tetramethyl-3-azabicyclo[3.3.1]nonan-6-amine (+)-103l



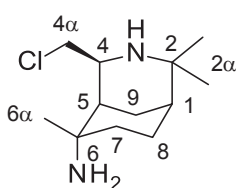
(71.1 mg, 0.363 mmol, 78%) light brown wax; *R*_f (EtOH) 0.10; [α]_D²² +15.24 (c 1.00, CHCl₃); IR *v*_{max} (neat) 3304, 2954, 2929, 2887, 1650, 1546, 1460, 1380, 1115, 1099, 1045 cm⁻¹; ¹H NMR (500 MHz, CDCl₃) δ 5.30 (br s, 1H, NH-3) 3.34 (qd, *J* = 7.5, 1.5 Hz, 1H, CH-4), 2.30 (td, *J* = 13.5, 5.0 Hz, 1H, CH₂-7), 2.02 (dt, *J* = 13.5, 3.0 Hz, 1H, CH₂-9a), 1.90-1.84 (m, 2H, CH₂-9b, CH₂-8a), 1.64-1.65 (m, 1H, CH₂-8b), 1.52 (br s, 1H, CH-5), 1.33-1.30 (m, 9H, CH₃-2α, CH₃-4α, CH₃-6α), 1.24-1.26 (m, 1H, CH-1), 1.12 (s, 3H, CH₃-2α); ¹³C NMR (125 MHz, CDCl₃) δ 53.7 (C-2), 52.7 (C-6), 52.3 (CH-4), 46.4 (CH-1), 36.8 (CH₂-7), 36.2 (CH-5), 33.0 (CH₃-2α), 30.5 (CH₂-9), 29.8 (CH₃-2α), 27.9 (CH₃-6α), 25.3 (CH₂-8), 23.8 (CH₃-4α); GC-MS *R*_t = 5.91 min, *m/z* 196 (11 M⁺), 181 (100), 164 (12), 124 (23), 84 (43%). HRMS: [M+H]⁺, found 197.2016, C₁₂H₂₄N₂ required 197.2012.

9.3 Miscellaneous Chemical Reaction Methods

9.3.1 Mild Amide De-protection of (+)-101m

A solution of 2-chloro-*N*-((1*S*,4*S*,5*R*,6*S*)-4-(chloromethyl)-2,2,6-trimethyl-3-azabicyclo[3.3.1]nonan-6-yl)acetamide (+)-101m (194.4 mg, 0.64 mmol) in dry methanol (10 mL), was added to a solution of thiourea (93.3 mg, 1.23 mmol), in dry methanol (5 mL) and glacial acetic acid (1 mL). The reaction mixture was refluxed overnight. The resulting suspension was cooled to room temperature before water (10 mL) was added. The solution was then basified with solution of NaOH (2 M) until pH > 10. The mixture was extracted with chloroform (2 X 15 mL). The combined organic extracts were dried over Na₂CO₃ and the solvent was removed under reduced pressure to give (+)-103m (123.6 mg, 0.54 mmol). NMR and GC-MS analysis indicated that the product was pure and was used for the bioassay without further purification.

(1S,4S,5R,6S)-4-(Chloromethyl)-2,2,6-trimethyl-3-azabicyclo[3.3.1]nonan-6-amine (+)-103m

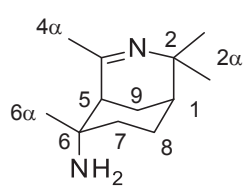


(124 mg, 0.537 mmol, 85%) yellow wax; $[\alpha]_D^{23} +18.83$ (c 1.63, MeOH); $\nu_{\max}(\text{neat})$ 3321, 2923, 2577, 2113, 1523, 1456, 1437, 1379, 1256, 1116, 720 cm^{-1} ; $^1\text{H NMR}$ (500 MHz, CDCl_3) δ 3.67-3.63 (m, 2H, CH_2 -4 α), 3.43 (dt, $J = 2.5, 9.5$ Hz, 1H, CH-4), 2.49 (td, $J = 5.0, 14.0$ Hz, 1H, CH_2 -7a), 2.12 (dt, $J = 3.0, 14.0$ Hz, 1H, CH_2 -9a), 1.91-1.86 (m, 2H, CH_2 -8a & CH_2 -9b), 1.74 (dt, $J = 5.0, 14.5$ Hz, 1H, CH_2 -8b), 1.69 (s, 1H, CH-5), 1.39-1.37 (m, 1H, CH-1), 1.37-1.34 (m, 1H, CH_2 -7b), 1.26 (s, 3H, CH_3 -6 α), 1.20 (s, 3H, CH_3 -2 α), 1.14 (s, 3H, CH_3 -2 α); $^{13}\text{C NMR}$ (125 MHz, CDCl_3) δ 54.8 (C-6), 60.3 (CH-4), 53.8 (C-2), 51.0 (CH_3 -6 α), 50.7 (CH_2 -4 α), 44.2 (CH-5), 36.4 (CH-1), 35.1 (CH_2 -7), 29.9 (CH_2 -9), 29.5 (CH_3 -2 α), 27.3 (CH_3 -2 α), 24.8 (CH_2 -8); GC-MS (EI) $R_t = 16.64$ min, m/z 230 (10 M^+), 215 (100), 195 (16), 118 (35), 70 (48%); HRMS (ESI): $\text{C}_{12}\text{H}_{23}\text{ClN}_2$ calcd: 231.1623 $[\text{M}+\text{H}]^+$; found: 231.1618 $[\text{M}+\text{H}]^+$.

9.3.2 C-6 Amide Hydrolysis with HCl

N-(2,2,4,6-Tetramethyl-3-azabicyclo[3.3.1]non-3-en-6-yl)acetamide (**+**)-59I (0.308 g, 1.305 mmol) was dissolved in HCl solution (20 mL, 6 M) and refluxed overnight. The HCl solution was removed under reduced pressure to give the HCl salt of the product as a pale yellow solid. The free base was recovered by dissolving the salt in water before basifying (pH > 12) with a solution of NaOH (4 M), and extracted with chloroform (2 X 15 mL), before drying over Na_2CO_3 . The solvent was removed under reduced pressure to give the free base as a viscous yellow oil.

2,2,4,6-Tetramethyl-3-azabicyclo[3.3.1]non-3-en-6-amine (+)-105I



(238 mg, 1.23 mmol, 94%) viscous yellow oil; $[\alpha]_D^{22} +122.98$ (c 1.58, CHCl_3); $\nu_{\max}(\text{neat})$ 3362, 3278, 2965, 2931, 1645, 1457, 1373, 1293, 1250, 1162 cm^{-1} ; $^1\text{H NMR}$ (500 MHz, CDCl_3) δ 5.34 (NH_2), 2.02 (s, 3H, CH_3 -4 α), 1.91-1.93 (m, 2H, CH-5 & CH_2 -9a), 1.71-1.78 (m, 2H, CH_2 -9b & CH_2 -8a), 1.67 (dt, $J = 14.0, 4.0$ Hz, 1H, CH_2 -8b), 1.61 (br. s, 1H, CH-1), 1.41 (td, $J = 14.0, 4.0$ Hz, 1H, CH_2 -7a), 1.25 (s, 3H, CH_3 -6 α), 1.18-1.21 (m, 1H, CH_2 -7b), 1.16 (s, 3H, CH_3 -2 α), 1.12 (s, 3H, CH_3 -2 α); $^{13}\text{C NMR}$ (125 MHz, CDCl_3) δ 167.6 (C-4), 58.2 (C-2), 51.6 (C-6), 47.5 (CH-5), 34.8 (CH_2 -7), 32.7 (CH-1), 32.6 (CH_3 -2 α), 32.2 (CH_3 -2 α), 30.1 (CH_3 -4 α), 26.7 (CH_3 -6 α), 25.1 (CH_2 -8), 24.3 (CH_2 -9); GC-MS $R_t = 5.849$ min, m/z 194 (6 M^+), 179 (100), 162 (7), 137 (44), 122 (90), 110 (21), 97 (29), 82 (43%). MS (ESI): $\text{C}_{12}\text{H}_{22}\text{N}_2$ calcd: 195.1856 $[\text{M}+\text{H}]^+$; found: 195.1859 $[\text{M}+\text{H}]^+$.

(2,2,4,6-Tetramethyl-3-azoniabicyclo[3.3.1]non-3-en-6-yl)ammonium; dichloride salt

(326 mg, 1.23 mmol, 94%) m.p. 175 °C, ^1H NMR (500 MHz, D_2O) δ 3.06 (br. s, 1H, CH-5), 2.48 (s, 3H, CH_3 -4 α), 2.08 (m, 1H, CH_2 9a), 2.03 (br. s, 1H, CH-1), 1.96 (m, 2H, CH_2 -9b & CH_2 -8a), 1.76 (m, 1H, CH_2 -7a), 1.69 (dt, $J = 15.5, 4.5$ Hz, 1H, CH_2 -8b), 1.51 (td, $J = 14.5, 4.5$ Hz, 1H, CH_2 -7b), 1.41 (s, 6H, CH_3 -6 α & CH_3 -2 α), 1.35 (s, 3H, CH_3 -2 α); ^{13}C NMR (125 MHz, D_2O) δ 190.0 (C-4), 654.0 (C-2), 58.6 (C-6), 45.8 (CH-5), 35.0 (CH-1), 31.8 (CH_2 -7), 31.0 (CH_3 -2 α), 29.3 (CH_3 -4 α), 28.6 (CH_3 -2 α), 25.0 (CH_3 -6 α), 24.6 (CH_2 -8), 23.4 (CH_2 -9).

9.3.3 $\text{S}_{\text{N}}2$ reaction of C-6 Amines with Benzyl Bromide

(4R)-2,2,4,6-Tetramethyl-3-azabicyclo[3.3.1]nonan-6-amine **(+)-103I** (47.5 mg, 0.245 mmol) was dissolved in dry *N,N*-dimethyl formamide (5 mL), to which powdered K_2CO_3 was added. While stirring, benzyl bromide (30.9 μL , 0.26 mmol) was added dropwise. The reaction was left to stir overnight before it was quenched by the addition of water (10 mL) and extracted with chloroform (2 X 20 mL). The combined extracts were dried over Na_2CO_3 and the solvent removed under reduced pressure to give 112.5 mg of crude product of **(+)-114**.

N-Benzyl-2,2,4,6-tetramethyl-3-azabicyclo[3.3.1]nonan-6-amine **(+)-114**

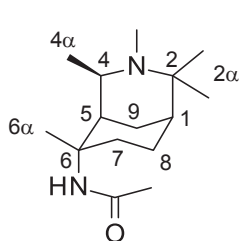
(58.7 mg, 0.205 mmol, 87%) light brown wax; R_f (EtOAc) 0.11; $[\alpha]_{\text{D}}^{22} +15.90$ (c. 1.00, CHCl_3); IR ν_{max} (neat) 3375, 3026, 2933, 1620, 1544, 1460, 1382, 1033, 1093, 910 cm^{-1} ; ^1H NMR (500 MHz, CDCl_3) δ 7.36-7.37 (m, 2H, Ar-CH-6 γ b), 7.32 (t, $J = 7.5$ Hz, 2H, Ar-CH-6 γ c), 7.25 (t, $J = 7.5$ Hz, 1H, Ar-CH-6 γ d), 5.49 (s, 1H, NH-6 α), 3.74 (qd, $J = 7.0, 2.5$ Hz, 1H, CH-4), 3.70 (d, $J = 12.0$ Hz, 1H, CH_2 -6 β), 3.63 (d, $J = 12.0$ Hz, 1H, CH_2 -6 β), 2.84 (s, 1H, NH-3), 2.51 (dt, $J = 10.5, 2.5$ Hz, 1H, CH_2 -9a), 1.96 (s, 3H, CH_3 -6 α), 1.87-1.80 (m, 2H, CH_2 -8), 1.77-1.73 (m, 2H, CH_2 -9b & CH-5), 1.66 (s, 3H, CH_3 -4 α), 1.58 (s, 3H, CH_3 -2 α), 1.54-1.53 (m, 5H, CH_2 -7 & CH_3 -2 α), 1.45 (s, 1H, CH-1); ^{13}C NMR (125 MHz, CDCl_3) δ 169.9 (Ar-C-6 γ a), 128.73 (2 Ar-CH-6 γ b), 128.70 (2 Ar-CH-6 γ c), 127.3 (Ar-CH-6 γ d), 58.9 (C-2), 57.4 (C-6), 53.4 (CH-4), 46.0 (CH_2 -6 β), 40.4 (CH-5), 36.4 (CH-1), 33.2 (CH_2 -7), 28.3 (CH_3 -4 α), 27.6 (CH_2 -9), 26.7 (CH_3 -2 α), 25.7 (CH_3 -2 α), 25.0 (CH_3 -6 α), 23.3 (CH_2 -8); GC-MS $R_t = 7.884$ min, m/z 286 (4 M^+), 271 (4), 228 (5), 214 (11), 195 (46), 160 (39), 147 (29), 126 (36), 106 (46), 91 (100%). HRMS: $[\text{M}+\text{H}]^+$, found 287.2491, $\text{C}_{19}\text{H}_{30}\text{N}_2$ required 287.2482.

9.3.4 Reductive Alkylation of **(+)-101I**

Compound **(+)-101I** (100 mg, 0.42 mmol) was dissolved in acetonitrile (5 mL), to which sodium cyanoborohydride (502.0 mg, 7.99 mmol), 28% formaldehyde solution (37 mL) and a few drops of glacial acetic acid were added. The solution was stirred for 3 h at room

temperature. The solvent was removed under reduced pressure to give both yellow and colourless crystals. The crude solid was triturated with hexane with the hexane decanted and the remaining solid dried under reduced pressure to give the yellow crystals of **(+)-104I** (48.0 mg, 0.19 mmol, 45%).

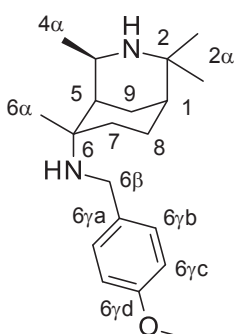
***N*-((1*S*,4*R*,5*R*,6*S*)-2,2,3,4,6-Pentamethyl-3-azabicyclo[3.3.1]nonan-6-yl)acetamide (+)-104I**



(48 mg, 0.19 mmol, 45%) pale yellow solid; m.p. 165 °C; $[\alpha]_D^{25} +13.89$ (c 0.37, CHCl₃); ν_{\max} (neat) 3313, 2981, 2960, 2943, 2881, 2846, 2802, 2789, 1638, 1545, 1465, 1439, 1380, 1370, 1310, 1299, 1246, 1223, 1030, 958, 718 cm⁻¹; ¹H NMR (500 MHz, CDCl₃) δ 5.28 (s, 1H, NH), 2.89 (qd, *J* = 2.0, 7.0 Hz, 1H, CH-4), 2.65 (td, *J* = 4.5, 14.0 Hz 1H, CH₂-7a), 2.41 (br s, 1H, CH-5), 2.08 (s, 3H, NCH₃), 1.96-1.94 (m, 1H, CH₂-8a), 1.94 (s, 3H, COCH₃), 1.81-1.83 (m, 1H, CH₂-9a), 1.75 (dt, *J* = 3.0, 13.5 Hz, 1H, CH₂-9b), 1.52 (s, 3H, CH₃-6 α), 1.46 (dt, *J* = 4.5, 14.0 Hz, 1H, CH₂-8b), 1.42-1.39 (m, 1H, CH₂-7b), 1.29 (br s, 1H, CH-1), 1.21 (d, *J* = 7.0 Hz, 3H, CH₃-4 α), 1.17 (s, 3H, CH₃-2 α), 0.98 (s, 3H, CH₃-2 α); ¹³C NMR (125 MHz, CDCl₃) δ 169.0 (C=O), 58.2 (CH-4), 57.5 (C-6), 57.4 (C-2), 41.8 (CH-5), 39.9 (CH-1), 34.4 (CH₂-9), 33.7 (CH₃-3 α), 30.0 (CH₂-7), 28.5 (CH₃-2 α), 28.1 (CH₃-6 α), 25.0 (CH₂-8), 24.5 (COCH₃), 22.5 (CH₃-4 α), 16.9 (CH₃-2 α); GC-MS (EI) *R*_t = 8.28 min, *m/z* 252 (4 M⁺), 237 (100), 178 (22), 58 (37%); HRMS (ESI): C₁₅H₂₈N₂O calcd: 253.2275 [M+H]⁺; found: 253.2276 [M+H]⁺.

9.3.5 Reductive *N*-alkylation of *N*-6 Amine (+)-105I with Anisaldehyde

2,2,4,6-Tetramethyl-3-azabicyclo[3.3.1]non-3-en-6-amine **(+)-105I** (184.6 mg, 0.952 mmol) was dissolved in dry methanol (15 mL). To this, *p*-anisaldehyde (115.7 μ L, 0.9516 mmol) was added before the addition of NaCNBH₃ (436.3 mg, 6.9430 mmol) and a few drops of glacial acetic acid. The reaction was stirred overnight at room temperature and then quenched with a saturated solution of NaHCO₃ (20 mL), before the products were extracted with chloroform (2 X 20 mL). The organic extracts were dried over Na₂CO₃ and the solvent was removed under reduced pressure to give a crude mass of 0.3295 g.



(4*R*)-*N*-[(4-Methoxyphenyl)methyl]-2,2,4,6-tetramethyl-3-azabicyclo[3.3.1]nonan-6-amine (+)-112

(231 mg, 0.729 mmol, 77%) yellow wax; *R*_f(EtOH) 0.22; $[\alpha]_D^{22} +7.64$ (c 1.00, CHCl₃); IR ν_{\max} (neat) 3440, 3345, 2959, 2933, 2840, 2402, 2251, 1665, 1613, 1512, 1460, 1248, 1106, 1033 912, 830 cm⁻¹; ¹H NMR (500 MHz, CDCl₃) δ 7.28 (d, *J* = 8.5 Hz, 2H, Ar-CH-6 γ b), 6.86 (d, *J* = 8.5 Hz, 2H, Ar-CH-

6 γ c), 6.16 (s, 1H, NH-6 α), 3.80 (s, 3H, OCH₃), 3.58 (dd, J = 8.5, 12.0 Hz, 2H, CH₂-6 β), 3.51 (qd, J = 7.0, 2.5 Hz, 1H, CH-4), 3.31-2.28 (m, 1H, CH₂-9a), 2.08-1.85 (m, 2H, CH₂-7), 1.80-1.75 (m, 3H, CH₂-9b & CH₂-8), 1.71-1.72 (m, 1H, CH-5), 1.56 (d, J = 7.0 Hz, 3H, CH₃-4 α), 1.50 (s, 1H, CH-1), 1.36 (s, 3H, CH₃-6 α), 1.35 (s, 3H, CH₃-2 α), 1.31 (s, 3H, CH₃-2 α); ¹³C NMR (125 MHz, CDCl₃) δ 165.6 (Ar-C-6 γ d), 159.0 (Ar-C-6 γ a), 129.8 (Ar-C-6 γ b), 114.3 (Ar-C-6 γ c), 57.8 (C-2), 25.8 (C-6), 55.7 (OCH₃), 52.7 (CH-4), 45.4 (CH₂-6 β), 41.2 (CH-5), 36.0 (CH-1), 30.0 (CH₂-7), 28.9 (CH₂-9), 28.4 (CH₃-2 α), 27.0 (CH₃-6 α), 26.8 (CH₃-2 α), 24.2 (CH₂-8), 21.7 (CH₃-4 α); GC-MS R_t = 8.745 min, m/z 316 (4 M⁺), 230 (7), 195 (21), 164 (21), 136 (32), 121 (100), 84 (39%). HRMS: [M+H]⁺, found 317.2587, C₂₀H₃₂N₂O required 317.2587.

9.3.6 Conversion of (+)-59I Imine to Nitrone

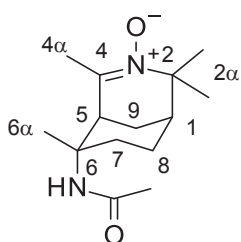
9.3.6.1 N-Oxidation with *m*-CPBA

N-(2,2,4,6-Tetramethyl-3-azabicyclo[3.3.1]non-3-en-6-yl)acetamide **(+)-59I** (197.3 mg, 0.836 mmol) was dissolved in methanol (10 mL), before the portion-wise addition of *m*-CPBA (145.1 mg, 0.841 mmol). The reaction was monitored by TLC analysis. After the reaction appeared complete, the solvent was removed by evaporation and the remaining residue was re-dissolved in dichloromethane before being washed with a saturated solution of NaHCO₃, followed by water. Methanesulfonic acid (100 μ L) was then added to the organic layer, which was stirred for 30 min at room temperature before the reaction mixture was quenched with a saturated solution of NaHCO₃, then washed with a saturated solution of NaCl. The organic extract was then dried over Na₂CO₃ before the solvent was removed by evaporation to give **(+)-125**.

9.3.6.2 N-Oxidation with UHP

N-(2,2,4,6-Tetramethyl-3-azabicyclo[3.3.1]non-3-en-6-yl)acetamide **(+)-59I** (117.2 mg, 0.497 mmol) was dissolved in methanol (10 mL), to which urea hydrogen peroxide (202.4 mg, 2.152 mmol) was added, prior to the addition of methylrhenum trioxide (8.2 mg, 0.033 mmol). The reaction mixture was stirred for an hour at room temperature before analysis of a reaction aliquot by GC-MS confirmed the reaction had gone to completion. The solvent was removed under reduced pressure before the crude residue was re-dissolved in cold dichloromethane to precipitate the remaining urea, which was removed by filtration. The organic extract was then dried over Na₂CO₃ before the solvent was removed by evaporation to give **(+)-125**.

***N*-(2,2,4,6-Tetramethyl-3-oxido-3-azoniabicyclo[3.3.1]non-3-en-6-yl)acetamide (+)-125**

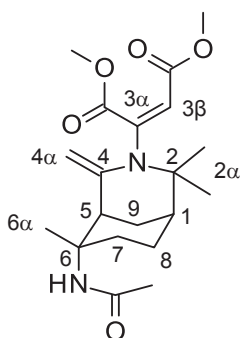


(107 mg, 0.422 mmol, 86%) bright green wax; $[\alpha]_D^{22} +5.08$ (c 1.00, CHCl_3); IR ν_{max} (neat) 3371, 3308, 3069, 2993, 2946, 2871, 1701, 1654, 1531, 1371, 1347, 1263 cm^{-1} ; ^1H NMR (500 MHz, CDCl_3) δ 5.53 (br s, 1H, NH), 3.74 (dd, $J = 3.5, 12.5$ Hz, 1H, CH-5), 2.51 (td, $J = 4.0, 13.0$ Hz, 1H, CH_2 -9a), 2.22-2.16 (m, 1H, CH-1), 2.15 (s, 3H, COCH_3), 1.97 (s, 3H, CH_3 -6 α), 1.82 (dt, $J = 13.5, 3.5$ Hz, 1H, CH_2 -9b), 1.61-1.55 (m, 6H, CH_3 -2 α , CH_2 -8 & CH_2 -7a), 1.50-1.46 (m, 1H, CH_2 -7b), 1.25 (s, 3H, CH_3 -2 α); ^{13}C NMR (125 MHz, CDCl_3) δ 211.3 (C-4), 170.3 (C=O), 91.6 (C-6), 55.8 (C-2), 52.9 (CH-5), 45.3 (CH-1), 36.3 (CH_2 -9), 31.3 (COCH_3), 26.4 (CH_2 -7), 25.0 (CH_3 -4 α), 23.8 (CH_2 -8), 23.8 (CH_3 -6 α), 23.4 (CH_3 -2 α), 20.7 (CH_3 -2 α); GC-MS $R_t = 7.934$ min, m/z 252 (21 M^+), 235 (20), 193 (50), 176 (20), 136 (100), 70 (24%). HRMS: $[\text{M}+\text{H}]^+$, found 253.1912, $\text{C}_{14}\text{H}_{24}\text{N}_2\text{O}_2$ required 253.1911.

9.3.7 DMAD addition of (+)-59I

N-(2,2,4,6-Tetramethyl-3-azabicyclo[3.3.1]non-3-en-6-yl)acetamide (+)-59I (502.3 mg, 2.13 mmol) was dissolved in chloroform (15 mL) and then heated to reflux. A solution of DMAD (309 mg, 2.18 mmol) dissolved in chloroform (5 mL) was added dropwise to the refluxed solution *via* the condenser. Once all the DMAD solution was added, the reaction was left to reflux for 4 h. The reaction was then cooled to room temperature before the solvent was removed under reduced pressure to obtain a dark yellow foam like the wax crude product (952 mg). The crude product was purified on an alumina column using a 40% *n*-hexane and 60% ethyl acetate as the mobile phase to give pure (-)-121 as a red-orange solid (458.6 mg, 1.21 mmol, 57%).

Dimethyl 2-((1*S*,5*S*,6*S*)-6-acetamido-2,2,6-trimethyl-4-methylene-3-azabicyclo[3.3.1]nonan-3-yl)maleate (-)-121



(459 mg, 1.21 mmol, 57%) red orange solid; m.p. 50 °C; R_f (4:6 hexane/ethyl acetate) 0.40; $[\alpha]_D^{25} -464.16$ (c 1.02, CHCl_3); ν_{max} (neat) 3309, 2950, 1715, 1654, 1585, 1542, 1433, 1370, 1340, 1277, 1234, 1205, 1144, 989, 943, 840, 727 cm^{-1} ; ^1H NMR (500 MHz, CDCl_3) δ 5.58 (s, 1H, H-3 β) 5.26 (s, 1H, NH), 4.61 (s, 1H, CH_2 -4 α a), 4.44 (s, 1H, CH_2 -4 α b), 3.73 (s, 3H, OCH_3), 3.70 (s, 3H, OCH_3), 3.34 (br s, 1H, CH-5), 2.63 (td, $J = 14.5, 5.0$ Hz, CH_2 -7a), 2.05 (s, 3H, NCOCH_3), 2.04-2.00 (m, 2H, CH_2 -8a & CH_2 -9a), 1.96 (s, 3H, CH_3 -2 α), 1.90 (dt, $J = 3.0, 10.5$ Hz, CH_2 -9b), 1.62-1.55 (m, 1H, CH_2 -8b), 1.52-1.51 (m, 1H, CH-1), 1.45 (s, 3H, CH_3 -6 α), 1.40 (s, 3H, CH_3 -2 α), 1.33 (dd, 1H, $J = 14.5, 5.0$ Hz, CH_2 -

7b); ^{13}C NMR (125 MHz, CDCl_3) δ 169.6 (C=O), 167.1 (C=O), 166.4 (C=O), 147.1 (C-4), 146.8 ($\text{C}=\text{CH}-3\alpha$), 106.7 ($\text{C}=\text{CH}_2-4\alpha$), 60.5 (C-6), 56.1 (C-2), 52.4 (OCH_3), 51.4 (OCH_3), 41.4 (CH-1), 41.3 (CH-5), 31.0 (CH_2-7), 26.0 (COCH_3), 25.9 ($\text{CH}_3-6\alpha$), 25.7 (CH_2-9), 24.7 ($\text{CH}_3-2\alpha$), 24.3 ($\text{CH}_3-2\alpha$), 23.8 (CH_2-8); GC-MS (EI) R_t = 18.27 min, m/z 378 (18 M^+), 363 (18), 319 (100), 287 (79), 260 (67) 208 (18), 70 (31%); HRMS (ESI): $\text{C}_{20}\text{H}_{30}\text{N}_2\text{O}_5$ calcd: 379.2227 $[\text{M}+\text{H}]^+$; found: 379.2229 $[\text{M}+\text{H}]^+$.

9.4 Attempted Reactions

The following is a list of the procedures used for the reactions attempted although they did not result in obtaining the desired product or useful yields, with the starting material generally being recovered. If more time permitted, several of these reactions could be attempted with alternative conditions and this may be carried out in future work, however, within the scope of this project, these reactions were deemed unviable synthetic procedures.

9.4.1 Bridged Ritter Reaction with Forced Oxidation

Sulfuric acid (18 M; 2 mL) is added to 4-bromobenzylcyanide (10.4681 g, 53.4 mmol) in a round bottom flask fitted with a condenser and drying tube at 0 °C. Whilst stirring, a solution of (-)- β -pinene (1.2 mL, 7.62 mmol) in benzene (5 mL) was added drop-wise. The reaction was left to stir for 30 min at 0 °C before continuing for 4 h at room temperature (ca. 21 °C), during which O_2 was bubbled through the reaction solution. The reaction mixture was washed with hexane, which was then discarded, before quenching with water (30 mL). The mixture was basified with a solution of NaOH (4M) until pH > 10. The product was extracted with chloroform (2 X 20 mL) and the combined extracts were dried over Na_2CO_3 before the solvent was removed under reduced pressure.

9.4.2 Bridged Ritter Reaction with Alternative Catalysts

9.4.2.1 I_2 Catalysed Bridged Ritter Reaction

Iodine (50.0 mg, 0.20 mmol), acetonitrile (0.2053 g, 0.25 mL, 5 mmol), (-)- β -pinene (0.1362 g, 0.1562 mL, 1 mmol) and distilled water (18 mg, 1.0 mmol) were stirred in a sealed reaction tube at 90 °C. After 18 h the reaction mixture was quenched with 20% aqueous sodium thiosulfate solution (5 mL) and extracted with chloroform (2 X 20mL). The combined extracts were dried over Na_2SO_4 before the solvent was removed under reduced pressure to give a dark yellow oil (0.1752 g) with the odour of pinene. The GC-MS analysis suggests that in addition to the pinene recovered, several rearrangements of the pinene structure were also present.

9.4.2.2 Zinc Triflate Catalysed Bridged Ritter Reaction

(-)- β -Pinene (1.2 mL, 7.62 mmol) was added with stirring to a solution of Zn(OTf)₂ (0.554 g, 1.524 mmol, 20% mol equiv.) and acetonitrile (1.99 mL, 1.564 g, 38.1 mmol) in water (1 mL). After 24 h at 100 °C, the mixture was cooled and aqueous KOH (20% w/v; 25 mL) was added to neutralise the acid and precipitate the catalyst. The product was extracted with dichloromethane (2 X 25 mL) and the combined extracts were dried over Na₂CO₃ before the solvent was removed under reduced pressure to give 1.0439 g of crude product containing mostly starting material and other impurities as determined by GC-MS and ¹H NMR analysis.

9.4.2.3 Copper Triflate Catalysed Bridged Ritter Reaction

(-)- β -Pinene (1.2 mL, 7.62 mmol) was added with stirring to a solution of Cu(OTf)₂ (0.5540 g, 1.524 mmol, 20% mol equiv.) and acetonitrile (1.99 mL, 1.564 g, 38.1 mmol) in water (1 mL). After 24 h at 100 °C, the mixture was cooled and aqueous NaOH (4 M; 25 mL) was added to neutralise the acid and precipitate the catalyst. The product was extracted with chloroform (2 X 25 mL) and the combined extracts were dried over Na₂CO₃ before the solvent was removed under reduced pressure to give 1.2951 g of crude product containing trace amounts of the expected products among mostly other impurities as determined by GC-MS and ¹H NMR analysis.

9.4.3 Controlled Mixed Ritter Reactions

9.4.3.1 Controlled Mixed Ritter Reaction with HCl

N-(2,2,4,6-Tetramethyl-3-azabicyclo[3.3.1]nonan-6-yl)acetamide **(+)-101I** (277.5 mg, 1.176 mmol) and propionitrile (10 mL) were added to a round bottom flask. Concentrated HCl (10 M; 10 mL) was added slowly while stirring before the mixture was heated at reflux overnight. After, the reaction was allowed to cool before water (20 mL) was added *via* the condenser. The crude mixture was basified with NaOH solution (4 M) until pH > 10, and extracted with chloroform (2 X 15 mL). The combined extracts were dried over Na₂SO₄ before the solvent was removed under reduced pressure to recover the starting material **(+)-101I** in addition to propanamide from the hydrolysis of the propionitrile.

9.4.3.2 Controlled Mixed Ritter Reaction with H₂SO₄

To sulfuric acid (18 M; 4.2 mL) in a round-bottom flask, acetonitrile (10 mL) was added at 0 °C. Whilst stirring, a solution of 2,2,6-trimethyl-4-phenyl-3-azabicyclo[3.3.1]nona-3,6-diene **(+)-60n** (105.4 mg, 0.441 mmol) in benzene (5 mL) was added drop-wise. The reaction was left to stir for 30 min at 0 °C before continuing for 24 h at room temperature (ca. 21°C). Afterwards, water (30 mL) was added to the reaction flask. The reaction mixture was basified

with a solution of NaOH (2 M) until pH > 10. The resulting mixture was then extracted with ethyl acetate (2 X 20 mL) and the combined extracts were dried over Na₂CO₃. The solvent was removed under reduced pressure to give the recovered starting material **(+)-60n**.

9.4.4 Reaction of **(+)-101l** with Benzenesulfonyl Chloride

N-((1*S*,4*R*,5*R*,6*S*)-2,2,4,6-Tetramethyl-3-azabicyclo[3.3.1]nonan-6-yl)acetamide **(+)-101l** (110.9 mg, 0.466 mmol) was dissolved in ethanol (5 mL). Benzenesulfonyl chloride (160 µL, 1.254 mmol) was added dropwise and the reaction stirred overnight at room temperature. The reaction solution was then acidified with HCl solution (10 M; 10 mL), before being extracted with chloroform (2 X 10 mL) and the combined extracts were dried over Na₂CO₃ before the solvent was removed under reduced pressure to give the recovered starting material **(+)-101l**. The reaction was attempted a second time, with **(+)-101l** dissolved in *N,N*-dimethyl formamide, to which a few drops of triethylamine was added before the addition of the benzenesulfonyl chloride. Again, only starting material was recovered.

9.4.5 Petasis-Borono Mannich Multicomponent Reaction

9.4.5.1 General Procedure for Petasis Reaction with Glyoxylic Acid

4-(Chloromethyl)-2,2,6-trimethyl-3-azabicyclo[3.3.1]nonan-6-amine **(+)-103m** (100 mg, 0.435 mmol), glyoxylic acid monohydrate (40.0 mg, 0.435 mmol) and boronic acid (1:1 mol equiv. of amine), were dissolved in toluene (10 mL) and stirred for 48 h at room temperature. The solvent was removed under reduced pressure to give the crude product. The same procedure was adapted for the reaction of imine-amine **(+)-105l**.

9.4.5.2 General Procedure for Copper Catalysed Petasis Reaction with Formaldehyde

Dry *N,N*-dimethyl formamide was added to copper(II) acetate (7.90 mg, 0.0435 mmol) and 2,2'-bipyridyl (6.79 mg, 0.044 mmol) under nitrogen and the solution stirred at 60 °C for 1 h. Afterwards, formaldehyde (13.06 mg, 0.435 mmol), 4-(chloromethyl)-2,2,6-trimethyl-3-azabicyclo[3.3.1]nonan-6-amine **(+)-103m** (100 mg, 0.435 mmol) and boronic acid (2 mol equiv. of amine) were added to the flask, along with powdered molecular sieves. The solution was stirred at 70 °C for 24 h and subsequently filtered on a short Celite® pad. The solvent was then removed under reduced pressure to give the crude product. The same procedure was adapted for the reaction of imine-amine **(+)-105l**.

9.4.6 C-6 Amide Hydrolysis with NaOH

9.4.6.1 NaOH Hydrolysis of (+)-59I

N-(2,2,4,6-Tetramethyl-3-azabicyclo[3.3.1]non-3-en-6-yl)acetamide **(+)-59I** (263.6 mg, 1.117 mmol) dissolved in isobutanol (5 mL) and NaOH solution (4 M; 10 mL) were added to a pressure tube. The mixture was stirred and heated to 150 °C for 48 h. Afterwards, the reaction was extracted with chloroform (2 X 15 mL), before drying over Na₂CO₃. The solvent was removed under reduced pressure to give the recovered starting material **(+)-59I**.

9.4.6.2 NaOH Hydrolysis of (+)-101I

N-((1*S*,4*R*,5*R*,6*S*)-2,2,4,6-Tetramethyl-3-azabicyclo[3.3.1]nonan-6-yl)acetamide **(+)-101I** (142.0 mg, 0.597 mmol) was dissolved in isobutanol (5 mL) and NaOH solution (4 M; 5 mL) were added to a pressure tube. The mixture was stirred and heated to 150 °C for 48 h. Afterwards, the reaction was extracted with chloroform (2 X 15 mL), before drying over Na₂CO₃. The solvent was removed under reduced pressure to recover the starting material **(+)-101I**.

9.4.7 C-6 Alkene Reactions with (+)-60I

9.4.7.1 Bromination of (+)-60I

2,2,4,6-Tetramethyl-3-azabicyclo[3.3.1]nona-3,6-diene **(+)-60I** (104.6 mg, 0.591 mmol) was dissolved in methanol (5 mL). Bromine water was added dropwise while stirring until the reaction mixture remained colourless. The solvent was then removed under reduced pressure to recover the starting material **(+)-60I**.

9.4.7.2 Oxidation of (+)-60I

A basic solution of potassium permanganate was prepared by dissolving 100.1 mg of KMnO₄ in a NaOH solution (2 M, 25 mL). This was then added dropwise to 2,2,4,6-tetramethyl-3-azabicyclo[3.3.1]nona-3,6-diene **(+)-60I** (149.1 mg, 0.842 mmol) dissolved in isopropanol (5 mL). The reaction mixture was filtered to remove precipitated MnO₂ before the solvent was removed under reduced pressure to recover the starting material **(+)-60I**.

9.4.8 Reactions with (+)-60a Imine

9.4.8.1 Reaction with 3-mercaptopropionic Acid

2,2,6-Trimethyl-3-azabicyclo[3.3.1]nona-3,6-diene **(+)-60a** (100 mg, 0.614 mmol) was dissolved in toluene (10 mL) in a round-bottom flask. 3-Mercaptopropionic acid (100 μL, 0.774 mmol) and *p*-toluenesulfonic acid monohydrate (100.6 mg, 0.529 mmol) were added. The reaction mixture was refluxed using a Dean-Stark apparatus for 24 h. The reaction mixture was

washed with a saturated solution of NaHCO₃ and then extracted with chloroform (2 X 20 mL) which was then dried over Na₂CO₃ before the solvent was removed under reduced pressure to recover the starting material **(+)-60a**.

9.4.8.2 Mannich Reaction with Ethyl Acetoacetate

2,2,6-Trimethyl-3-azabicyclo[3.3.1]nona-3,6-diene **(+)-60a** (66.8 mg, 0.41 mmol) was dissolved in acetonitrile (10 mL) before ethyl acetoacetate (54 µL, 0.41 mmol) and L-proline (9.4 mg, 20% mole equiv.) were added. The reaction was stirred at room temperature overnight before the solvent was removed under reduced pressure and the crude residue analysed by GC-MS and ¹H NMR but only **(+)-60a** was recovered. When attempted for a second time with the absence of L-proline, 102.3 mg of **(+)-60a** and 89.9 mg of ethyl acetoacetate were used. Again, only starting material was recovered.

9.4.8.3 Reaction with Malonic Acid

2,2,6-Trimethyl-3-azabicyclo[3.3.1]nona-3,6-diene **(+)-60a** (154.2 mg, 0.946 mmol) and malonic acid (128.8 mg, 1.238 mmol) were dissolved in methanol (10 mL), before the solvent was removed under reduced pressure to give a uniform mixture of the two reactants as a residue in a round bottom flask. The flask was then heated to 120 °C for 2 h. After cooling, the crude residue was attempted to be recrystallised using aqueous methanol, however, not solid formed and the starting material was recovered.

9.4.8.4 Grignard Reaction with Phenylmagnesium Bromide

2,2,6-Trimethyl-3-azabicyclo[3.3.1]nona-3,6-diene **(+)-60a** (12.8 mg, 0.079 mmol) was reacted with phenylmagnesium bromide (78.5 µL, 1 M) in tetrahydrofuran. The reaction was left to stir overnight. The crude reaction mixture was filtered before the solvent was removed under reduced pressure and the remaining residue analysed.

9.4.9 1,3-Dipolar Cycloaddition of **(+)-128** with Maleic Anhydride

The nitron **(+)-128** (85.3 mg, 0.336 mmol) was dissolved in dichloromethane and reacted for 10 min at room temperature under N₂ atmosphere with maleic anhydride (52.2 mg, 0.532 mmol). The solvent was removed by evaporation and re-dissolved in methanol-HCl (5:3 w/w) at 0 °C and stirred for 2 h. Afterwards, saturated K₂CO₃ solution was added (10 mL) and the product was extracted with dichloromethane (3 X 15 mL) and dried over MgSO₄ before removing the solvent *via* evaporation.

9.4.10 Hinsberg Reaction of (+)-101I with Benzenesulfonyl Chloride

N-(2,2,4,6-Tetramethyl-3-azabicyclo[3.3.1]nonan-6-yl)acetamide **(+)-101I** (110.9 mg, 0.466 mmol) was dissolved in dichloromethane (5 mL), to which a few drops of triethylamine was added. Then benzenesulfonyl chloride (160 μ L, 1.221 mmol) was added dropwise. The reaction was stirred for 4 h before being acidified with HCl solution (10 M). Crystallisation in ice was attempted, however, no solid was formed so the reaction solution was extracted with chloroform and 0.1696 g of crude product was obtained.

9.4.11 Methylchlorine Elimination of IBA with Base

2-Chloro-*N*-(1,7,7-trimethylnorbornan-2-yl)acetamide **76** (45.9 mg, 0.200 mmol) was stirred overnight in NaOH solution (4 M; 4 mL). The reaction mixture was extracted with chloroform (2 X 10 mL) and the combined organic extracts were dried over Na₂CO₃ before the solvent was removed under reduced pressure and the crude product analysed by GC-MS and ¹H NMR.

9.5 X-ray Structure Analysis

9.5.1 Diffraction Data Collection

Suitable single crystals of compounds **(-)-66h**, **(+)-101I**, **(+)-101b**, **(+)-80** and **(+)-67** were selected under the polarizing microscope (Leica M165Z), were moved on a MicroMount (MiTeGen, USA) consisting of a thin polymer tip with a wicking aperture. The X-ray diffraction measurements of **(-)-66h**, **(+)-101I**, **(+)-80** and **(+)-101b** were performed on a Bruker kappa-II CCD diffractometer at 150 K by using graphite-monochromated Mo-K α radiation (λ = 0.710723 Å). The single crystals, mounted on the goniometer using cryo loops for intensity measurements, were coated with paraffin oil and then quickly transferred to the cold stream using an Oxford Cryo stream attachment.

The X-ray diffraction measurements of **(+)-67** were carried out at MX1 beamline at the Australian Synchrotron Facility, Melbourne. The crystal was mounted on the goniometer using a cryo-loop for diffraction measurements, was coated with paraffin oil and then quickly transferred to the cold stream using Cryo stream attachment. Data were collected using Si<111> monochromated synchrotron X-ray radiation (λ = 0.71023 Å) at 100 K and were corrected for Lorentz and polarization effects using the XDS software.^[216] The structure was solved by direct methods, and the full-matrix least-squares refinements were carried out using SHELXL^[217] with the program Olex-2.^[218]

9.5.2 Solution and Refinement

Symmetry-related absorption corrections using the program SADABS^[219] were applied, and the data were corrected for Lorentz and polarisation effects using Bruker APEX2 software.^[220] All structures were solved by direct methods and the full-matrix least-square refinements were carried out using SHELXL.^[217] The non-hydrogen atoms were refined anisotropically. The molecular graphics were generated using Olex2^[218] and Mercury.^[221] The key crystallographic data and refinement details for each compound are presented in Table 9.1, Table 9.2, Table 9.3, Table 9.4 and Table 9.5.

Table 9.1 X-ray crystal data for (-)-66h.

(-)-66h	
Crystal data	
Chemical formula	2(C ₁₅ H ₂₅ NO ₃)
<i>M_r</i>	534.72
Crystal system, space group	Monoclinic, <i>Cc</i>
Temperature (K)	152
<i>a</i> , <i>b</i> , <i>c</i> (Å)	9.9601 (8), 19.406 (2), 7.8544 (6)
β (°)	98.746 (5)
<i>V</i> (Å ³)	1500.5 (2)
<i>Z</i>	2
Radiation type	Mo Kα
μ (mm ⁻¹)	0.08
Crystal size (mm)	0.16 × 0.13 × 0.07
Data collection	
Diffractometer	Bruker APEX-II CCD
Absorption correction	Multi-scan <i>SADABS2014/5</i> (Bruker, 2014/5) was used for absorption correction. <i>wR2(int)</i> was 0.1524 before and 0.0504 after correction. The Ratio of minimum to maximum transmission is 0.8365. The λ/2 correction factor is 0.00150.
No. of measured, independent and observed [<i>I</i> > 2σ(<i>I</i>)] reflections	0.624, 0.746
<i>R</i> _{int}	11273, 3088, 2334
(sin θ/λ) _{max} (Å ⁻¹)	0.056
Refinement	
<i>R</i> [<i>F</i> ² > 2σ(<i>F</i> ²)], <i>wR</i> (<i>F</i> ²), <i>S</i>	0.047, 0.113, 1.05
No. of reflections	3088
No. of parameters	177
No. of restraints	2
H-atom treatment	H-atom parameters constrained
Δρ _{max} , Δρ _{min} (e Å ⁻³)	0.17, -0.17
CCDC deposition Number	1485895

Table 9.2 X-ray crystal data for (+)-1011.

(+)-1011	
Crystal data	
Chemical formula	C ₁₄ H ₂₆ N ₂ O
<i>M_r</i>	238.37
Crystal system, space group	Monoclinic, <i>P</i> 2 ₁
Temperature (K)	155
<i>a</i> , <i>b</i> , <i>c</i> (Å)	8.4055 (5), 9.5712 (5), 9.4883 (5)
β (°)	112.922 (1)
<i>V</i> (Å ³)	703.06 (7)
<i>Z</i>	2
Radiation type	Mo Kα
μ (mm ⁻¹)	0.07
Crystal size (mm)	0.20 × 0.14 × 0.04
Data collection	
Diffractometer	Bruker APEX II
Absorption correction	Multi-scan <i>SADABS2007/4</i> (Bruker, 2007/4) was used for absorption correction. <i>wR2(int)</i> was 0.0482 before and 0.0371 after correction. The Ratio of minimum to maximum transmission is 0.8847. The λ/2 correction factor is 0.0015.
No. of measured, independent and observed [<i>I</i> > 2σ(<i>I</i>)] reflections	0.660, 0.746
<i>R</i> _{int}	5997, 2937, 2874
(sin θ/λ) _{max} (Å ⁻¹)	0.025
Refinement	
<i>R</i> [<i>F</i> ² > 2σ(<i>F</i> ²)], <i>wR</i> (<i>F</i> ²), <i>S</i>	0.031, 0.083, 1.05
No. of reflections	2937
No. of parameters	258
No. of restraints	1
H-atom treatment	All H-atom parameters refined
Δρ _{max} , Δρ _{min} (e Å ⁻³)	0.22, -0.13
CCDC deposition Number	1485896

Table 9.3 X-ray crystal data for **(+)-101b**.

(+)-101b	
Crystal data	
Chemical formula	C ₁₆ H ₃₀ N ₂ O
<i>M_r</i>	266.42
Crystal system, space group	Monoclinic, <i>P</i> 2 ₁
Temperature (K)	151
<i>a</i> , <i>b</i> , <i>c</i> (Å)	9.259 (2), 9.523 (2), 10.244 (3)
β (°)	115.841 (7)
<i>V</i> (Å ³)	813.0 (4)
<i>Z</i>	2
Radiation type	Mo Kα
μ (mm ⁻¹)	0.07
Crystal size (mm)	0.23 × 0.13 × 0.03
Data collection	
Diffractometer	Bruker APEX-II CCD
Absorption correction	Multi-scan <i>SADABS2014/5</i> (Bruker, 2014/5) was used for absorption correction. <i>wR2(int)</i> was 0.1284 before and 0.0603 after correction. The Ratio of minimum to maximum transmission is 0.8287. The λ/2 correction factor is 0.00150.
No. of measured, independent and observed [<i>I</i> > 2σ(<i>I</i>)] reflections	0.618, 0.746
<i>R</i> _{int}	5777, 2504, 1629
(sin θ/λ) _{max} (Å ⁻¹)	0.061
Refinement	
<i>R</i> [<i>F</i> ² > 2σ(<i>F</i> ²)], <i>wR</i> (<i>F</i> ²), <i>S</i>	0.051, 0.121, 0.99
No. of reflections	2504
No. of parameters	191
No. of restraints	2
H-atom treatment	H atoms treated by a mixture of independent and constrained refinement
Δρ _{max} , Δρ _{min} (e Å ⁻³)	0.21, -0.22
CCDC deposition Number	1485897

Table 9.4 X-ray crystal data for **(+)-67**.

(+)-67	
Crystal data	
Chemical formula	C ₁₄ H ₂₂ N ₂ O ₂
<i>M_r</i>	250.33
Crystal system, space group	Monoclinic, <i>P</i> 2 ₁
Temperature (K)	100
<i>a</i> , <i>b</i> , <i>c</i> (Å)	8.6120 (17), 7.4570 (15), 11.189 (2)
β (°)	110.16 (3)
<i>V</i> (Å ³)	674.5 (3)
<i>Z</i>	2
Radiation type	Mo Kα
μ (mm ⁻¹)	0.08
Crystal size (mm)	0.04 × 0.02 × 0.02
Data collection	
Diffractometer	Australian Synchrotron
Absorption correction	–
No. of measured, independent and observed [<i>I</i> > 2σ(<i>I</i>)] reflections	11209, 3006, 2935
<i>R</i> _{int}	0.024
(sin θ/λ) _{max} (Å ⁻¹)	0.659
Refinement	
<i>R</i> [<i>F</i> ² > 2σ(<i>F</i> ²)], <i>wR</i> (<i>F</i> ²), <i>S</i>	0.039, 0.102, 1.14
No. of reflections	3006
No. of parameters	171
No. of restraints	1
H-atom treatment	H atoms treated by a mixture of independent and constrained refinement
Δρ _{max} , Δρ _{min} (e Å ⁻³)	0.30, -0.21
Absolute structure	Flack <i>x</i> determined using 1310 quotients [(<i>I</i> ^{+)-(<i>I</i>⁻)]/[(<i>I</i>⁺)+(<i>I</i>⁻)] (Parsons, Flack and Wagner, Acta Cryst. B69 (2013) 249-259).}
Absolute structure parameter	0.3 (3)
CCDC deposition Number	1454979

Table 9.5 X-ray crystal data for **(+)-80**.

(+)-80	
Crystal data	
Chemical formula	C ₁₉ H ₂₆ N ₂ O
<i>M_r</i>	298.42
Crystal system, space group	orthorhombic, P _b ca
Temperature (K)	152.61
<i>a</i> , <i>b</i> , <i>c</i> (Å)	9.8285(11), 12.2145(15), 28.041(3)
β (°)	90
<i>V</i> (Å ³)	3366.4(7)
<i>Z</i>	8
Radiation type	Mo Kα (λ = 0.71073)
μ (mm ⁻¹)	0.073
Crystal size (mm)	0.398 × 0.104 × 0.052
Data collection	
Diffractometer	Bruker APEX-II CCD
Absorption correction	Multi-scan SADABS2014/5 (Bruker, 2014/5) was used for absorption correction. <i>wR2</i> (int) was 0.1781 before and 0.0650 after correction. The Ratio of minimum to maximum transmission is 0.7961. The λ/2 correction factor is 0.00150.
No. of measured, independent and observed [<i>I</i> > 2σ(<i>I</i>)] reflections	0.0502, 0.1126
<i>R</i> _{int}	0.107
(sin θ/λ) _{max} (Å ⁻¹)	0.638
Refinement	
<i>R</i> [<i>F</i> ² > 2σ(<i>F</i> ²)], <i>wR</i> (<i>F</i> ²), <i>S</i>	0.0502, 0.1288, 1.023
No. of reflections	3630
No. of parameters	204
No. of restraints	0
H-atom treatment	H-atom parameters constrained
Δρ _{max} , Δρ _{min} (e Å ⁻³)	0.23/-0.21
CCDC deposition Number	not deposited

9.5.3 Crystal Structure Data

Crystallographic data (excluding structure factors) for the structures in this paper have been deposited with the Cambridge Crystallographic Data Centre as supplementary publication numbers listed in Table 9.1, Table 9.2, Table 9.3 and Table 9.4. The data can be obtained free of charge *via* <http://www.ccdc.cam.ac.uk>, or by e-mailing data_request@ccdc.cam.ac.uk or by contacting The Cambridge Crystallographic Data Centre, 12, Union Road, Cambridge CB2 1EZ, UK; fax: (+44) 1223/336-033, Tel.: (+44) 1223/336-408.

9.6 Biological Assays

9.6.4 MTS Assay

General reagents for cell culture

Penicillin and Streptomycin, Trypsin and fetal bovine serum were purchased from Thermo Fisher Scientific (Scoresby, Vic, Australia). Dulbecco's Modified Eagle's Medium (DMEM), phosphate-buffered saline (PBS) and DMSO were purchased from Sigma-Aldrich (Castle Hill, NSW, Australia). The CellTiter 96[®] AQueous One Solution Reagent was purchased from Promega (Alexandria, NSW, Australia).

Cell culture

Human MDA-MB-231 breast cancer cells were obtained as a gift from Professor Michael Murray (University of Sydney) and grown at 37 °C in a humidified atmosphere of 5% CO₂ in DMEM supplemented with 10% fetal bovine serum and 1% Penicillin/Streptomycin. Confluent cells (80 – 90%) were harvested using trypsin/EDTA after washing with PBS.

Cell Viability

For the MTS assay cells were seeded in 96-well flat-bottom plates at a density of 7×10^4 cells/well. Serum was removed after 24 hours, after which cells were treated with various concentrations of drug candidates (1 – 50 μ M) in DMSO (final concentration 0.1%) for 48 hours; control cells received solvent alone. MTS activity was determined spectrophotometrically.

9.6.5 External Cancer Cell Growth Inhibition Assay

The selected compounds were screened against cancerous human KB cell line (epidermoid carcinoma of oral cavity, ATCCCL-17), cancerous human breast cancer cell line (MCF-7) and healthy mammalian cell line (African green monkey kidney epithelial cell, Vero), each at 50 μ g/mL. These assays were performed using the method described by O'Brien *et al.*^[170] In brief, cells at a logarithmic growth phase were harvested and diluted to 2.2×10^4

cells/ml, in fresh medium. Successively, 5 μ L of the test sample diluted in 5% DMSO, and 45 μ L of cell suspension were added to 384-well plates, incubated at 37 °C in a 5% CO₂ incubator. After the incubation period of 3 days, 12.5 μ L of 62.5 μ g/ml resazurin solution was added to each well and the plates were then incubated at 37 °C for 4 hours. Fluorescence signal was measured using SpectraMax M5 multi-detection microplate reader (Molecular Devices, USA) at the excitation and emission wavelengths of 530 nm and 590 nm.

Ellipticine and doxorubicin were used as a positive control, and 0.5% DMSO and water were used as a negative control.

9.6.6 AChE TLC Bioautographic Method

The AChE used in this assay was extracted from electric eels and purchased from Sigma-Aldrich (EC 3.1.1.7). The enzyme stock solution was prepared from a solution of AChE (1000 U) in 150 mL of 0.05 M Tris-hydrochloric acid buffer at pH 7.8 to which was added bovine serum albumin (150 mg) to stabilise the enzyme. The stock solution was kept at 4 °C. TLC plates (3 X 7 cm) used for the bioautography were washed with acetone and then thoroughly dried.

The samples were prepared as solutions in MeOH at concentrations of 1000, 200, 40, 8, 1.6, 0.32 and 0.064 ppm. The samples were applied to the TLC plates (3 X 7cm) in varying quantities using Camag Nanomat 4 TLC spotter with 0.5 μ L capillaries. Each plate was also spotted with Galantamine at 8, 1.6 and 0.32 ppm, as a positive control. The plate layout is shown in Figure 9.1.

The plate was sprayed with AChE enzyme stock solution so that the plate was visibly wet. Before the plate can dry, it was placed in an incubation chamber filled with water so that the plate sits above the water and is exposed to 100% humidity as this was vital. The chamber was kept at a constant 37 °C and the plate was incubated for 20 minutes. Upon removal of the plate, it was immediately (before it is allowed to dry) sprayed with a freshly prepared indicator solution which was a mixture of two solutions, a solution of 1-naphthyl acetate (25 mg) in EtOH (10 mL) and a solution of Fast Blue B salt (40 mg) in H₂O (16 mL). After between about 2-5 minutes, a purple coloration on the TLC plates appeared and white spots indicated inhibition of AChE by Galantamine as shown in Figure 5.1.

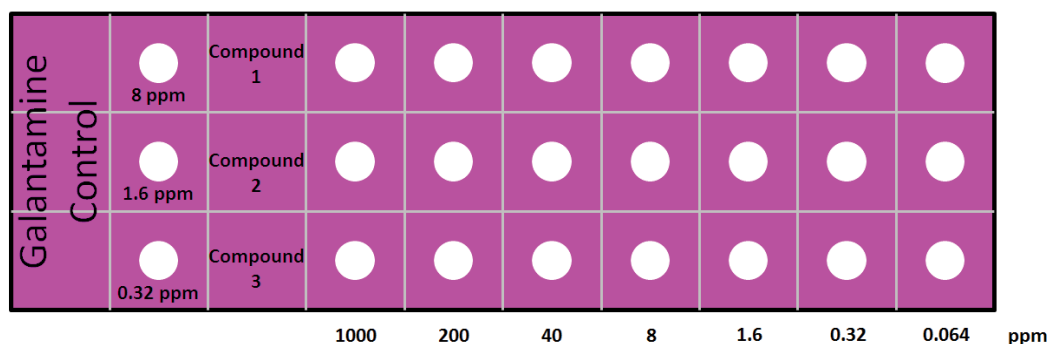


Figure 9.1 Layout of TLC bioautograph showing the inhibition of acetylcholinesterase activity by an inhibitor (0.5-1000 ng) with Galantamine as a positive control.

9.6.7 Ellman Assay Procedure

The assay used to determine the IC_{50} values of AChE inhibition was a modified version of the Ellman method, as described by Ingkaninan *et al.*^[179] Tris-buffer was prepared using Tris-HCl and Tris-Base to give pH 8 at 37 °C. The enzyme stock solution was prepared to 0.28 U/mL using the Tris-buffer with 0.1% bovine serum albumin. The colour reagent was prepared by making a 3 mM stock solution of DTNB in Tris-buffer also containing NaCl (0.1008 M) and $MgCl_2 \cdot 6H_2O$ (0.0200 M). The substrate was prepared by making a stock solution of 14 mM ATCh in Millipore water. Inhibitor samples were dissolved in 10% MeOH and Tris-buffer at 1 mg/mL and diluted to concentrations of 1000, 200, 40, 8, 1.6, 0.32 and 0.064 ppm).

Falcon Polystyrene 96-well, flat-bottom plates were used and for each concentration of inhibitor each well contained 25 μ L of enzyme solution, 25 μ L of inhibitor solution, 125 μ L of colour reagent (DTNB) solution and 50 μ L of buffer before the reaction was started by the addition of 25 μ L of substrate (ATCh) solution. BIO-TEK Synergy HT plate reader was used to read the absorbance in each well at 412 nm, every 15 seconds for 30 minutes at 37 °C. Each concentration was measured in triplicate in addition to an assay using a buffer without any inhibitor. Galantamine hydrobromide was used as a positive control. The AChE inhibitory data was analysed with the software package GraphPad Prism.

9.7 Molecular Modeling

The parameters used in each of the molecular modeling calculations used in Discovery Studio 4.5 are listed in the Appendices (Chapter 10).

CHAPTER 10: Appendices

10.1 Docking Parameters

10.1.1 Protein Preparation

Build Loops	True
Loop Definition	SEQRES
Loop List	
Maximal Loop Length	20
Use Looper	False
Use Looper Maximal	12
Loop Length	
Use CHARMM	True
Minimization	
Flexible Stem	0
Residues	
Protonate	True
Protein Dielectric	10
Constant	
pH for Protonation	7.4
Ionic Strength	0.145
Energy Cutoff	0.9
Advanced	
Forcefield	CHARMM
Keep Ligands	True
Keep Water	None
Disulfide Bridges	

10.1.2 Ligand Minimisation

Input Forcefield	CHARMM
Minimization	
Algorithm	Adopted Basis NR
Max Steps	2000
RMS Gradient	0.01
Energy Change	0.0
Save Results	0
Frequency	
Implicit Solvent	None
Model	
Dielectric Constant	1
Nonbond List Radius	18.0
Advanced	
Partial Charge	Momany-Rone
Estimation	

10.1.3 Ligand Preparation

Change Ionization	True
Ionization Method	pH Based
pH Based	
Minimum pH	7.4
Maximum pH	7.4
Rule Based	
Acid Ionization	Carboxylate
Base Ionization	Amine (primary) Amine (secondary) Amine (tertiary)
Ionization	One Protomer
Enumeration	
Filter SMARTS	Positive 1-Bond Positive 2-Bonds Positive 3-Bonds Negative 1-Bonds Negative 2-Bonds Negative 3-Bonds
Generate Tautomers	False
Enumerate What	AllTautomers
Maximum Number of	10
Tautomers	

ConsiderCarbonAsDonor	Never
MakeAllSp2AtomsAcceptors	False
Perceive Charge	False
Tautomerization	
Amides Tautomerization	Tautomerize
	Only Diamides
Preserve Aromaticity	False
Generate Isomers	True
EnumerateWhat	MarkedStereoatoms
SkipStereoAtomsAtBridgeHeads	True
AcceptInputStereoAsMarked	True
Fix Bad Valencies	True
Generate Coordinates	3D
Advanced	
Duplicate Structures	Remove

10.1.4 Docking with CDOCKER

Top Hits	1
Pose Cluster Radius	0.1
Random Conformations	10
Dynamics Steps	1000
Dynamics Target Temperature	1000
Include Electrostatic Interactions	True
Orientations to Refine	10
Maximum Bad Orientations	800
Orientation vdW Energy Threshold	300
Simulated Annealing	True
Heating Steps	2000
Heating Target Temperature	700
Cooling Steps	5000
Cooling Target Temperature	300
Advanced	
Forcefield	CHARMm
Use Full Potential	False
Ligand Partial Charge Method	Momany-Rone
Final Minimization	Full Potential
Final Minimization	0
Gradient Tolerance	
Prepare Input Receptor	True
Grid Extension	8.0
Random Number	314159 314159
Seed	314159 314159

10.1.5 In Situ Ligand Minimization

Flexible Receptor	Receptor.Positions,Gold.Protein.RotatedAtoms
Atom Property	
Flexible Residues	
Input Forcefield	CHARMm
Minimization	
Substructure Constraints	False
Substructure Constraints Input	
Substructure	

Substructure Constraints Input	Nearest
Substructure Selection	
Substructure Constraints Type	None
Substructure Constraints Force	10
Hydrogen Flexibility	False
Hydrogen Flexibility Radius	3.0
Algorithm	Adopted Basis NR
Steps	1000
RMS Gradient	0.001
Energy Change	0.0
Dielectric Constant	1.0
Distance-Dependent Dielectrics	True
Nonbond Cutoff	13.0
Constraints	

10.1.6 Ligand Scoring

Rotated Atoms	Receptor.Positions,Gold.Protein.RotatedAtoms,Gold.Protein.RotatedWaterAtoms
Property	
Input Control	
Ligands	
Input Preserve	True
Controls In Input	
Input Control Ligand	Control
Property	
Scoring Functions	CDOCKER Scores Ludi Energy Estimate 3
CDOCKER Scores	
Scores	-CDOCKER_ENERGY _
Ligand Partial Charge Method	CDOCKER_INTERACTION_ENERGY Momany-Rone
LigScore Scoring	Dreiding
LigScore Forcefield Scoring	5.0
LigScore Energy Grid Extension	
Scoring LigScore1	LigScore1
Label	
Scoring LigScore1 Minimum Score	
Scoring LigScore1 Report	False
Individual Contributions	
Scoring LigScore2	LigScore2
Label	
Scoring LigScore2 Minimum Score	
Scoring LigScore2 Report	False

Individual Contributions
PLP
Scoring PLP1 -PLP1
Label
Scoring PLP1
Minimum
Negative
Score
Scoring PLP2 -PLP2
Label
Scoring PLP2
Minimum
Negative
Score
Jain
Scoring Jain Jain
Label
Scoring Jain
Minimum
Score
Scoring Jain False
Ignore Non-Polar
Hydrogens
Scoring Jain False
Ignore Water
PMF
Scoring PMF -PMF
Label
Scoring PMF
Minimum
Negative
Score
Scoring PMF True
Ignore
Hydrogens
Scoring PMF 12.0
Carbon-Carbon
Cutoff
Scoring PMF 12.0
Other
Interactions
Cutoff
PMF04
Scoring -PMF04
PMF04 Label
Scoring
PMF04
Minimum
Negative
Score
Scoring PMF04 True
Ignore
Hydrogens
Scoring PMF04 6.0
Carbon-Carbon
Cutoff
Scoring PMF04 Other 9.0
Interactions
Cutoff
Ludi
Scoring Ludi Ludi
Score Label
Scoring Ludi
1 Minimum
Score
Scoring Ludi
2 Minimum
Score

Scoring Ludi
3 Minimum
Score
Scoring Ludi False
Report
Individual
Contributions
GOLD
Perform True
Local
Optimization
Retrieve False
Rotatable H
Positions
Receptor False
Depth
Scaling
Report False
Individual
Contributions
Fix All False
Receptor
Rotatable
Bonds
Parameter
Files
Parameter
Files
Goldscore
Parameter
Files
Chemscore
Parameter
Files ASP
Parameter
Files
CHEMPLP
Advanced
Use Input Binding False
Site
Input Binding Site

10.2 Common Feature Pharmacophore Generation

Conformation BEST
Generation
Maximum 255
Conformations
Discard Existing True
Conformations
Energy Threshold 20.0
Ring Fragments File
Save Conformations False
Parallel Processing False
Parallel Processing 4
Batch Size
Parallel Processing localhost
Server
Parallel Processing 2
Server Processes
Parallel Processing True
Preserve Order
Features HB_ACCEPTOR 0
5,HB_DONOR 0
5,HYDROPHOBIC 0
5,HYDROPHOBIC_aromatic
0 5,POS_IONIZABLE 0
5,NEG_IONIZABLE 0
5,RING_AROMATIC 0 5
Maximum 5
Pharmacophores
Minimum Interfeature 0.4
Distance

Maximum Excluded Volumes	0
Validation	False
Active Ligands	
Inactive Ligands	
Conformation Generation	FAST
Conformation Generation Maximum Conformations	250
Conformation Generation Discard Existing Conformations	True
Conformation Generation Ring Fragments File	
Conformation Generation Energy Threshold	20.0
Fitting Method	Rigid
Maximum Omitted Features	0
Advanced	
Minimum Features	1
Maximum Features	10
Number of Leads That May Miss	0
Minimum Feature Points	3
Minimum Features in Moderately Active	4
Feature Misses	1
Complete Misses	0
Stereoisomers As Different Molecules	False
Align Ligands to Hypothesis	True
Best Mapping Only	True
Check Superposition	True
Superposition Error	1.0
Scale Feature Blob Size	1.0
Maximum Mappings	1000
Maximum Confs Per Mapping	1000
Memory	512
Explore Exhaustive HBond Geometry Catalyst Parameter File	True

CHAPTER 11: References

- [1] J. Drews, *Science* **2000**, 287, 1960-1964.
- [2] M. Congreve, C. W. Murray and T. L. Blundell, *Drug Discovery Today* **2005**, 10, 895-907.
- [3] J. B. Dressman, G. L. Amidon, C. Reppas and V. P. Shah, *Pharmaceutical Research* **1998**, 15, 11-22.
- [4] D. J. Diller and K. M. Merz, *Proteins: Structure, Function, and Bioinformatics* **2001**, 43, 113-124.
- [5] D. A. Winkler, *Briefings in Bioinformatics* **2002**, 3, 73-86.
- [6] S. Y. Yang, *Drug Discovery Today* **2010**, 15, 444-450.
- [7] D. J. Newman and G. M. Cragg, *Journal of Natural Products* **2012**, 75, 311-335.
- [8] F. E. Koehn and G. T. Carter, *Nature Reviews Drug Discovery* **2005**, 4, 206-220.
- [9] C. A. Lipinski, F. Lombardo, B. W. Dominy and P. J. Feeney, *Advanced Drug Delivery Reviews* **1997**, 23, 3-25.
- [10] M. L. Lee and G. Schneider, *Journal of Combinatorial Chemistry* **2001**, 3, 284-289.
- [11] J. McMurry, *Organic Chemistry*, Thomson-Brooks/Cole, Belmont, CA, **2008**, p. 63.
- [12] A. L. Harvey, *Drug Discovery Today* **2008**, 13, 894-901.
- [13] G. L. Patrick and J. Spencer, *An Introduction to Medicinal Chemistry*, Oxford University Press, Oxford; New York, **2009**, p. 137.
- [14] P. J. Houghton, Y. Ren and M. J. Howes, *Natural Product Reports* **2006**, 23, 181-199.
- [15] E. E. Müller, A. E. Panerai, D. Cocchi and P. Mantegazza, *Life Sciences* **1977**, 21, 1545-1558.
- [16] *Erythroxylon coca.*, N. d. Piérola Camino Verde,
http://www.caminoverde.org/sites/default/files/imagecache/52_restore.jpg
3/4/2015.
- [17] M. S. Butler, *Journal of Natural Products* **2004**, 67, 2141-2153.
- [18] D. G. Kingston, *Journal of Natural Products* **2011**, 74, 1352-1352.
- [19] C. Hemtasin, A. T. Ung, S. Kanokmedhakul, K. Kanokmedhakul, R. Bishop, T. Satraruji and D. Bishop, *Monatshefte für Chemie* **2012**, 143, 955-963.
- [20] R. J. Quinn, A. R. Carroll, N. B. Pham, P. Baron, M. E. Palframan, L. Suraweera, G. K. Pierens and S. Muresan, *Journal of Natural Products* **2008**, 71, 464-468.
- [21] D. Camp, R. A. Davis, M. Campitelli, J. Ebdon and R. J. Quinn, *Journal of Natural Products* **2011**, 75, 72-81.
- [22] M. Feher and J. M. Schmidt, *Journal of Chemical Information and Computer Sciences* **2002**, 43, 218-227.

- [23] D. A. Goff, *Tetrahedron* **2013**, *69*, 242-256.
- [24] M. Suwalsky, P. Vargas, M. Avello, F. Villena and C. P. Sotomayor, *International Journal of Pharmaceutics* **2008**, *363*, 85-90.
- [25] C. L. Céspedes, M. El-Hafidi, N. Pavon and J. Alarcon, *Food Chemistry* **2008**, *107*, 820-829.
- [26] M. Silva and M. Bittner, *Química de la Flora de Chile* **1992**, 153-164.
- [27] O. Muñoz, P. Christen, S. Cretton, N. Backhouse, V. Torres, O. Correa, E. Costa, H. Miranda and C. Delporte, *Journal of Pharmacy and Pharmacology* **2011**, *63*, 849-859.
- [28] R. T. Wall, *Tetrahedron* **1970**, *26*, 2107-2117.
- [29] C. Mirand, G. Massiot and J. Levy, *The Journal of Organic Chemistry* **1982**, *47*, 4169-4170.
- [30] J. Degenhardt, T. G. Köllner and J. Gershenzon, *Phytochemistry* **2009**, *70*, 1621-1637.
- [31] *Picea abies*, H. Medicine
http://cdn.hauschka.com/images/system/plant_library/picea-abies-l.jpg 2/2/2014.
- [32] P. Tan and N. Auersperg, *Cancer Research* **1973**, *33*, 2320-2329.
- [33] X. Li, K. Jiang and Z. Lin, *Chinese Journal of Pharmacology and Toxicology* **1987**, *1*, 4.
- [34] M. A. Jordan, D. Thrower and L. Wilson, *Cancer Research* **1991**, *51*, 2212-2222.
- [35] M. Casanova, A. Ferrari, F. Spreafico, M. Terenziani, M. Massimino, R. Luksch, G. Cefalo, D. Polastri, I. Marcon and F. F. Bellani, *Cancer* **2002**, *94*, 3263-3268.
- [36] D. Baunbæk, N. Trinkler, Y. Ferandin, O. Lozach, P. Ploypradith, S. Rucirawat, F. Ishibashi, M. Iwao and L. Meijer, *Marine Drugs* **2008**, *6*, 514-527.
- [37] F. Lamchouri, H. Toufik, S. Bouzzine, M. Hamidi and M. Bouachrine, *Journal of Materials and Environmental Science* **2010**, *1*, 343-352.
- [38] B. Stewart and C. Wild, World Cancer Report 2014, *World Health Organization* **2014**.
- [39] *Cancer in Australia: an overview 2014*, Australian Institute of Health and Welfare, **2014**.
- [40] *How cancer starts*, The Cancer Council, <https://www.cancercouncil.com.au/wp-content/uploads/2010/11/How-cancer-starts.jpg> 6/4/2016.
- [41] V. T. DeVita and E. Chu, *Cancer Research* **2008**, *68*, 8643-8653.
- [42] J. P. Dheyongera, W. J. Geldenhuys, T. G. Dekker and C. J. Van der Schyf, *Bioorganic & Medicinal Chemistry* **2005**, *13*, 689-698.
- [43] D. Bhowmik, M. Hossain, F. Buzzetti, R. D'Auria, P. Lombardi and G. S. Kumar, *The Journal of Physical Chemistry B* **2012**, *116*, 2314-2324.

- [44] E. Thomas, F. Yu-jie, Z. Yuan-gang, S. Gunter, K. Venkata Sai Badireenath and W. Michael, *Current Medicinal Chemistry* **2007**, *14*, 2024-2032.
- [45] Y. Nakao, S. Yoshida, S. Matsunaga and N. Fusetani, *Journal of Natural Products* **2003**, *66*, 524-527.
- [46] S. R. Walker, E. J. Carter, B. C. Huff and J. C. Morris, *Chemical Reviews* **2009**, *109*, 3080-3098.
- [47] D. S. Shewach and R. D. Kuchta, *Chemical Reviews* **2009**, *109*, 2859-2861.
- [48] L. M. Heiser, A. Sadanandam, W. L. Kuo, S. C. Benz, T. C. Goldstein, S. Ng, W. J. Gibb, N. J. Wang, S. Ziyad, F. Tong, N. Bayani, Z. Hu, J. I. Billig, A. Dueregger, S. Lewis, L. Jakkula, J. E. Korkola, S. Durinck, F. Pepin, Y. Guan, E. Purdom, P. Neuvial, H. Bengtsson, K. W. Wood, P. G. Smith, L. T. Vassilev, B. T. Hennessy, J. Greshock, K. E. Bachman, M. A. Hardwicke, J. W. Park, L. J. Marton, D. M. Wolf, E. A. Collisson, R. M. Neve, G. B. Mills, T. P. Speed, H. S. Feiler, R. F. Wooster, D. Haussler, J. M. Stuart, J. W. Gray and P. T. Spellman, *Proceedings of the National Academy of Sciences* **2012**, *109*, 2724-2729.
- [49] C. Sotiriou and L. Pusztai *New England Journal of Medicine* **2009**, *360*, 790-800.
- [50] J. C. Chang, *American Association for Cancer Research* **2007**, *13*, 1-3.
- [51] W. L. McGuire and G. M. Clark, *CA: A Cancer Journal for Clinicians* **1986**, *36*, 302-309.
- [52] M. Lacroix, R.-A. Toillon and G. Leclercq, *Endocrine-Related Cancer* **2006**, *13*, 293-325.
- [53] J. Hugh, J. Hanson, M. C. U. Cheang, T. O. Nielsen, C. M. Perou, C. Dumontet, J. Reed, M. Krajewska, I. Treilleux, M. Rupin, E. Magherini, J. Mackey, M. Martin and C. Vogel, *Journal of Clinical Oncology* **2009**, *27*, 1168-1176.
- [54] S. Y. Park, *Archives of Pharmacal Research* **2010**, *33*, 1589-1609.
- [55] L. E. Hebert, P. A. Scherr, J. L. Bienias, D. A. Bennett and D. A. Evans, *Archives of Neurology* **2003**, *60*, 1119-1122.
- [56] Y. Brian, C. L. Masters, K. J. Barnham, A. I. Bush and P. A. Adlard, *Journal of Cellular and Molecular Medicine* **2009**, *13*, 61-86.
- [57] A. D. Kinghorn, L. Pan, J. N. Fletcher and H. Chai, *Journal of Natural Products* **2011**, *74*, 1539-1555.
- [58] L. Huang, A. Shi, F. He and X. Li, *Bioorganic & Medicinal Chemistry* **2010**, *18*, 1244-1251.
- [59] M. Kawahara, Y. Kuroda, N. Arispe and E. Rojas, *Journal of Biological Chemistry* **2000**, *275*, 14077-14083.
- [60] C. Priller, T. Bauer, G. Mitteregger, B. Krebs, H. A. Kretzschmar and J. Herms, *The Journal of Neuroscience* **2006**, *26*, 7212-7221.

- [61] K. S. KoSIK, C. L. Joachim and D. J. Selkoe, *Proceedings of the National Academy of Sciences* **1986**, *83*, 4044-4048.
- [62] K. Wallin, K. Blennow, N. Andreasen and L. Minthon, *Dementia and Geriatric Cognitive Disorders* **2006**, *21*, 131-138.
- [63] J. Busciglio, A. Lorenzo, J. Yeh and B. A. Yankner, *Neuron* **1995**, *14*, 879-888.
- [64] *Pathology of Alzheimer's disease*, Alzheimer's Disease Education and Referral Center, http://www.nia.nih.gov/NR/rdonlyres/A01D12CE-17E3-4D3D-BCEF-9ABC4FF91900/0/TANGLES_HIGH.JPG 3/5/2014.
- [65] H. Yu, W. M. Li, K. K. Kan, J. M. Ho, P. R. Carlier, Y. P. Pang, Z. M. Gu, Z. Zhong, K. Chan and Y. T. Wang, *Journal of Pharmaceutical and Biomedical Analysis* **2008**, *46*, 75-81.
- [66] M. Pohanka, *Expert Opinion on Therapeutic Patents* **2012**, *22*, 871-886.
- [67] D. M. Quinn, *Chemical Reviews* **1987**, *87*, 955-979.
- [68] R. Boopathy, R. V. Rajesh, S. Darvesh and P. G. Layer, *Clinica Chimica Acta* **2007**, *380*, 151-156.
- [69] *ACh and AChE in the synaptic cleft*, Unknown Author, http://faculty.pasadena.edu/dkwon/chap%208_files/textmostly/slide58.html 18/6/2013.
- [70] J. Sussman, M. Harel, F. Frolova, C. Oefner, A. Goldman, L. Toker and I. Silman, *Science* **1991**, *253*, 872-879.
- [71] Y. Xu, J. P. Colletier, M. Weik, H. Jiang, J. Moulton, I. Silman and J. L. Sussman, *Biophysical Journal* **2008**, *95*, 2500-2511.
- [72] U. Holzgrabe, P. Kapková, V. Alptüzün, J. Scheiber and E. Kugelmann, *Expert Opinion on Therapeutic Targets, Informa Healthcare* **2007**, *11*, 161-179.
- [73] M. Yusoff, H. Hamid and P. Houghton, *Molecules* **2014**, *19*, 1201-1211.
- [74] M. Gilson, T. Straatsma, J. McCammon, D. Ripoll, C. Faerman, P. Axelsen, I. Silman and J. Sussman, *Science* **1994**, 1276-1276.
- [75] M. Bajda, A. Więckowska, M. Hebda, N. Guzior, C. Sotriffer and B. Malawska, *International Journal of Molecular Sciences* **2013**, *14*, 5608-5632.
- [76] I. Silman and J. L. Sussman, *Current Opinion in Pharmacology* **2005**, *5*, 293-302.
- [77] M. Pakaski, Z. Rakonczay and P. Kasa, *Neurochemistry International* **2001**, *38*, 219-226.
- [78] J. Järv, T. Kesvatera and A. Aaviksaar, *European Journal of Biochemistry* **1976**, *67*, 315-322.
- [79] J. M. Rollinger, A. Hornick, T. Langer, H. Stuppner and H. Prast, *Journal of Medicinal Chemistry* **2004**, *47*, 6248-6254.

- [80] J. M. Barbosa Filho, K. C. P. Medeiros, M. d. F. F. Diniz, L. M. Batista, P. F. Athayde-Filho, M. S. Silva, E. V. d. Cunha, J. R. Almeida and L. J. Quintans-Júnior, *Revista Brasileira de Farmacognosia* **2006**, *16*, 258-285.
- [81] F. H. Shaw and G. A. Bentley, *The Australian Journal of Experimental Biology and Medical Science* **1953**, *31*, 573-576.
- [82] T. Thomsen and H. Kewitz, *Life Sciences* **1990**, *46*, 1553-1558.
- [83] X. C. Tang and Y. F. Han, *CNS Drug Reviews* **1999**, *5*, 281-300.
- [84] A. Lleo, S. Greenberg and J. Growdon, *Annual Review of Medicine* **2006**, *57*, 513-533.
- [85] B. Küenburg, L. Czollner, J. Fröhlich and U. Jordis, *Organic Process Research & Development* **1999**, *3*, 425-431.
- [86] A. Rampa, A. Bisi, F. Belluti, S. Gobbi, P. Valenti, V. Andrisano, V. Cavrini, A. Cavalli and M. Recanatini, *Bioorganic & Medicinal Chemistry* **2000**, *8*, 497-506.
- [87] P. Mungkornasawakul, S. G. Pyne, A. Jatisatienr, D. Supyen, W. Lie, A. T. Ung, B. W. Skelton and A. H. White, *Journal of Natural Products* **2003**, *66*, 980-982.
- [88] P. Mungkornasawakul, S. G. Pyne, A. Jatisatienr, W. Lie, A. T. Ung, K. Issakul, A. Sawatwanich, D. Supyen and C. Jatisatienr, *Journal of Natural Products* **2004**, *67*, 1740-1743.
- [89] P. Mungkornasawakul, S. G. Pyne, A. Jatisatienr, D. Supyen, C. Jatisatienr, W. Lie, A. T. Ung, B. W. Skelton and A. H. White, *Journal of Natural Products* **2004**, *67*, 675-677.
- [90] C. Mount and C. Downton, *Nature Medicine* **2006**, *12*, 780-784.
- [91] D. Fournier and A. Mutero, *Comparative Biochemistry and Physiology Part C: Pharmacology, Toxicology and Endocrinology* **1994**, *108*, 19-31.
- [92] P. Xia, H. S. V. Chen, D. Zhang and S. A. Lipton, *The Journal of Neuroscience* **2010**, *30*, 11246-11250.
- [93] C. G. Parsons, A. Stöffler and W. Danysz, *Neuropharmacology* **2007**, *53*, 699-723.
- [94] H. S. Chen and S. A. Lipton, *The Journal of Physiology* **1997**, *499*, 27-46.
- [95] N. C. Inestrosa, A. Alvarez, C. A. Pérez, R. D. Moreno, M. Vicente, C. Linker, O. I. Casanueva, C. Soto and J. Garrido, *Neuron* **1996**, *16*, 881-891.
- [96] E. Giacobini, *Neurochemical Research* **2000**, *25*, 1185-1190.
- [97] R. Morphy and Z. Rankovic, *Journal of Medicinal Chemistry* **2005**, *48*, 6523-6543.
- [98] S. D. Bembenek, J. M. Keith, M. A. Letavic, R. Apodaca, A. J. Barbier, L. Dvorak, L. Aluisio, K. L. Miller, T. W. Lovenberg and N. I. Carruthers, *Bioorganic & Medicinal Chemistry* **2008**, *16*, 2968-2973.
- [99] M. L. Weidenbaum, *Murray Weidenbaum Publications* **1993**, *Policy Study* 116.

- [100] A. T. Ung, R. Bishop, D. C. Craig, M. L. Scudder and J. Yunus, *Australian Journal of Chemistry* **1992**, *45*, 553-565.
- [101] I. C. C. Bong, A. T. Ung, D. C. Craig, M. L. Scudder and R. Bishop, *Australian Journal of Chemistry* **1989**, *42*, 1929-1937.
- [102] J. J. Ritter and P. P. Minieri, *Journal of the American Chemical Society* **1948**, *70*, 4045-4048.
- [103] R. Bishop, *Ritter-type Reactions*. In *Comprehensive Organic Synthesis*, Trost, B. M.; Fleming, I, Eds.; Pergamon: Oxford, **1991**, Vol. 6, Winterfeldt, E. Ed., Chapter 1.9, 213-325.
- [104] L. I. Krimen and D. J. Cota in *The Ritter Reaction*, Vol. 17 John Wiley & Sons, Inc., **1969**, pp. 312-356.
- [105] G. A. Olah and B. G. Balaram Gupta, *The Journal of Organic Chemistry* **1980**, *45*, 3532-3533.
- [106] E. E. Magat, B. F. Faris, J. E. Reith and L. F. Salisbury, *Journal of the American Chemical Society* **1951**, *73*, 1028-1031.
- [107] B. T. G. Glikmans, M. Hellin, and F. Coussebant, *Bulletin de la Société Chimique de France* **1966**, 1383-1388.
- [108] H. Christol and G. Solladié, *Bulletin de la Société Chimique de France* **1966**, 1299-1307.
- [109] C. L. Parris and R. M. Christenson, *The Journal of Organic Chemistry* **1960**, *25*, 331-334.
- [110] F. R. Benson and J. J. Ritter, *Journal of the American Chemical Society* **1949**, *71*, 4128-4129.
- [111] J. R. Norell, *The Journal of Organic Chemistry* **1970**, *35*, 1611-1618.
- [112] S. Edwards and F. H. Marquardt, *The Journal of Organic Chemistry* **1974**, *39*, 1963-1963.
- [113] S. E. Tadashi Sasaki, Takeshi Toru, Katsumi Ito, *Bulletin of the Chemical Society of Japan* **1970**, *43*, 1820-1824.
- [114] N. C. Deno, R. W. Gaugler and M. J. Wisotsky, *The Journal of Organic Chemistry* **1966**, *31*, 1967-1968.
- [115] F. Cacace, G. Ciranni and P. Giacomello, *Journal of the American Chemical Society* **1982**, *104*, 2258-2261.
- [116] J. K. Kochi and M. A. Ratcliff, *The Journal of Organic Chemistry* **1971**, *36*, 3112-3120.
- [117] L. Eberson and K. Nyberg, *Tetrahedron* **1976**, *32*, 2185-2206.
- [118] H. C. Cowen, F. Riding, E. Warhurst, A. D. Buckingham, R. J. W. Le Fevre, G. D. Meakins, R. N. Haszeldine, J. Jander, G. R. Clemo, B. W. Fox, R. Raper, J. F. W. McOmie, I. M.

- White, O. L. Brady, P. E. Halstead, A. G. Sharpe, G. W. Gray, B. Jones, J. Cast, T. S. Stevens, F. Bell, J. W. Cook, L. Hunter, R. M. Barrer, N. Mackenzie, D. MacLeod, C. C. Barker, F. D. Casson, G. F. Laws, W. Carruthers, E. S. Lane and C. Williams, *Journal of the Chemical Society (Resumed)* **1953**, 4168-4188.
- [119] H. C. Brown and P. J. Geoghegan, *The Journal of Organic Chemistry* **1970**, *35*, 1844-1850.
- [120] L. S. Hegedus, T. A. Mulhern and H. Asada, *Journal of the American Chemical Society* **1986**, *108*, 6224-6228.
- [121] R. Sanz, A. Martínez, V. Guilarte, J. M. Álvarez-Gutiérrez and F. Rodríguez, *European Journal of Organic Chemistry* **2007**, *2007*, 4642-4645.
- [122] A. I. Meyers and J. C. Sircar in *Additions to the Cyano Group to Form Heterocycles*, Vol. 1 John Wiley & Sons, Ltd., **1970**, pp. 341-421.
- [123] H. Stetter and J. Gärtner, *Chemische Berichte* **1966**, *99*, 925-929.
- [124] I. Z. Kaboré, Q. Khuong-Huu and A. Pancrazi, *Tetrahedron* **1978**, *34*, 2815-2819.
- [125] M. R. Monaco, P. Renzi, D. M. Scarpino Schietroma and M. Bella, *Organic Letters* **2011**, *13*, 4546-4549.
- [126] A. T. Ung, S. G. Williams, A. Angeloski, J. Ashmore, U. Kuzhiumparambil, M. Bhadbhade and R. Bishop, *Monatshefte für Chemie-Chemical Monthly* **2014**, *145*, 983-992.
- [127] J. Wang, L. Lai and Y. Tang, *Journal of Chemical Information and Computer Sciences* **1999**, *39*, 1173-1189.
- [128] L. Ma'mani, A. Heydari and M. Sheykhani, *Applied Catalysis A: General* **2010**, *384*, 122-127.
- [129] I. Bong, A. Ung, D. Craig, M. Scudder and R. Bishop, *Australian Journal of Chemistry* **1989**, *42*, 1929-1937.
- [130] R. Bishop, *Ritter-Type Reactions*, Elsevier, Oxford, **2014**, p. 239-295.
- [131] T. Gajda, A. Koziara, S. Zawadzki and A. Zweirzak, *Synthesis* **1979**, *1979*, 549-552.
- [132] J. A. Caram, B. E. Rivero, O. E. Piro, E. G. Gros and C. M. Marschoff, *Canadian Journal of Chemistry* **1990**, *68*, 334-338.
- [133] V. D. Dyachenko and E. B. Rusanov, *Chemistry of Heterocyclic Compounds* **2003**, *39*, 645-690.
- [134] S. N. Bizyaev, Y. V. Gatilov and A. V. Tkachev, *Mendeleev Communications* **2015**, *25*, 93-95.
- [135] V. Shreevidhyaa Suresh, S. Sathya, A. Akila, S. Ponnuswamy and G. Usha, *Acta Crystallographica Section E* **2014**, *70*, 1171-1172.

- [136] A. Akila, S. Ponnuswamy, V. Shreevidhyaa Suresh and G. Usha, *Journal of Molecular Structure* **2015**, *1093*, 113-118.
- [137] F. F. Fleming and Z. Zhang, *Tetrahedron* **2005**, *61*, 747-789.
- [138] R. E. Moser and C. N. Matthews, *Experientia* **1968**, *24*, 658-659.
- [139] Y. Hanzawa, Y. Kasashima, K. Tomono, T. Mino, M. Sakamoto and T. Fujita, *Journal of Oleo Science* **2011**, *61*, 715-721.
- [140] E. Callens, A. J. Burton and A. G. M. Barrett, *Tetrahedron Letters* **2006**, *47*, 8699-8701.
- [141] G. R. Qu, Y. W. Song, H. Y. Niu, H. M. Guo and J. S. Fossey, *RSC Advances* **2012**, *2*, 6161-6163.
- [142] W. N. Samaniego, A. Baldessari, M. A. Ponce, J. B. Rodriguez, E. G. Gros, J. A. Caram and C. M. Marschoff, *Tetrahedron Letters* **1994**, *35*, 6967-6970.
- [143] S. R. Taylor, A. T. Ung and S. G. Pyne, *Tetrahedron* **2007**, *63*, 10896-10901.
- [144] E. Torres, R. Fernández, S. Miquet, M. Font-Bardia, E. Vanderlinden, L. Naesens and S. Vázquez, *ACS Medicinal Chemistry Letters* **2012**, *3*, 1065-1069.
- [145] J. R. Luly, G. Bolis, N. BaMaung, J. Soderquist, J. F. Dellaria, H. Stein, J. Cohen, T. J. Perun, J. Greer and J. J. Plattner, *Journal of Medicinal Chemistry* **1988**, *31*, 532-539.
- [146] R. C. Neuman, C. T. Berge, G. A. Binengar, W. Adam and Y. Nishizawa, *The Journal of Organic Chemistry* **1990**, *55*, 4564-4568.
- [147] B. Witkop, *Journal of the American Chemical Society* **1956**, *78*, 2873-2882.
- [148] S. Kandambeth, A. Mallick, B. Lukose, M. V. Mane, T. Heine and R. Banerjee, *Journal of the American Chemical Society* **2012**, *134*, 19524-19527.
- [149] R. N. Lacey, *Journal of the Chemical Society (Resumed)* **1960**, 1633-1639.
- [150] N. A. Petasis, A. Goodman and I. A. Zavialov, *Tetrahedron* **1997**, *53*, 16463-16470.
- [151] R. Frauenlob, C. García, G. A. Bradshaw, H. M. Burke and E. Bergin, *The Journal of Organic Chemistry* **2012**, *77*, 4445-4449.
- [152] C. E. Cleeton and N. H. Williams, *Physical Review* **1934**, *45*, 234-237.
- [153] M. Jafarpour, A. Rezaeifard and T. Golshani, *Phosphorus, Sulfur, and Silicon and the Related Elements* **2010**, *186*, 140-148.
- [154] M. Mokhtar, T. S. Saleh, N. S. Ahmed, S. A. Al-Thabaiti and R. A. Al-Shareef, *Ultrasonics Sonochemistry* **2011**, *18*, 172-176.
- [155] N. T. Thuan, D. T. M. Dung, D. N. Que, P. T. P. Dung, T. K. Vu, H. Hahn, B. W. Han, Y. Kim, S. B. Han and N. H. Nam, *Medicinal Chemistry Research* **2015**, *24*, 3803-3812.
- [156] Q. Lin, D. Djaidi, R. Bishop, D. C. Craig and M. L. Scudder, *Australian Journal of Chemistry* **1998**, *51*, 799-806.

- [157] S. A. Ali, J. H. Khan, M. I. M. Wazeer and H. P. Perzanowski, *Tetrahedron* **1989**, *45*, 5979-5986.
- [158] J. C. Pelletier and M. P. Cava, *The Journal of Organic Chemistry* **1987**, *52*, 616-622.
- [159] Q. Lin, G. E. Ball and R. Bishop, *Tetrahedron* **1997**, *53*, 10899-10910.
- [160] G. Soldaini, F. Cardona and A. Goti, *Organic Letters* **2007**, *9*, 473-476.
- [161] V. D. Sen', G. V. Shilov and V. A. Golubev, *Russian Journal of Organic Chemistry* **2014**, *50*, 1124-1132.
- [162] M. Kammoun, H. B. Salah and M. Damak, *Synthetic Communications* **2011**, *41*, 1520-1528.
- [163] P. Bilski, K. Reszka, M. Bilska and C. F. Chignell, *Journal of the American Chemical Society* **1996**, *118*, 1330-1338.
- [164] J. F. French, C. E. Thomas, T. R. Downs, D. F. Ohlweiler, A. A. Carr and R. C. Dage, *Circulatory Shock* **1994**, *43*, 130-136.
- [165] S. A. Alexander, C. Kyi and C. H. Schiesser, *Organic & Biomolecular Chemistry* **2015**, *13*, 4751-4759.
- [166] R. Suarez-Bertoa, F. Saliu, M. Bruschi and B. Rindone, *Tetrahedron* **2012**, *68*, 8267-8275.
- [167] *Bioassay Laboratory, National Center for Genetic Engineering and Biotechnology (BIOTEC)*, 113 Thailand Science Park, Phahonyothin Road, Khlong Nueng, Khlong Luang, Pathum Thani 12120 Thailand.
- [168] T. Mosmann, *Journal of Immunological Methods* **1983**, *65*, 55-63.
- [169] P. A. Bernabei, V. Santini, L. Silvestro, O. D. Pozzo, R. Bezzini, I. Viano, V. Gattei, R. Saccardi and P. R. Ferrini, *Hematological Oncology* **1989**, *7*, 243-253.
- [170] J. O'Brien, I. Wilson, T. Orton and F. Pognan, *European Journal of Biochemistry* **2000**, *267*, 5421-5426.
- [171] R. E. Erb and M. H. Ehlers, *Journal of Dairy Science* **1950**, *33*, 853-864.
- [172] R. C. Squatrito, J. P. Connor and R. E. Buller, *Gynecologic Oncology* **1995**, *58*, 101-105.
- [173] G. L. Ellman, K. D. Courtney and R. M. Featherstone, *Biochemical Pharmacology* **1961**, *7*, 88-95.
- [174] I. K. Rhee, N. Appels, T. Luijendijk, H. Irth and R. Verpoorte, *Phytochemical Analysis* **2003**, *14*, 145-149.
- [175] W. Liu, Y. Yang, X. Cheng, C. Gong, S. Li, D. He, L. Yang, Z. Wang and C. Wang, *Journal of Pharmaceutical and Biomedical Analysis* **2014**, *94*, 215-220.
- [176] A. Marston, J. Kissling and K. Hostettmann, *Phytochemical Analysis* **2002**, *13*, 51-54.

- [177] F. Marcelo, C. Dias, A. Martins, P. J. Madeira, T. Jorge, M. H. Florêncio, F. J. Cañada, E. J. Cabrita, J. Jiménez-Barbero and A. P. Rauter, *Chemistry-A European Journal* **2013**, *19*, 6641-6649.
- [178] K. Sastraruji, *Semi-synthesis and Structure-Activity Relationship Studies of Stemona Alkaloids and Related Analogues, Doctor of Philosophy Dissertation* University of Wollongong, Wollongong, **2011**.
- [179] K. Ingkaninan, P. Temkitthawon, K. Chuenchom, T. Yuyaem and W. Thongnoi, *Journal of Ethnopharmacology* **2003**, *89*, 261-264.
- [180] N. S. L. Perry, P. J. Houghton, A. Theobald, P. Jenner and E. K. Perry, *Journal of Pharmacy and Pharmacology* **2000**, *52*, 895-902.
- [181] C. Brühlmann, A. Marston, K. Hostettmann, P. A. Carrupt and B. Testa, *Chemistry & Biodiversity* **2004**, *1*, 819-829.
- [182] Y. Özkay and Ü. D. Özkay, *European International Journal of Science and Technology* **2014**, *3*, 115-120.
- [183] S. R. Lee, J. R. D. Pronto, B. E. Sarankhuu, K. S. Ko, B. D. Rhee, N. Kim, N. P. Mishchenko, S. A. Fedoreyev, V. A. Stonik and J. Han, *Marine Drugs* **2014**, *12*, 3560-3573.
- [184] R. F. Bruns and I. A. Watson, *Journal of Medicinal Chemistry* **2012**, *55*, 9763-9772.
- [185] T. J. Cheeseright, M. D. Mackey, J. L. Melville and J. G. Vinter, *Journal of Chemical Information and Modeling* **2008**, *48*, 2108-2117.
- [186] R. A. Vogel, *Journal of the American College of Cardiology* **2012**, *59*, 2354-2355.
- [187] J. D. Horton, J. C. Cohen and H. H. Hobbs, *Journal of Lipid Research* **2009**, *50*, 172-177.
- [188] K. Dungan and J. B. Buse, *Clinical Diabetes* **2005**, *23*, 56-62.
- [189] D. Wootten, E. E. Savage, C. Valant, L. T. May, K. W. Sloop, J. Ficorilli, A. D. Showalter, F. S. Willard, A. Christopoulos and P. M. Sexton, *Molecular Pharmacology* **2012**, *82*, 281-290.
- [190] F. S. Willard, D. Wootten, A. D. Showalter, E. E. Savage, J. Ficorilli, T. B. Farb, K. Bokvist, J. Alsina-Fernandez, S. G. B. Furness, A. Christopoulos, P. M. Sexton and K. W. Sloop, *Molecular Pharmacology* **2012**, *82*, 1066-1073.
- [191] A. Ichimura, A. Hirasawa, O. Poulain Godefroy, A. Bonnefond, T. Hara, L. Yengo, I. Kimura, A. Leloire, N. Liu, K. Iida, H. Choquet, P. Besnard, C. Lecoœur, S. Vivequin, K. Ayukawa, M. Takeuchi, K. Ozawa, M. Tauber, C. Maffei, A. Morandi, R. Buzzetti, P. Elliott, A. Pouta, M. R. Jarvelin, A. Korner, W. Kiess, M. Pigeyre, R. Caiazzo, W. Van Hul, L. Van Gaal, F. Horber, B. Balkau, C. Levy Marchal, K. Rouskas, A. Kouvatsi, J.

- Hebebrand, A. Hinney, A. Scherag, F. Pattou, D. Meyre, T. a. Koshimizu, I. Wolowczuk, G. Tsujimoto and P. Froguel, *Nature* **2012**, *483*, 350-354.
- [192] D. Y. Oh, E. Walenta, T. E. Akiyama, W. S. Lagakos, D. Lackey, A. R. Pessentheiner, R. Sasik, N. Hah, T. J. Chi, J. M. Cox, M. A. Powels, J. Di Salvo, C. Sinz, S. M. Watkins, A. M. Armando, H. Chung, R. M. Evans, O. Quehenberger, J. McNelis, J. G. Bogner-Strauss and J. M. Olefsky, *Nature Medicine* **2014**, *20*, 942-947.
- [193] S. D. Dib-Hajj, Y. Yang, J. A. Black and S. G. Waxman, *Nature Reviews Neuroscience* **2013**, *14*, 49-62.
- [194] S. A. Yuzwa, X. Shan, M. S. Macauley, T. Clark, Y. Skorobogatko, K. Vosseller and D. J. Vocadlo, *Nature Chemical Biology* **2012**, *8*, 393-399.
- [195] S. A. Yuzwa, A. H. Cheung, M. Okon, L. P. McIntosh and D. J. Vocadlo, *Journal of Molecular Biology* **2014**, *426*, 1736-1752.
- [196] W. Ouyang, J. K. Kolls and Y. Zheng, *Immunity* **2008**, *28*, 454-467.
- [197] S. L. Gaffen, R. Jain, A. V. Garg and D. J. Cua, *Nature Reviews Immunology* **2014**, *14*, 585-600.
- [198] A. Young, D. Mittal, J. Stagg and M. J. Smyth, *Cancer Discovery* **2014**, *4*, 879-888.
- [199] D. L. Cohn, F. Bustreo and M. C. Raviglione, *Clinical Infectious Diseases* **1997**, *24*, 121-130.
- [200] J. Tavares, P. Formaglio, S. Thiberge, E. Mordelet, N. Van Rooijen, A. Medvinsky, R. Ménard and R. Amino, *The Journal of Experimental Medicine* **2013**, *210*, 905-915.
- [201] W. H. Organization, **2016**.
- [202] *Discovery Studio Client*, Dassault Systèmes Biovia Corp, **2016**.
- [203] W. J. Egan, K. M. Merz and J. J. Baldwin, *Journal of Medicinal Chemistry* **2000**, *43*, 3867-3877.
- [204] W. J. Egan and G. Lauri, *Advanced Drug Delivery Reviews* **2002**, *54*, 273-289.
- [205] R. G. Susnow and S. L. Dixon, *Journal of Chemical Information and Computer Sciences* **2003**, *43*, 1308-1315.
- [206] T. K. Woo, P. M. Margl, L. Deng, L. Cavallo and T. Ziegler, *Catalysis Today* **1999**, *50*, 479-500.
- [207] J. R. Votano, M. Parham, L. M. Hall, L. H. Hall, L. B. Kier, S. Oloff and A. Tropsha, *Journal of Medicinal Chemistry* **2006**, *49*, 7169-7181.
- [208] B. Wang, L. P. Yang, X. Z. Zhang, S. Q. Huang, M. Bartlam and S. F. Zhou, *Drug Metabolism Reviews* **2009**, *41*, 573-643.
- [209] L. K. Teh and L. Bertilsson, *Drug Metabolism and Pharmacokinetics* **2012**, *27*, 55-67.

- [210] H. M. Greenblatt, G. Kryger, T. Lewis, I. Silman and J. L. Sussman, *FEBS Letters* **1999**, *463*, 321-326.
- [211] G. Kumari, Nutan, M. Modi, S. K. Gupta and R. K. Singh, *European Journal of Medicinal Chemistry* **2011**, *46*, 1181-1188.
- [212] G. Wu, D. H. Robertson, C. L. Brooks and M. Vieth, *Journal of Computational Chemistry* **2003**, *24*, 1549-1562.
- [213] N. Brooijmans and I. D. Kuntz, *Annual Review of Biophysics and Biomolecular Structure* **2003**, *32*, 335-373.
- [214] H. J. Böhm, *Journal of Computer-Aided Molecular Design* **1994**, *8*, 243-256.
- [215] H. J. Böhm, *Journal of Computer-Aided Molecular Design* **1998**, *12*, 309-309.
- [216] W. Kabsch, *Journal of Applied Crystallography* **1993**, *26*, 795-800.
- [217] G. M. Sheldrick, *Acta Cryst. A* **2008**, *71*, 64-112.
- [218] O. V. Dolomanov, L. J. Bourhis, R. J. Gildea, J. A. K. Howard and H. Puschmann, *Journal of Applied Crystallography* **2009**, *42*, 339-341.
- [219] SADABS, Bruker AXS Inc, Madison, Wisconsin, USA, **2001**.
- [220] APEX2 and SAINT, Bruker AXS Inc., Madison, Wisconsin, USA, **2007**.
- [221] C. F. Macrae, P. R. Edgington, P. McCabe, E. Pidcock, G. P. Shields, R. Taylor, M. Towler and J. van de Streek, *Journal of Applied Crystallography* **2006**, *39*, 453-457.